Effect of citric acid on hydrotreating activity of NiMo catalysts

A thesis

submitted to the college of graduate studies and research

in partial fulfillment of the requirements for the degree of

Masters of Science

in the Department of Chemical and Biological Engineering

University of Saskatchewan

Saskatoon, Saskatchewan

by

Sidhartha Mohanty

December 2011

COPYRIGHT

The Department Head of Chemical and Biological Engineering
College of Engineering
University of Saskatchewan
57 Campus Drive
Saskatoon SK Canada
S7N 5A9

ABSTRACT

With depleting reserves of sweet crude oil, there is an increasing demand world over to process heavy crudes. Canada's Athabasca oil sands basin is a rich source of this heavy feedstock derived from bitumen. However, the heavy gas oil feedstock derived from this bitumen has very high quantities of S (4 wt %) and N (0.4 wt %). In order to meet today's strict environmental regulations, design of hydrotreating catalysts with increased active site density and improved intrinsic catalytic activity per site is critical. This work, in the first phase deals with the modification of the Al_2O_3 support to increase its acidity and in subsequent phases, citric acid has been used as an additive to enhance the formation of Type II NiMoS sites.

Mesostructured alumino-silicate (MAS) materials were synthesized from ZSM-5 nanoclusters and used as catalysts supports for the hydrotreatment of a model compound and real feed stock. The alumino-silicate materials exhibited different acid strengths and textural properties depending on the duration of hydrothermal treatment of the zeolite seeds. The acidity of the MAS materials were found significantly higher than Al-SBA-15 and Al_2O_3 materials. The activity of NiMo catalysts supported on MAS materials were evaluated using the hydrodesulfurization of dibenzothiophene (DBT). The NiMo catalyst supported on mesoporous alumino silicate obtained after 16 hrs of hydrothermal treatment of the ZSM-5 precursors was found to be the most active in the HDS of DBT. Similarly, hydrotreating tests revealed that the composite made of 5 wt % MAS-16 and 95 wt % γ-Al_2O_3 was best suited for hydrotreating reactions with real feedstock. This support showed optimum acidity and excellent dispersion of the active species and was selected as the support of choice for all further hydrotreating reactions with real feed stock.

In the second stage of this work citric acid (CA) in varying ratios was used to prepare NiMo catalysts supported on a composite of γ-Al_2O_3 and mesoporous alumino-silicates. Citric acid was found to form a complex with both Ni and Mo simultaneously. However, the promoting effect of citric acid in the hydrotreating was observed mostly due to the formation of a stable nickel-citrate complex. The hydrotreating activity of the synthesized catalysts is evaluated using heavy gas oil (HGO) derived from Athabasca bitumen, in a trickle bed continuous reactor. The Mo loading, Ni loading and the citric acid to nickel molar ratios were optimized on the basis of hydrodesulfurization (HDS) and hydrodenitrogenation (HDN) activity of HGO. The best performing catalyst for the hydrotreating of heavy gas oil was obtained for a Mo loading of 13 wt %, Ni loading of 7 wt % and CA/Ni molar ratio of 1. The sulfur and nitrogen conversions for the best catalyst were found to be 93 wt % and 74 wt % respectively.

ACKNOWLEDGEMENT

I would first like to thank my supervisors, Dr. Ajay Dalai and Dr. John Adjaye, for their valuable guidance and supervision throughout my research work. I greatly appreciate the effort made by them to review and provide recommendations to my written materials. I would also like to thank the other two members of my MSc. supervisory committee, Dr. Yongfeng Hu and Dr. Hui Wang, for their contributions to my graduate studies. Secondly, I would also like to thank Mr. Richard Blondin, Mr. Dragan Cekic, and Heli Eunike for their assistance in the laboratory work that contributed to my project. My thanks also go to the Natural Sciences and Engineering Research Council of Canada and Syncrude Canada Limited for their much-appreciated financial assistance. I also greatly appreciate the work done by the Saskatchewan Structural Science Center and Geology Department of University of Saskatchewan, University of New Brunswick, and the University of Western Ontario for their assistance in the catalyst characterizations. Lastly, I would like to express my gratitude to all the professors, post-doctorate fellows, and graduate students that have contributed to my graduate study at the University of Saskatchewan. Finally, I thank God Almighty for his blessings.

DEDICATION

In loving memory of my jeje (Grandfather), Shri Jadumani Mohanty (1923- 2010)

TABLE OF CONTENTS

LIST OF TABLES

LIST OF FIGURES

NOMENCLATURE

ΔH_R	heat of reaction kJ/mol
ΔE_o	inner-potential correction
$\sigma_s{}^2$	debye–Waller factor
°*API*	american Petroleum Institute gravity of petroleum liquids, dimensionless
A	surface area of catalysts and catalyst supports found from BET analysis, m^2/g
Al	aluminum
Al_2O_3	aluminium oxide
ATM	atmospheric
B	boron
BET	brunauer-emmett-teller method
BP	biphenyl
BT	benzothiophene
BTU	British thermal unit
CA	citric acid
CHB	cyclohexyl benzene
Co	cobalt
d	average pore diameter of catalysts and catalyst supports, nm
DBT	dibenzothiophene
DDS	direct desulfurization
DM	demineralized water
DMDBT	dimethyl dibenzothiophene
DRU	diluents recovery unit

EDTA ethylene diammine tetra aceitic acid

EXAFS extended x-ray absorption fine spectroscopy

FBP final boiling point

FCC fluid catalytic cracking unit

FID flame ionization detector

FT fourier Transform

FTIR fourier transform infrared spectroscopy

G/O ratio of volumetric flow rates between hydrogen gas and gas oil

HC hydrocarbon

HDA hydrodearomatization

HDM hydrodemetallization

HDN hydrodenitrogenation

HDS hydrodesulfurization

HGO heavy gas oil

HMS hexagonal mesoporous silica

HRTEM high resolution transmission electron microscopy

IBP initial boiling point

ICP-MS inductively coupled plasma mass spectroscopy

KIT-6 korean institute of technology – 6

LGO light gas oil

LHSV liquid hourly space velocity, s^{-1}

LPG liquefied petroleum gas

MAS mesoporous alumino silicate

MAS magic angle spinning

MCM-41 Mobil Composition of Matter no. 41

MCM-48 Mobil Composition of Matter no. 48

Me methyl

Mo molybdenum

MoO_3 molybdenum trioxide

MPa megapascal

N coordination number

Ni nickel

NiO nickel oxide

$NiMoO_4$ nickel molybdate

nm nanometer

NMR nuclear magnetic resonance

NOx nitrogen oxides

NTA nitrilo aceitic acid

OMS ordered mesoporous silica

P phosphorus

P123 poly (ethylene oxide)20-poly (propylene oxide)70-poly(ethylene oxide)20

($EO_{20}PO_{70}EO_{20}$)

PEO poly (ethylene oxide)

PPO poly (propylene oxode)

P_{H2} partial pressure of hydrogen gas, Pa

P_{H2S} partial pressure of hydrogen sulfide, Pa

Py pyridine

RDF radial distribution fucntion

S sulfur

SAXS small-angle X-ray scattering

SBA-15 santa Barbara amorpous-15

SBET surface area found from BET analysis, m^2/g

SCO synthetic crude oil

SEM scanning electron microscopy

SG specific gravity, dimensionless

SOx sulfur oxides

STEM scanning tunneling electronic microscopy

T_b average boiling point of HGO, K

TEOS tetraethyl orthosilicate

TEM transmission

TGA thermogravimetric analysis

Ti titanium

TiO_2 titanium oxide

TIPB triisopropyl benzene

TMB trimethyl benzene

TPAOH tetra propyl ammonium hydroxide

UV-DRS ultra violet diffuse reflection spectroscopy

VDU vacuum distillation unit

VGO vacuum gas oil

V_P total pore volume found for catalysts and catalyst supports, cm^3/g

XANES x-ray absorption near edge spectroscopy

XAS x-ray absorption spectroscopy

XRD x-ray diffraction

Zr zirconium

ZrO_2 zirconium oxide

CHAPTER 1
INTRODUCTION

1.1 Research Background

Strict environment regulations around the world coupled with rapidly decreasing sources of low sulfur crude oil has underlined the importance of upgrading the available heavy feed stock to meet current norms. Many European countries have already imposed a 50 wppm sulphur restriction on diesel. It is expected that, similar or more stringent restrictions on permissible sulfur in diesel will be brought in place in North America. Global demand for oil has increased over the last 40 years by 150% and by 20% in the past two decades to the current 80 million barrels per day. It is projected to grow 1.3 to 1.4% per annum in the next 30 years and reach 116 to 118 million barrels per day by 2030 (Kjarstad and Johnsson, 2009). Due to this, the supply of sweet crude oil is depleting at a very fast rate. The world's energy dependence therefore is growing on the heavy feed-stocks to meet demands. Canada's oil sands located in Athabasca region forms an important source of this heavy feed stock. The oil sands collectively contain vast bitumen resources, one of the largest known hydrocarbon deposits in the world. Established reserves are estimated to be 28.3 billion cubic metres (178 billion barrels) (Berkowitz and Speight, 1975). In 2004, oil sands production surpassed 160 000 cubic metres (one million barrels) per day; by 2015, production is expected to more than double to about 340 000 cubic metres (2.2 million barrels) per day (Ball and Wietschel, 2010). The heavy gas oil which is derived from the Athabasca bitumen forms the bottom cut for the Synthetic Crude Oil (Chrones and Germain, 1989). The SCO with very low quantities of impurities like sulphur and

nitrogen is comparable to other conventional lighter feed-stocks is further sent to the FCC to produce middle distillates. A poor quality HGO would mean that SCO also yields poor quality middle distillate (potentially jet and diesel fuel blending components). These potential motor fuel components have low cetane numbers and poor ignition qualities owing to their extra heavy nature (Cooper and Donnis, 1996). Heavy gas oil (HGO) quality as FCC feedstock is one of the most severe problems faced by the upgrading industry. There is, therefore a need to improve the quality of the heavy gas oil prior to sending it for further processing. The heavy gas oil derived from Athabasca bitumen suffers from the presence of high percentage of impure hetero atoms like Sulfur and Nitrogen (Ferdous et al., 2004; Smith et al., 2008).

Ever since hydroprocessing and hydrotreating specifically gained industrial prominence, Co and Ni promoted Mo catalyst supported on γ-Al_2O_3 has been used in industries for hydrodesulphurization and hydrodenitrogenation respectively. Commercially available catalysts show high HDS and HDN activity for feed stocks derived from sweet crude sources like those in the Middle East. However, gas oil obtained from the processing of tar sands contains very high levels of impurities (sulfur ~ 4 wt % and nitrogen ~ 0.32 wt %), which are difficult to remove using conventional NiMo/γ-Al2O3 and CoMo/γ-Al2O3 catalysts (Bej et al., 2002; Ferdous et al., 2004; Ferdous et al., 2006). Also, hydrotreating of such lower quality feed stock with the conventional catalysts needs more severe operating conditions (temperature, pressure), resulting in accelerated catalyst deactivation (Absi-Halabi et al., 1991; Ancheyta et al., 2002). Thus with the growing requirement to process heavy feed stocks, there is a mounting need to design new catalyst systems capable of producing sulphur and nitrogen free fuel from such heavy feed stocks.

Various authors have previously reported new combinations of the promoter, active metal and the support based on the studies of the reaction mechanism and metal-support interactions in a general hydrotreating reaction (Babich and Moulijn, 2003; Breysse et al., 2003; Prins et al., 1989; van Veen, J. A. Rob et al., 1987). The generally accepted active phase of Ni(Co)-Mo-S phase, which consists of sulfided Ni(Co) atoms positioned at the edges and corners of the MoS_2 slabs (Topsoe et al., 1981; Wivel et al., 1981). The number of Ni-Mo-S phases on the catalyst directly influences the catalytic activity. On the other hand, the morphology of the MoS_2 structure is also important for the HDS and HDN activity. The Ni-Mo-S Type II phase, which is located at the edges of the multi layers of MoS_2 structure is probably much more accessible to large molecules than the Ni-Mo-S Type I phase, which is located at the edges of the single layer of MoS_2 (Topsoe and Clausen, 1984). Therefore it is necessary to find final preparation methods to increase the density of Ni-Mo-S Type II phase on the catalyst. In addition to extensive studies on active sites and metal-support interaction, support modifications leading to enhanced textural properties of the catalysts and improved metal-support interaction has also been a subject of keen interest to researchers. Significant improvements in catalytic activity can be obtained by addition of chelating ligands to the impregnation solution during the preparation of the hydrotreating (HDT) catalyst. Complexing (chelating) agents such as ethylenediamine tetra-acetic acid (EDTA), nitrilo acetic acid (NTA) and citric acid (CA) contain chelating ligands with two or more donor atoms that can bind to a metal cation to form a complex cation or chelate during synthesis. By interacting with the cations in solution, the chelating agents can be used to tailor the final catalyst. For example, Sun et al. reported that the strong interaction between NTA or EDTA chelating ligands and Al^{3+} led to weaker interactions of molybdenum (Mo) and tungsten (W) with alumina, ultimately resulting in higher stacks of MoS_2 and WS_2 crystallites (Sun et al., 2003). These chelating agents (EDTA and NTA) have also been shown to interact strongly with

nickel (Ni) and cobalt (Co) cations (Al-Dalama and Stanislaus, 2006; Escobar et al., 2008; van Dillen et al.). These strong interactions led to delayed sulfidation of the Ni and Co species such that more active hydrodesulfurization catalysts were formed. In addition to generating more hydrogenating sites in the catalysts, the acidity of the γ-Al_2O_3 support also needs to be improved to promote mild hydrocracking of the heavy gas oil (Leyva et al., 2007; Yui and Sanford, 1989). The conventional CoMo and NiMo catalysts show excellent HDS activity but they are less active for hydrodenitrogenation (HDN) and hydrodealkylation (HDA) reactions. The isomerization and dealkylation activities of a catalyst can be imparted by the addition of acidic component to the catalysts. Various studies have been done in the past to improve the acidic Lewis and Bronsted sites on the γ-Al_2O_3 support. Amorphous silica-alumina (ASA), physical mixtures of zeolites and alumina have yielded mixed results. Zeolites mixed with alumina owing to strong acidic sites have shown promising results with light feed stocks. Among all the acidic components available, acidic zeolites are demonstrated to be the most effective. Yumoto et al. (Yumoto et al., 1997) found that the addition of less than 10 % zeolite (no type was mentioned in the literature) in a CoMo supported on Al_2O_3 catalyst can increase HDS activity by 40% compared with conventional CoMo/Al_2O_3 when evaluating with straight run gas oil (sulfur content 1.38 wt%). However rapid deactivation of the catalyst is observed while hydrotreating heavy gas oil. The reason for this has been attributed to the microporous nature of zeolites (pore size < 1 nm) (Larocca et al., 1990; Rajagopalan et al., 1986). Small pores present in zeolites prevent the diffusion of large bulky molecules present in HGO onto the active sites, resulting in pore blockage and a decrease in the catalyst life. In this context, the modification of γ- Al_2O_3 with mesoporous alumino-silicates with higher surface areas and larger pore diameters (between 3 nm to 10 nm) is particularly useful for overcoming the mass transfer limitations posed by the narrow pore channels of microporous zeolites (Bej et al., 2004; Sambi and Mann, 1989). Incorporation

of the mesoporous alumino-silicate materials into γ-Al_2O_3 support also enhances the acidity of the resulting support. The increase in acidity is a result of the creation of strong Bronsted acid sites in the modified support.

A novel preparation method of nickel molybdenum catalyst incorporating the use of citric acid as a chelating ligand supported on γ-Al_2O_3 modified with mesoporous alumino silicates synthesized from zeolite nano-seeds is proposed in this work. The hydrotreating activities of the synthesized catalysts are evaluated using heavy gas oil derived from Athabasca bitumen as a feedstock. The hydrodesulphurization (HDS) and hydrodenitrogenation (HDN) activity of the above mentioned series of catalysts are subsequently compared with the hydrotreating (HDT) performance of a commercial catalyst.

1.2 Knowledge Gaps

After a thorough review of research articles published on the hydrotreating activity, the active phase, the role of promoters, the effect of chelating ligands and the role of citric acid in particular and the modification of γ-Al_2O_3 with mesoporous alumino-silicates, it was found that the following topics have not been studied or have not been explored extensively :

- The modification of γ-Al_2O_3 support with mesoporous alumino-silicate materials synthesized from ZSM-5 nano-seeds has not been reported in literature previously. There are only few studies on mesoporous alumino-silicate (MAS) materials from zeolite nano-seeds used as supports in hydrotreating reactions. However, studies of this kind have only been restricted to hydrotreating of simple model compounds. Usage of a complex real feedstock like heavy gas oil for hydrotreating reactions involving MAS as support materials is absent.

- The role of citric acid in improving the activity of hydrotreating catalysts is very unclear. Various works have attributed the resulting improvement in hydrotreating activity to the better edge dispersion of Ni (Co) on the MoS_2 particles whereas other studies have pointed to the better dispersion of MoO_x phase due to the formation of molybdenum-citrate complex. Nonetheless, all activity studies have been carried out with model compounds with no mention of real feedstock. The detailed role of citric acid as a chelating ligand still remains ambiguous in literature.
- Furthermore, studies related to the various stages of sulfidation in catalysts prepared with citric acid as chelating ligand is very rare. Although, there have been some reports on the effect of other chelating ligands like EDTA, NTA etc on the sulfidation mechanism of NiMo catalyst, the effects of addition of citric acid on the sulfidation of NiMo catalysts is not found in literature.

1.3 Hypothesis

Based on the comprehensive literature review of articles pertaining to hydrotreatment and above knowledge gaps the following points can be hypothesized for this work.

- The modification of γ-Al_2O_3 support with mesoporous alumino-silicates synthesized from zeolite nano-seeds will improve the acidity of the support material due to the creation of strong Bronsted acid sites. The physico-chemical properties like surface area, pore diameter and acidity of the MAS materials can be adjusted by the hydrothermal treatment of the zeolite precursor solutions.
- The use of citric acid as a chelating ligand will help form a nickel-citrate complex. The formation of this nickel citrate complex will delay the sulfidation of nickel. The retarded

sulfidation of Ni will allow the formation of more active Ni-Mo-S Type II sites with higher intrinsic hydrotreating activity.

- The sulfidation of the NiMo catalysts can be improved by controlling the metal/citrate molar ratios. A higher concentration of nickel-citrate complex would favour the edge promotion of MoS_2 leading to more active Type II hydrotreating sites.

1.4 Research Objectives

The primary objective of this work is to synthesize, characterize and evaluate the hydrodesulphurization and hydrodenitrogenation activities of sulfided NiMo catalysts supported on γ-Al_2O_3 modified with mesoporous alumino-silicates using heavy gas oil derived from Athabasca bitumen as the feedstock. The primary objective of the work was further divided into three different phases or sub-objectives:

Phase I: Synthesis and modification of γ-Al_2O_3 support with mesoporous alumino-silicates prepared from ZSM-5 nano-seeds

Mesoporous alumino-silicate materials were prepared from ZSM-5 nano-seeds using tetra propyl ammonium hydroxide (TPAOH) as a structure directing agent (SDA). The nano-particles thus obtained were organized into hexagonal arrays by using a surfactant based approach. Pluronic 123 (P123) a neutral polymer was used as the surfactant in the assembly of the ZSM-5 nano-particles. The ZSM-5 nano particles were subjected to various lengths of hydrothermal treatment to tune the physic-chemical properties of the final material. The synthesized materials were then extensively characterized and evaluated as support for NiMo catalyst using hydrodesulfurization of dibenzothiophene (DBT) in a batch reactor. After the determination of the optimum hydrothermal treatment time, hydrotreatment reactions were carried out using a mixture of γ-

Al_2O_3 and MAS material as support for NiMo catalysts. Light Gas Oil (LGO) was used the feedstock for the above screening reactions. The reactions performed gave the most suitable γ-Al_2O_3 and MAS support mixture composition. This support composition was used for all subsequent hydrotreatment reactions.

Phase II: Synthesize and characterize catalysts with varying Citric acid/ Nickel molar ratios and to study the effects of citric acid on the sulfided phase hydrotreating activity of NiMo catalysts

Three different catalysts were prepared with varying citric acid (CA) to nickel (Ni) molar ratios of 0, 1 and 2. The Mo and Ni loadings of the catalysts were kept constant at 15 wt % and 5 wt % respectively. The chemical nature of the synthesized catalysts was characterized using FT-IR spectroscopy, Raman spectroscopy and Extended X-ray absorption spectroscopy (EXAFS) of the Mo K edge. Further, characterization studies were performed on the catalysts after various levels of sulfidation. The catalysts were sulfided and characterized after sulfidation at 150 ^oC, 250 ^oC and 350 ^oC using X-ray absorption spectroscopy techniques. Finally, the hydrotreating performance of the synthesized catalysts was checked in a trickle bed reactor using heavy gas oil (HGO) as the feedstock. Based on the sulfur and nitrogen conversions, the optimum CA/Ni molar ratio was chosen for further studies.

Phase III: Optimization of metal loading for the NiMo/Al_2O_3- MAS catalysts

After the determination of the optimum CA/Ni molar ratios, the metal content of the catalysts were varied to further improve the hydrotreating performance of the catalysts. Four different catalysts were synthesized with Mo loadings of 10 wt %, 13 wt %, 15 wt % and 17 wt %. For this series of catalysts, the Ni loading was kept constant at 5 wt %. HDS and HDN activities were determined in a trickle bed reactor with heavy gas oil as the feedstock. Subsequently the

catalyst with optimal Mo loading was considered for further tests. Four different catalysts were then prepared with the optimal Mo loading but varying Ni loadings. The synthesized catalysts had Ni loadings of 3 wt %, 5 wt % 7wt % and 9 wt %. Again, the most favorable Ni loading was determined based on the S and N conversions of HGO. In all, 8 different catalysts were synthesized by changing the Mo and Ni contents in the catalysts. All the catalysts were well characterized for evaluating the physical and chemical properties of the same.

Phase IV: Long term activity study of the optimum catalyst

The HDS and HDN activity of the best performing catalyst obtained from the previous phase of research was checked after subjecting the catalyst to 45 days of time on stream (TOS). The catalysts were checked for any decrease in performance due to deactivation. Further, the effects of H_2/Oil ratio, LHSV, H_2 partial pressure and sulfidation temperature were also studied in this phase of work. The catalytic activity of the best catalyst was then compared to the hydrotreating performance of a commercial catalyst.

CHAPTER 2

LITERATURE REVIEW

This chapter deals with a comprehensive analysis of research articles dealing with hydroprocessing and hydrotreating in general. The increasing need to produce cleaner fuels from dirtier feedstock fuelled by the growing consumption of oil has been investigated in the first section of this chapter. Subsequent sections deals with hydrotreating process, common hydrotreating catalysts and its components and the hydrodesulphurization and hydrodenitrogenation process in general. Finally, a review of new methods available to increase the intrinsic activity of hydrotreating catalysts is given. The modification of Al_2O_3 support by the incorporation of mesoporous alumino-silicate materials synthesized from ZSM-5 nano-particles combined with the use of citric acid as a chelating ligand forms a part of this chapter.

2.1 Global Demand for Oil

Crude oil is one of the most important sources of energy. During the period from 1980 to 2006, the proportion of petroleum consumption in total energy consumption has been the largest (36.36% in 2006). Oil has been a key element of the growing economy. Since 1845, oil production has increased from virtually nothing to approximately 86 million barrels per day (Mb/d) today (Kjarstad and Johnsson, 2009), which has permitted living standards to increase around the world. In 2004, oil production growth stopped while energy hungry and growing countries like China and India continued increasing their demand. Since 2004 world oil production has remained within 5% of its peak despite historically high prices (Fig. 2.1).

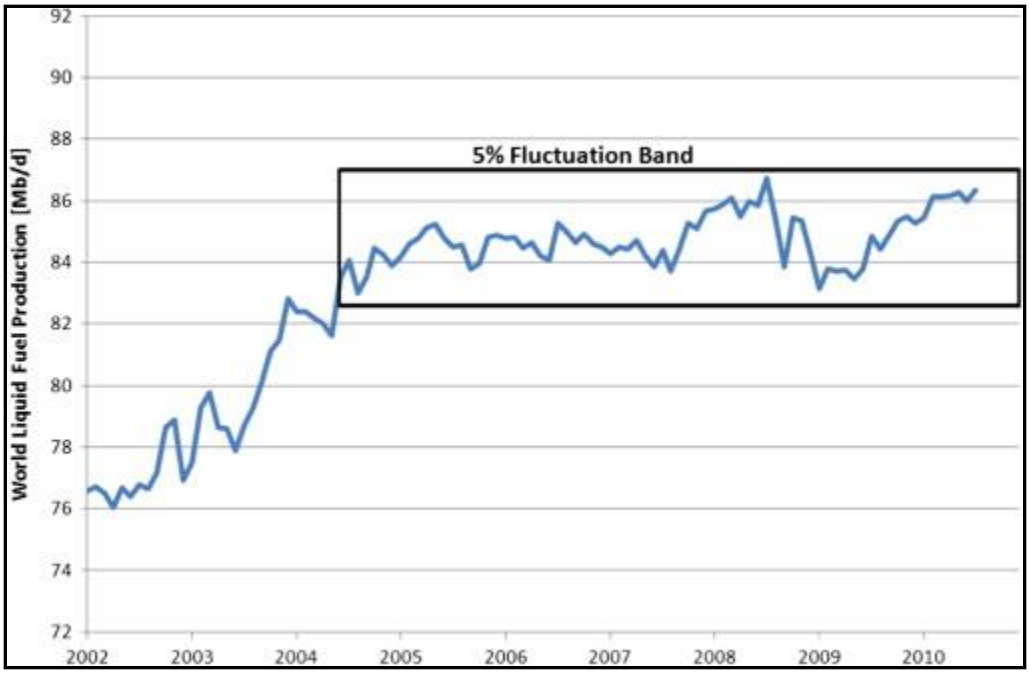

Figure 2.1: World production of oil (Fantazzini et al., 2011)

The combination of increasingly difficult-to-extract conventional oil combined with depleting supergiant and giant oil fields, some of which have been producing for seven decades, has led the International Energy Agency (IEA) to declare in late 2010 that the peak of conventional oil production occurred in 2006 (Bentley, 2002). Conventional crude oil makes up the largest share of all liquids commonly counted as "oil" and refers to reservoirs that primarily allow oil to be recovered as a free-flowing dark to light-colored liquid (Speight, 2003). Given the likely peak in conventional oil production, it is important to examine unconventional oil resources and possible production. In this context, the non-conventional oil production, such as Canadian oil sands production, may play an important role in bridging the coming gap between the world's soaring oil demand and global oil supply.

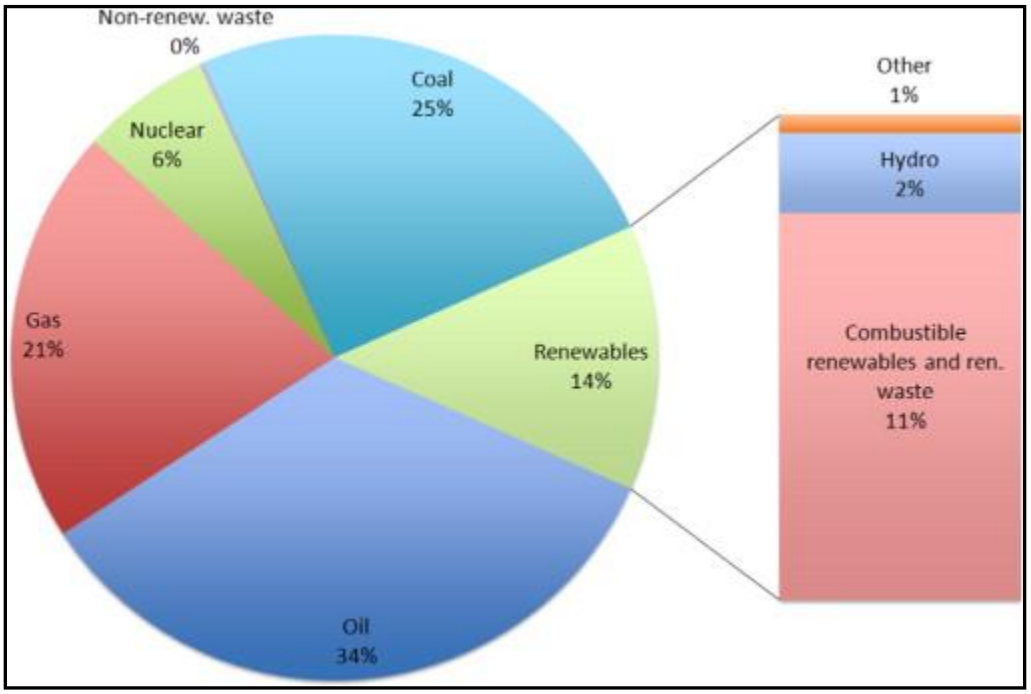

Figure 2.2: Fuel share of the world (Fantazzini et al., 2011)

Canada's oil sands are a significant resource, and the initial volume of crude bitumen in place is estimated to be approximately 1.7 trillion barrels (279 billion m^3), with 11% or 174 billion barrels (27.7 billion m^3) recoverable under current economic conditions (Berkowitz and Speight, 1975; Soderbergh et al., 2007). Canada's resources of crude bitumen occur entirely within the province of Alberta in sand and carbonate formations in the northeastern part of the province. These oil sands areas consist of three regions defined as the Athabasca (43 km^2), Cold Lake (7.3 km^2) and Peace River Oil Sands Areas (9.8 km^2). The oil sands themselves typically consist of friable rock of which 75–80% consists of sand, silt and clay, impregnated with bitumen (Soderbergh et al., 2007). Heavy minerals including rutile, zircon, tourmaline and pyrite are also present. The deposits are however far from homogenous being subject to important, and not

always recognized, variations from area to area. The bitumen itself is a thick black tar-like substance, with high sulfur and metal content. The density lies in the range of 970–1015 kg/m^3 (8–14 ^oAPI) and viscosity is greater than 50,000 centipoises. Since bitumen is deficient in hydrogen it must be upgraded into higher quality synthetic crude oil (SCO) to make it an acceptable feedstock for conventional refineries (Berkowitz and Speight, 1975). This is accomplished through the addition of hydrogen or the rejection of carbon, or both. Upgrading bitumen utilizes natural gas as a source of heat and steam for processing, and also as a source of hydrogen for hydroprocessing. Depending on the upgrading employed and depending on the degree of quality improvement of the final product, varying amounts of hydrogen are required.

2.2 Bitumen and Heavy Gas Oil

Bitumen is a black, oily, viscous material that is a naturally-occurring organic byproduct of decomposed organic materials. Krishnan et al define bitumen as mixtures of natural or pyrogenous origin or combination of both, frequently accompanied by their nonmetallic derivatives which can be gaseous, liquid, semisolid, or solid, and which are completely soluble in carbon disulphide (Krishnan and Rajagopal, 2003). Chemically, it is a complex mixture of chemical species including aromatics, substituted aromatics, organo sulfur and nitrogen compounds. Table 2.1 gives a comparison of the physical and chemical properties between conventional crude oil, Athabsca bitumen and heavy gas oil derived from Athabasca bitumen(Gray, 1994; Speight, 2007).

Table 2.1: Comparison of the physical and chemical properties between conventional crude oil, Athabsca bitumen (Gray, 1994)and heavy gas oil derived from Athabasca bitumen (Gray, 1994; Speight, 2007)

Material	Conventional Crude Oil	Athabasca Bitumen	Heavy Gas Oil
API Gravity	25-37	< 10	20- 25
Viscousity, mPa.s	10	> 105	102 - 105
Carbon (wt%)	83-87	83.1	84.1
Hydrogen (wt%)	10.1 - 14	10.3	10.1
Sulfur (wt%)	0.05 - 6	5.14	4.3
Nitrogen (wt%)	0.1-0.2	0.56	0.4
Metals	< 0.1	> 0.1	< < 0.1

Heavy gas oil on the other hand is a distillate product from bitumen upgradation. The heavy gas oil can be broadly defined as the distillate cut with a boiling point range of 343 ^{o}C – 524 ^{o}C (Speight, 1999; Meyers; Speight, 2007). The definition of heavy gas oil varies depending on the source of the crude oil. Heavy gas oils derived from sweet crude oil have different boiling point ranges. The heavy gas oil derived from Athabasca bitumen is generally a mixture of distillate product from the vacuum distillation unit (VDU) and the delayed coker unit (DCU). After primary upgradation of the bitumen, the distillate cuts obtained are HGO, light gas oil (LGO) and other heavy and lighter fractions. Coke also forms a part of the bitumen upgradation product stream. The heavy gas oil obtained from bitumen upgradation has very high levels of sulfur and nitrogen contents. The aromatic content is also substantially higher than conventional crude oil

(Cooper and Donnis, 1996; Stanislaus and Cooper, 1994). The HGO after blending is further routed for secondary upgradation through various hydrotreaters and mild hydrocrackers (Yui and Sanford, 1989). The hydrotreated HGO then forms a feedstock for the catalyst cracker units.

2.3 Hydroprocessing

The heavy or extra heavy oil conversion processes are either based on carbon rejection (thermal process), deasphalting (solvent), or hydrogen addition (hydroprocessing). This latter is relatively costly and requires strict operating conditions, large size units, and high hydrogen and catalyst consumptions(Leyva et al., 2007; Rana et al., 2007). The basis of process selection for hydroconversion is dependent on the quality of the feedstock, such as metal, carbon, and sulfur content and API gravity. The hydroprocessing application range has been reported to cover feeds with heavier amount of contaminants with lower API gravity, which is mainly due to the use of catalyst with improved stability as well as the selection of proper reactor and operating conditions to work under moderate conversion (Leyva et al., 2007). The hydroprocessing of gas oils can be broadly classified into three categories depending on the process and the purpose.

2.3.1 Hydrodemetallization

Hydrodemetallization (HDM) is defined as the removal of metal contents particularly Ni and V from the crude oil through the catalytic addition of hydrogen. Nickel and vandaium exist in the petroleum fraction as chelating complexes, either in porphyrinic or nonporphyrinic structure, as illustrated in Figure 2.3.(Leyva et al., 2007). The removal of these metallic impurities assumes importance as the presence of the metallic elements leads to rapid deactivation of the catalysts in downstream processes. General HDM catalysts include NiMo supported on wide pored clay materials with substantially higher pore diameters (Hauser et al., 2008).

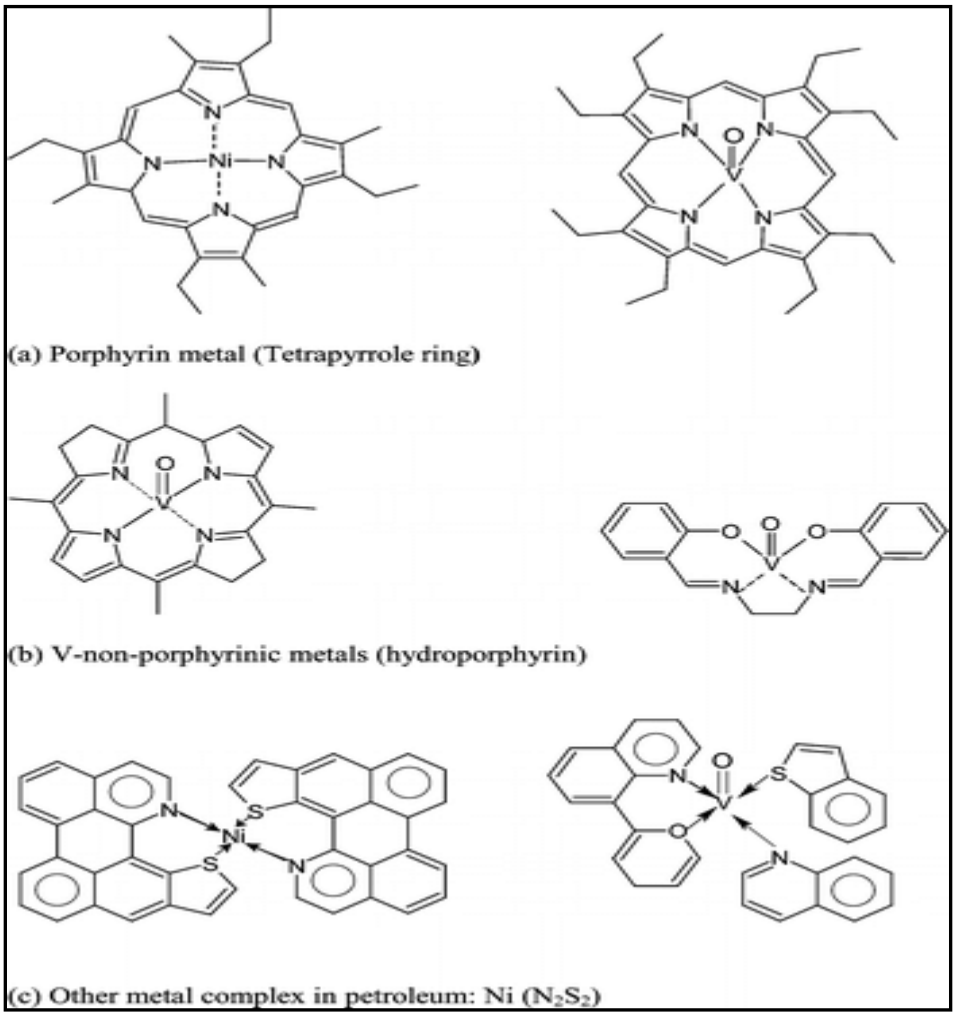

Figure 2.3: Hypothetical porphyrinic, nonporphyrinic, and other types of organo-metallic compounds in heavy oil (Leyva et al., 2007)

2.3.2 Hydrodcracking

It is the catalytic addition of hydrogen along with simultaneous cracking of the feedstock to yield smaller products with more value. In case of heavy feedstocks or during bitumen upgradation, hydrocracking is done to mainly to break the large carbon chains into smaller molecules, which are then fed into the light gas oil (LGO) and heavy gas oil (HGO) hydrotreaters. The top end product of the hydrocracker unit is also sent to the naptha hydrotreaters for further processing. This process is a hydrogen intensive process, wherein the catalytic hydrogenation and cracking is done at very high pressures. Normally a dual functional catalyst with high hydrogenation and acidic functionality is chosen for this process. NiMo supported on amorphous silica alumina is the most common catalyst for hydrocracking (John W., 1993).

2.3.3 Hydrotreating

The catalytic removal of impurities present in the feedstock with the addition of hydrogen is referred to as hydrotreatment. The feedstock for hydrotreatment reactions is very wide depending on the concentration of S and N required in the product. Mild hydrocracking of the feed also occurs along with the cleavage or the C-S or C-N bond (Botchwey et al., 2003). The general catalyst that is used in industries is NiMo supported on γ-Al_2O_3. With stringent environmental regulations being imposed around the world, hydrotreating has been gaining importance over the years. In addition, with depleting reserves of sweeter crude there is an increased dependency on heavier and dirtier feedstocks. Refiners around the world have to deal with feedstocks with high contents of sulfur and nitrogen. Hydrotreatment has significant importance in improving the quality of heavy gas oil derived from the Athabasca bitumen (Speight and Ancheyta, 2007) . This HGO has very high contents of sulfur and nitrogen at 4 wt % and 0.4 wt % respectively. For

refiners to be able to process this feedstock with existing technologies, the removal of S and N to acceptable limits is a must.

2.4 Need for Hydroprocessing

Today, hydroprocessing forms a significant part of refineries around the world. Hydroprocessing catalysts constitutes about one third of the catalysts sold around the world. The need for hydroprocessing is driven by several factors:

2.4.1 Strict Environmental Regulations

The stringent regulations on the permissible amounts of SO_x and NO_x emissions have led many countries to restrict the maximum sulfur in fuels to less than 15 ppm or Ultra Low Sulfur Diesel (ULSD). Table 2.2 shows the current US EPA regulations for gasoline, and diesel fuels , and including non-road diesel fuels , respectively, along with earlier fuel specification data in the US for comparison (Chunshan, 2003a; Swain, 1991) . With the new US EPA Tier II regulations to reduce the gasoline sulfur from current maximum of 350 to 30 ppm (refinery average, with 80 ppm as per-gallon (1 US gallon = 3.7854 ltrs) cap by 2006, and to cut the highway diesel fuel sulfur from current 500 ppm down to 15 ppm (per-gallon average) by June 2006, refineries are facing major challenges to meet the fuel sulfur specification along with the required reduction of aromatics contents.

Table 2.2: The current US EPA regulations for gasoline, and diesel fuels, and including non-road diesel fuels

Category	Year			
	1989	1993	2006	2010
Highway Diesel (ppmw)	5000	500	15	< 15
Non-road Diesel (ppmw)	20000	5000	500	< 15
Jet Fuel (ppmw)	3000	3000	3000	< 3000

Similarly Canada and the European Union have also imposed stricter regulations of maximum S levels in diesel fuels . The challenges faced by refiners for producing ULSD is mainly due to the presence of refractory sulfur compounds like 4, 6 DMDBT which are extremely difficult to remove (Gates and Topsoe, 1997; Kabe et al., 1992; Ma et al., 1994; Ma et al., 1995). By improving current methods of hydrotreatment, refractory compounds can be effectively treated to meet environmental norms.

2.4.2 Increasing middle distillate fraction

The profitability of hydroprocessing for heavy crude oil upgrading is a function of product value (the price differential between the feed and the product) (Huang et al., 2010). The high prices of middle distillates and naphtha have a strong contribution toward the crude oil conversion, as well as the production of upgraded crude oil with low metal and asphaltene content, which can be one alternative route to improve the entire crude oil feedstock to refineries to produce better feeds for fluidized catalytic cracking (FCC), hydrocracking, and other downstream processes with the

consequent enhancement in catalyst performance and life cycle. With a tremendous increase in demand for middle distillates, hydrocracking and mild hydrocracking methods along with hydrotreatment provides refiners around the world to add value to their products.

2.4.3 Improving Product Quality

The presence of aromatics and unsaturates in the product is detrimental to the cetane number and hence the quality of the fuel. Cetane number or CN is a measurement of the combustion quality of diesel fuel during compression ignition. It is a significant expression of diesel fuel quality among a number of other measurements that determine overall diesel fuel quality. Processing of heavy feedstocks poses a significant challenge in the sense that, the aromatic content of the feed is very high. Hence, saturating the aromatics is required to achieve the acceptable cetane number for the fuel. Hydrodearomatization and hydrocracking reactions are two common processes to achieve the same.

2.5 Hydrotreatment

Hydrotreatment refers to the hydrogenative removal of hetero-atoms like sulfur. Nitrogen, metals and oxygen followed by hydrogenation. The main objectives of hydrotreating are (a) to remove impurities such as S and N and metal containing compounds, from a feedstock, (b) to increase the hydrogen content of the feedstock, and (c) to lower molecular weight without a substantial loss in liquid product yield. Hydrotreatment is generally done at various stages of refining and on different kinds of feedstock. Lower molecular weight feedstocks such as naptha, gasoline, middle distillates have substantially lower levels of sulfur and nitrogen as compared to higher molecular feedstocks like vacuum distillates and atmospheric residues. In addition to high levels of S and N in heavy feedstocks, the metal content particularly Ni and V is also higher. In general,

the concentration of these impurities increases with increasing boiling point. Thus, the hydrotreating process of choice depends mostly on the molecular weight of the feedstock being processed. A NiMo catalyst supported on γ-Al_2O_3 is the most favoured catalyst for hydrotreating (Bej et al., 2001).

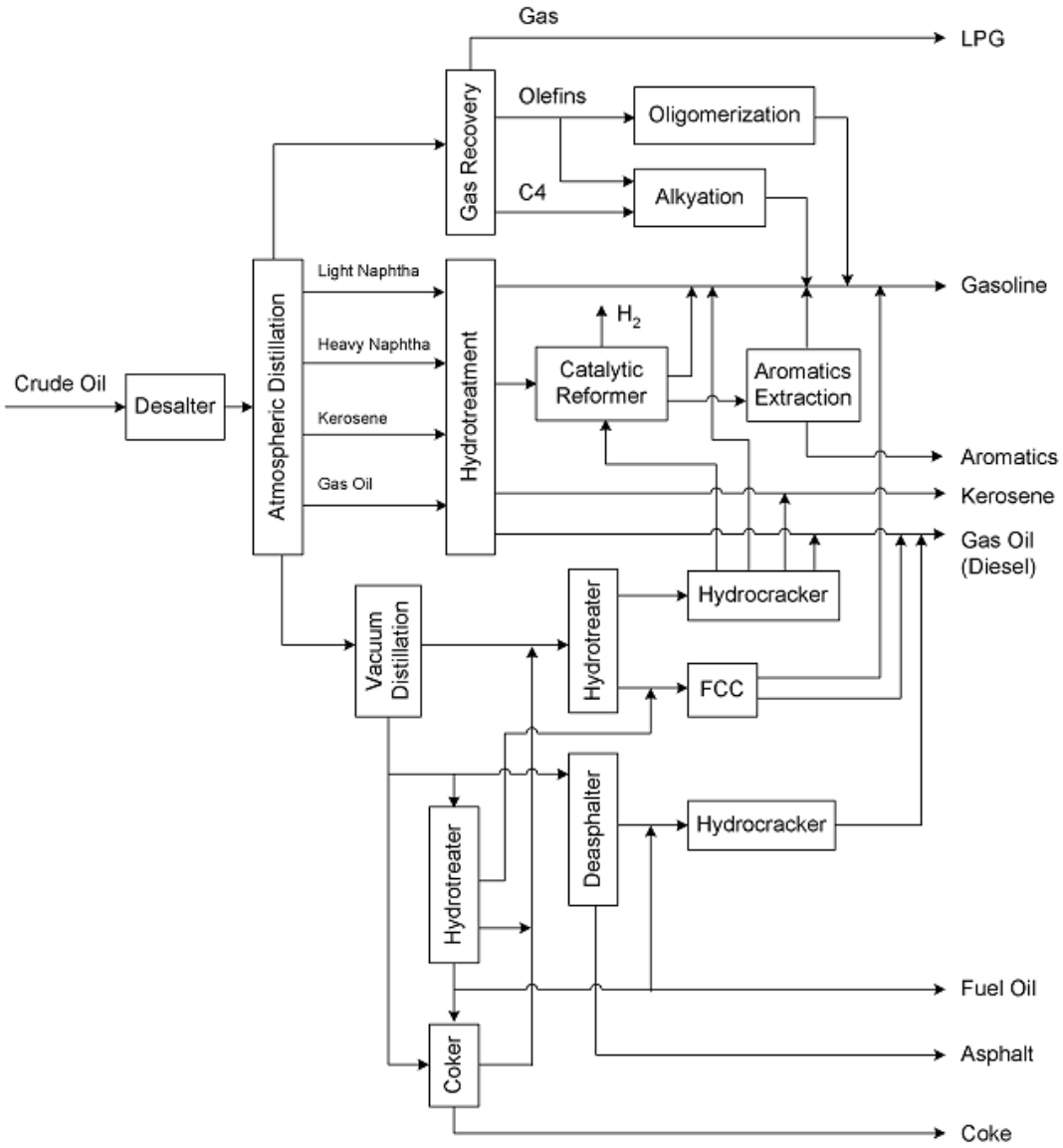

Figure 2.4: Application of hydrotreating in a modern refinery (Mochida and Choi, 2006)

2.5.1 Hydrotreating Process Description

Although hydrotreating is done for a variety of purposes and on a variety of feedstocks, the essential process for hydrotreating remains almost the same. The central unit of a hydrotreating process is generally a high pressure fixed bed reactor with multiple beds for catalysts. The surround units are mainly heat exchangers, high pressure separators and fractionating columns to separate the desulfurized and denitrogentaed products. Figure 2.5 gives a detailed description of a generic hydrotreating process (Gruia, 2006).

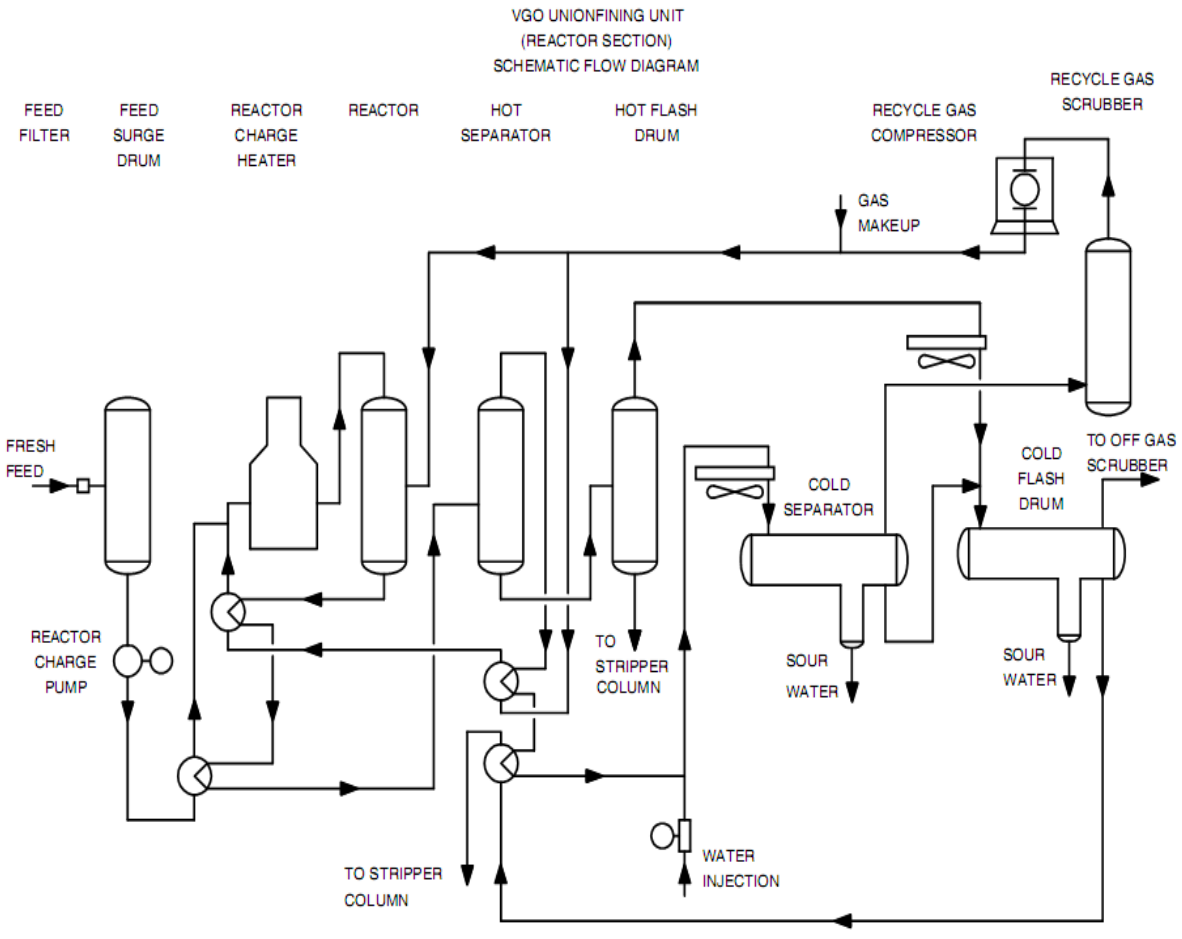

Figure 2.5 Generic schematic of a hydrotreating process (Gruia, 2006)

Based on the above process, a brief description of some of the units and functionalities is given below:

1. **Reactor Charge Heater** In most units, the combined feed and recycle gas is heated together to desired reactor inlet temperature in a combined charge heater. In units processing heavy feed, especially the atmospheric residue units, the liquid feed is preheated separately with reactor effluent exchange and only the recycle gas is heated in the heater upstream of the reactor.
2. **Reactor –** Once the feed and recycle gas have been heated to the desired temperature, the reactants enter the top of the reactor. As the reactants flow downward through the catalyst bed, various exothermic reactions occur and the temperature increases. Multiple catalyst beds (and possibly additional reactor may be required depending on the heat of reaction, unit capacity and/or type of hydrotreating unit. Specific reactor designs will depend upon several variables.
3. **Vapour Liquid Separation** The exact method of separating vapour and liquid will vary depending on the optimum heat integration scheme. Upto four separate vessels may be used to disengage and individually remove vapour, water and hydrocarbon liquid. A hot separator is sometimes installed after the feed/effluent exchangers to collect the heavier hydrocarbon material from the reactor effluent and send it to fractionation via the hot flash drum. The overhead vapour from the hot separator continues through an air cooler into a cold separator.

2.5.2 Hydrotreating Reactions

Hydrotreating reactions are characterized by the cleavage of C-X bond (where X is S, N, O or metal) and/or saturation of the molecule. Chemically, the boundary between hydrotreating, mild

hydrocracking and hydrocracking reactions is very narrow. Hydrocracking reactions also takes place in hydrotreaters generally at high temperatures at the near ends of the reactor (Gruia, 2006). Thermodynamically these reactions are exothermic in nature, so controlling this release of heat is a major factor while designing reactors. On the basis of enthalpies of formation, the reactions taking place can be categorized into 3 different classes: For HDS, HDN, HDO, HDM, and aromatics saturation, ΔH_R are about -2.5 to -3.0 kJ per standard cubic meter of consumed H_2. For reactions that break carbon-to-carbon bonds, ΔH_R are about -1.3 to -1.7 kJ per m^3 of consumed H_2. And for saturation of olefins, ΔH_R are about -5.5 kJ per m^3 of consumed H_2. Isomerization reactions produce a small amount of heat, but this can be neglected. The ΔH_R values are summarized in Table 2.3 (Robinson and Dolbear, 2006). The following reactions form a part of hydrotreating reactions

1. Hydrodesulfurization – Removal of S atom
2. Hydrodenitrogenation – Removal of N atom
3. Hydrodeoxygenation – Removal of O atom
4. Hydrodemetallation – Removal of metallic impurities
5. Aromatic Saturation – Hydrogenation of aromatic rings

Of all these classes of reactions, O-compounds are generally not considered as major environmental hazards in petroleum products. Nevertheless, some O-impurity compounds such as phenols and naphthenic acids lead to corrosion problems in the reactor and storage vessels. Similrly, hydrodemetallation is generally carried out at very early stage of crude processing. Further, a guard bed is also provided in the reactors to prevent metal deactivation of the more sensitive catalysts. Heavy gas oil derived from Athabasca bitumen is hydrotreated primarily to lower the S and N level in the product.

Table 2.3: ΔH_R values for some common hydroprocessing reactions (Robinson and Dolbear, 2006)

Reaction Type	Illustration	Heat of Reaction*
C-X Bond Breaking		
Hydrodesulfurization (HDS)	R-S-R' + $3H_2$ → RH + R'H + H_2S	-2.5 to 3
Hydrodenitrogenation (HDN)	R≡N-R' + $3H_2$ → RH + R'H + NH_3	-2.5 to 3
Hydrodeoxygenation (HDO)	R-O-R' + $3H_2$ → RH + R'H + H_2O	-2.5 to 3
Hydrodemetallization (HDM)	R-M + $1/2H_2$ + A → R-H + M-A	-3
Aromatic Saturation	$C_{10}H_8 + 2H_2 \rightarrow C_{10}H_{12}$	-3
Olefin Saturation	R=R' + H_2 → HR-R'H	-5.5
C-C Bond Breaking		
Dealkylation of aromatics	θ-CH_2-R + H_2 → θ-CH_3 + RH	-1.3 to -1.7
Ring Opening of Napthenes	Cyclo-$C_6H_{12} \rightarrow C_6H_{14}$	-1.3 to -1.7
Hydrocracking of paraffins	R-R' + H_2 → RH + R'H	-1.3 to -1.7
Other Reactions		
Coke Formation	2θH → θ-θ + $2H_2$	+3

* Kilojoules per standard m^3 of H_2 consumed. For exothermic reactions, ΔH_R is negative.

† R = alkyl; θ = aromatic; M = Fe, Ni or V; A = metals-adsorbing material

2.6 Hydrodesulphurization (HDS)

Removal of sulfur via the conversion of organic sulfur compounds into H_2S is known as desulfurization or hydrodesulfurization, since it occurs along with addition of hydrogen. Typical quantities of sulfur in feedstocks can range from 40,000 ppm in heavy gas oils to 300 ppm in low sulfur diesel. Sulfur is found throughout the boiling range of petroleum fraction in the form of many hundreds of different organic sulfur compounds which, in the naphtha to atmospheric residue range, can all be classified as belonging to one of the following six sulfur types: mercaptans, sulfides, di-sulfides, thiophenes, benzo-thiophenes, and di-benzo-thiophenes. The mercaptans, sulfides, di-sulfides and thiophenes are relatively easier to desulfurize. The HDS reaction follows the direct desulfurization route for these reactions. In comparison, alkyl substituted benzothiophenes forms a class of refractory sulfur compounds which are exceedingly difficult to remove (Kabe et al., 1997). The discussion of the mechanism is done in the later sections.

Mercaptans

$$R\text{-}SH + H_2 \rightarrow R\text{-}H + H_2S$$

Sulfides

$$R1\text{-}S\text{-}R2 + 2H_2 \rightarrow R1\text{-}H + R2\text{-}H + H_2S$$

Di-sulfides

$$R1\text{-}S\text{-}S\text{-}R2 + 3H_2 \rightarrow R1\text{-}H + R2\text{-}H + 2H_2S$$

Thiophenes

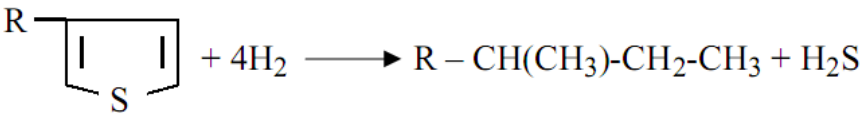

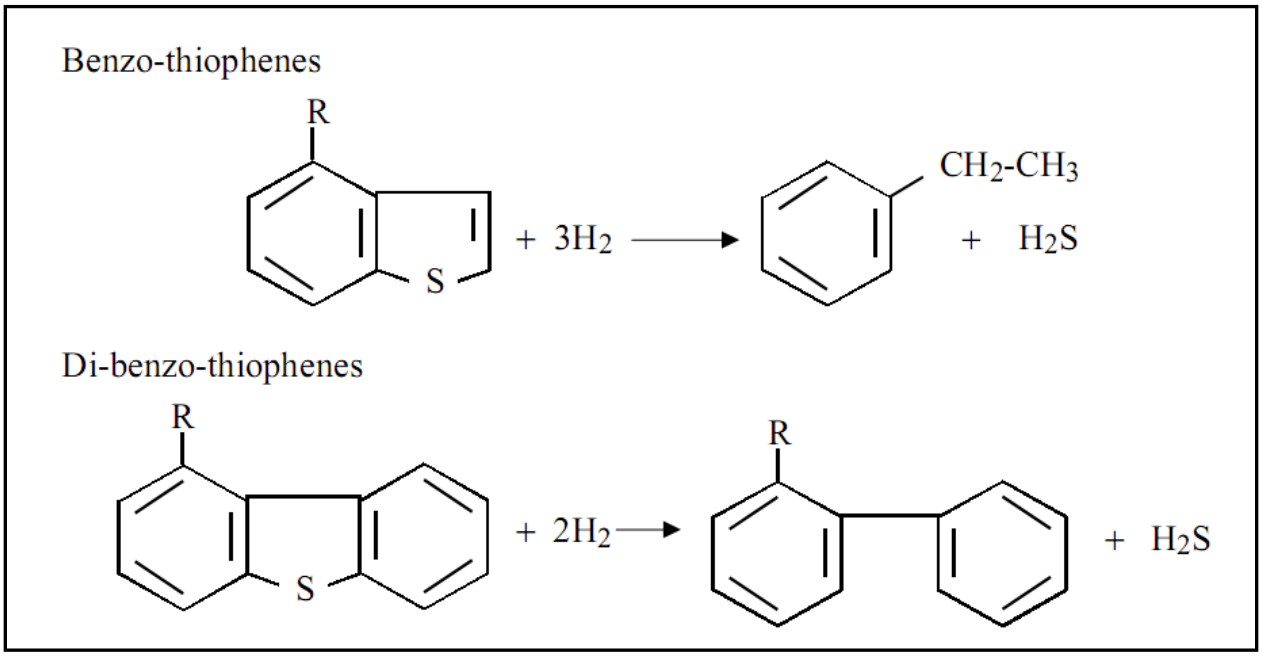

Figure 2.6: Examples of hydrodesulfurization reactions (Gruia, 2006)

2.6.1 Reactivity of organo-sulfur compounds

The ease of removal of sulfur from a petroleum stream depends greatly on the structure of the sulfur compound being treated. The rates of sulfur removal can vary by several orders of magnitude. Generally, acyclic sulfur compounds such as thiols and disulfides are highly reactive and can be removed under very mild conditions. Saturated cyclic sulfur compounds and aromatic systems in which sulfur is present in six-membered rings are also highly reactive (Mochida and Choi, 2006; Whitehurst et al., 1998). However, compounds in which the sulfur atom is incorporated into a five-membered aromatic ring structure (such as thiophene), are much less reactive and the reactivity decreases as the ring structure becomes increasingly condensed (e.g. one ring > two rings > three rings) (Whitehurst et al., 1998). For highly condensed ring structures (four or more rings), the reactivity trend reverses and reactivity tends to increase as the

ring structure increases in size. The reason for such behaviour is that there are several different chemical pathways through which sulfur can be removed from a molecule and the preferred pathway changes for different sulfur compound structures. Figure 2.7 gives a representation of the reactivity of different sulfur based compounds.

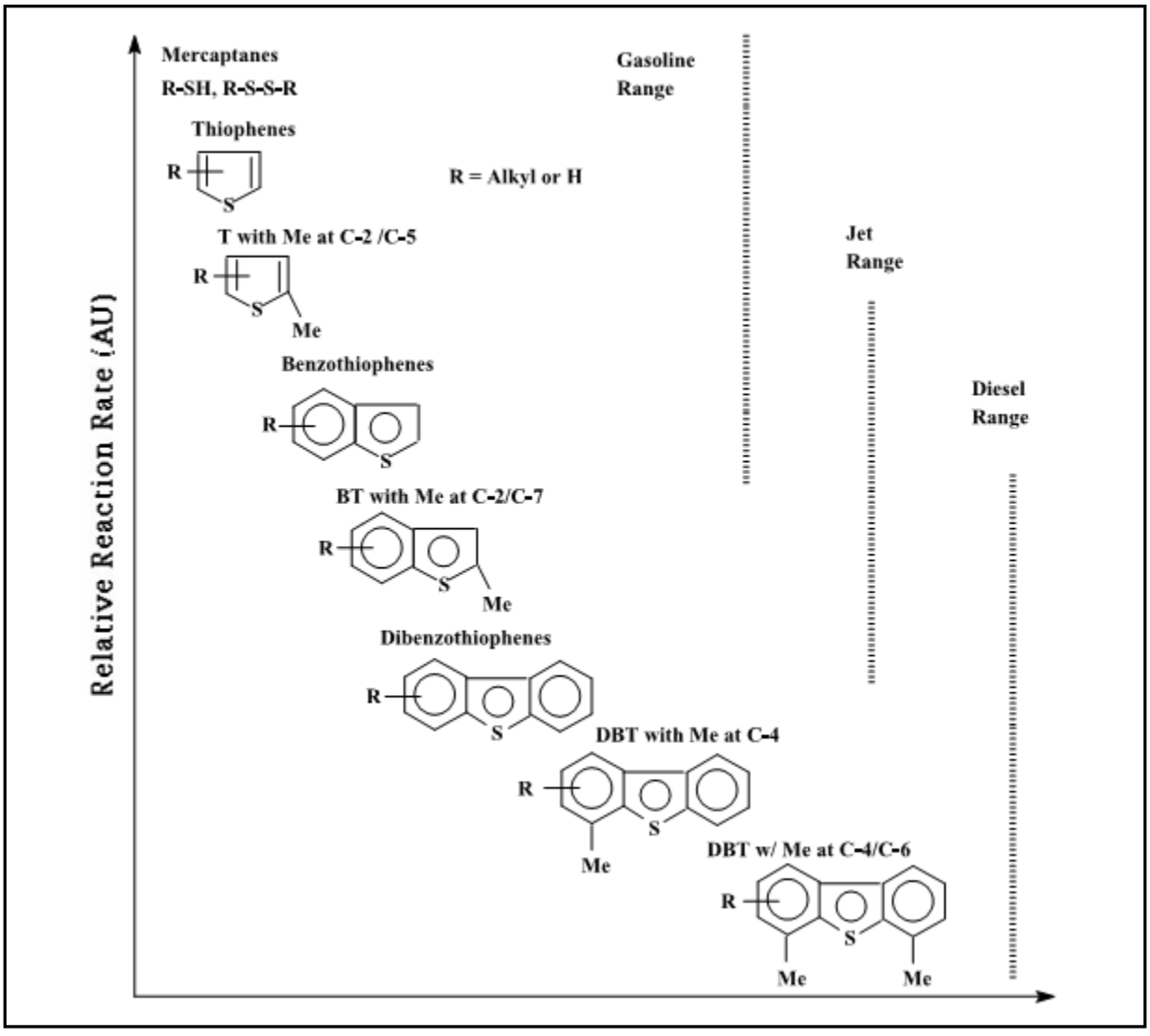

Figure 2.7: Reactivity of various organic sulfur compounds in HDS versus their ring sizes and positions of alkyl substitutions on the ring (Chunshan, 2003; Song, 2002)

Alkyl subsistents in dibenzo-thiophenic compounds greatly increase the difficulty of hydrodesulfurization. Steric hindrance caused by the methyl substituents at 4,6 position is mainly said to be the main reason behind the refractory nature of this compound.

2.6.2 Mechanism of Hydrodesulfurization

Hydrodesulfurization reactions are known to proceed via two pathways (Prins et al., 2006). These 2 pathways are discussed below for dibenzothiophene :

1) **Direct Desulfurization (DDS) Pathway** – In this pathway, the sulfur atom is first removed from the structure and replaced by hydrogen, without hydrogenation of any unsaturated C-C bonds. This pathway is believed to involve the insertion of metal atom on the surface of the catalyst into the sulfur–carbon bond in the sulfur containing compound. This insertion can occur even for fully aromatic sulfur compounds. This pathway is possible because of the energetically favourable metal-sulfur bond that is formed (Mochida and Choi, 2006; Whitehurst et al., 1998).

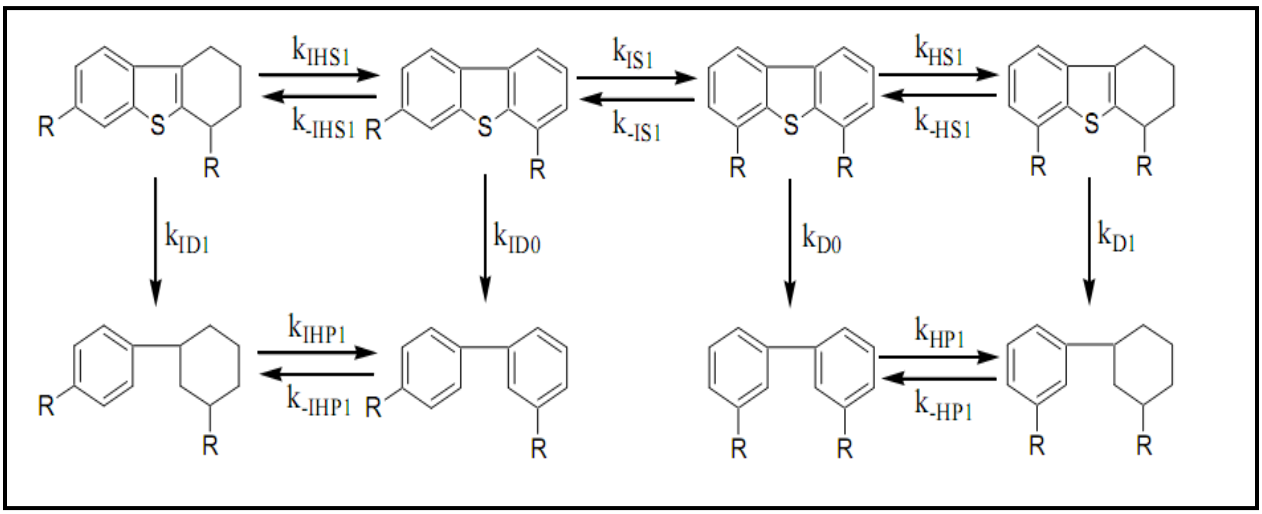

Figure 2.8: Reaction Pathways for Desulfurization of Dibenzothiophenes (Mochida and Choi, 2006).

2) **Hydrogenation (HYD) Pathway** – In this pathway at least one aromatic ring adjacent to the sulfur containing ring is hydrogenated before the sulfur atom is removed and replaced by hydrogen. In addition to hydrogenation of an aromatic ring before sulfur is removed, an aromatic ring may be hydrogenated after sulfur removal. The hydrogenation pathways are subject to thermodynamic equilibrium constraints. Thus, the partially hydrogenated intermediates (such as tetrahydrodibenzothiophenes) have lower equilibrium concentrations at higher temperatures. This results in a maximum in the observed rates of HDS via the hydrogenative route, as a function of temperature. Thus, hydrodesulfurization via the hydrogenative route becomes limited at low pressures and high temperatures (Mochida and Choi, 2006).

   In addition to the above defined pathways, certain desulfurization reactions can be imagined to proceed via an isomerization pathway. For example, in presence of an acidic site in the catalyst, 4, 6 DMDBT may first isomerize into 3, 6 DMDBT and then proceed through the DDS pathway. The isomerization of the methyl group is achieved due to the acidic functionality of the catalyst.

2.7 Hydrodenitrogenation (HDN)

Nitrogen is essentially found in the bottom end of the petroleum fraction mostly as present as five or six membered rings. Basic compounds are mainly 6-membered-ring nitrogen compounds, such as quinolines and benzoquinolines. Non basic compounds are mainly 5-membered-ring compounds, such as indoles and carbazoles. Some chemical structures are shown in Figure 2.9 for reference (Wiwel et al., 2010). Both the molecular complexity and quantity of nitrogen containing molecules increases with increasing boiling range, making them more difficult to

remove. The denitrogenation reaction proceeds through a different path from that of desulfurization. While in desulfurization the sulfur is first removed and the olefin created as an intermediate is saturated, in denitrogenation, the aromatic is saturated first and then the nitrogen is removed (Gruia, 2006). HDN reactions of a few nitrogen containing compounds are shown below in Figure 2.10 (Gruia, 2006).

2.7.1 Reaction Network of Nitrogen Compounds

The HDN reaction network is more complicated than the HDS reaction network, because the heterocyclic ring has to be hydrogenated prior to the cleavage of the carbon−nitrogen bond. The reason is that the dissociation energy of double bonds in the heterocyclic rings is approximately twice that of the single bond in the hydrogenated heterocyclic rings. Quinoline is a typical nitrogen-containing compound in middle distillates, and its reaction network is shown in Figure 2.11 (Lu et al., 2007).

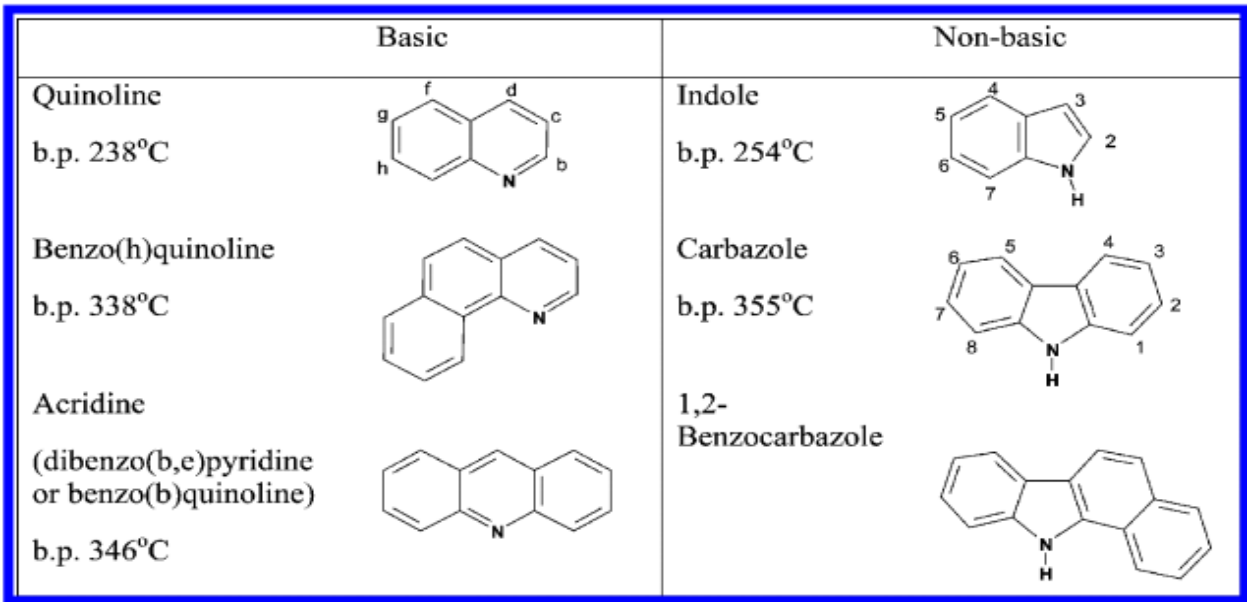

Figure 2.9: Structures of selected organic nitrogen compounds (Wiwel et al., 2010)

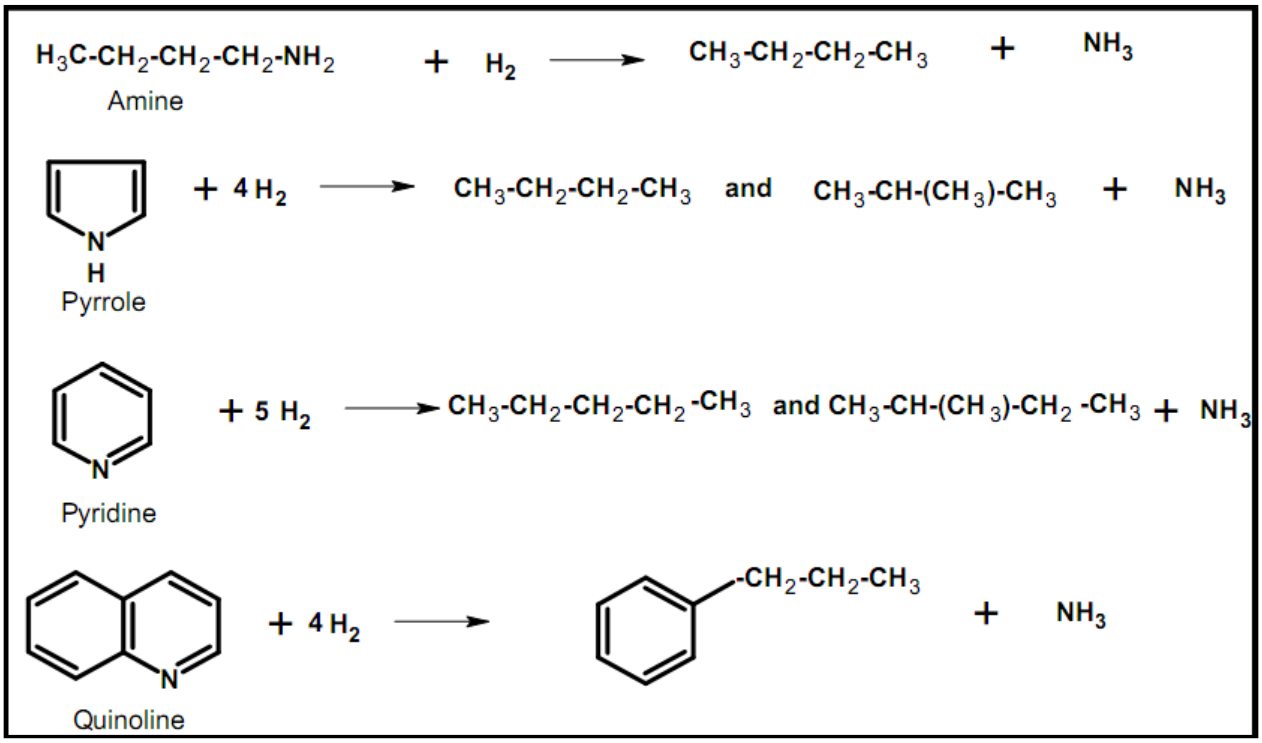

Figure 2.10 Examples of Hydrodenitrogenation reactions (Gruia, 2006).

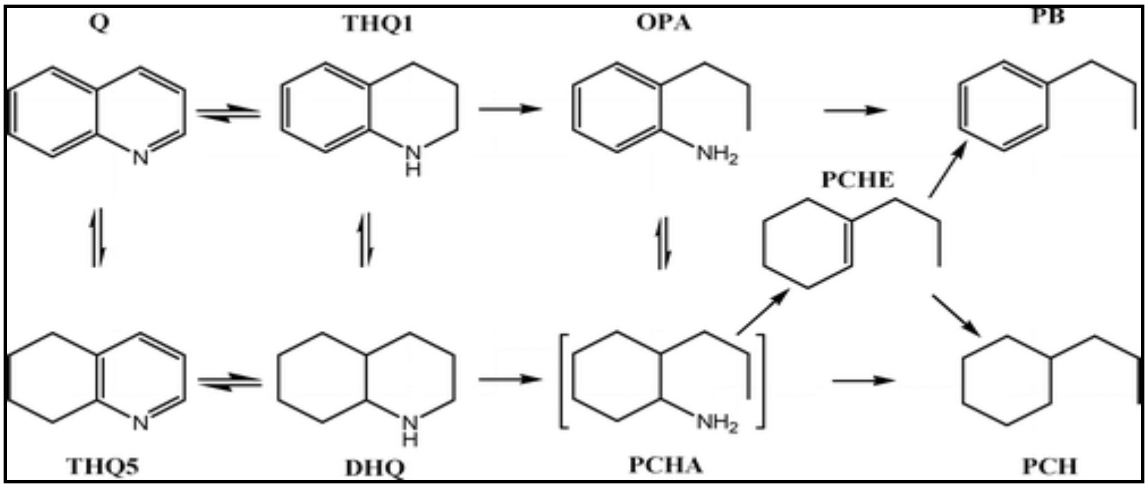

Figure 2.11 Reaction Network of Quinoline (Lu et al., 2007)

Q, quinoline; THQ1, 1,2,3,4-tetrahydroquinoline; OPA, ortho-propylaniline; PB, propylbenzene; THQ5, 5,6,7,8-tetrahydroquinoline; DHQ, decahydroquinoline; PCHA, 2-propylcyclohexylamine; PCHE, propylcyclohexene; PCH, propylcyclohexane

Shabtai et al. studied the HYD of Q, THQ, and BzTHQ to DHQ over sulfided NiMo, CoMo, and NiW catalysts supported on γ-Al_2O_3 at 573 K and 16 MPa of H_2 (Shabtai et al., 1988; Shabtai et al., 1989). Following rapid equilibrium Q to THQ, the favored subsequent path was to DHQ. They found high ratios of trans/cis- DHQ isomers in all cases. The effect of H_2S was to lower the rate constant for the trans-reaction, while having little effect on the cis-reaction. Two separate active sites were proposed to account for the two different reaction paths, viz., adsorption in a vacancy site, in which the N-molecule is exposed to addition of surface hydrogen from SH from both sides to give DHQ, and adsorption flat wise with addition of surface hydrogen to the same side to give cis-DHQ (Furimsky and Massoth, 2005).

2.7.2 Reactivity of Nitrogen Compounds

Basic nitrogen compounds with 6 membered rings are generally more reactive than their five membered ring counterparts. In basic nitrogen compounds the lone pair of electrons on nitrogen does not take part in resonance and is hence available for donation as a lewis base. However, in five membered ring the lone pair is not available due to delocalization in the ring. In general, the reactivity of nitrogen compounds in 6 membered ring follows the order Pyridine > Quinoline > Acridine. In 5 membered rings the order of reactivity is as follows Pyrrole > Indole > Carbazole (Furimsky and Massoth, 2005) .

2.8 Hydrotreating Catalysts

Hydrotreating catalysts contain at least two elements from the Group VI and Group VIII of the periodic table. The most common hydrotreating catalysts contain the active metal as Molybdenum or Tungsten, a promoter metal most commonly Nickel or Cobalt. γ-Al_2O_3 is by far

the most universally used support owing to excellent physical and chemical properties suitable to hydrotreating and associated reactions. Molybdenum precursor (15- 20wt %) is first impregnated to be highly dispersed onto alumina and then the Co or Ni precursor (1-5 wt %) is impregnated hopefully onto the Mo phase. The impregnated catalyst is carefully calcined and sulfided in the commercial application for the stable catalytic activity. The active species is believed to be the Ni(Co) MoS phase (Clausen et al., 1981; Topsoe et al., 1981b; Topsoe and Topsoe, 1983; Wivel et al., 1981b). Commercial catalysts also contain isolated Ni_3S_2 and the corresponding cobal sulfides (Co_9S_8) and $Co(Ni)/Al_2O_3$ spinels. The final phase of the formed catalysts depends on a variety of factors including but not restricted to a) synthesis method, b) calcination temperature c) metal loading, d) sulfidation and e) nature of support. The amount of active phase is roughly the same and a maximum catalytic activity is observed for a Ni(Co)/[Ni(Co) + Mo(W)] ratio at approximately 0.3, whatever the catalytic active phase and the nature of the main reaction. However, the active phase and exact nature of active sites is still a matter of much debate. As many as 17 or more theories have been proposed in order to explain the active phase and the catalytic synergy between the promoter and the active metal in the sulfide phase. A brief summary of some of the main theories has been tabulated below

Table 2.4: Various theories proposed on the active phase of the Co(Ni)Mo/Al_2O_3 catalyst

Authors	Theory	References
Lipsch and Schuit	Monolayer of Oxide	(Lipsch and Schuit, 1969)
Delmon	Contact Synergy	(Delmon, 1979; Delmon and Froment, 1996)
Schuits and Gates	Oxysulfide Monolayer	(Schuit and Gates, 1973)
Voorhoeve and Stuiver	Intercalation of Co	(Voorhoeve and Stuiver, 1971)
Farragher	Pseduo Intercalation	(R.J.H., 1971)
Harris and Chianelli	Electronic Effect	(Harris and Chianelli, 1986b)
Topsoe	CoMoS Phase	(Topsoe et al., 1981b; Wivel et al., 1981b)
Delmon	Remote Control	(B., 1994)
Chianelli and Daage	Rim/Edge Contribution	(Daage and Chianelli, 1994)

Further the choice of the active metal and promoter is generally made based on the catalytic reactions it is used for. Mo based catalysts promoted with Co are known to be excellent for hydrodesulfurization reactions (HDS) whereas Mo promoted with Ni are highly active for HDN reactions. On the other hand, W based catalysts show high activity towards hydrogenation of aromatics. The results are summarized in the table below

Table 2.5: Typical activities of catalyst used for hydrotreating process (Speight, 1999)

Catalyst[a]	**HDS Activity**	**HDN Activity**	**Aromatics Hydrogenation**
Co-Mo-Al_2O_3	XXXX[b]	XX	X
Ni-Mo-Al_2O_3	XXX	XXX	XX
Ni-W-Al_2O_3	XX	XX	XXXX

[a] All catalysts are in the sulfide state with the average chemical composition CoO (NiO) 2- 4 wt % ; MoO_3 12 – 15 wt %; and Al_2O_3 81 – 86 wt %

[b] Reactivities: X – fair; XX – good; XXX – very good; XXXX - excellent

The physical and textural properties of the hydrotreating catalyst can be designed and tailored according to feedstock being processed. For example, for hydrotreating of heavy feedstocks and residua large pore diameter of the catalysts is desirable to avoid diffusion limitations whereas relatively leaner naptha and gasoline can be processed with catalysts having small pore diameter. A few physical properties of hydrotreating catalysts are tabulated below (Speight, 1999).

Table 2.6: Typical composition of catalyst used for hydrotreating process (Speight, 1999)

Property	Low	High
Surface area (m^2/g)	150	250
Pore diameter (nm)	7.5	25
Pore Volume (ml/g)	0.5	1
Bulk density (kg/m^3)	490	980
Ni(Co) as NiO(CoO) wt%	3	8
Mo(W) as MoO_3(WoO_3) wt%	10	30

2.8.1 Hydrotreating Catalyst Life Cycle

The formation and dispersion of the active phase changes drastically during a typical catalyst cycle. A typical life cycle of a NiMo/γ-Al_2O_3 catalyst is shown in Figure 2.12 (Sonja, 1997). The catalysts in oxide phase usually have a high Mo dispersion (well dispersed MoO_3 or polymolybdate phase), with well dispersed CoO (NiO) present in the proximity of Mo (Apecetche and Delmon, 1979; Delmon, 1985; Massoth et al., 1984; Sonnemans and Mars, 1973). Finely dispersed $CoMoO_4$ ($NiMoO_4$) may also be observed resulting from the direct interaction of Mo and Ni. Mo is usually assumed to be bound to the support via -O-A1 bridges (Delannay, 1985; Hayden and Dumesic, 1987). During the sulfidation, finely dispersed MoO_3 and CoO (NiO) are transformed into sulfides (De Boer et al., 1994; Mangnus et al., 1992;

Mangnus et al., 1993; Scheffer et al., 1986). A direct interaction between sulfidic Co (Ni) and MoS_2 is generated resulting in the formation of MoS_2, with edges decorated with sulfidic Co(Ni) (Bouwens et al., 1988; Bouwens et al., 1990). Sulfidation of crystalline phases of MoO_3 and CoO(NiO) only takes place on the surface, where the core retains it oxide character. If present, crystalline $A1_2(MoO_4)_3$, $CoA1_2O_4$ ($NiA1_2O_4$), $CoMoO_4$ ($NiMoO_4$), CoO (NiO) and MoO_3 do not get (fully) sulfided (Pratt et al., 1990) . Depending on the metal-support interaction a part of the Mo remains incompletely sulfided, maintaining the Mo-O-A1 bridges (Hayden et al., 1987; Louwers et al., 1993) . With increase in the extent of sulfidation, MoS_2 clusters, no longer linked to the support, can migrate over the $A1_2O_3$ surface and sinter (Kameoka et al., 1995). Except for large crystals, sulfides of Mo and Co (Ni) are transformed back into oxides during the oxidative regeneration (Eijsbouts et al., 1993a; Yoshimura et al., 1991; Yoshimura, 1991). During this process, coke is removed and a redispersion of Mo takes place through solid-solid wetting of MoO_3 on $A1_2O_3$ (Arteaga et al., 1987; Delmon, 1990; Madeley and Wanke, 1988). Under typical regeneration conditions, large MoS_2 crystals get oxidized only on their surface and their redispersion is incomplete . Although the regeneration increases the surface exposure of the Co (Ni) and Mo species the redistribution is incomplete, leading to a lower dispersion and less intimate contact of the active phase components. This distinguishes the regenerated catalyst from the fresh one and explains its lower activity (Yoshimura et al., 1994).

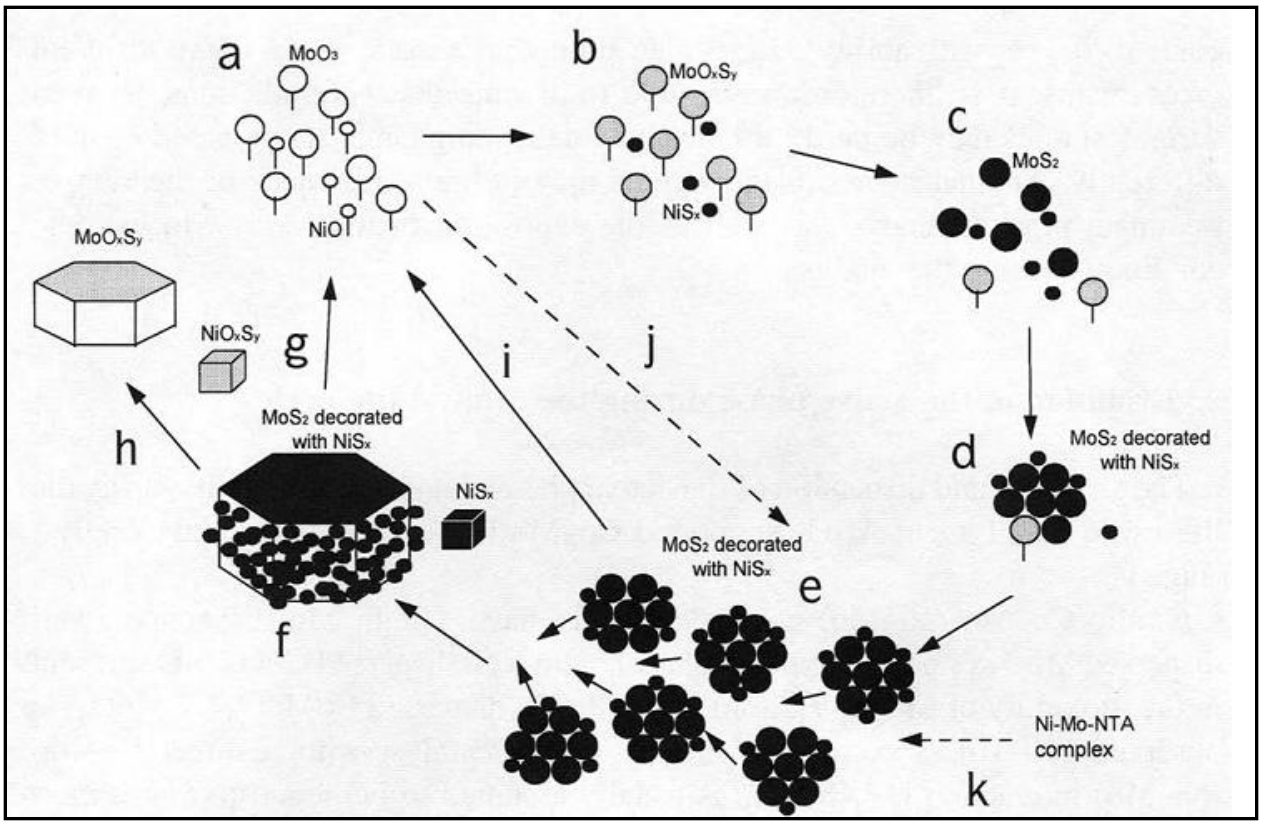

Figure 2.12: A typical life cycle of a NiMo/γ-Al_2O_3 catalyst: (a) Oxidic catalyst - oxidic Mo and Ni (or Co) are bound to Al_2O_3; (b) Partly sulfided catalyst - sulfidic Ni (or Co) is no longer linked to Al_2O_3, Mo oxysulfide is still bound to Al_2O_3; (c) Partly sulfided catalyst - part of Mo is no longer bound to Al_2O_3; (d) Partly sulfided catalyst - small MoS_2 slabs decorated with Ni (or Co) are formed, these slabs are still anchored to Al_2O_3; (e) Fully sulfided catalyst - Mo gets completely sulfided so that MoS_2 slabs decorated with sulfidic Ni (or Co) become mobile; (f) Deactivation - small MoS_2 slabs decorated with sulfidic Ni (or Co) sinter to form larger slabs, stacks and crystals, the edge surface area of these crystals is insufficient to accommodate all of Ni (or Co) so that separate Ni (or Co) sulfide crystals are formed; (g) Regeneration - MoS_2 crystals along with some decorating Ni (or Co) sulfide get partly redispersed; (h) Regeneration - large MoS_2 crystals get only oxidized on the surface, Ni (or Co) sulfide crystals cannot redisperse on oxidation; (i) Regeneration - small structures get fully oxidized and return nearly to their original state; (j) High temperature sulfidation - Mo gets completely sulfided so rapidly that the intermediate steps can be neglected; (k) NTA preparation route - Ni-Mo-NTA complex gets completely sulfided. No linkages with the support are formed at any stage of the process (Sonja, 1997).

2.8.2 Components of Hydrotreating Catalysts

As discussed above a typical hydrotreating catalyst consists of several components. These components are decided by the nature of catalyzed reactions. Generally a hydrotreating catalyst consists of a) Active metal, b) Promoter, c) Support, d) Other additives

2.8.2.1 Active Metal

The active metal when dispersed over the support, in its active phase provides hydrogenating sites for the reactions. Hydrogenation of the organo-sulfur or organo-nitrogen compound is believed to be the first step before the cleavage of the C-S or C-N bond takes place. Group VIII metals, usually molybdenum (Mo) or in some cases tungsten (W) are used as the active metals for hydrotreating reactions. In some cases, noble metals like Pd and Pt may also be used to synthesize very active hydrogenating catalysts. However their use is limited owing to their high costs. The active metal is generally loaded on the support surface in its oxide form. After drying and subsequent calcination, the catalyst is sulfided in presence of H_2S/H_2 to convert the oxide phase of the active metal into its sulfide phase. The sulfide phase of the catalyst MoS_2 or WS_2 forms the active phase wherein the hydrogenation reactions take place.

2.8.2.2 Promoter

All hydrotreating catalysts are invariably promoted systems, where the Group VIII active metal is promoted by a Group VI metal most frequently Cobalt or Nickel. The promoter has the effect of substantially increasing (approximately 100-fold) the activity of the active metal sulfide. Upon sulfidation, the promoter atom occupies the edge site of the MoS_2 slabs. Studies have shown that the presence of Co or Ni does not affect the basic slab size of the MoS_2 slabs, being located at

the edge of the slabs. The Co or Ni does not appear to appreciably increase the number of vacancies, but the vacancies associated with the Co or Ni are considerably more active than those associated with only Mo, leading to the increased promotional activity of the catalyst.

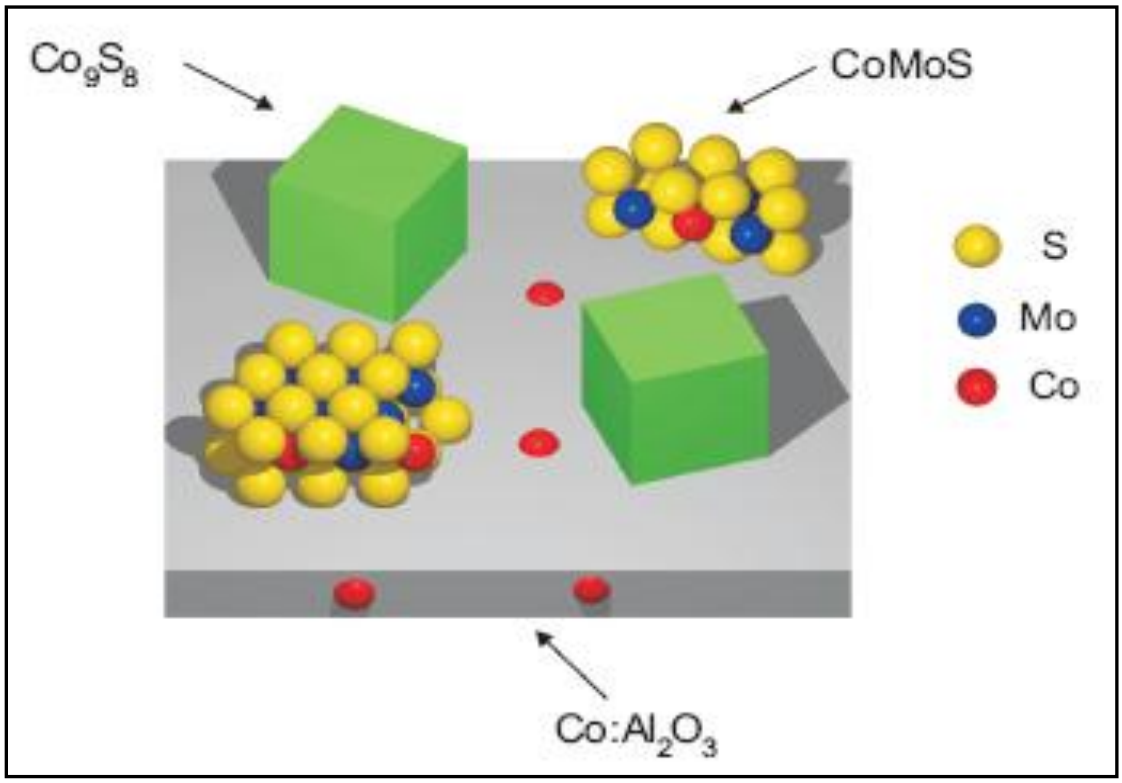

Figure 2.13: The Structure of CoMo Catalyst (Mochida and Choi, 2006)

2.8.2.3 Support

The support forms the carrier material on which the metals are loaded. γ-Al_2O_3 is by far the most commonly used support for hydrotreating. γ-Al_2O_3 has various desirable physical and chemical properties which makes it an excellent carrier material. Other oxides like TiO_2, ZrO_2, MgO and SiO_2, mixed oxides like TiO_2-Al_2O_3, TiO_2-ZrO_2, Al_2O_3-ZrO_2, SiO_2-Al_2O_3 etc have also been used as supports. Similarly crystalline zeolites and very recently mesoporous silica materials

have also been used as supports for hydrotreating reactions. The role of support in hydrotreating reactions of much importance. A few functionalities of supports are given below:

1) Textural Properties – Hydrotreating support surfaces need to have high surface areas, large pore diameters and good mechanical strength. High surface area in supports is desirable to achieve maximum dispersion of the active metal without the formation of bulk phases. Similarly, large pore diameter prevents any mass transfer limitations. High mechanical strength is essential to maintain the integrity of the catalyst during catalyst loading in the reactors and to withstand high temperature and pressure conditions in the reactor.
2) Acidity – In addition to having good textural properties, the presence of acidic sites is also very important. Attempts were made to increase the conversion of 4,6-dimethyl dibenzothiophene (4,6,DMDBT) by transforming it into a more reactive compound, either through demethylation or isomerization. These reactions are acid-catalyzed, and consequently were carried out on bifunctional catalysts, such as mechanical mixtures of the alumina-supported sulfide catalyst with an acidic component, silica–alumina or zeolite, or by associating a hydrotreating catalyst such as CoMo/alumina to a Ni/HY catalyst.
3) Metal support interaction – The chemical nature of the support material dictates the nature of the active sulfide species. A strongly metal interacting support like Al_2O_3 has very strong Mo-O-Al bridging bonds. The strong nature of this bond ensures excellent dispersion of the MoOx species even for high loadings of Mo (~ 21 wt %). However, some Mo-O-Al bonds still remain even after sulfidation which decrease the activity of the catalyst. On the other hand SiO_2 has very weak interaction with Mo. As a result, the formation of bulk MoO_3 is accelerated in SiO_2 supports

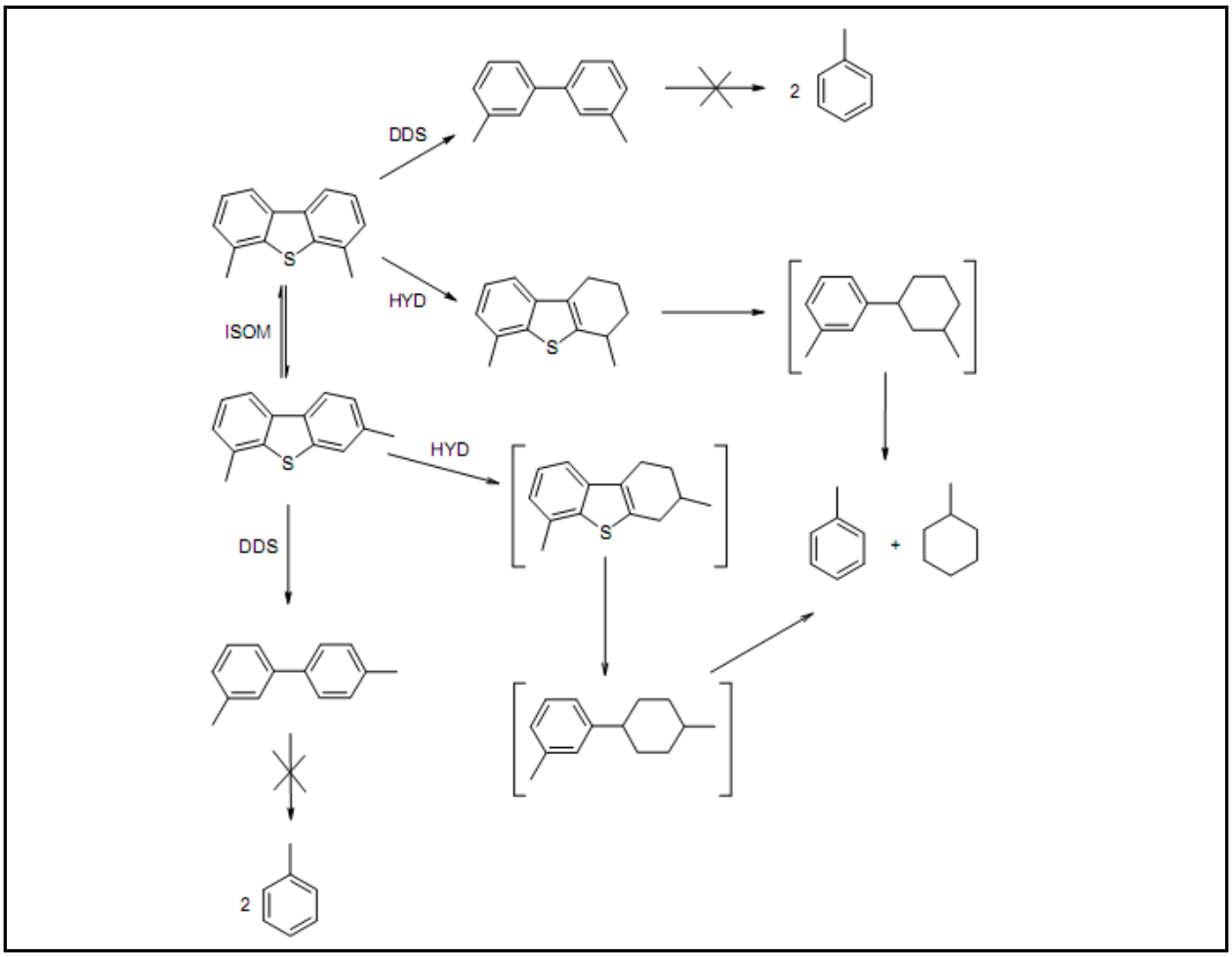

Figure 2.14: Transformation of 4,6-DMDBT acid-containing hydrotreating catalysts. Main reaction steps for the HDS of the reactant and of its 3,6-dimethylisomer. Isomerization (ISOM); DDS pathway; HYD.

2.8.2.4 Additive

In addition to the promoter atoms, certain additives are most frequently used in hydrotreating catalysts to further improve the activity. The most common additive that is used is phosphorus. Various other works have also focussed on boron as an alternative to phosphorus yielding good results. Addition of phosphorus leads to an increase in the acidity of the catalytic system and a decrease in the metal support interaction in alumina supports resulting in higher activities.

2.8.2.5 Active Phase

The most common active phase for hydrotreating reactions is the sulfide phase with the Ni-Mo-S phase accepted as the active catalyst phase. Various other models have also been suggested in the literature. Some important ones are discussed below:

1) Monolayer Model – The monolayer model was first proposed by Lipsch, et al in 1961 (Lipsch and Schuit, 1969). They dealt with the oxide form of Co/Mo catalysts and concluded that the molybdenum is dispersed as MoO_3 over the alumina surface while the cobalt is distributed throughout the support as cobalt aluminate. The role of the promoter was further studied by Ratnaswamy et al who found that in agreement with the model a certain portion of the promoter cations penetrates some distance into the support, Co preferring tetrahedral sites, and Ni, octahedral sites (Ratnasamy and Sivasanker, 1980).
2) Pseduo Intercalation Model – This model was proposed by Voorhove et al and later modified by Farragher et al (Voorhoeve, 1971; Voorhoeve and Stuiver, 1971). It starts from the layer structure of of MoS_2 and WS_2 where the metal cation occupies trigonal prismatic sites.

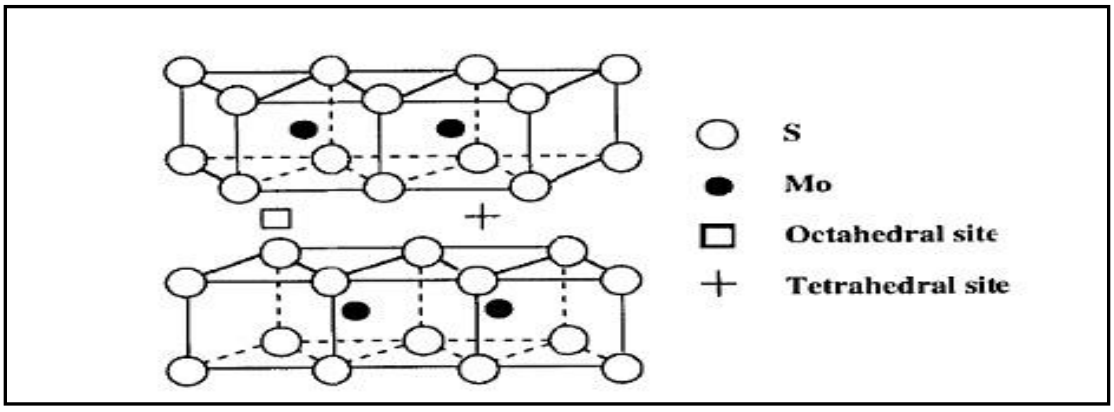

Figure 2.15: The pseudo inter-calaction model of MoS_2

The cationic sites between successive sulfur layers being alternately all empty or all filled. Because of the symmetry of the trigonal prismatic crystal intercalation between the empty sulfur layers should not occur.

3) Remote Control Model –In this model the synergistic effect is a result of the mere contact of the Group VIII sulfide (e.g., Co_9S_8) with the Group VI sulfide (e.g., MoS_2). Delmon et al have proposed that the interaction might be electron transfer at the junction or perhaps hydrogen atom spillover from one phase to another (Delmon, 1994). Also in the contact synergy model, the role of support is not considered essential.

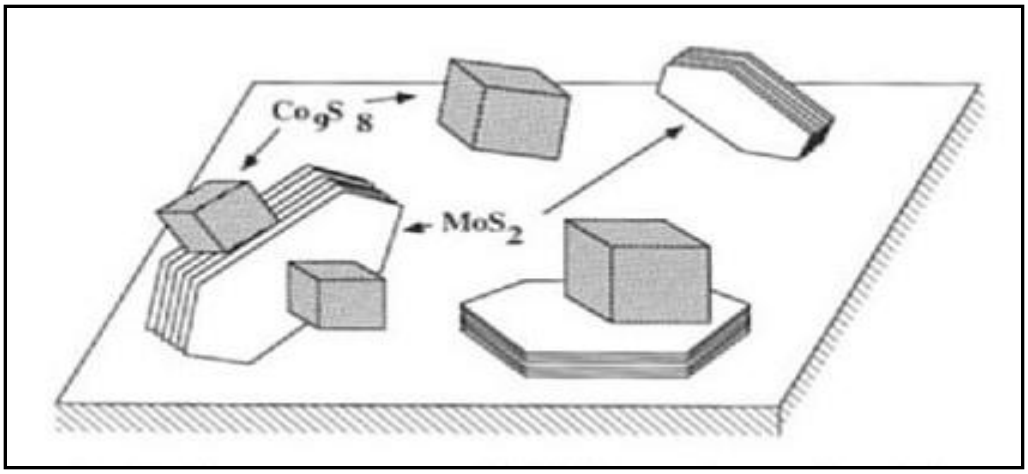

Figure 2.16: The remote control model of Co promoted MoS_2 catalyst(Topsoe et al., 1981; Wivel et al., 1981)

4) Ni(Co)-Mo-S Model – This model was developed by Topsoe, et al in a series of papers (Topsoe et al., 1981; Wivel et al., 1981) . As in the pseudo intercalation model Topsoe suggests that the cobalt is located at the edge of a molybdenum disulfide crystallite, however, there is no stacking of MoS_2 to form multiple layers as suggested earlier by Voorheve (Voorhoeve and Stuiver, 1971). A further refinement to this model suggests that there are

infact two different Co-Mo-S phases present. For alumina supported Co-Mo catalysts high temperature sulfiding studies have revealed the existence of a “low temperature” (Type I) and a “high temperature” (Type II) Co-Mo-S structures.

2.8.2.6 Type I and Type II phase

The Co-Mo-S model proposed by Topsoe et al is the most widely accepted depiction of the active phase in a hydrotreating catalyst. The typical properties of the "Type I" phases are the lower S coordination of Mo and Co (Ni) and the high dispersion of the underlying MoS_2, mostly single slabs having maintained their (Mo-O-A1) interactions with the support (Bouwens et al., 1994; Topsoe and Clausen, 1986; van Veen et al., 1993). The "Type II" phases are fully sulfided, i.e. have higher S coordination of Mo and Co (Ni), and the underlying MoS2 is less disperse, consisting mainly of stacks not linked with the support . "Type II" phases have higher intrinsic activities in thiophene hydrodesulfurization (HDS) than the "Type I". To depict just Type I and II phases seems, however, too static to describe the dynamic changes of the catalyst during its sulfidation and deactivation. TEM (Eijsbouts et al., 1993b) as well as MES (Carvill and Thompson, 1991; Craje et al., 1994; Craje et al., 1991; Harris and Chianelli, 1986; Van et al., 1988) results indicate strongly that the active phase transforms gradually. The initial state may be described as the "Type I" phase (very small active phase clusters deposited directly on the support). During the catalyst use, the "Type II" (active phase situated on the surface of larger MoS_2 crystallites) is slowly formed. As the deactivation proceeds, the catalyst components reach a highly sintered state with segregated small entities of Co (Ni) sulfides of different stoichiometries. Finally, even large crystals of MoS_2, Co_9S_8 (Ni_3S_2, NiS) are present. The synergetic effect in the "Type I and II" structures is often explained by the electron transfer from Co (Ni) to Mo, removing metal-S

anti-bonding electrons from Co (Ni). These changes of electron densities on Mo and Co (Ni) sites are suggested to increase the intrinsic activity of the Mo sites or of the Co (Ni) sites (Harris and Chianelli, 1986a; Topsoe et al., 1987) . This electron donation model , similarly to the catalyst model based on the formation of ternary sulfides (Chevrel compounds), assumes a strong interaction between Mo and Co (Ni).

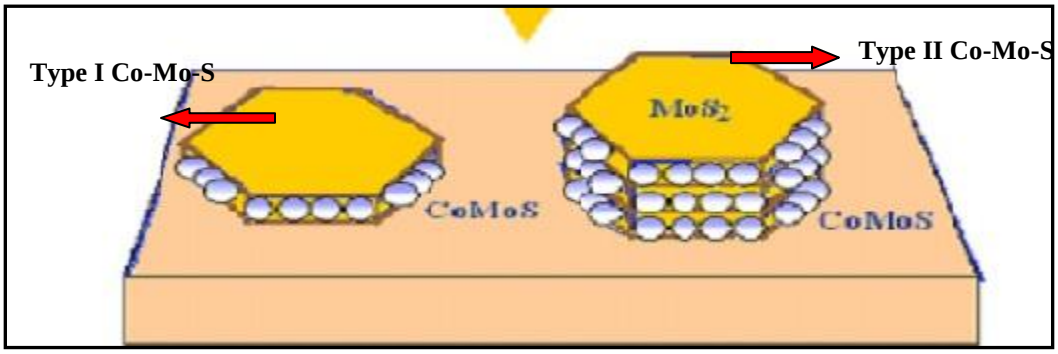

Figure 2.17: Type I and Type II CoMoS phases

2.8.3 Sulfidation

HDS catalysts are initially prepared in the form of highly dispersed molybdenum oxides on high-surface-area supports to which promoters such as Co or Ni may be added and are subsequently converted into the catalytically active phase by sulfidation, typically in H_2S/H_2 atmospheres at temperatures between 300 and 400 °C:

$$MoO_3 \xrightarrow[H_2S/H_2]{300^oC - 400^oC} MoS_2 \quad \ldots\ldots\ldots\ldots\ldots\ldots\ldots (2.1)$$

The transition of the oxidic MoO_3 to the final sulfided state of MoS_2 takes place in various stages. At low temperatures (< 200 ^oC), the terminal bonds of MoO_3 react with H_2S to form

oxyslufides. The initial sulfidation of MoO_3 results in the reduction of Mo^{+6} to Mo^{+5} and the oxidation of sulfide ligands to bridging S_2^{2-} ones. The Mo-O-Mo bridging bonds disappear between 50 to 100 ^oC and are transformed into terminal bonds (Weber et al., 1996).

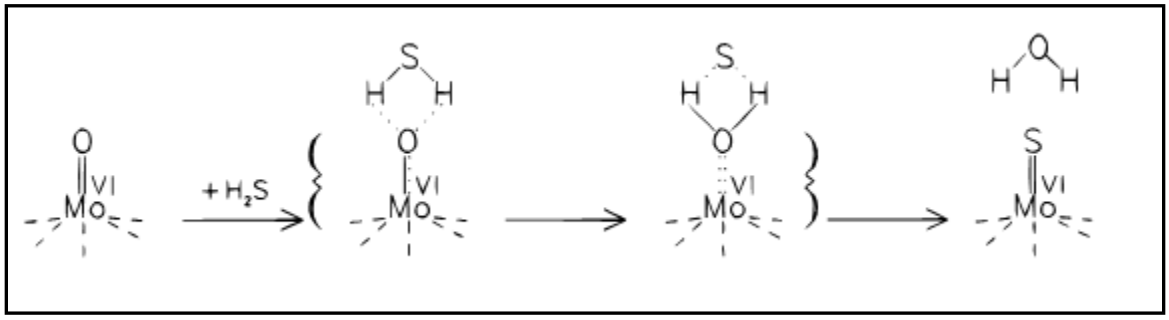

Figure 2.18: Sulfidation of Mo^{+6} (Weber et al., 1996)

As the temperature is increased from 200 to 400 ^oC, the oxysulfides react further to give the final metal sulfides. Mo^{6+} and Mo^{5+} have largely reduced to Mo^{4+}, and the contribution of bridging S_2^{2-} disappears. Formation of a perfect MoS_2 lattice would require much higher temperatures of about 800 °C. Hence, the sulfidation of MoO_3 at temperatures typically employed in catalyst pre-treatments (about 400 °C) leads to a microcrystalline MoS_2 phase, relatively rich in defects.

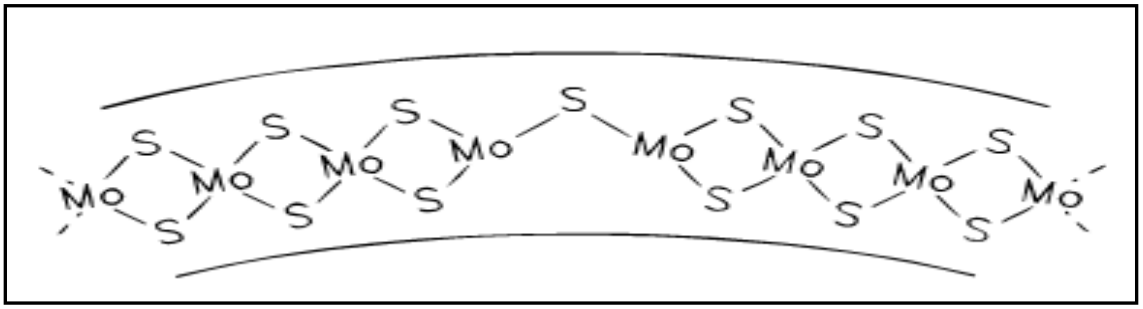

Figure 2.19: Structure showing small region of MoS2 interconnected by Mo−S−Mo bridges (Weber et al., 1996)

The vacancy model is a widely accepted approach to understanding the mechanism of hydrodesulphurization reaction (Kwart et al., 1980). Vacancies in the catalyst are generated due to reaction of hydrogen with surface sulfide group. Thermodynamically unstable vacant sites then tend to regain the stability by forming metal bonded sulfide group. According to this concept, S in thiophene attaches to a surface anionic vacancy; its interaction with hydrogen results in the formation of a surface –SH group.

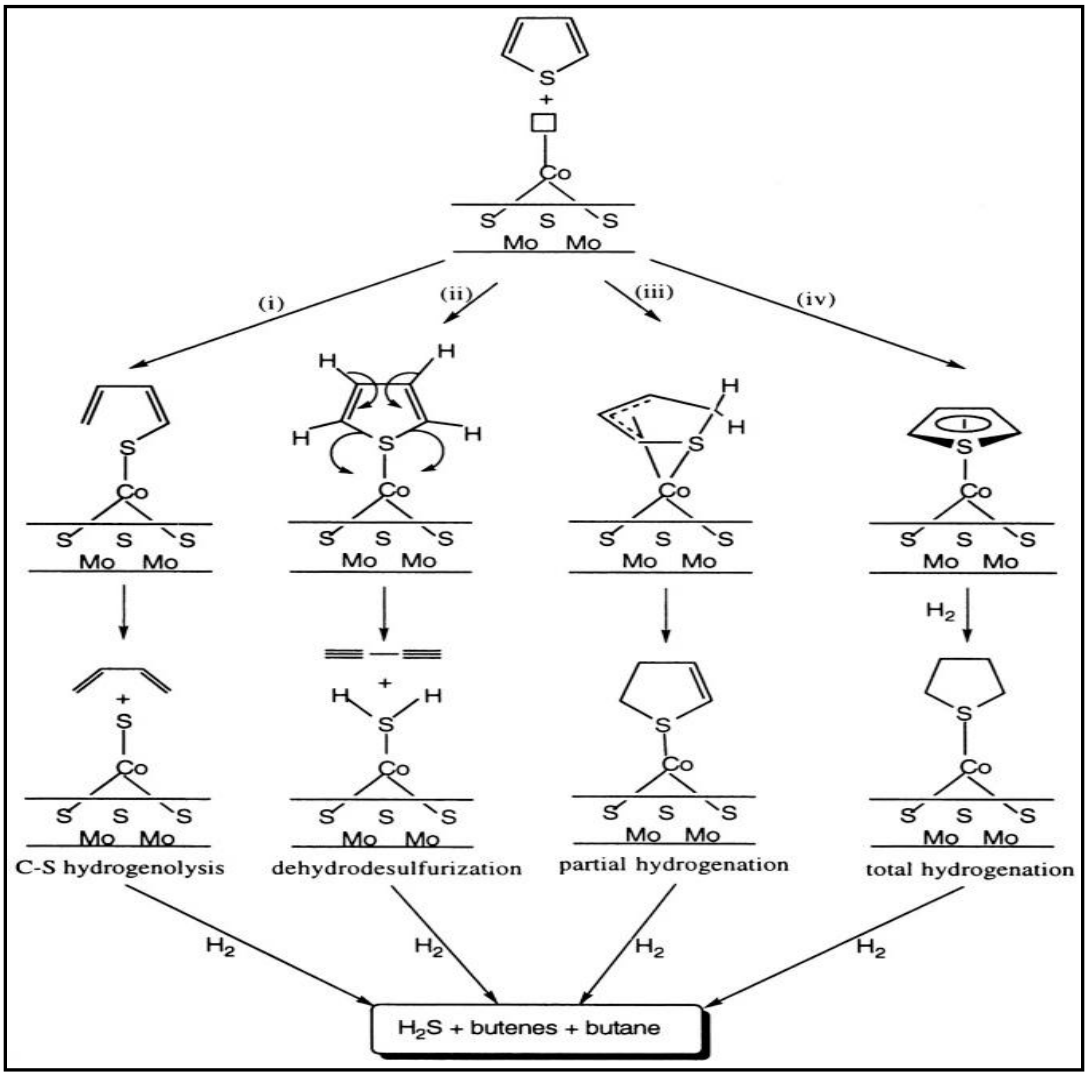

Figure 2.20: Thiophene hydrodesulfurization through the vacancy model

Consequently, the number of vacancies (V) and the V: SH ratio decreases. This would stop the catalytic reaction; however, the V: SH ratio becomes re-established due to surface SH interaction with gas phase hydrogen (possibly via H_2 dissociation) and H_2S release. Following this, the ratio of the acting vacancy, the mobile –SH group number, is the determining factor in the HDS activity of the catalyst.

2.9 Challenges in HGO hydrotreatment

Hydrotreatment of heavy gas oils is quite challenging as compared to hydrotreatment of lighter fractions. In spite of a few similarities, hydrotreating of heavy gas oils or heavy feedstocks in general differs markedly from that of light feeds. The larger molecules present mostly as asphaltenes or organo-metallic compounds make the catalyst prone to deactivation and poisoning. Further, there are significantly higher concentrations of hetero atoms like S, N and metals which make hydrotreating using a conventional catalyst difficult. Few challenges pertaining to heavy gas oil hydrotreating are listed below:

1) Bulky molecules – Heavy gas oil derived from Athabasca bitumen has a boiling point distribution of 343 ^{o}C – 525 ^{o}C. Such a high range of boiling point indicates the presence of high molecular weight molecules including asphaltenes. The large size of the molecules poses mass transfer limitations in the catalyst. The inability of the bulky molecules to diffuse through the pores of the catalyst or the pore blockage of the catalysts by the larger molecules results in rapid loss in activity of the catalyst. Further diffusion of bulky reactants, such as DBT (molecular size 0.8 nm) and 4, 6-DMDBT (molecular size 0.9 nm), into the catalyst pores significantly affects the activity of the catalyst having smaller pore size (Jayne et al., 2005)

2) High Concentrations of sulfur and nitrogen – The S and N content in heavy gas oil is very high at 4 wt % and 0.4 wt % respectively. The presence of such high concentrations of hetero atoms requires catalysts with significantly higher intrinsic activity. Additionally, previous studies have determined that the non basic nitrogen compounds are more difficult to remove as compared to the basic ones. These non basic nitrogen compounds are a major source of reversible and irreversible poisoning of the active sites in the catalyst (Furimsky and Massoth, 2005).
3) Catalyst Deactivation - For relatively light feeds, deactivation of the catalyst is minimal and the process can operate for long periods of time before there is a need for catalyst replacement. However, during hydrotreatment of heavy gas oils deactivation can be rather severe and quick. Deactivation of the catalyst can occur due to different reasons. Poisoning of the active sites, blockage of the active sites by coke, sintering of the active phase etc are a few causes of deactivation. Initial deactivation is quite common and is caused by coke deposition on some of the active sites of the catalyst. Catalyst deactivation by poisoning of the active sites however is observed mostly in heavy gas oil processing. Most common form of catalyst deactivation through poisoning occurs due to nitrogen compounds present in the feedstock. Non basic nitrogen compounds are adsorbed very strongly on the acidic sites of the catalyst blocking the site either permanently or temporarily. Besides strongly adsorbing on the Lewis sites via the N- electron pair or via the aromatic π system, N compounds can also interact with the protons from Bronsted acid sites, forming positively charged species. The basic strength and extent of adsorption of several N compounds are listed in Table 2.7 (Furimsky and Massoth, 1999)

Table 2.7: Nitrogen-compound poisons (Furimsky and Massoth, 1999)

Name	Structure	pK^a	Adsorbtion[c] (μmol/g)
Piperidine (PIP)		11.1	0.15
Pyridine (PY)		5.3	0.16
2,6-Lutidine (26L)	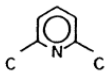	7[b]	0.045
3,5-Lutidine (35L)	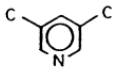	6.2	0.215
Aniline (AN)	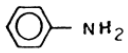	4.6	0.13
N,*N*-dimethylaniline (NAN)	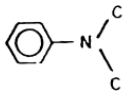	5.2	0.085
Quinoline (Q)		4.9	0.25
Quinaldine (MQ)	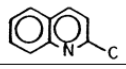	5.8	0.08

2.10 Scope for improvement in hydrotreating catalysts

Keeping in mind the difficulties posed by heavy gas oil hydrotreatment, the design of hydroprocessing catalysts for heavy feedstocks should be optimized for excellent textural and chemical properties, tolerance to poisoning by nitrogen compounds and metals and high intrinsic activity. Recent studies on hydrotreating catalysts for heavy oil processing have reviewed the above characteristics (Massoth, 1979; Grange, 1980; Ratnasamy and Sivasanker, 1980; Topsoe et al., 1996). A few desirable properties in context with heavy gas oil hydroprocessing are discussed below:

1) Physical Properties – Textural properties such as pore volume, pore size distribution, average pore diameter and surface area have to be optimized in order to maximize catalyst utilization and maximum exposure of the reactants to the active sites. A high surface area and moderate

pore volume catalysis are very active for HDS because of the efficient dispersion of active metals in the pores. However, in case of heavy feeds, these pores become gradually unavailable because of pore mouth plugging. On the contrary, catalysts with high pore diameter and low surface areas are less active because the available surface area for metal dispersion is less. But the effects of catalyst deactivation are less pronounced. Figure 2.21 shows the effect of surface area and pore volume/pore diameter on catalyst deactivation and their applicability to different feedstocks (Ancheyta et al., 2005),

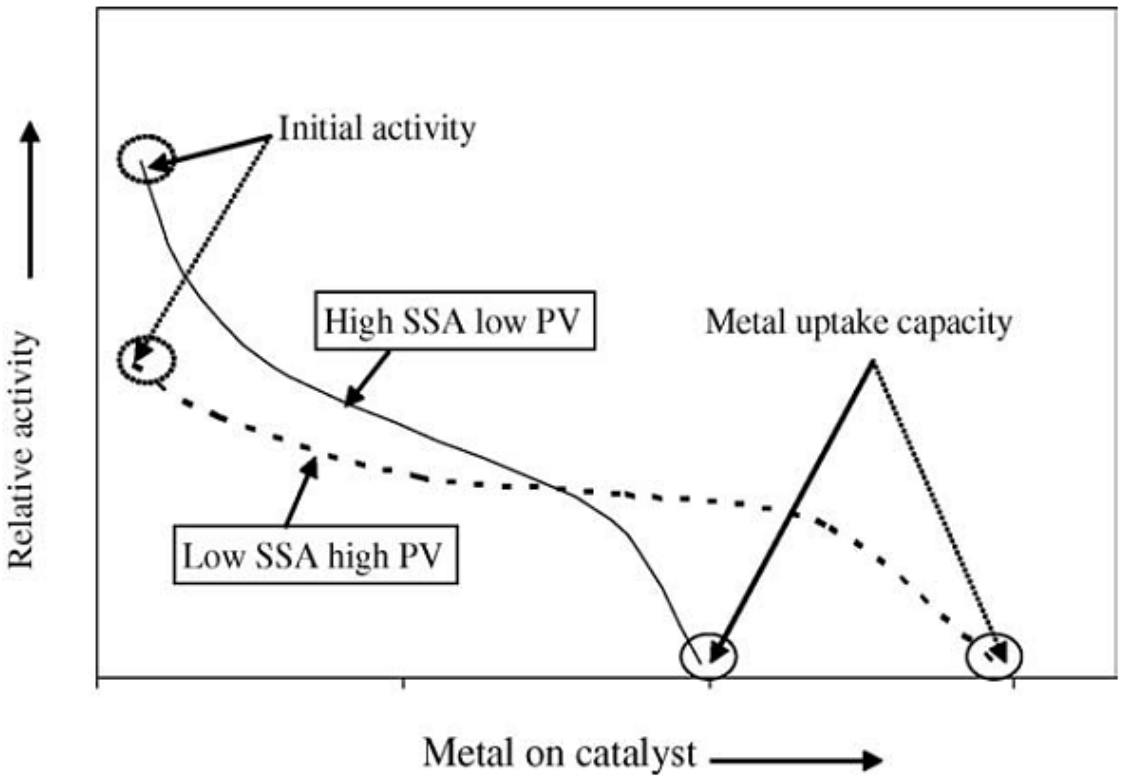

Figure 2.21: Relationship between catalyst activity and metal accumulation (SSA: specific surface area, PV: pore volume) (Ancheyta et al., 2005)

From the above discussion, it is evident that for each catalyst there is an optimal surface area and pore diameter/pore volume to obtain highest activity. Further, the catalyst textural

properties to obtain highest sulfur and nitrogen conversions also depend on the feedstock. For heavy gas oil derived from Athabasca bitumen pore diameter in excess of 10 nm is desirable largely due to the high molecular weight compounds being hydrotreated. Similarly, the surface area must be greater than 250 m^2/g to provide sufficient active sites for HDS and HDN reactions.

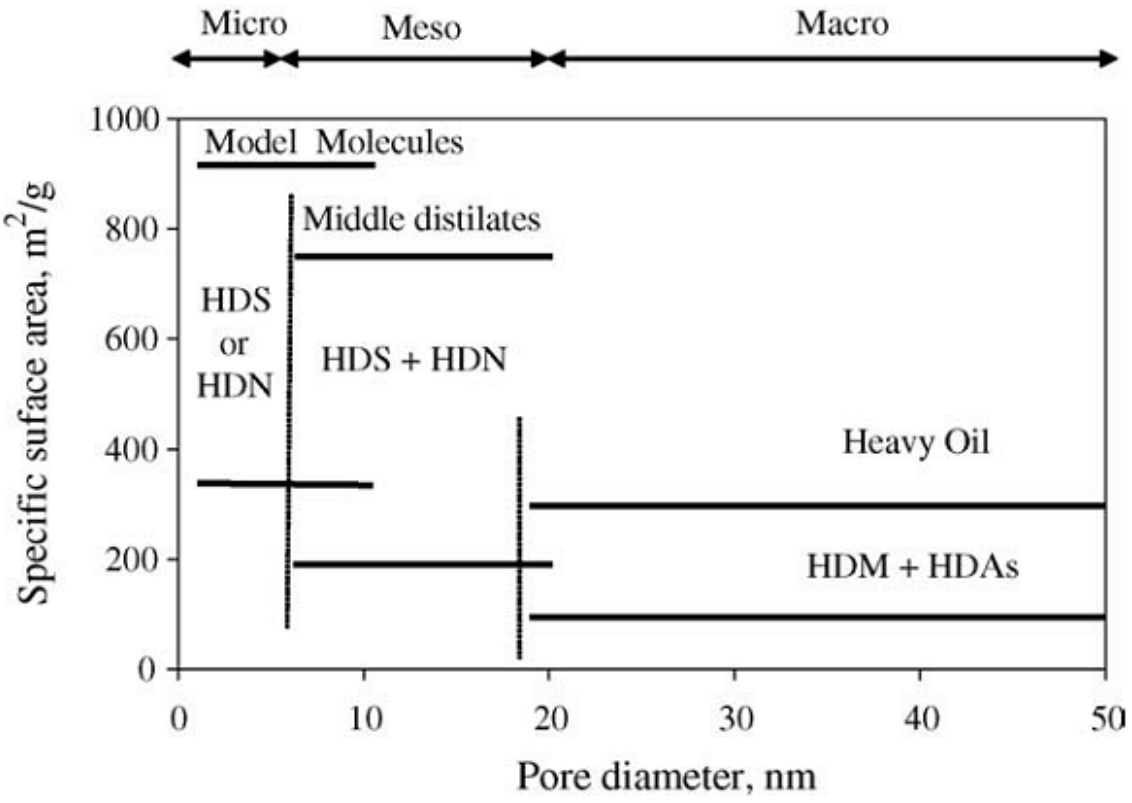

Figure 2.22: Effect of pore diameter and specific surface area on hydrotreating catalyst activities (Ancheyta et al., 2005)

2) Acidic functionalities – In heavy oil hydroprocessing, the role of acidic catalysts has been highlighted by numerous studies (Absi-Halabi et al., 1991; Ancheyta et al., 2005; Perot, 2003). Certain isomerization and dealkylation reactions necessary to remove the refractory

dialkyl dibenzothiophenes are only specific to acidic sites in the catalyst. These acidic sites could be either Bronsted or Lewis depending on the catalyst support used. Further, with increasing demand for middle distillates, mild hydrocracking along with hydrotreating is desirable. The C-C bond scission reactions takes place on acidic sites of the catalyst. Alumina is the most widely utilized carrier for hydrotreating reactions, but has mainly Lewis acid sites. As a result, certain reactions like shifting the methyl groups from 4,6 to 3,7 or to 2,8 positions in 4,6 DMDBT through an isomerization reaction to decrease the steric hindrance is not possible in pure alumina supports. Other support materials with strong acidic functionalities such as TiO_2, ZrO_2, zeolites, amorphous silica alumina (ASA) or other alumina mixed supports easily carry out the isomerization of the methyl groups in 4,6 DMDBT, thus increasing the rate of HDS as compared to catalysts supported on alumina (Bej et al., 2004b). However, highly acidic catalysts may lead to successive scission of the C-C bonds leading to the formation of coke on the catalyst surface. The effect is even more observed in heavy gas oil hydrocracking where the life of an acidic catalyst is greatly reduced due to coke formation (Absi-Halabi et al., 1991b). Thus there is a need to optimize the acidic functionalities and the hydrogenating properties of the catalyst.

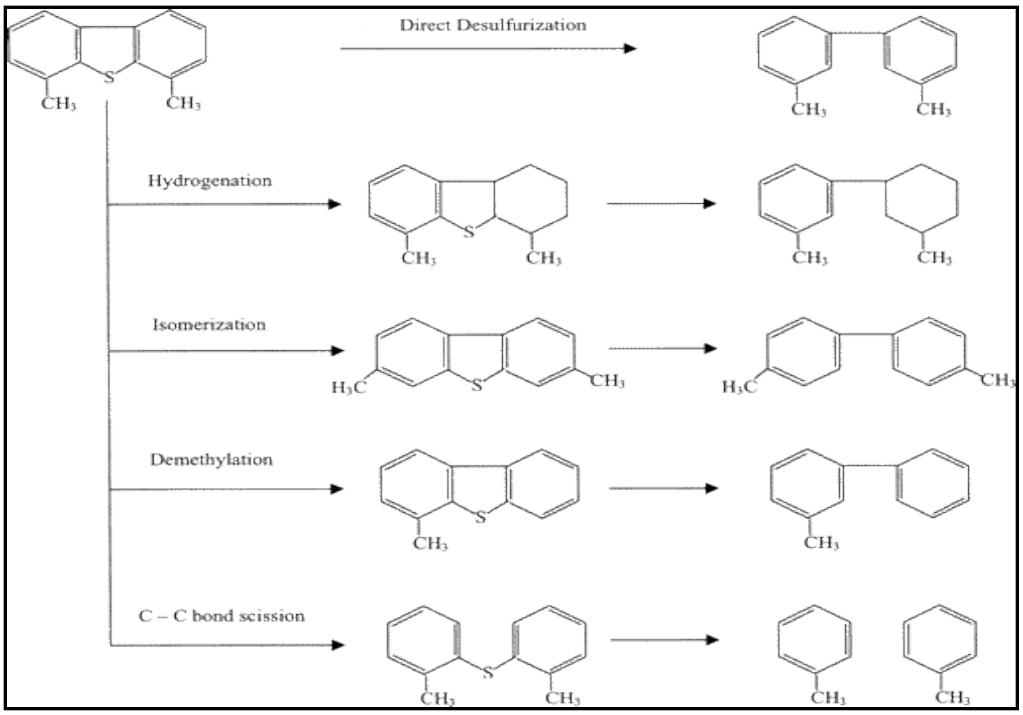

Figure 2.23: Possible reaction pathways for enhancing the reactivity of 4,6-DMDBT (Bej et al., 2004)

3) Genesis of Active Phase - The terms active site and active phase are used as follows: The active site is the transition metal ion facilitating (through its S vacancies or S ions) the adsorption of the reactant molecule (heterocyclic compound or hydrogen). The active phase is the active site plus the ensemble of transition metal and sulfur ions making this site active. The active phase is situated either on the surface of larger metal sulfide crystallites or, as very small clusters, directly on the support. The creation and the number of available active sites depend on a lot of factors. The preparation method of the catalyst, the active metals used in the catalyst, sulfidation procedures employed for catalyst activation, the metal support interaction in the catalyst etc. Some of the above have already been discussed and some of the other key factors will be discussed in the later sections.

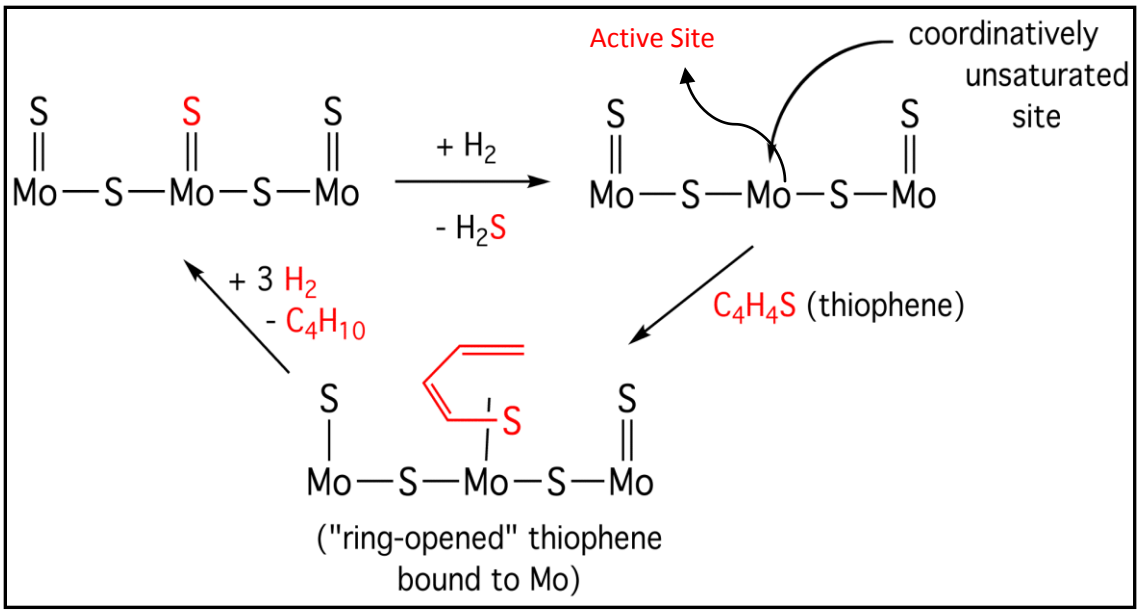

Figure 2.24: Mechanism of thiophene HDS on active site

The creation of Type I and Type II sites has already been discussed. Additionally, various studies have proved that Type II sites with multiple stacks of MoS_2 have higher intrinsic activity than single layered Type I sites. For heavy gas oil hydrotreatment, it is important that the catalyst sulfidation is maximized with the focus on creating more active Type II sites.

In the above context, some of the important properties of conventionally used NiMo/γ-Al_2O_3 catalyst are tabulated below:

Table 2.8: Desirable properties in a conventional NiMo/ γ-Al_2O_3 catalyst

Properties	NiMo/γ-Al_2O_3	Comments
Textural Properties	Surface Area - 150 - 300m^2/g	Can be improved
	Pore Diameter - 7 -15 nm	Mostly bimodal
Acidity	Moderate, Mostly Lewis acid sites	Low acidity, hydrocracking not favorable
Metal Support Interaction	Very Strong	Leads to incomplete sulfidation and Type I sites
Dispersion	Mo Loading of ~ 21 wt % without bulk formation	Excellent

There have been various attempts to improve the acidity as well as textural properties of γ-Al_2O_3 support. The use of mixed oxides, ordered mesoporous materials, zeolites etc have focused on improving the textural properties and the acidity of the support material. Similarly, a lot of research has also been done to optimize the metal-support interaction to increase the concentration of Type II sites. The use of carbon and silica with relatively lower metal support interaction has been a topic of numerous studies. Similarly, chelating ligands like ethylene diammine tetra acetic acid (EDTA), citric acid (CA), nitrilo acetic acid (NTA) etc have been used to improve the sulfidation of the NiMo catalyst and generate more Type II active sites.

2.11 Approaches for Developing Better Catalysts

Based on the previous works, various experiments and studies have been undertaken to develop better catalysts with higher HDS and HDN activities. These have included the use of new supports or modifications of the existing alumina based supports, use of different active phases like nitride, carbide, phosphide etc, different synthesis procedures and precursors like CVD and organo-metallic compounds, use of noble metals like Pt, Pd to improve hydrogenating functionalities etc. Figure 2.25 gives a general classification of various ways to improve the HDS of the most refractory 4,6 DMDBT compound.

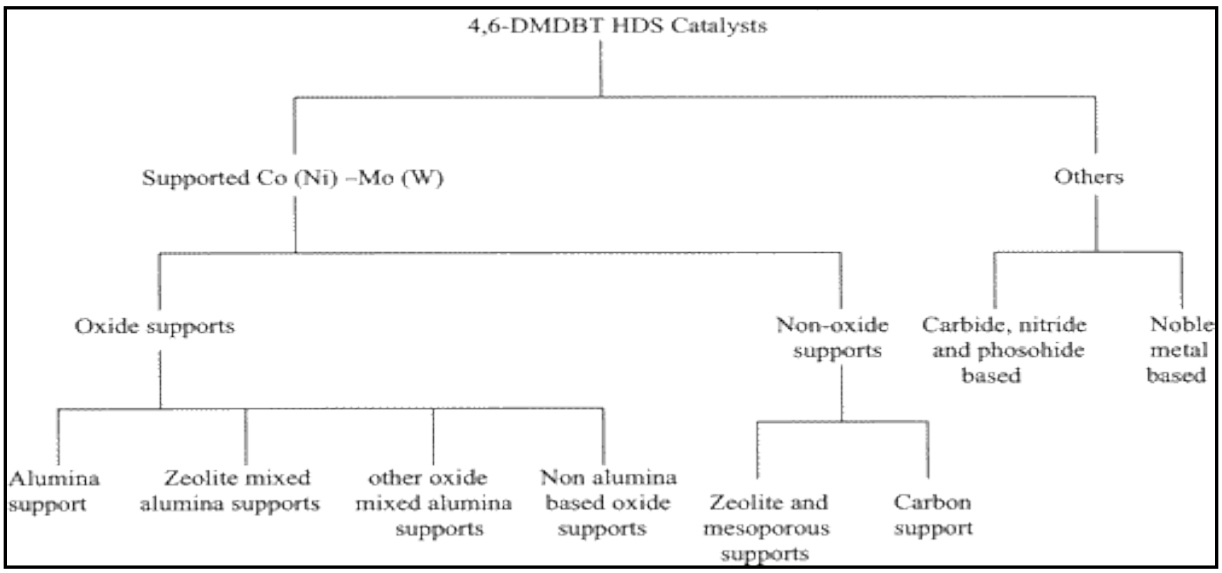

Figure 2.25: A general classification of the catalysts holding potential for the removal of 4,6-DMDBT(Bej et al., 2004).

2.11.1 Review of Support Materials

A lot of focus has been on the modification of the γ-Al_2O_3 support. The role of support in hydrotreating reactions has been discussed in numerous articles and reviews (Breysse et al.,

1991; Breysse et al., 2003; Breysse et al., 2008; Ramirez and Sanchez-Minero, 2008). Some of the most important functions of the catalysts support are listed below:

1) Stabilization of the active phase and active sites
2) Provide good dispersion to the active metals
3) Provide good surface and textural properties to the catalyst
4) Improve the acidity of the catalyst to promote isomerization and dealkylation reactions
5) Reduce the formation of spinel phases of promoter atoms ($NiAl_2O_4$ and $CoAl_2O_4$)
6) Modification of the reducibility of oxide precursor through change of the interaction between the active phase and support (Grange and Vanhaeren, 1997)

2.11.1.1 Oxide Supported Catalysts

Oxide based catalysts have received considerable attention as means to improve the hydrotreating activity of the catalysts. NiMo, NiW and CoMo catalysts have generally been used as the active components supported on γ-Al_2O_3. Various efforts have been made to increase the activities of conventional CoMo-based alumina catalysts by incorporating more hydrogenation capabilities in these materials. These include loading of the active metals in greater amounts, improving dispersion of the active metals, and manipulating the acidity level of the alumina support. The first two objectives have been achieved by increasing the surface area of the support and also by using better metal loading techniques (Mignard et al., 1996) .

The use of mixed oxide alumina-supported CoMo- or NiMo-based catalysts have provided encouraging results for the HDS of thiophene and benzothiophene (Barrio et al., 2003; Dhar et al., 2003; Grzechowiak et al., 2003; Rana et al., 1999). Lecrenay et al reported that activities of the mixed Al_2O_3–TiO_2-supported catalysts were higher than that of the alumina-supported ones

in the HDS of 4,6 DMDBT. The highest activity was observed for a CoMo-based catalyst supported on Al_2O_3−TiO_2 mixture containing 25 wt % of TiO_2. They attributed the increase in activity to the improvement in acidity and hydrogenation capabilities of the catalyst with incorporation of TiO_2 into the support framework (Lecrenay et al., 1998a; Lecrenay et al., 1998b).

The same group of researchers studied the activities of CoMo and NiMo catalysts supported on alumina mixed with other oxides such as ZrO_2−Al_2O_3 and B_2O_3−Al_2O_3 for the HDS of 4,6-DMDBT (Lecrenay et al., 1998b). The ZrO_2 and B_2O_3 contents in the mixed support were 20 and 15 wt %, respectively. The acidity of these supported materials, increased with the addition of the second oxide. In this case also, all the CoMo-based catalysts showed higher acidity as compared to that of the NiMo-based materials. The hydrogenation capabilities of the catalysts, as evident from the naphthalene hydrogenation activities, also increased.

A mixture of alumina and amorphous silica−alumina was also used as a support for loading CoMo oxides (Lecrenay et al., 1997). The activity of the alumina and amorphous silica−alumina mixed supported CoMo catalyst was higher than the conventional $CoMo/Al_2O_3$ catalyst. Robinson et al. used amorphous silica alumina (ASA) as a support for NiMo catalysts for the HDS of 4, 6-M-DBT in the hopes of taking advantage of the strongly acidic properties of ASA. The HDS rate for the ASA-supported NiMo catalyst was higher than that of alumina-supported commercial CoMo as well as NiMo catalysts (Robinson et al., 1999).

Similarly non alumina based oxide supports have also been studied in great details. Landau et al. reported that the activity of a SiO_2-supported NiMo catalyst for the HDS of 4,6-DMDBT was higher than that of $CoMo/Al_2O_3$ and $NiMo/Al_2O_3$ catalysts (Landau et al., 1996; Maity et al., 2001). Also, the combinations of two mixed oxides supports such as TiO_2- ZrO_2, SiO_2-ZrO_2 and

SiO_2-TiO_2 have been tested as hydrotreating catalyst. The combination of two oxides observed to be more effective as HDT catalyst supports. For example, ZrO_2 –TiO_2 mixed oxide with specific surface area 254 m^2/g was studied as catalyst support and proved to be promising for the HDS reaction (Maity et al., 2001).

2.11.1.2 Zeolite – Alumina Supported Catalysts

The use of zeolites (ZSM-5, HY and β-zeolites) in hydroprocessing of heavy gas oils has been reported in literature before. However, the application of pure zeolites as supports is limited due to the small pore size of the zeolites, especially for heavy gas oil hydrotreating and hydrocracking. On the other hand, the incorporation of zeolites into the framework of alumina can have an important effect on product selectivity and conversion (Isoda et al., 1996; Turaga et al., 2003). The important steps for synthesis of zeolite based catalysts are shown in Figure 2.26 (Leyva et al., 2007).

Several studies have found that a combination of Ni–Mo sulfide catalyst with zeolites is a promising approach to next generation hydrotreating catalysts. Mann et al. studied the HDS and hydrodenitrogenation (HDN) of heavy gas oil over NiMo sulfide catalysts supported on zeolite–alumina–silica at 350 – 425 ^oC, and they found that this combination of catalysts can remove as much as 99% S and 86% N at 425 ^oC (Mann et al., 1988). Shimada et al. compared the catalytic activities of coal derived liquids over a series of Ni–Mo/Al_2O_3–HY zeolite catalysts. They found that the HYD activity decreased and HC activity increased with the proportion of Y zeolite in the support and that the HDN and HYD activities of the zeolite-supported catalysts are generally poorer than those of alumina-supported catalysts (Shimada et al., 1990). More recently, Yumoto

et al reported a new type of Al_2O_3–zeolite-based catalyst for deep HDS, and found that a small amount of zeolite accelerates the hydrogenation rate of the DBT ring (Yumoto et al., 1997).

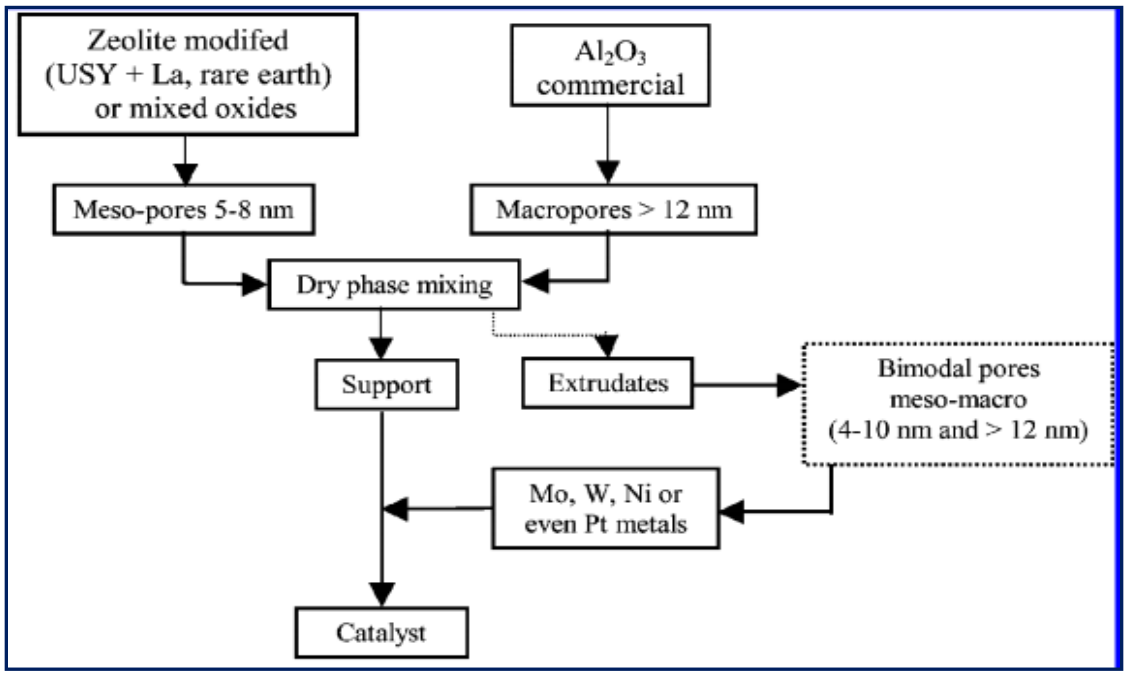

Figure 2.26: Synthesis of catalysts for (a) zeolite-based or dry extrusion method of support preparation on the use of acid, (Leyva et al., 2007)

Kunisada et al attempted to optimize the coating of USY-zeolite with alumina, aiming at the best supports of alumina and alumina coated USY-mixture for NiMoS to achieve deep HDS of gas oil with the least cracked hydrocarbon product and probably lower deactivation. By optimizing the acidic strength, reducing the direct contact of acidic surface with the substrates, and locating NiMoS in the vicinity of the acidic site to hydrogenate the adsorbed species, they were able to achieve high HDS activity (Kunisada et al., 2004).

2.11.1.3 Mesoporous Materials Supported Catalysts

Very recently, ordered mesoporous materials with high surface areas and large pore diameters with a narrow pore size distribution have been shown to have interesting properties in hydrotreating reactions. Mesoporous materials have pore diameters in the range 5 nm – 30 nm. These materials have high hydrothermal stability, their textural properties are better than those of the traditional γ-alumina support and the pore size and shape are especially appropriate for the transformation of large organic molecules, such as sulfur-containing compounds of the dibenzothiophene type. Variety of ordered mesoporous silica (OMS) materials have been synthesized and tested for catalytic activity in hydrotreating reactions. Dhar et al reported the HDS and hydrogenation activity of Mo/SBA-15, CoMo/SBA-15 and NiMo/SBA-15 using thiophene and cyclohexene as the feedstock respectively. They found that the catalysts supported on SBA-15 showed superior hydrodesulfurization and hydrogenating activities compared to their γ-Al_2O_3 counterparts (Dhar et al., 2005). Sundarmurthy et al compared the hydrotreating activities of SBA-15, Al-SBA-15 and B-SBA-15 using light gas oil as the feedstock. The catalytic studies with different Mo loadings revealed that an optimum Mo loading of 17 wt %. The NiMo/Al-SBA-15 sulfide catalyst with Mo loading (17 wt %) showed HDN and HDS activities similar to the conventional NiMo/γ-Al_2O_3 sulfide catalyst with real feedstock (Sundaramurthy et al., 2008). Similar studies using the same feedstock was done by Soni et al who reported the influence of frame connectivity of SBA-15 and KIT-6 supported NiMo catalysts for hydrotreating of gas oil. In their work they demonstrated that KIT-6 supported catalysts shows much higher hydrodesulfurization (HDS) and hydrodenitrogenation (HDN) activities compared to SBA-15 counterpart due to the fact that 3D-interconnected

mesopores caused better dispersion of active species and faster diffusion of reactants and products (Soni et al., 2010).

Obtained results clearly show the advantages of the SBA-15 materials in comparison with the conventionally used γ-alumina support, even though it is well-known that the interaction between silica and Mo(W) species is very weak, and the dispersion of the sulfided active phases is low and inhomogeneous (Hensen et al., 2001). In further works, attempts to overwhelm the drawbacks of the pure silica SBA-15 support and improve its interaction with HDS active species were made. Thus, it was proposed to modify SBA-15 with different heteroatoms using synthetic or post-synthetic methods (Garg et al., 2008; Gutierrez et al., 2006; Gutierrez et al., 2007; Gutierrez et al., 2008; Hensen et al., 2001; Klimova et al., 2009). In general, improvement of the catalytic activity and some changes in the selectivity were observed when M-SBA-15 supports of different chemical compositions (M = Al, Ti, Zr, W, etc.) were tested. These changes were attributed to an increase in the dispersion of Ni and Mo(W) species and in their reducibility. The most promising results were obtained when Zr- and W-containing SBA-15 materials were used as supports for NiMo and NiW catalysts for deep hydrodesulfurization. Murali Dhar and co-workers prepared SBA-15 and ZrO_2-containing SBA-15 materials with zirconia loading between 10 and 50 wt.% and tested them as supports for Mo, CoMo and NiMo catalysts (Garg et al., 2008b). Catalytic activities of these catalysts were evaluated for hydrodesulfurization of thiophene and hydrogenation (HYD) of cyclohexene. For HDS of thiophene over Mo, CoMo, and NiMo catalysts increased when SBA-15 was substituted by ZrO_2-SBA-15 with 25 wt.% of zirconia. At the same time, Mo and CoMo/ZrO_2-SBA-15 catalysts showed lower HYD activity than the corresponding catalysts supported on pure silica SBA-15, while the HYD activity of NiMo/ZrO_2-SBA-15 was higher than that of NiMo/SBA-15. A comparison of HDS and HYD activities of CoMo catalysts supported on SBA-15 and TiO_2- and ZrO_2-containing SBA-15

materials also confirmed the above observation, namely, while the incorporation of titania and zirconia into SBA-15 material resulted in an increase in the activity for HDS, activity for HYD decreased.

2.11.1.4 Carbon Supported Catalysts

Carbon support present many advantages such as minimized metal–support interaction which facilitates sulfidation and dispersion, large specific surface area and controlled pore volume (Klimova et al., 1998). CoMo carbon-supported catalysts were found to be more active than alumina-supported catalysts for both DBT and 4,6-DMDBT hydrodesulfurization (Wang et al., 2002) . Prabhu et al evaluated the catalytic properties of NiMo supported on mesoporous carbon with light gas oil as feedstock. The HDS and HDN activity was found to be higher than a commercial NiMo/γ-Al_2O_3 catalyst. They attributed the higher activity to weaker metal support interaction and the large surface of mesoporous carbon (Prabhu et al., 2011).

2.11.2 Effect of Chelating Ligands

As discussed earlier, the active phase in a typical NiMo catalyst is categorized into two types; Type I phase and Type II phase. The Type I NiMoS phase is marked by single layers of MoS_2 slabs with Ni atoms decorating the edges of the slabs. On the contrary, the Type II NiMoS phase has multiple layers of MoS_2 slabs with Ni atoms on the edge of the slabs. Another key difference is the presence of the sulfided metal-support interaction of the type Mo-O-Al in the Type I phase. This feature is generally absent in the Type II active phase, where the Mo is assumed to be completely sulfided. Further, the activity of the Type II sites has been reported to be twice that of the Type I site. It is, accordingly, expected that highly active nickel molybdenum catalysts are

composed of a highly dispersed NiMoS Type II phase. An important step in the effective formation of Type II NiMoS phase is that the transition of oxidic Ni to sulfided Ni should occur during or after the transformation of MoO_3 into MoS_2. Chelating agents such as nitrilotriacetic acid (NTA), ethylenediaminetetraacetic acid (EDTA), and derivatives of these molecules stabilize Ni and Co with respect to sulfide formation to temperatures where all or most of the Mo have converted to sulfides(Sundaramurthy et al., 2005) . These procedures enable one to prepare highly active CoMoS, NiMoS catalysts irrespective of the support. Thereafter, Medici and Prins compared the chemistry of $NiMo/SiO_2$ catalysts prepared in presence and absence of nitrilo acetic acid (NTA) (Medici and Prins, 1996b). NiMo Catalyst precursors prepared with the NTA-recipe and supported on either SiO_2 or Al_2O_3 were complexed with NTA. Ni was mainly present as $[Ni(NTA)(H_2O)_2]^-$, independent of the Ni:Mo and Ni:NTA ratios. During drying, NH_3 evaporated and coordinated H_2O was replaced by surface groups of the support. The catalysts made by sequential impregnation in the absence of NTA have different Ni^{2+} environments from their NTA counterparts. When Ni was impregnated first, $Ni(OH)_2$ crystallites were formed on the SiO_2 surface, and Mo is attracted by the positive surface of the $Ni(OH)_2$ crystallites during the second impregnation step . In their subsequent work, Medici and Prins, reported the HDS of thiophene on $NiMo/SiO_2$ catalysts prepared with and without NTA (Medici and Prins, 1996a). Using, Ni and Mo K edge EXAFS, they concluded that in the absence of NTA, Ni was present in the sulfided catalysts as a mixture of Ni_3S_2 and the catalytically active NiMoS phase. However, no Ni_3S_2 was determined when the catalyst was prepared using NTA. They attributed the the stability of the $[Ni(NTA)(H_2O)_2]^-$ complex at temperatures upto 220 ^oC against the very aggressive H_2S/H_2 mixture. Therefore, the Ni is sulfided just before the MoS_2 phase is formed and does not sinter to Ni_3S_2 but is deposited on the edges of the MoS_2 crystallites forming large amounts of the "NiMoS" phase. In contrast, when the Ni is already sulfided at low temperature,

the nickel sulfides into other thermodynamically stable Ni_3S_2 phase due to the absence of MoS_2 (Coulier et al., 2000). In order to further elucidate the effect of the $[Ni(NTA)(H_2O)_2]^-$ complex on the sulfidation of Ni, Cattaneo et al studied the activity of $NiMo/SiO_2$ prepared using a host of organic ligands in the hydrodesulfurization of thiophene at atmospheric pressure(Cattaneo et al., 1999). They observed that catalysts prepared using ethylene diaamine (EN) and NTA exhibited significantly higher catalytic activity for EN/Ni and NTA/Ni ratios of 0 to 4. A comparison of the catalytic activities is given in Figure 2.27.

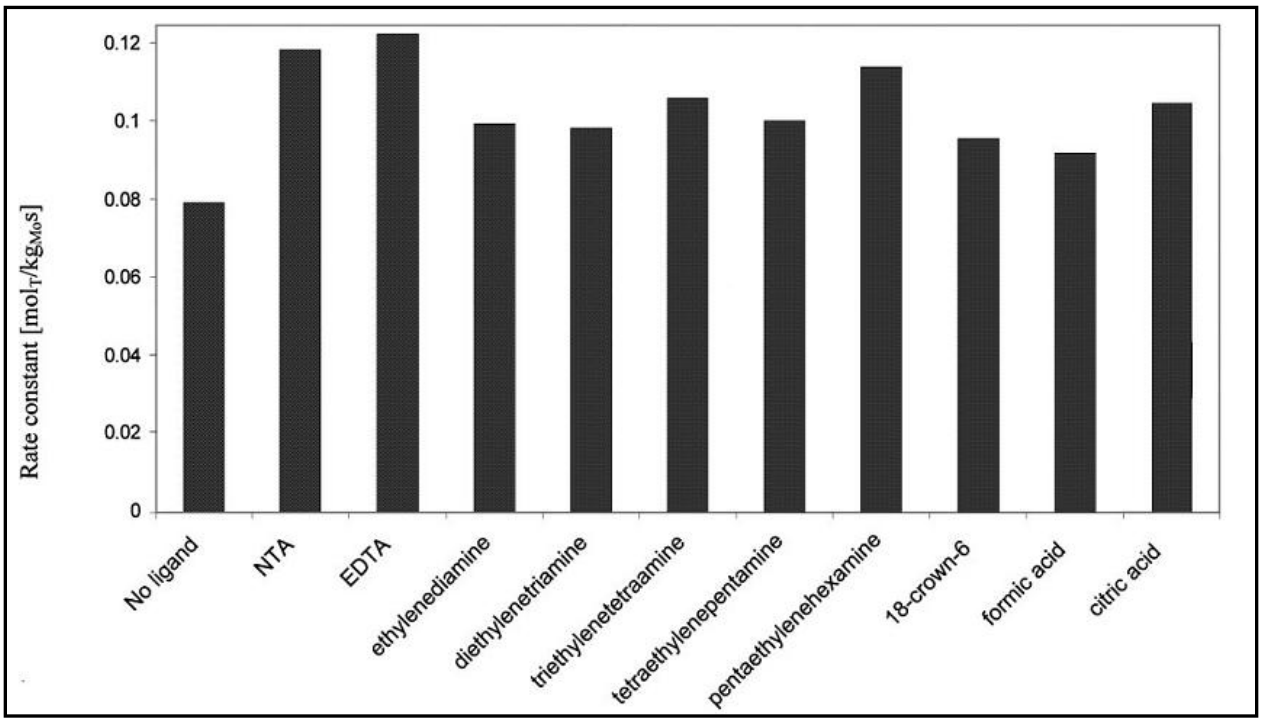

Figure 2.27: Activity of $NiMo/SiO_2$ catalysts prepared by adding different ligands (Cattaneo et al., 1999)

They explained the increase in activity to be due to the decreased interaction of Ni with the support. Further in case of NTA, the stable $[Ni(NTA)(H_2O)_2]^-$ was seen to retard the sulfidation of Ni at lower temperatures (Cattaneo et al., 1999).

The effects of chelating ligands on the activity of hydrotreating catalysts have also been reported with real feedstocks. Sundarmurthy et al reported the catalytic activity of sulfided CoMo/γ-Al_2O_3 on the hydrotreating of heavy gas oil derived from Athabasca bitumen. On EDTA addition to CoMo catalyst, the apparent rate constant for HDN bitumen at 400 ^oC increased by 24.2%, and 36% for dimethyl aniline (DMA) at 300 ^oC (Sundaramurthy et al., 2005). Escobar et al used ethylenediamine tetraacetic acid (EDTA) and citric acid (CA) organic chelating additives in NiMo catalysts with wide-pore ZrO_2–TiO_2 mixed oxides as carrier (Escobar et al., 2008b). They observed a clear beneficial effect of either chelator in the dibenzothiophene hydrodesulfurization reactions. Additionally, they pointed out that augmented chelators concentration resulted in catalysts of decreased hydrodesulfurizating properties probably due to delayed sulfidation of complexated molybdenum that could be formed by reaction of Mo^{6+} containing species with organic additive excess.

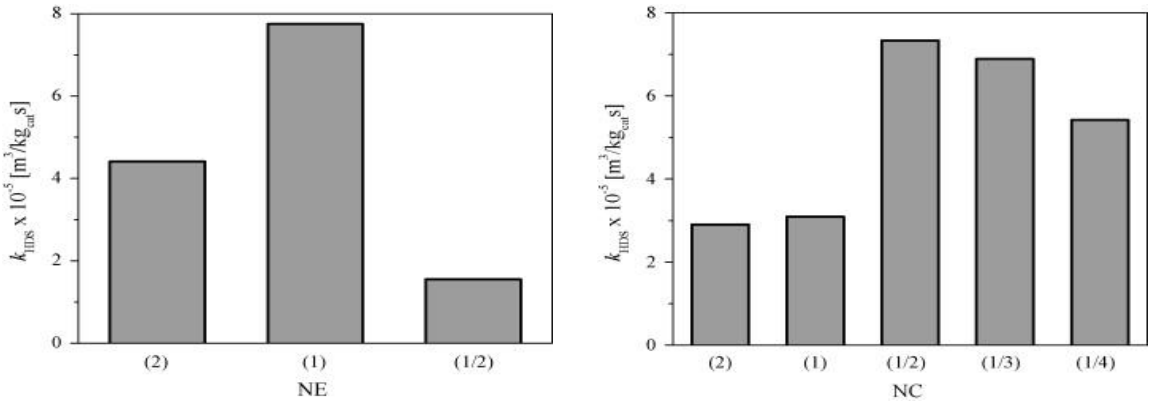

Figure 2.28: Dibenzothiophene hydrodesulfurization activity of sulfided NiMo/ZrO_2–TiO_2 catalysts impregnated at various a) Ni/EDTA ratios and b) Ni/CA ratios (Escobar et al., 2008).

Characterization by thermal analyses (TGA, DTA) and infrared spectroscopy pointed out to delayed Ni^{2+} sulfidation (to temperature high enough to be efficiently integrated to then already

formed MoS_2) as the main cause of HDS activity improvement in catalysts prepared in presence of organic chelators.

2.12 Mesoporous alumino-silicates (MAS) assembled from zeolite nano seeds

Mesoporous silica materials such as MCM-41, HMS, SBA-15 and KIT-6 with open porous channels are ideal catalyst supports for the catalytic conversions of large molecules as they can overcome the diffusion barrier for reactants and products (Nava et al., 2007; Soni et al., 2009; Turaga and Song, 2003; Dhar et al., 2005). In spite of their excellent textural properties the applications of these materials in catalytic reactions where acidity plays an important role is very limited. This restriction stems from the absence of strong Bronsted acid sites as their surface is predominantly made of silanol groups (Prabhu et al., 2009). In order to overcome the disadvantages of both zeolites and siliceous mesoporous materials, various teams have synthesized materials with strong acidity in open porosity through the surfactant based assembly of zeolite nano clusters present in the precursors that nucleate to form the final crystalline zeolite. This approach has been demonstrated by the successful assembly of ZSM-5 (MFI), Beta (BEA), HY (FAU) zeolite nano clusters resulting in a mesoporous structure with strong acid sites (Han et al., 2002 Liu et al., 2000; Liu et al., 2001; Liu and Pinnavaia, 2002; Liu and Pinnavaia, 2004). The main advantage of this type of approach is the complete or nearly complete incorporation of aluminum atoms into the silica framework in a tetrahedral coordination similar to that observed in zeolites. In comparison post synthesis and direct synthesis methods for Al incorporation into silica framework of various mesoporous materials have resulted in octahedral aluminum being present as extra framework atoms.

The fine characterization and the study of the mechanistic assembly of the zeolite nano clusters present in the precursor solution have led to the conclusion that the duration of hydrothermal treatment of the zeolite precursor solution containing the zeolite nano clusters is a key parameter to adjust the final properties of the resulting material (Klimova et al., 2008). Zebib et al reported the transition of MCM-41 type material synthesized from β zeolite seeds from an amorphous phase to a crystalline one for hydrothermal treatment durations between 6 to 16 hours (Zebib et al., 2005). Assembly of metal-silicate nano-clusters into mesoporous materials by the use of a templating agent as a possible method for incorporating hetero metal atoms into silica framework has been the focus of a lot of studies. Mesoporous structures with high hydrothermal stability and catalytic activity have been prepared from zeolite Y seeds and zeolite β primary structures. A thorough study of the aggregation mechanism of the zeolite seeds has been proposed by deMoor et al, who showed the existence of two different species of zeolite nano-particles (2.8 nm and 6 nm) using SAXS and DLS (de Moor, Peter-Paul E. A. et al., 1999). Similarly Zhang et al have synthesized mesoporous materials using preformed zeolite nano-clusters as precursors to assembly with surfactant templates in acidic (Zhang et al., 2001) and basic media (de Moor, Peter-Paul E. A. et al., 2000) alike. In all cases, a higher catalytic activity of the materials has arisen from zeolite-like connectivity of AlO_4 and SiO_4 tetrahedra in the frame work walls, and also high thermal stability of the resulting meso-structures was observed.

In this context the assembly mechanism of zeolite seeds into crystals has received a lot of attention. The different phases of the growth of the crystals from the precursor solution have been elucidated using techniques like NMR, SAXS, USASXS, DLS etc (Aerts et al., 2007; Ravishankar et al., 1998). The formation of ZSM-5 and Silicalite, the all silica counterpart of ZSM-5 has been well documented in literature. The formation of unusual silicate oligomers during the hydrolysis of tetraethylorthosilicate (TEOS) in aqueous TPAOH was recently

observed using ^{29}Si NMR (Follens et al., 2008; Kirschhock et al., 1999). A model was then proposed by Kirschhock et al in which silicalite-1 crystallization takes place via nano-slab aggregation mechanism (Kirschhock et al., 1999). The effect of hydrothermal treatment has been known to play a major role on the rate of assembly of the nano slabs and subsequent crystallization. Hydrothermal treatment plays an even greater role while assembling zeolite nano-crystals into mesoporous materials. Larger nano-particles are often difficult to assemble using a surfactant templating approach owing to thin pore walls of the resulting structure. The resulting structure is observed to be made of two separate phases then instead of a composite. MCM-41 type materials which are synthesized in basic medium are seen to collapse due to the growth of zeolite nano-particles which are favored under basic conditions (Huang et al., 2000; Trong On et al., 2001).

Interestingly all works conclude an enhanced catalytic activity for such materials in acid catalyzed reactions. The cumene cracking activity was found to be comparable to ZSM-5 and higher than ZSM-5 for the cracking of Tri iso propyl benzene (TIPB) (Frunz et al., 2006). Similarly favorable results were obtained in hydrocracking reactions and HDS of 4,6 DMDBT when these materials were used as supports for the NiW sulfide phase (Zeng et al., 2005).

2.12.1 MAS as hydrotreating catalyst supports

Very limited studies are available on the use of mesoporous alumino silicate materials prepared from zeolite nano seeds as catalyst support in hydrotreating and hydrocracking reactions. Zeng et al have reported the use of nickel-tungsten sulfides catalysts supported on silica–alumina mesostructures assembled form zeolite BEA seeds for hydrocracking reactions (Zeng et al., 2005; Zeng et al., 2006). They observed that the nature of the acidic support, either a purely mesoporous material or a mixture of BEA zeolite and mesoporous material can be adjusted by varying the duration of the hydrothermal treatment leading to the zeolite seeds solution. For low duration of the thermal treatment, the material resembled to a MCM-41 mesoporous solid but almost all the Al atoms are inserted in tetrahedral substitution in the silica network (even after calcination). The catalyst composed of a nickel-tungsten sulfide active phase supported on this support is more active and more selective toward isomerized products than the amorphous silica–alumina counterpart. When the duration of the thermal treatment increases, the materials formed resemble more to a zeolite, which leads for the NiW catalysts to a high activity but also to a low selectivity to isomerized products. In another study the same group reported the catalytic properties of the same catalysts for deep desulfurization reactions. They concluded that by using mesoporous materials assembled from BEA zeolite seeds as supports for a nickel–tungsten sulfide active phase, more active catalysts than their alumina-supported counterpart could be obtained for the conversion of 4,6-DMDBT. This enhancement of activity was also observed in the presence of dimethyldisulfide, carbazole and tetralin. They ascribed the modification of the catalytic properties to an electronic effect in and to a bifunctional type mechanism involving the migration of methyl groups through isomerization. Further, they showed that using the mesoporous-like material, it was possible to limit the undesirable side reactions, such as cracking

into light products, which were observed with zeolites and to a lesser extent with the mesoporous alumino silicate support prepared with higher hydrothermal treatment duration.

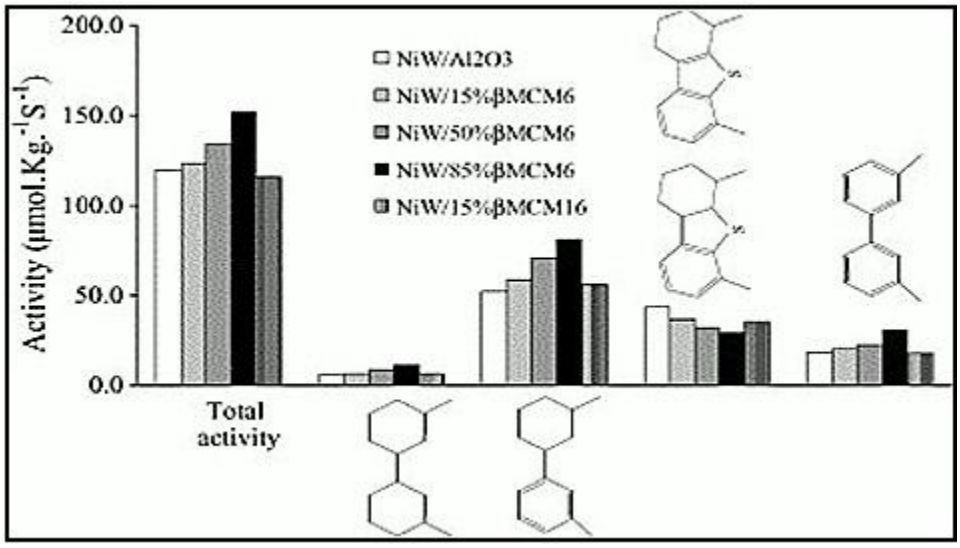

Figure 2.29: Activities of the NiW catalysts for the transformation of 4,6-DMDBT at 280 °C (Zeng et al., 2006).

Similarly, Huo et al synthesized a novel mesoporous zeolite L by the self-assembly of zeolite L nanocrystal clusters in the presence of template Triton X 100 (Huo et al., 2010). They demonstrated that the material possessed relatively high acid amount and acid strength, appropriate acid types, and a composite pore structure with micropores and mesopores. The catalyst with mesoporous zeolite L showed the excellent performances of deep desulfurization, aromatization, isomerization and preserving the research octane number (RON) for the hydrodesulfurization reaction of full-range FCC gasoline. They attributed the excellent catalytic performances of the catalyst to appropriate acidity distribution, high amount of Lewis acid sites and open pore structure of material M-L.

2.13 Effect of citric acid addition on the preparation of hydrotreating catalysts

The use of chelating ligands has been very effective in improving Type II NiMoS and CoMoS sites. When a chelating agent is added to the impregnation solution containing Co (or Ni) and Mo precursors, the formation of Co(Ni)–chelating agent complexes retards the sulfidation of the Co or Ni promoter until the sulfidation of Mo, leading to an increased number of Co(Ni)–Mo–S with suppressed formation of bulk Co or Ni sulfides. The use of citric acid (CA) as a chelating ligand is well documented in literature. From economic considerations, citric acid has advantages over other chelating agents like EDTA, NTA and CyDTA. Various authors have studied the hydrotreating activity of Ni(Co)Mo catalysts prepared with citric acid using various synthesis routes. Fujikawa et al prepared CoMo catalysts with citric acid and phosphorus and reported higher stability and ultra low sulfur products in pilot plant studies of straight run gas oil (Fujikawa et al., 2005a; Fujikawa et al., 2005b; Fujikawa, 2006). They ascribed the increased formation of highly active CoMoS Type II sites to the enhanced thermal stability of cobalt during sulfidation, due to the formation of the stable cobalt citrate complex. The influence of drying condition of the $CoMo/Al_2O_3$ catalyst prepared using citric acid as a chelating agent on the sulfidation behavior and on the catalytic activity to hydrodesulfurization of straight-run gas oil (SRGO) was investigated by Pashigreva et al. In another work, Klimov et al synthesized highly active bimetallic Co-Mo catalysts (Figure 2.30) for hydrodesulfurization of SRGO (Klimov et al., 2009; Klimov et al., 2010a; Klimov et al., 2010b). The bimetallic compounds with Co/Mo atomic ratio between 1:3 and 1:2 (i.e. the same stoichiometry as in the best reported HDS catalysts) were synthesized by coordination of Co^{2+} cations towards Mo-containing anions as follows: $[Mo_2O_4(C_2O_4)_2(H_2O)_2]^{2-}$, $[Mo_3O_4(C_2O_4)_3(H_2O)_3]^{2-}$, $[Mo_4O_{11}(C_6H_5O_7)_2]^{4-}$ and $[H_2Mo_5P_2O_{23}]^{4-}$. Sulfidation of the synthesized supported catalysts yielded bimetallic sulfide particles with the average size of 3 – 4 nm and the mean stacking number of 1.95–2.35 evenly

dispersed over the alumina surface. The surface composition of the obtained samples was found to be typical of catalysts containing CoMoS Phase Type II as an active phase.

Rinaldi et al, demonstrated the advantages of citric acid addition on $CoMo/B_2O_3/Al_2O_3$ a catalysts prepared using a post treatment route (Rinaldi et al., 2009a; Rinaldi et al., 2009b; Rinaldi et al., 2010). They concluded that the addition of citric acid by the post-treatment method to CoMo calcined catalysts [CA/CoMo/(B/)Al] improves the thiophene HDS activity more significantly than the addition of citric acid by the simultaneous-impregnation method [Co−Mo−CA/(B/)Al]. They observed that citric acid consumed the already dispersed $CoMoO_4$ and polymolybdate phase, thus increasing the dispersion of Co and Mo, resulting in larger amount of CoMoS phase. Further, they obtained an optimum CA/Mo molar ratio of 2. However, on further increase of CA, the HDS activity and the surface properties of the support were found to deteriorate.

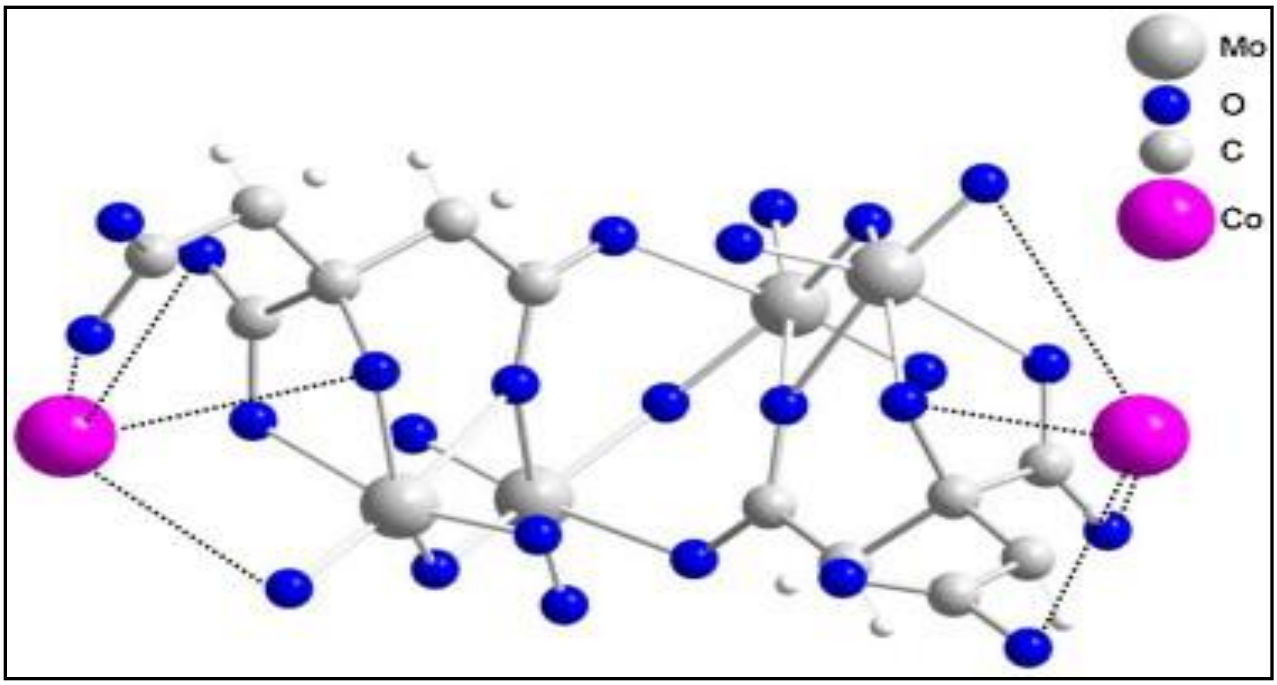

Figure 2.30: Tentative structure of the bimetallic complex $Co_2[Mo_4(C_6H_5O_7)_2O_{11}]$ (Klimov et al., 2010b)

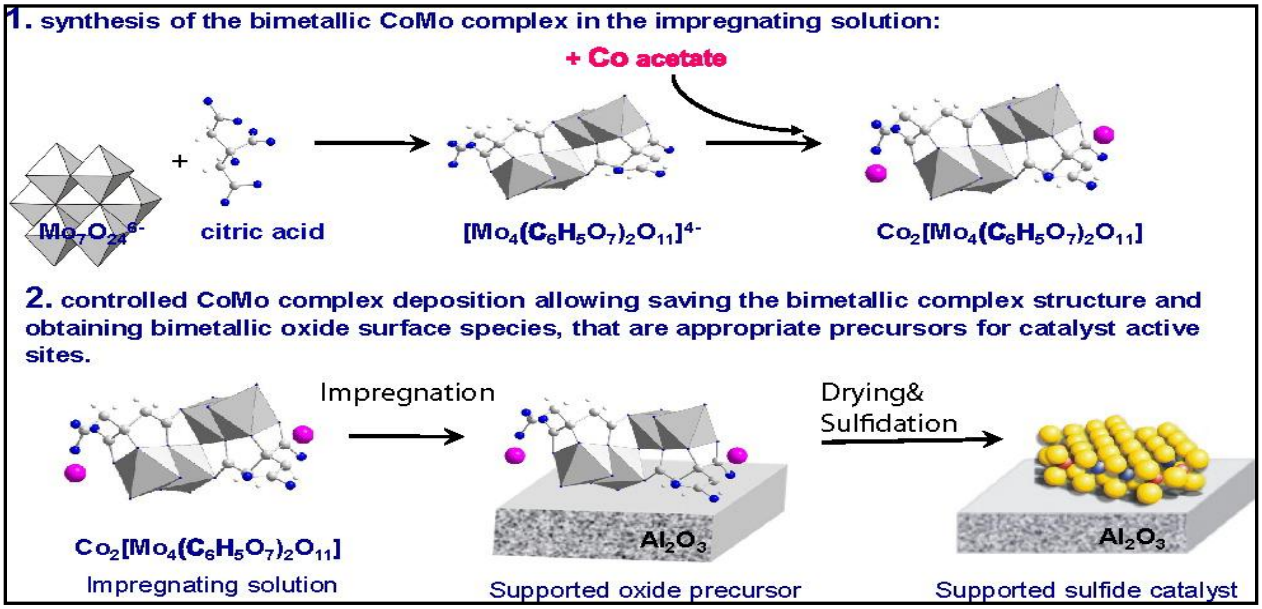

Figure 2.31: The preparation of catalysts via synthesis of bimetallic Co–Mo compounds from ammonium heptamolybdate, citric acid and cobalt acetate (Klimov et al., 2010a; Klimov et al., 2010b).

Regardless of the synthesis route, the sulfidation of Co is strongly suppressed by the CA addition to Co–Mo/B_2O_3/Al_2O_3 catalysts due to the formation of Co–CA complexes. Bergwerff et al. (Bergwerff et al., 2006) showed an increased Mo dispersion and enhanced HDS activity by the addition of citric acid in the impregnation solution.

In brief the role of citric acid on the hydrotreating activity of Co(Ni)Mo catalysts can be summarized as below :

1) It forms a stable complex with the promoter atom (Co, Ni) which delays the sulfidation of Co such that cobalt starts to sulfide just before the sulfidation of molybdenum. The near simultaneous sulfidation of cobalt and molybdenum leads to the formation of more Type II CoMoS sites.
2) Citric acid improves the dispersion of molybdenum oxide on the support surface by forming molybdenum citrate complex. Even at high loadings of Mo, crystalline phase of MoO_3 is not observed.
3) A bimetallic cobalt and molybdenum complex can be synthesized using citric acid. The sulfidation of the stable bimetallic complex results in the formation of a very active CoMoS phase.

CHAPTER 3
EXPERIMENTAL

This chapter deals with the synthesis of mesoporous alumino silicate materials (MAS) from ZSM-5 nano-seeds, preparation of the MAS mixed alumina materials as supports for the hydrotreating catalysts. Subsequent sections elaborate on the preparation of NiMo catalysts supported on the MAS - Al_2O_3 support using the pore volume impregnation method. A detailed description of the methods and equipments used for the characterization of the synthesized materials and catalysts is also given. In addition, a separate account of X-ray absorption technique is also provided. This section also describes the experimental conditions, hydrotreaters system set up and the trickle bed reactor configuration and loading procedure.

3.1 Preparation of Mesoporous Alumino Silicate from ZSM-5 nano seeds

The synthesis method was adopted from Han et al (Han et al., 2001). A typical synthesis procedure consisted of two steps; a) preparation of the ZSM-5 nano-seed solution, and b) Assembling the synthesized nano seeds in a surfactant based approach to form the final mesoporous material. The chemicals used for the syntheses were tetraethoxy silane (TEOS) (>98%, Aldrich), tetrapropylammonium hydroxide (TPAOH) (1.0 M in water, Aldrich), a triblock copolymer based surfactant P123 ($EO_{20}PO_{70}EO_{20}$) and sodium aluminate (BDH, Canada) as the aluminium source. The zeolite precursor solution was prepared mixing 14 mL of tetrapropylammonium hydroxide (TPAOH) aqueous solution , 0.35 g of $NaAlO_2$, and 24 mL of tetraethyl orthosilicate (TEOS) with 68 mL of H_2O under stirring

($Al_2O_3/SiO_2/Na_2O/(TPA)_2O/H_2O$ with molar ratios of 1.0/50/1.0/7/1800). The clear solution thus obtained was subjected to hydrothermal treatment at 100^oC in an autoclave for various durations. In all three precursor solution with the same chemical composition but different seeding times of 4, 16 and 24 hrs were prepared. Another precursor solution was prepared without any heating, but was aged for 2 hrs after stirring. The organization of the polymerizing silica present in the precursor solution was done using the ampiphilic triblock copolymer P123 as described by Zhao et al (Zhao et al., 1998). 10 g of $EO_{20}PO_{70}EO_{20}$ (Pluronic P123) was dissolved in 265 mL of H_2O with mL of HCl (10 M/L), followed by the addition of the precursor solution (containing 8 mmol of SiO_2) obtained in step one. The mixture was stirred at 40 °C for 24 h and then transferred into an autoclave for additional reaction at 100 °C for 36 h. The product was collected by filtration, dried in air, and calcined at 550 °C for 5 h to remove the organic template. The final samples were labeled as MAS-4, MAS-16 and MAS-24 in accordance with the heating times of the precursor solution.

3.2 Preparation of mixed MAS-γAl_2O_3 Support

The supports for the hydrotreating reactions were prepared by a physically mixing the MAS material and γ-Al_2O_3. Three different weight ratios of MAS were used for mixing. The support materials were so prepared that, the content of MAS in the final material was 0 wt %, 5 wt % and 10 wt % respectively. Subsequently the alumina content in the mixtures was 100 wt %, 95 wt % and 90 wt % respectively. De-ionized water was added to the MAS and alumina powder mixture and the wet mixture dried in an oven at 100 ^oC overnight. The mixture was then calcined at 450 ^oC for 4 hrs in order to get a homogenous mixture of MAS and alumina in the desired quantity.

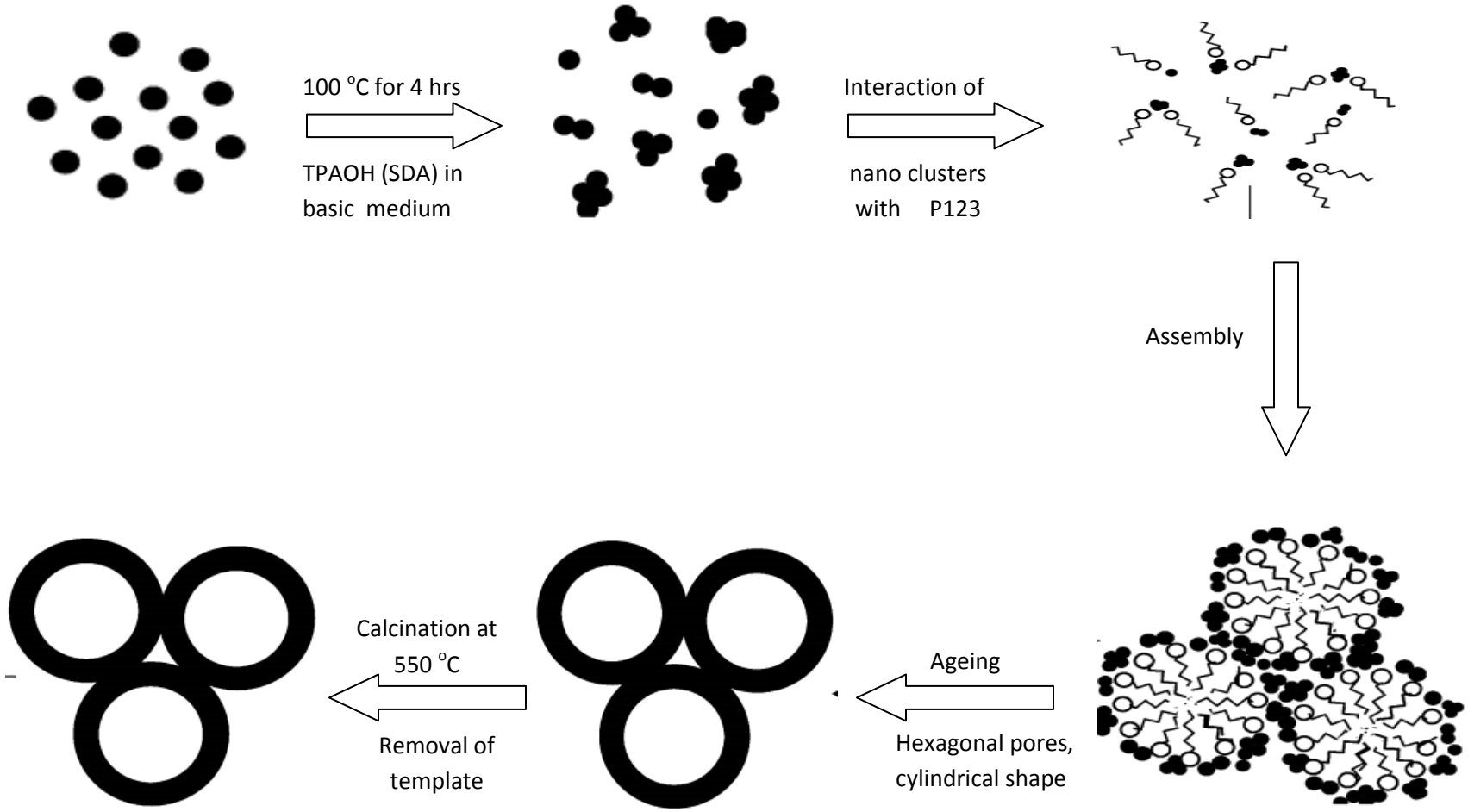

Figure 3.1: Schematic of the synthesis procedure for mesoporous alumino silicate (MAS) materials from ZSM-5 nano seeds

3.3 Preparation of reference materials

Al-SBA-15 and γ Al_2O_3 were used as the reference materials in this study. Al-SBA-15 was prepared using the direct synthesis route as described by Yue et al (Yue et al., 1999). The same Si/Al ratio of 25 was maintained for Al-SBA-15 as well. Aluminum nitrate was used at the Al source in the preparation method. The γ-Al_2O_3 support was procured from *La Roche Chemicals* and was used without any further modification.

3.4 Preparation of NiMo/MAS-γ Al_2O_3 Catalysts

NiMo loading on the MAS-Al_2O_3 supports were carried out through the standard pore volume impregnation technique. Ammonium heptamolybdate ($(NH_4)_6Mo_7O_{24}.4H_2O$) and nickel nitrate hexahydrate ($Ni(NO_3)_2.6H_2O$) were used as the molybdenum and nickel precursors respectively. Both the chemicals were procured from Sigma Aldrich Canada. The loading fractions of the metals on the catalyst have been described in the subsequent chapters. Standard successive impregnation approach was used while preparing the NiMo catalysts. Molybdenum was first impregnated on the support. The mixture was then dried overnight at 100 ^oC and then calcined at 550 ^oC for 4 hrs. Nickel was then impregnated on the calcined mixture. The final mixture was then dried and calcined at 500 ^oC for 4 hrs.

3.5 Preparation of Ni(Cit)Mo/MAS-Al_2O_3 Catalysts

The preparation route for the catalysts was a little different when citric acid was used. Molybdenum was first impregnated on the support and the mixture was then dried and calcined for 4 hrs and 550 ^oC. Citric acid was then dissolved in an ammonium hydroxide solution (20 wt

%) followed by dissolution of the nickel nitrate crystals. The color of the solution was observed to turn blue on the addition of nickel nitrate to the solution. The solution was then impregnated on the calcined Mo/MAS-Al_2O_3 using the standard pore volume impregnation method. The catalysts were then dried overnight at 120 ^oC. No calcination of the final catalysts were done when citric acid was present in the mixture. The detailed compositions of the catalysts are described in subsequent chapters.

3.6 Support and Catalyst Characterization

The synthesized supports and catalysts were characterized to determine the various physico-chemical properties and compositions. The characterization techniques and their protocols are described below.

3.6.1 Elemental Composition (ICP/MS)

Quantitative estimation of Si/Al ratio, Ni and Mo loadings was performed using inductively coupled plasma - mass spectrometer (ICP-MS). A catalyst sample (0.1 g) was dissolved in concentrated hydrofluoric acid (48-51 %) at a temperature of 100-150 °C for three days. After cooling, samples were further dissolved in concentrated HNO_3 to ensure the complete dissolution of the metals. The final solution was prepared using 0.2 N HNO_3 and analyzed with a mass spectrometer.

3.6.2 Small Angle X-ray Scattering (SAXS)

The low-angle X-ray diffraction patterns of the samples were measured using Bruker D8 Advance Powder diffractometer with a Ge monochromator, producing a monochromatic Cu Kα

(λ = 1.54 A^o) radiation. The scanning was made from 1.5^o to 10^o for the small angle measurements and 15^o to 60^o for the high angle measurements with a 2θ step size of 0.02^o, and a step time of 2s. In all cases, the generator was operated at 40 kV and 30 mA. To avoid the problem of illuminated areas at low 2θ angles, all the samples were measured using the same sample holder.

3.6.3 N_2 Adsorption-Desorption

The BET surface area, pore volume, and pore size distribution of the samples were measured with a Micromeritics ASAP 2000 instrument using low temperature N_2 adsorption–desorption isotherms. Before the measurement, each sample was degassed in vacuum at 200°C. The surface area was computed from these isotherms using the multi-point Brunauer-Emmett-Teller (BET) method based on the adsorption data in the partial pressure P/P_0 range from 0.01 to 0.2. The mesopore volume was determined from the N_2 adsorbed at a P/P_0 = 0.4. The total pore volume was calculated from the amount of nitrogen adsorbed at P/P_0 = 0.95, assuming that adsorption on the external surface was negligible compared with adsorption in pores. The pore diameter and pore volume were determined using the BJH method. In all cases, correlation coefficients above 0.999 were obtained.

3.6.4 Fourier Transformed Infrared Spectroscopy (FT-IR)

The Fourier transform infra red (FT-IR) spectra were recorded in the range 400–1400 cm^{-1} wave numbers using 64 scans and a resolution of 4 cm^{-1} with a JASCO FT-IR 4100 using pellets with spectroscopic grade potassium bromide (KBr).

3.6.5 Pyridine Adsorption FT-IR

The pyridine adsorption experiments were performed using a Perkin-Elmer Spectrum GX instrument. Prior to the pyridine adsorption, the samples were dried at 500 °C and maintained under vacuum (10^{-7} bar) for 3 hrs. Pyridine was then injected into the sample by saturating the He carrier gas for 30 mins at room temperature followed by degassing and evacuation at 250 ^{o}C. Molar extinction coefficients of 1.67 cm/μmol and 2.22 cm/μmol were used to determine the absolute amount of Bronsted and Lewis acid sites (Emeis, 1993).

3.6.6 Transmission Electron Microscopy

The morphologies of the materials were characterized by transmission electron microscopy (TEM). Sample specimens for TEM studies were prepared by ultrasonic dispersion of the catalysts in ethanol, and the suspensions were dropped onto a carbon-coated copper grid. TEM investigations were carried out using a Philips CM20 (100 kV) transmission electron microscope equipped with a NARON energy-dispersive spectrometer with a germanium detector.

3.6.7 ^{27}Al MAS NMR

^{27}Al MAS NMR experiments were performed on a Bruker AMX-400 FT NMR spectrometer operated at 104.2 MHz. All spectra were acquired using single-pulse excitation and spinning speeds ranging from 14–15 kHz. The spectra were typically obtained with a pulse width of 1.5 μs, and recycle delay of 1 s. Baselines were corrected and smoothed using the Bruker baseline correction routine. All spectra were externally referenced to aluminum nitrate solution (δ = 0 ppm).

3.6.8 Raman Spectroscopy

Raman Spectroscopic analysis was carried out using the vibrational modes of NiMo catalysts measured in the range of 100–1200 cm^{-1} using Raman spectrometer (Renishaw) equipped with a Nd:YAG laser source.

3.6.9 Extended X-ray Absorption Fine Spectroscopy (EXAFS)

1) Data Collection

Mo K-edge XAS data were collected for 3 sulfided catalyst samples sat the Hard X-ray Microanalysis beamline (HXMA, 06ID-1) at the Canadian Light Source. The synchrotron source at the HXMA beamline is a superconducting wiggler and the beamline is equipped with a double-crystal Si(220) monochromator and Rh-coated, upstream collimating and downstream focusing mirrors. The operational current in the storage ring of CLS is 200-250 mA at 2.9 GeV. The harmonic rejection was accomplished by detuning the second monochromator crystal to 50% of the maximum intensity. XAS data for the sulfided samples were collected in fluorescence mode using a 32 element solid state germanium detector. The XAS data for the catalyst samples were collected at ambient temperature and pressure with the simultaneous measurement of a Mo reference foil spectra for energy calibration. Approximately 200 mg of the sample was pressed into the 10 mm ID quartz sample holder. The weight of the sample was calculated to have a total absorption length of about 2.0 for optimal signal to noise ratio.

2) Data Analysis

The XAS spectral data collected were analyzed using Athena (Ravel and Newville, 2005). The data reduction of the XAS spectra included the standard procedures for energy calibration,

averaging of multiple scans, background subtraction as well as per atom normalization. Ab initio theoretical phase shifts and amplitude functions for the Mo-O, Mo-S and Mo-Mo contributions were calculated using the program FEFF version 8. Multiple shell fitting of the Mo K edge EXAFS data was done in R- space using the program Artemis (Ravel and Newville, 2005). The fitting was done over a k range of 3.5 – 13.98 $(A^o)^{-1}$ range. The fitting in R space ranged from 1–4 A^o. This data and modeled regions contain approximately 18 independent points. This model is a well constrained model as the number of independent parameters was roughly twice more than the number of parameters determined in the fit. The estimated accuracies of the EXAFS fit parameters were ± 20% for the coordination number (N), ± 0.04 A˚ for the coordination distance (R), ± 20% for the Debye–Waller factor σ_s^2 and ± 10% for the inner-potential correction ΔE_0.

3.6.10 X-ray Absorption Near Edge Spectroscopy (XANES)

A medium energy, bending magnet based Soft X-ray Micro-characterization Beamline (SXRMB) with an energy range of 1.7 to 10keV at Canadian Light Source (CLS) was used for XAS analysis of the catalysts. The data was recorded in the total electron yield (TEY) mode for S K edge and Mo L3 edge and the Ni K edge data was recorded in the fluorescence yield mode.

3.7 Batch Reactor Studies

Hydrodesulfurization of the model compound DBT was performed in a 500 mL autoclave type Parr reactor equipped with a sampling port. The reactor was closed and pressurized with hydrogen and heated to 325 ^oC at the heating rate of 2.5 ^oC /min. The reaction began when the agitation (1000 rpm) started at 325 ^oC and 600 psi. Liquid samples were removed periodically and analyzed by GC. Reaction mass balances were found to be more than 95% in all

experiments, for each reactants using dodecane as internal reference for analysis. In a typical experiment, about 6 liquid samples of approximately 0.5 mL each were withdrawn, so that the volume feed could be considered constant throughout the experiment. The liquid product samples were diluted in ethanol (500mL) and analyzed by GC for cyclohexyl benzene (CHB) and biphenyl (BP) using an FID detector and a DB wax capillary column at a temperature programmed from 50 to 230^{o}C (15^{o}C/min). DBT in the product was analyzed in the same GC but using a different Varian CP-Sil 8CB column using an FID detector at a temperature programmed from 80 to 280^{o}C (15^{o}C/min). Conversions were calculated according to the disappearance of reactant or the formation of products. The conversions for DBT are reported here for 6 hrs of reaction-on-time.

3.8 Hydrotreating Reactions in Trickle Bed Reactor

The heavy gas oil (HGO) derived from Athabasca bitumen is used as a feed for hydrotreating activity studies. Catalytic experiments were performed in a trickle bed reactor under typical industrial conditions. The high pressure reaction set up used in this study simulates the process that takes place in industrial hydrotreater. The system consist of liquid and gas feeding sections, a high pressure reactor, a heater with temperature controller for precisely controlling the

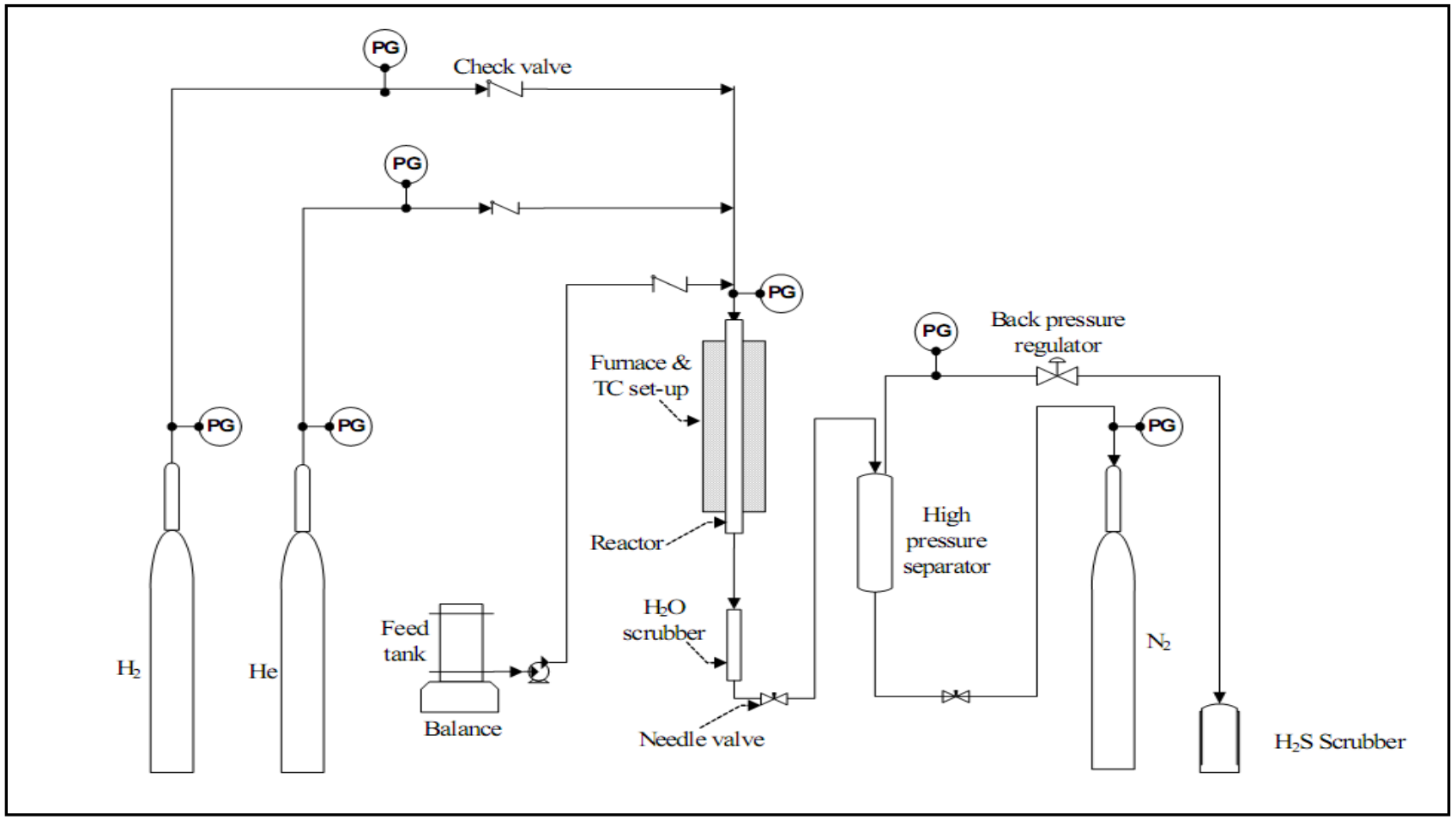

Figure 3.2: Schematic of the lab scale hydrotreaters set up.

temperature of the catalyst bed, a scrubber for removing the ammonium sulfide from the reaction products, and a high pressure gas–liquid separator. The length and internal diameter of the reactor were 240 and 14 mm, respectively. Typically, the catalyst bed, approximately 10.5 cm long, was packed with 5 cm^3 of catalyst (2.0 g) and 12 cm^3 of 90 mesh silicon carbide.

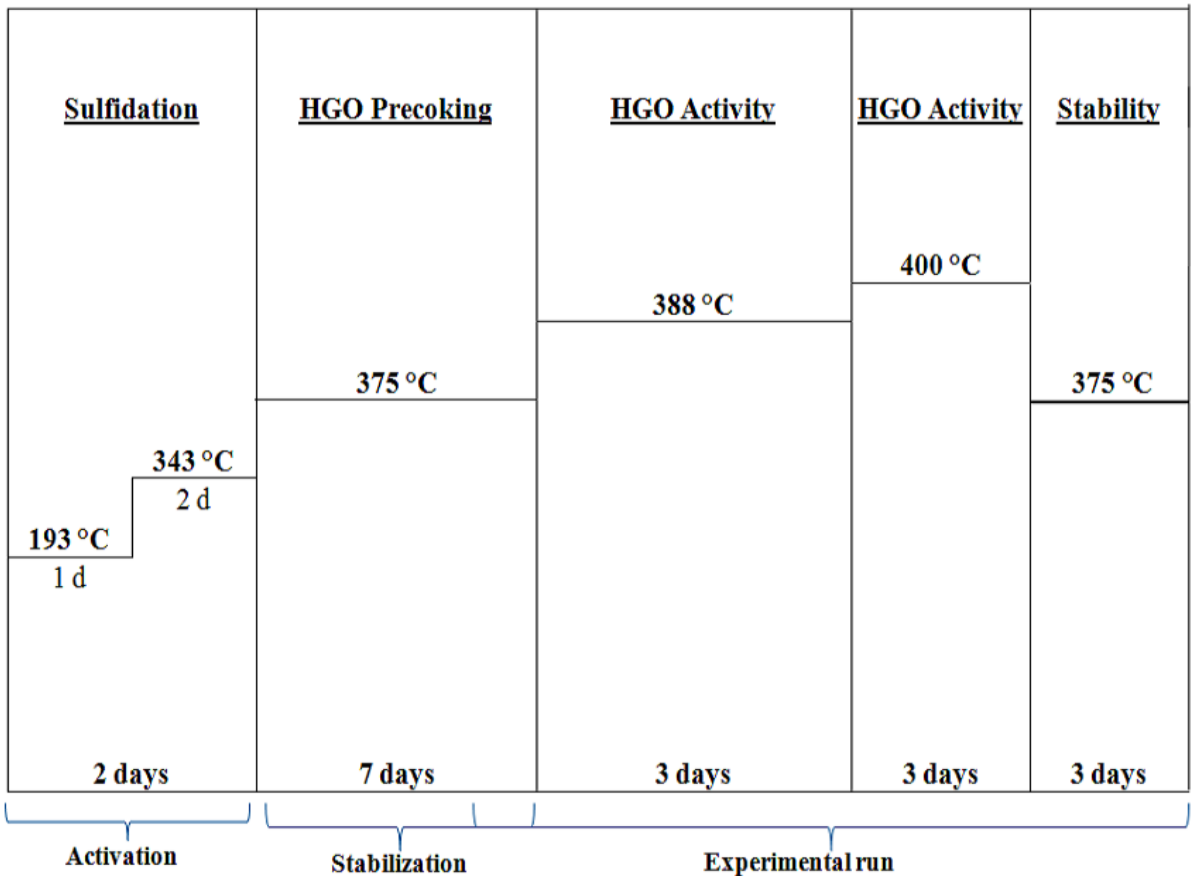

Figure 3.3: A typical temperature program followed for the hydrotreatment of heavy gas oil

The catalyst was sulfided by injecting sulfidation solution containing 2.9 vol.% of butanethiol in straight run atmospheric gas oil at a pressure and temperature of 8.8 MPa and 193 °C, respectively, for 24 h. The flow rate of the sulfiding solution was 5 mL/min. The H_2 flow rate

was kept at a rate corresponding to H_2/sulfiding solution ratio of 600 mL/mL. The temperature of the reactor was increased to 350 °C and maintained for another 24 h. Following sulfidation, the catalyst was precoked (stabilized) with HGO for 5 days at a temperature of 370 °C, pressure of 8.8 MPa, and LHSV of 1 h^{-1}. After precoking, hydrodenitrogenation (HDN) and HDS activities of catalysts were studied at 370 °C and 390 °C for 3 days at each temperature. The pressure, H_2/feed ratio and LHSV were maintained constant at 8.8 MPa, 600 ml/ml and 1 h^{-1}, respectively. The products were collected at 12 h interval. The products were stripped with nitrogen for removing the dissolved ammonia and hydrogen sulfide.

3.9 Feed and Product Analysis

3.9.1 N-S Analysis

The concentrations of sulfur and nitrogen compounds present in feed and products were determined using an Antek 9000 NS analyzer. The sulfur content was measured using the combustion-fluorescence technique of the ASTM D5463 method. The nitrogen content of the liquid product was determined by the combustion-chemiluminescence technique of the ASTM D4629 method. The instrumental error for both N and S analysis was found to be approximately ±2%, based on analyzing standard solutions of known composition.

3.9.2 Simulated Distillation

To determine the boiling point distribution of the liquid feeds and products, a simulated distillation ASTM D6352 method was used. The simulated distillation of the heavy gas oil feed and product liquids was performed using a Varian Model CP 3800 Gas Chromatograph coupled with a Varian CP 8400 Auto sampler. The components boiling range were determined using a

flame ionization detector (FID). The boiling fractions were determined by comparing them against a calibration curve.

3.10 Summary of Characterization Techniques

Table 3.1: Summary of characterization techniques used in this work

Characterization Technique	Description
X-Ray Diffraction (XRD)	Detection of crystalline phases and verification of geometry
BET Analysis	Surface area, pore volume and pore size
ICP/MS	Bulk elemental composition
TEM, HRTEM	Surface morphology
^{27}Al NMR	Coordination state of Aluminium
FT-IR	Presence of functional groups
Py- FTIR	Bronsted and Lewis acid sites
Raman Spectroscopy	Determination of various MoO_x phases
EXAFS	Coordination number and Bond distance
XANES	Coordination number and Oxidation state
N-S Analyzer	Determination of nitrogen and sulfur concentration in feed and products
Simulated Distillation	Boiling point distribution of feed and products

CHAPTER 4

SYNTHESIS AND MODIFICATION OF γ-Al_2O_3 SUPPORT WITH MESOPOROUS ALUMINO-SILICATES PREPARED FROM ZSM-5 NANO-SEEDS

This chapter describes the synthesis and characterization mesoporous alumino-silicates prepared from the assembly of ZSM-5 nano-seeds. The first section of the chapter deals with the effect of hydrothermal treatment on the physic-chemical properties of the MAS materials. The catalytic activities of the MAS materials synthesized with various hydrothermal treatment durations are evaluated in the hydrodesulfurization of dibenzothiophene (DBT) in a batch reactor. The MAS with highest activity was then mixed with Al_2O_3 in various weight ratios to prepare support for hydrotreatment reactions of real feedstock.

4.1 Synthesis and Characterization of MAS

Three different mesoporous alumino silicates (MAS) materials were prepared using the synthesis procedure described earlier. A uniform Si/Al molar ratio of 25 was maintained for all the materials. Only the hydrothermal treatment duration of the ZSM-5 precursors was varied. The MAS materials were named as MAS-4, MAS-16 and MAS-24. Further, Al-SBA-15 was synthesized as the reference material.

4.1.1 N_2 Adsorption-Desorption Analysis

The N_2 adsorption and desorption isotherms of Al-SBA-15, MAS-4, MAS (16) and MAS-24 are shown in Figure 4.1. Also, the various textural properties for these materials along with Al_2O_3

are tabulated in Table 4.1. MAS-4 and Al-SBA-15 exhibit a typical Type IV with a hysteresis loop which is characteristic of regular mesoporous channels structure. The initial increase in volume of adsorption at low pressure is due to monolayer adsorption in micropores and mesopores, and the upward deviation in the 0.6-0.8 P/Po range is associated with capillary condensation inside the mesopores. An alteration in type of isotherm and relative shift in the point of inflection with increasing hydrothermal treatment duration can be observed due to a change in nature or pores. The surface area as well as the pore volume decreased continuously with increase in seeding time, The contribution of mesopores to the total surface area of the material decreases with seeding time. This effect is particularly visible in the reduction of surface area of MAS-24 as compared to MAS-16. In MAS-16 mesopores constitute almost 70 % of the total surface area whereas the mesoporous area in MAS-24 is as low as 50 % of the total surface area. The decline in mesopores is accompanied with a rapid growth of micropores in the materials especially in MAS-24. The increase in microporosity in MAS-24 can be ascribed to the degree of connection of the alumino-silicate network of the hydrothermal gel. The alumino silicate framework after 24 hrs of hydrothermal treatment is nearly completely connected. The large connected alumino silicate network in MAS-24 is able to resist the capillary stress of evaporative drying and calcination. As a result the micropores are retained by the final material. In contrast, hydrothermal gel with low seeding durations (t_{seed} = 4 hrs.) possesses a very high content of silanols, which corresponds to interruption of the alumino-silicate framework. The presence of weaker silanol groups instead of a stronger alumino-silicate network allows the micropores to grow into mesopores (Morsli et al., 2007).

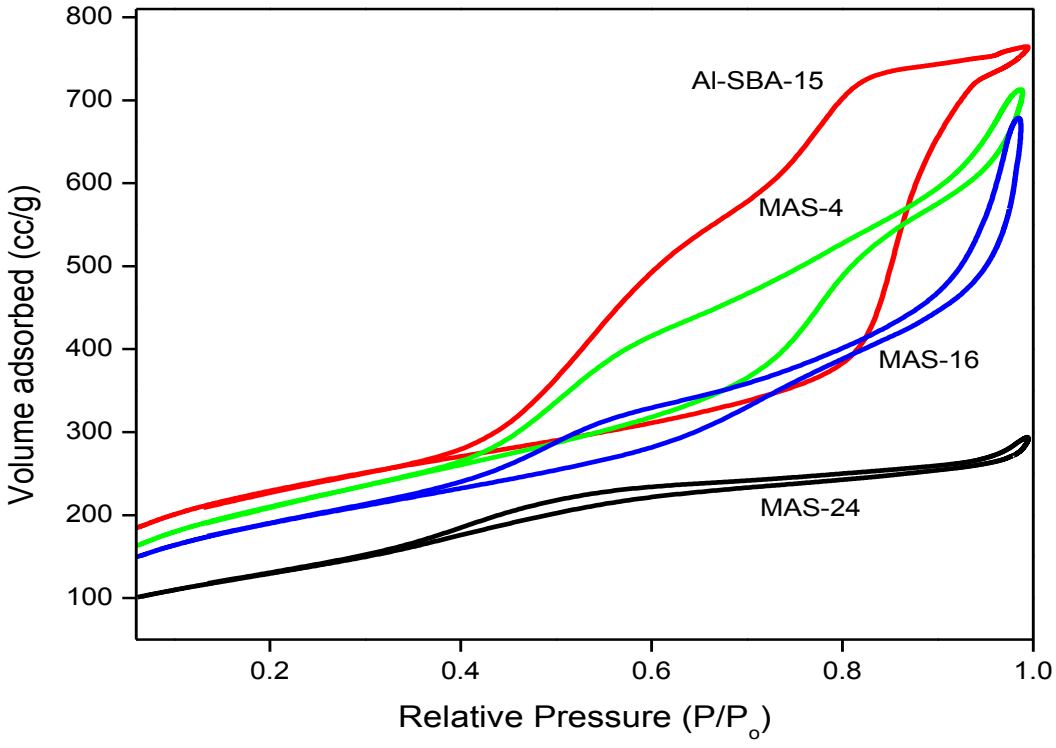

Figure 4.1: N_2 adsorption-desorption isotherms of a) Al-SBA-15, b), MAS-4, c) MAS-16 and d) MAS-24

Table 4.1: Textural properties of the MAS supports and reference materials

Sample	$S_{tot}(m^2/g)^a$	d_{BJH} (nm)[b]	PV (cc/g)	S_{micro} (m^2/g)	S_{meso} (m^2/g)	S_{micro}/ S_{tot}	Si/Al[c]
Al-SBA-15	887	7.1	1.58	71	816	0.08	24.8
MAS-4	759	6.5	1.36	68	691	0.09	24.7
MAS-16	683	5.4	1.03	128	455	0.18	24.4
MAS-24	478	3.3	0.53	245	223	0.51	24.6
Al_2O_3	267	9.2	0.72	--	--	--	--

a) Calculated by the BET method.
b) Calculated by BJH method.
c) Determined using ICP-MS

4.1.2 XRD Analysis

The structural arrangement of MAS and Al-SBA-15 materials were examined using XRD at low and high angles. The low angle XRD pattern of Al-SBA-15, MAS-4, MAS-16 and MAS-24 are given in Fig.4.2. The reference Al-SBA-15 exhibited an intense peak at $2\theta = 0.81^{o}$ and two small humps at $2\theta = 1.42^{o}$ and 1.65^{o}. The peaks are typical of ordered SBA-15 like material with p6mm symmetry (Zhao et al., 1998a). In comparison with Al-SBA-15, the synthesized MAS family of materials have one broad peak around $2\theta = 1.4^{o}$. The poor resolution of the 110 and 200 planes and a relative broadening of the peak width in MAS materials as compared to Al-SBA-15 may indicate that the long range ordered hexagonal symmetry is absent in materials assembled from zeolite nano clusters. In addition, a very small peak at $2\theta = 8^{o}$ can be observed only for MAS-24 which is a characteristic peak of ZSM-5. From these results it can be concluded that the duration of hydrothermal treatment of the zeolite seed solution is a very important factor in deciding the nature of the final material. At low seeding times of t_{seed} = 4 hrs, the final material is essentially similar to mesoporous Al-SBA-15 with associated long range ordered structure exhibiting p6mm symmetry as observed from XRD at low angles. Further, no peaks associated with crystalline structure was observed for materials with t_{seed} = 16 hrs. In contrast MAS-24 exhibited sharp XRD peaks similar to ZSM-5. The results from the low angle XRD are well supported by the TEM images of the MAS materials (Fig. 4.4). In contrast to the well-ordered 2D hexagonal arrays of mesopores in Al-SBA-15, MAS materials have very low areas of ordered structure. Hexagonal arrays are visible only but sporadically. The ill formed hexagonal mesoporous arrays to be due to the modification in the structure.

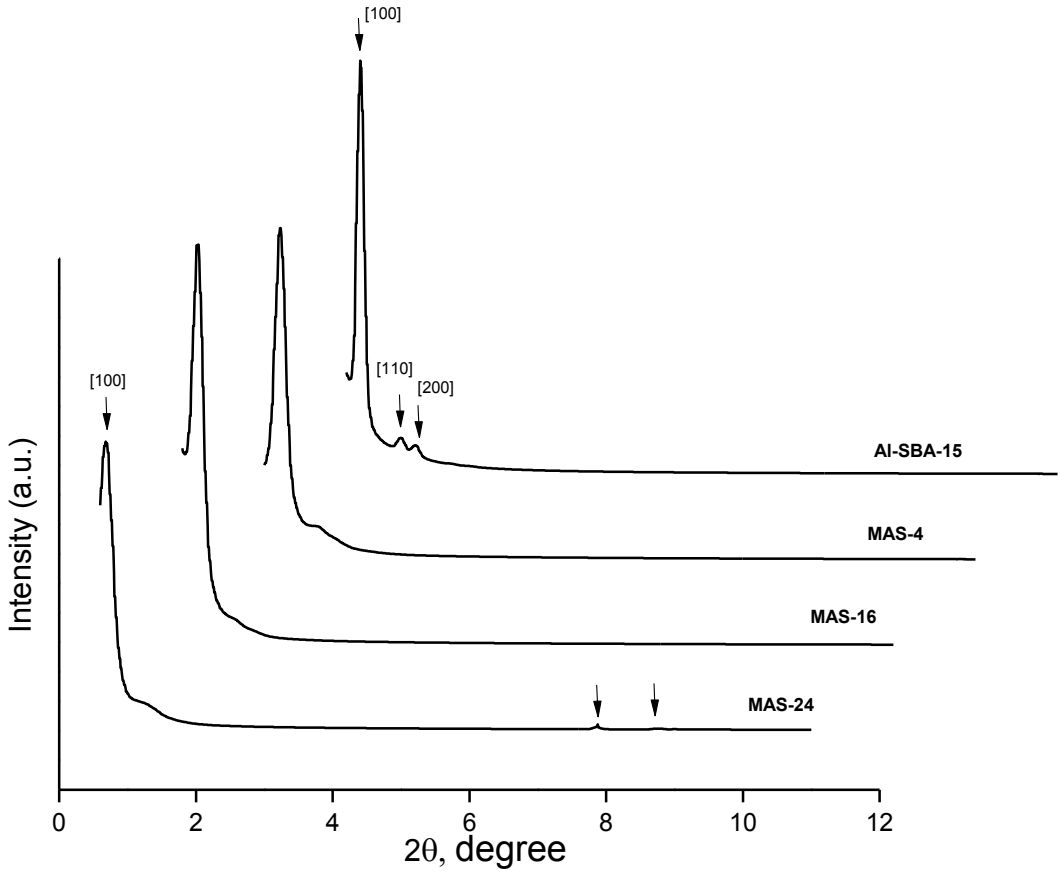

Figure 4.2: XRD pattern of a) Al-SBA-15, b), MAS-4, c) MAS-16 and d) MAS-24 in small angle range plotted in cascading format

The findings of the XRD at low angles are further confirmed by the diffraction pattern observed at higher angles (Fig. 4.3). MAS-24 showed intense peaks similar to ZSM-5 at $2\theta = 22.2^{o}$ (Cheng et al., 2005). However, this peak is absent for the materials synthesized with seeding times less than 24 hours. A broad peak typical of amorphous material is observed in MAS-4, indicating very little or no crystalline phase formation in the material after 4 hours of hydrothermal treatment.

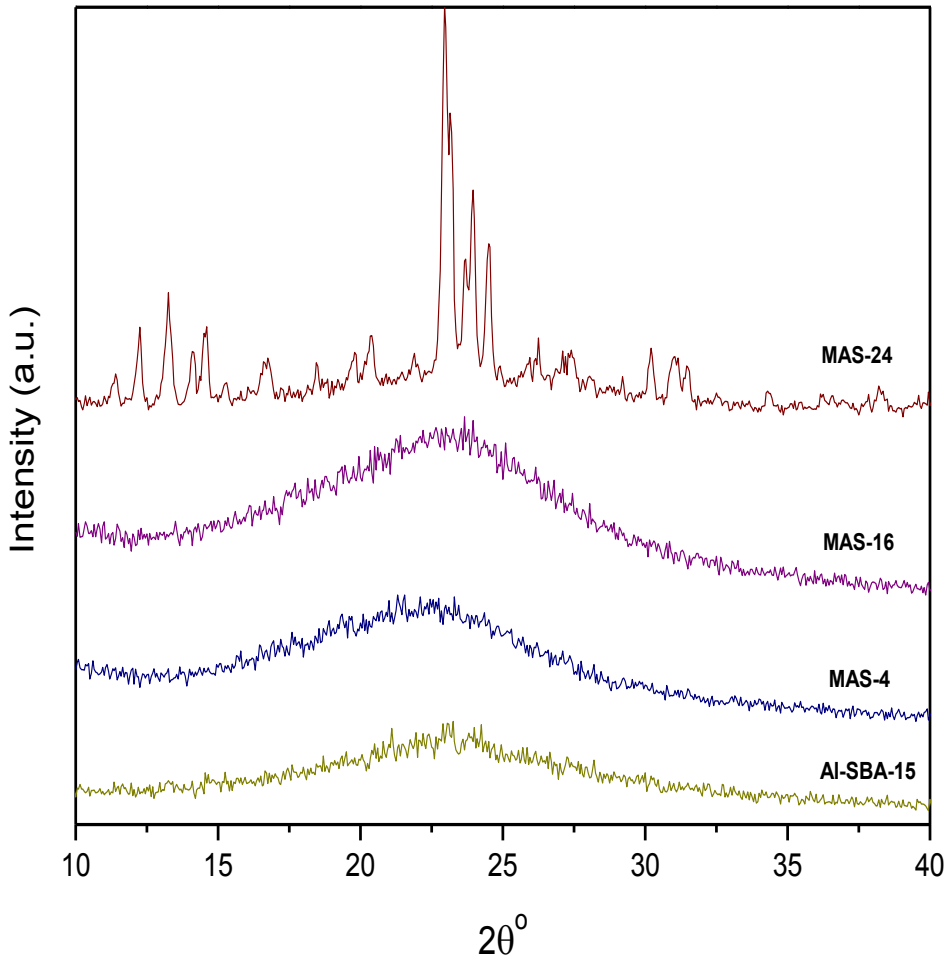

Figure 4.3: XRD pattern of a) MAS-24 , b) MAS-16, c) MAS-4 and d) Al-SBA-15 in high angle domain

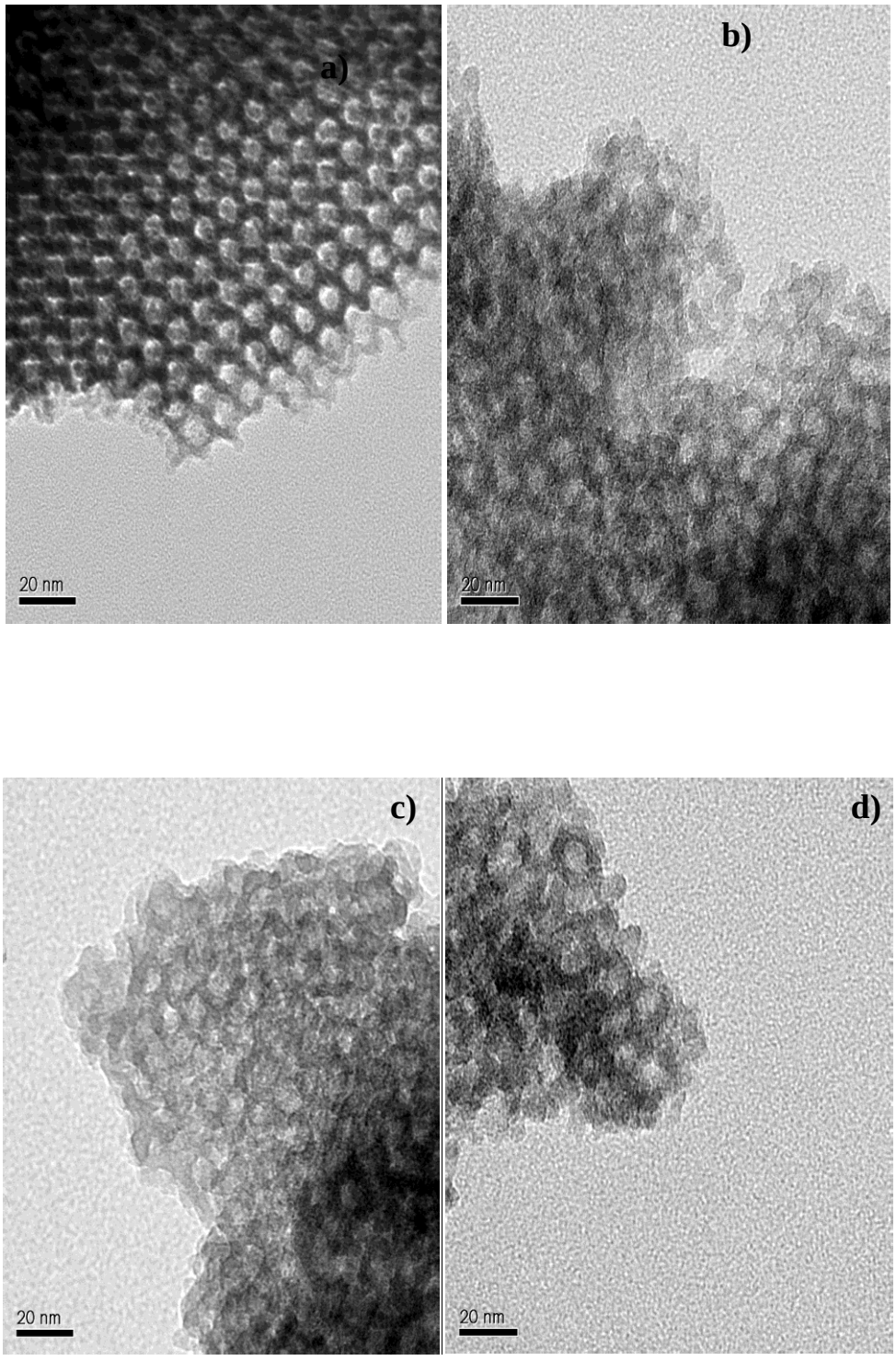

Figure 4.4: TEM images of a) Al-SBA-15, b), MAS-4, c) MAS-16 and d) MAS-24

4.1.3 FT-IR Analysis

The FTIR spectra of Al-SBA-15, MAS-4, MAS-16 and MAS-24 samples plotted in transmittance mode are shown in Fig.4.5. All the MAS materials showed a band at 550 cm^{-1} which is assigned to the double five ring (D5R) stretching present in MFI type zeolites (Jacobs et al., 1981).

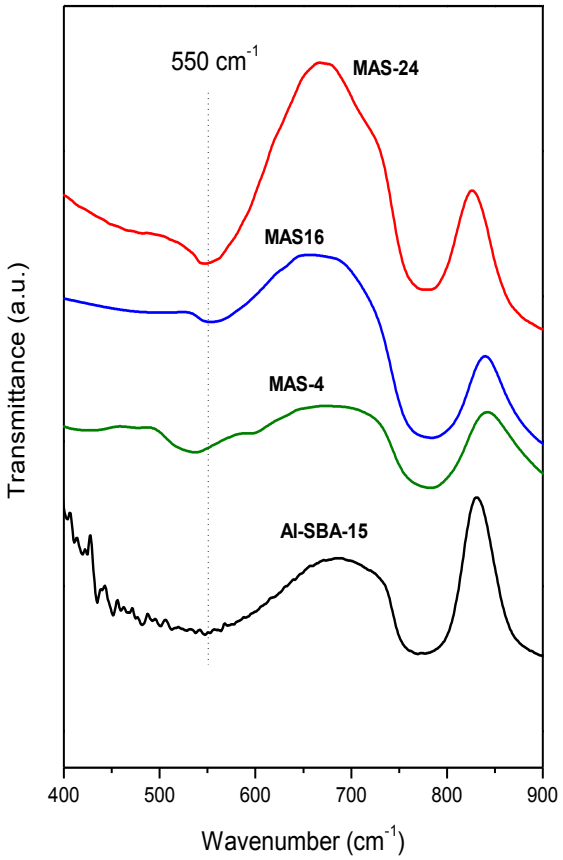

Figure 4.5: FTIR spectra of a) MAS-24 , b) MAS-16, c) MAS-4 and d) Al-SBA-15 in 400-900 cm^{-1}

This shows that the nano-crystal segments or nano crystals of ZSM-5 were embedded into the framework of the mesoporous matrix. The intensity of this band is increases with seeding time and is highest for MAS-24, indicating that the alumino silicate network is predominantly present as five membered rings of Si-O-Al similar to those present in ZSM-5. The results are in good agreement with the findings of Han et al who also reported Si-O-Al band in the 550 cm^{-1} region for similar materials (Han et al., 2002).

4.1.4 ^{27}Al MAS NMR Analysis

The ^{27}Al NMR spectrum provides evidence of the framework connectivity of the alumino-silicate network. ^{27}Al MAS NMR spectra of Al-SBA-15, MAS-4, MAS-16 and MAS-24 materials are shown in Fig 4.6. The sharp peak at ~ 58 ppm is generally assigned to tetrahedral Al species present in zeolite frameworks, whereas the peak at 0 ppm is indicative of the extra framework aluminum present in an octahedral coordination. The extra framework Al peaks are only observed for Al-SBA-15 and MAS-4. In addition to the 0 ppm peak, Al-SBA-15 also gave a shoulder at ~ 10 ppm. This peak can be assigned to a hexa-coordinated aluminum species with SiO groups around the AlO_6 structural units (Atwood and Harvey, 2001). These results show the existence of extra framework Al-O-Si species in Al-SBA-15 and MAS-4 materials, probably generated by the dealumination of the precursor in an acidic media during the surfactant based assembly procedure. Another interesting aspect of the ^{27}Al MAS NMR spectra is the gradual shift in the position of the tetrahedral aluminum peak. The tetrahedral peak signal for Al present in Al-SBA-15 is observed at a chemical shift δ = 53 ppm, whereas in MAS-16 and MAS-24 the peak shifts to δ = 57 and 58 ppm respectively. The shift in the peak position is reported in literature to be due to the difference in the locating environment of Al . The 4 coordinated Al

atoms in MAS materials are present as five membered ring structures similar to the pentasil unit present in ZSM-5.

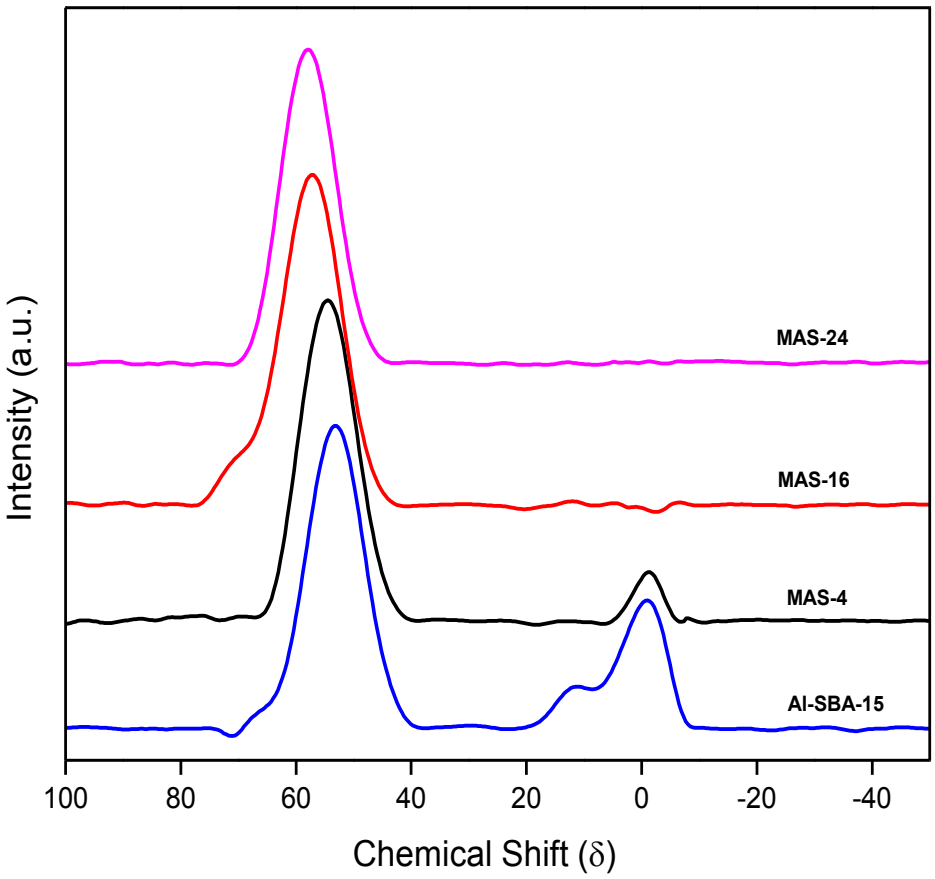

Figure 4.6: ^{27}Al MAS NMR spectra of a) MAS-24 , b) MAS-16, c) MAS-4 and d) Al-SBA-15

4.2 Characterization of MAS supported NiMo catalysts

The acid strength of the supported catalyst systems was studied using the Pyridine FTIR method. Py-FTIR spectra of the protonated samples were measured in the region of 1700-1400 cm^{-1}. According to literature, pyridine adsorbed on Lewis acid sites exhibits signals at 1450, 1596 and 1615 cm^{-1} (Barzetti et al., 1996). Bands at 1540 and 1640 cm^{-1} are assigned to Bronsted acid sites present in the material. Further, pyridine co-adsorbed on both Bronsted and Lewis acid sites gives rise to a band at 1495 cm^{-1} (Hughes and White, 1967). Fig 4.7 clearly shows the presence of Bronsted acid sites in NiMo/MAS-24 and NiMo/MAS-16. In contrast NiMo/MAS-4 exhibits only a weak band at 1640 cm^{-1} which corresponds to a very low concentration of Bronsted acid sites in MAS-4. The reference Al-SBA-15 however shows no peaks at 1640 or 1540 cm^{-1}, possibly due to the absence of Bronsted acid sites. Nevertheless Lewis acid sites are present in all the four catalysts. A peak at 1490 cm^{-1} corresponding to presence of both Bronsted and Lewis acid sites is observed for all the catalysts. Table 4.2 lists the acid sites distribution in the four catalysts. The results are calculated after degassing of the adsorbed pyridine at 300 ^{o}C. NiMo/MAS-24 possesses more Bronsted acid sites than NiMo/MAS-16. Presence of Bronsted acid sites is fairly minimal in NiMo/MAS-4 and almost absent in NiMo/Al-SBA-15. The presence of Bronsted acid sites may be linked to the distinctive Al chemical environment present in the framework in a zeolite like Si-O-Al network. In agreement with the ^{27}Al MAS NMR results, the FTIR-Py technique demonstrates that with increase in hydrothermal treatment duration, the extent of Al incorporation into the framework through tetrahedral AlO_4 units increases. Indeed, the number of AlO_4 tetrahedron sharing an oxygen with the SiO_4 tetrahedron involved in the Bronsted acid site determines the Si-O(H)-Al angle deprotoantion energy and hence the acid strength (Grajciar et al., 2010).

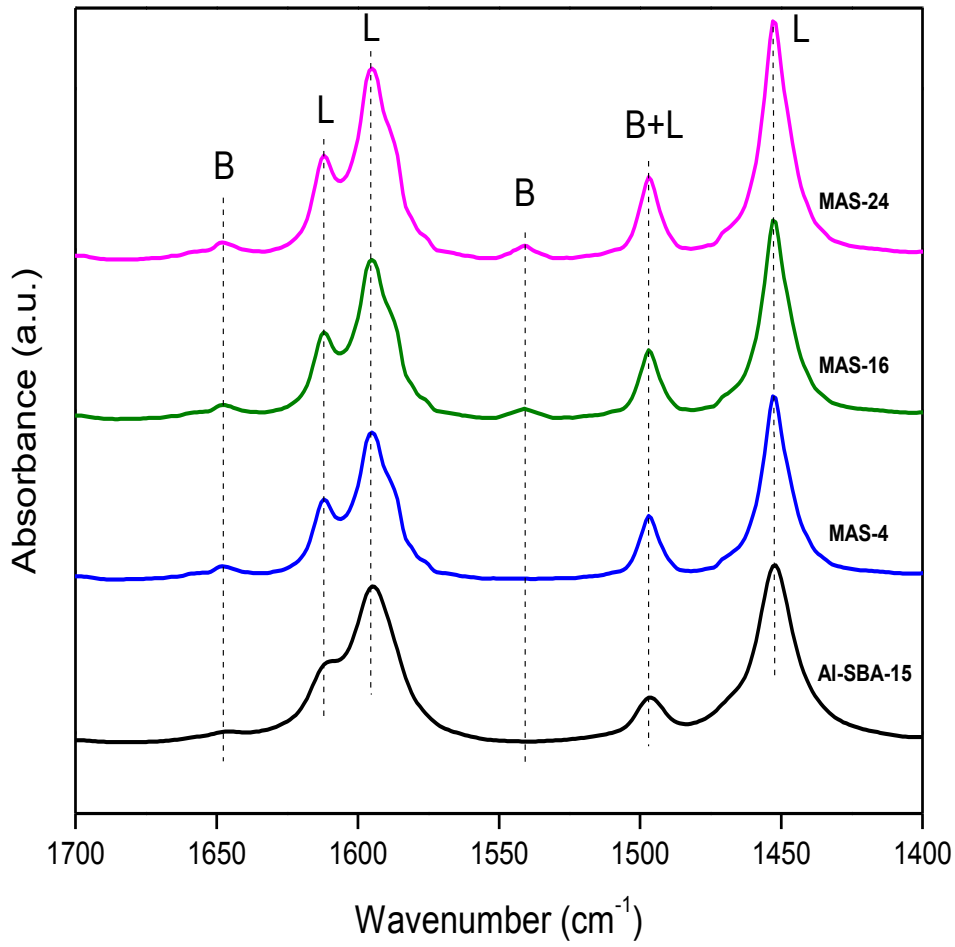

Figure 4.7: FTIR spectra of pyridine adsorbed spectra of a) MAS-24 , b) MAS-16, c) MAS-4 and d) Al-SBA-15 after degassing at 250 ^{o}C

Table 4.2.shows the surface area and other textural properties of the NiMo supported catalysts. The actual metal loading is very close to the targeted values, indicating a good deposition of the metals on the support surface by the employed wetness impregnation procedure. NiMo loading

on MAS-24, however leads to an appreciable decrease in the pore diameter of the catalyst support. A possible reason may be the micropore and mesopore blockage of the already constricted MAS-24. A non uniform dispersion of the metal phase may also be a probable reason for the reduction in surface area and pore volume in MAS-24.

Table 4.2: Textural properties and concentration of acid sites of the supported catalysts systems

			Amount of acid sites (μmol/gm)		
Sample	$S_{tot}(m^2/g)$	d_{BJH} (nm)	Lewis	Bronsted	Lewis + Bronsted
NiMo/Al-SBA-15	465	6.9	385	2	387
NiMo/MAS-4	398	6.2	453	5	455
NiMo/MAS-16	373	5.2	476	29	505
NiMo/MAS-24	202	3.4	513	43	556
$NiMo/Al_2O_3$	189	8.6	396	--	396

The Raman spectra for the NiMo oxide catalysts are presented in Fig.4.8. A Raman band at ~ 958 cm^{-1} appeared in NiMo/MAS-16 and NiMo/MAS-24. This band is attributed to the vibration of Mo=O bond of the Mo species interacting with the MAS support. Low frequency bands at 220 cm^{-1} characteristic of Mo-O-Mo deformation is also observed in all the catalysts. The Mo-O-Mo linkages can be attributed to the presence of polymolybdates with similar linkages. The results are in confirmation with Mestl et al who concluded that Mo exists as polymolybdates at intermediate loadings of 15-20 wt % on alumina silica based supports (Mestl and Srinivasan, 1998).

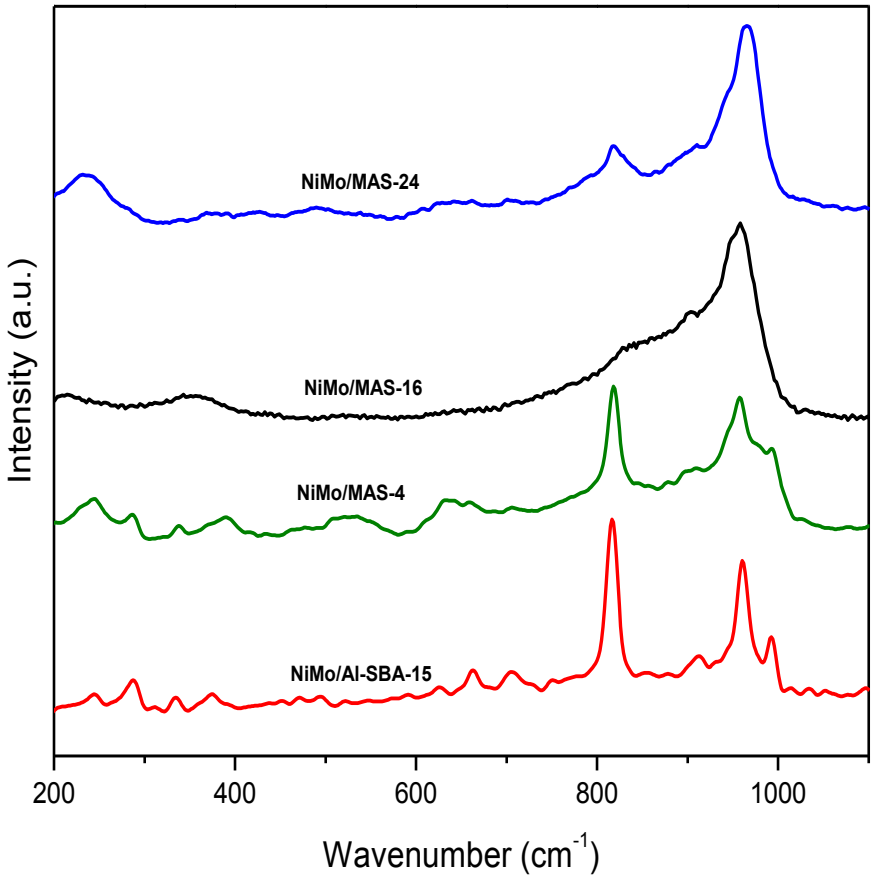

Figure 4.8: Raman spectra of NiMo loaded on a) MAS-24, b) MAS-16, c) MAS-4 and d) Al-SBA-15

Another interesting feature is the appearance of bands at 820 cm^{-1} and 996 cm^{-1} for NiMo/MAS-4, NiMo/MAS-24 and Al-SBA-15. These bands are however not observed for NiMo/MAS-16. Bands at 820 cm^{-1} and 996 cm^{-1} are assigned to Mo=O stretching and Mo-O-Mo asymmetrical stretching in crystalline MoO_3. A relatively weak interaction between MoO_x and the supports

MAS-4 and MAS-24 appears to be the reason for the formation of bulk MoO_3. Thus the duration of hydrothermal treatment which directs the Al incorporation into the mesoporous framework seems to be a controlling factor for the dispersion of the MoO_x species on the surface of the support. The HRTEM image (Fig.4.9) of sulfided NiMo/MAS-16 shows a very well dispersed MoS_2 phase with only single slabs of the MoS_2 phase. However the HRTEM image of sulfided NiMo catalysts supported on Al-SBA-15 shows stacked layers of MoS_2. Silica based materials like SBA-15, KIT-6, MCM-41 are known to favor multiple stacked layers of MoS_2 due to the low metal support interactions (Huang et al., 2008a). Single slabs of MoS_2 dispersed over the MAS-16 support suggest an improvement in the metal support interaction similar to those present in alumina supports. This may be due to an extensive bonding of Mo with the framework Al atoms resulting in Mo-O-Al linkage instead of Mo-O-Si linkages. Preparation of mesoporous alumino-silicates from ZSM-5 nano seeds seems to have a positive impact on the metal support interaction and hence the dispersion of the MoO_x phase on the support. A well dispersed MoO_x upon sulfidation resulted in single slabs of MoS_2 uniformly spread throughout the surface of the support.

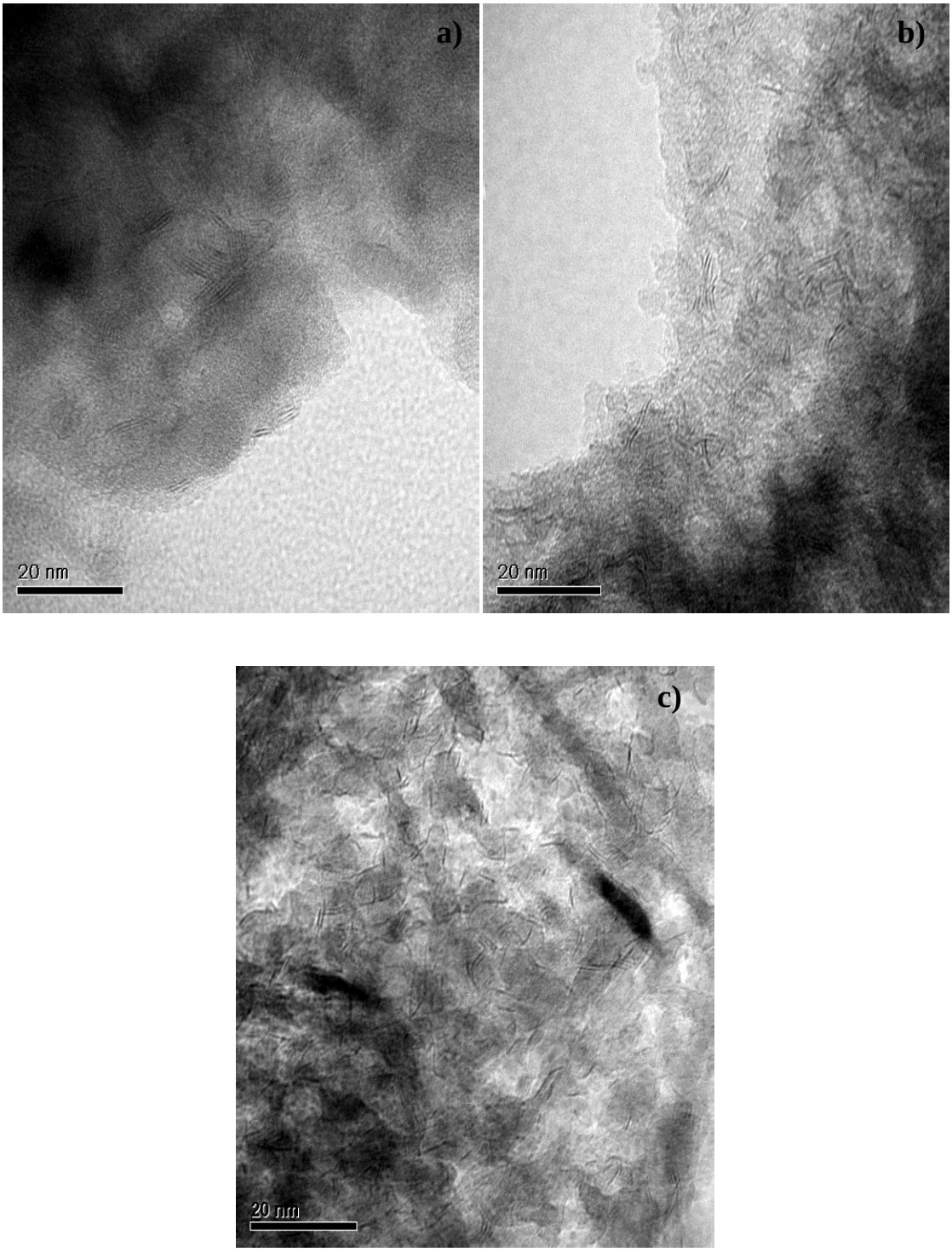

Figure 4.9: HRTEM images of sulfided a) NiMo/Al-SBA-15, b) NiMo/MAS-4 and c) NiMo/MAS-16

4.3 Catalytic activity of NiMo/MAS in HDS of DBT

The MAS-16 supported NiMo catalyst showed the highest DBT conversion at all times, with DBT conversion being 30 % higher than Al-SBA-15 and MAS-4 supported catalyst. DBT conversion in Al-SBA-15 and MAS-4 supported catalyst were similar. This is probably due to similar properties of Al-SBA-15 and MAS-4 since at lower durations of hydrothermal treatment; the nano clusters do not fully exhibit zeolite like connectivity and thus have properties similar to Al-SBA-15. In contrast, the conversion of DBT over MAS-4 was higher than that of MAS-24 despite of MAS-24 having the maximum growth of the zeolite like phase. This is probably due to the small pore size and pore volume observed in MAS-24. In addition, structural collapse of the mesophase due to the rapid growth of crystals on the walls of MAS-24 as observed from the N_2 adsorption and desorption isotherms could be another possible reason for the low DBT conversion. A good dispersion of the active phase combined with excellent textural properties and presence of strong Bronsted acid sites resulted in NiMo supported on MAS-16 exhibiting the highest conversion among all 4 catalysts. The product distribution analysis was done only for cyclohexyl benzene (CHB) and biphenyl (BP) using a GC. Biphenyl is known to be a product of the direct desulfurization (DDS) pathway whereas CHB is formed in the hydrogenation (HYD) pathway. The simplified reaction scheme for the HDS of DBT is given in Fig. 4.10. The selectivity for BP over CHB is highest for catalyst supported on MAS-24. This indicates that NiMo/MAS-24 favors the DDS pathway for the HDS of DBT. The acceleration of the DDS pathway may be attributed to the presence of Bronsted acid sites which act as proton donors to the metal sulfide particles and lead to a direct C-S bond cleavage. NiMo/MAS-16 with similar acid sites also yields more BP as compared to NiMo/MAS-4 and NiMo/Al-SBA-15. The product analysis for CHB, however gives different results. NiMo/MAS-4 and NiMo/Al-SBA-15 show comparable concentrations of CHB and BP in the products as compared to catalysts supported on

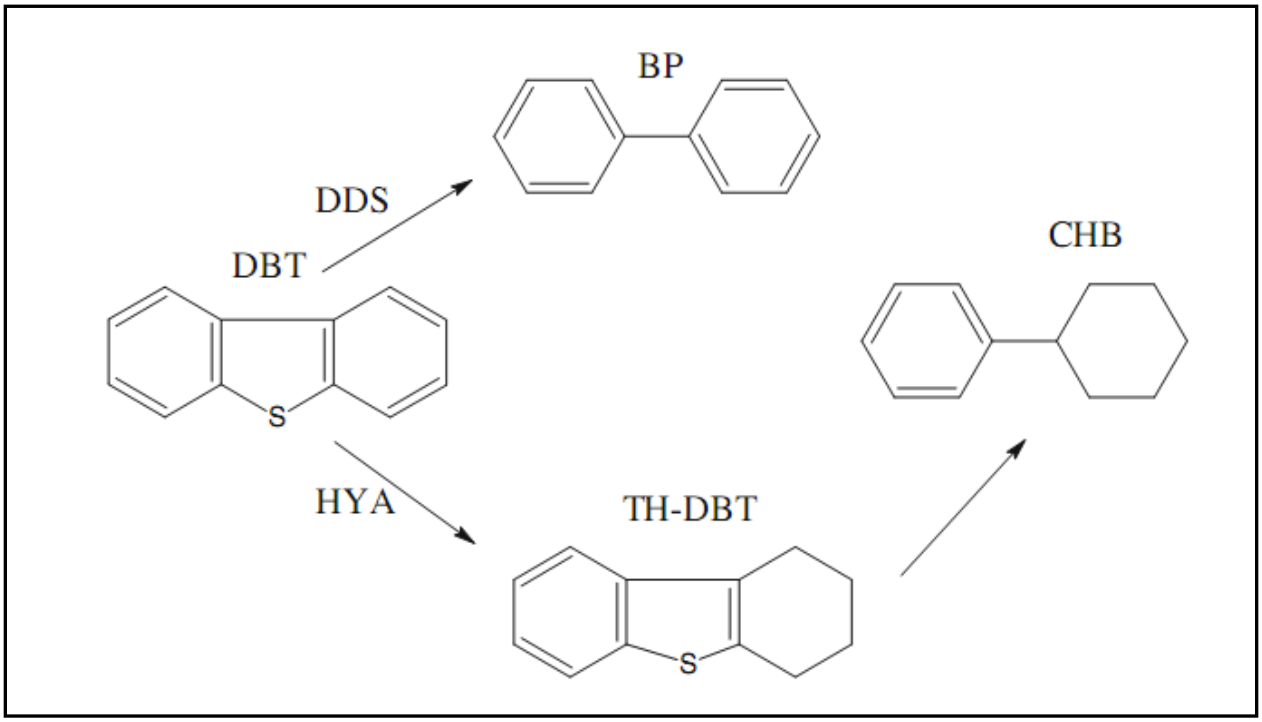

Figure 4.10: Simplified reaction schematic of HDS of DBT (Linares and Fernandez, 2008)

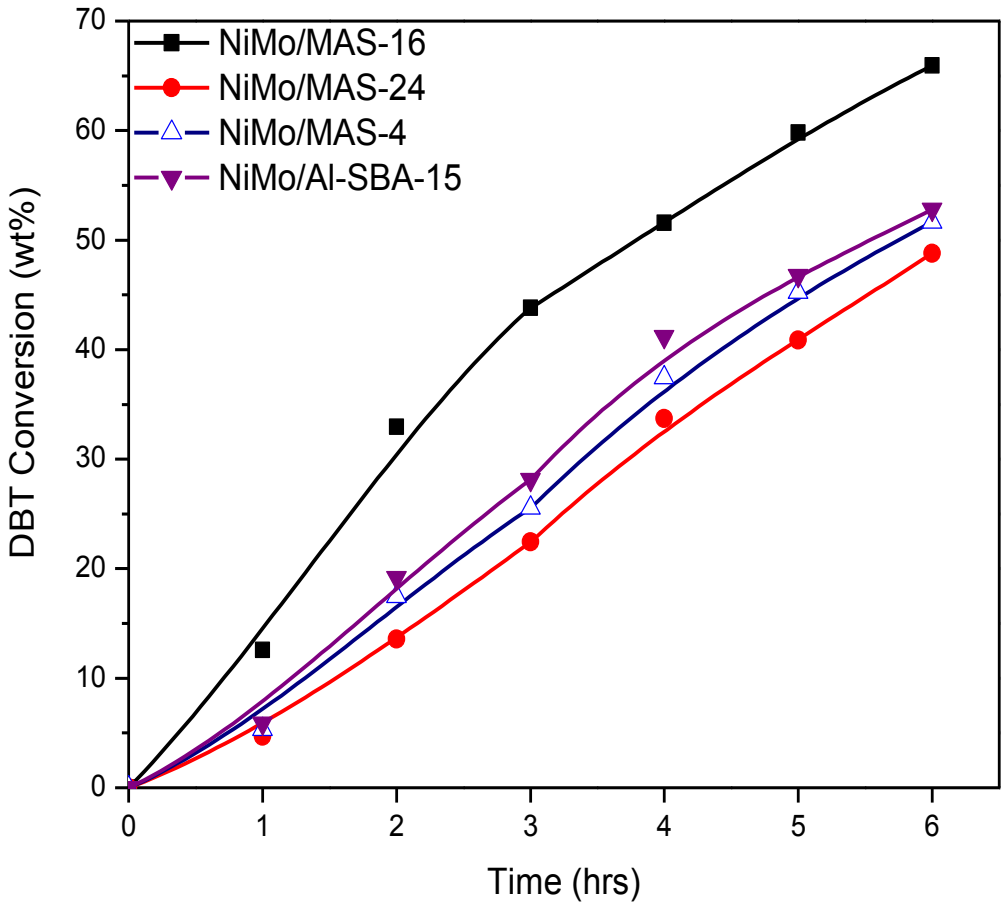

Figure 4.11: DBT conversions of sulfided NiMo catalysts at various times over different supports. Reactions conditions: Temperature – 325 ^{o}C, H_2 Pressure – 600 psi, Stirring speed – 1000 rpm

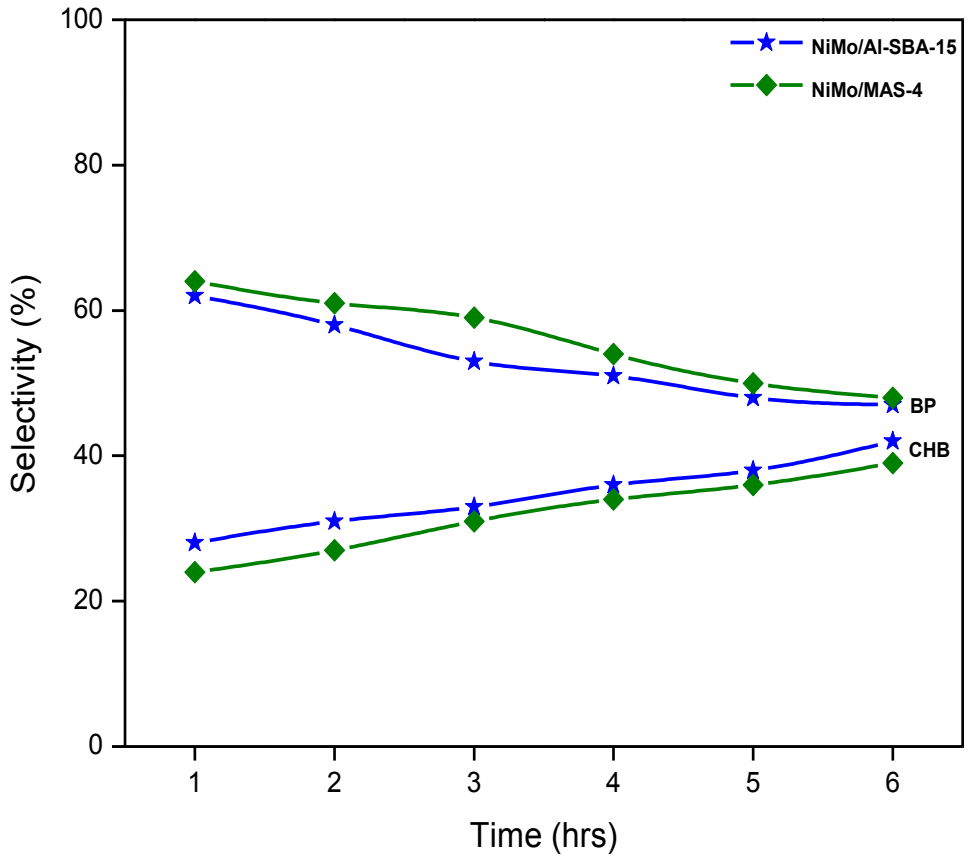

Figure 4.12 a): Product distribution of BP and CHB in the HDS of DBT over NiMo/Al-SBA-15 and NiMo/MAS-4. Reactions conditions: Temperature – 325 ^{o}C, H_2 Pressure – 600 psi, Stirring speed – 1000 rpm

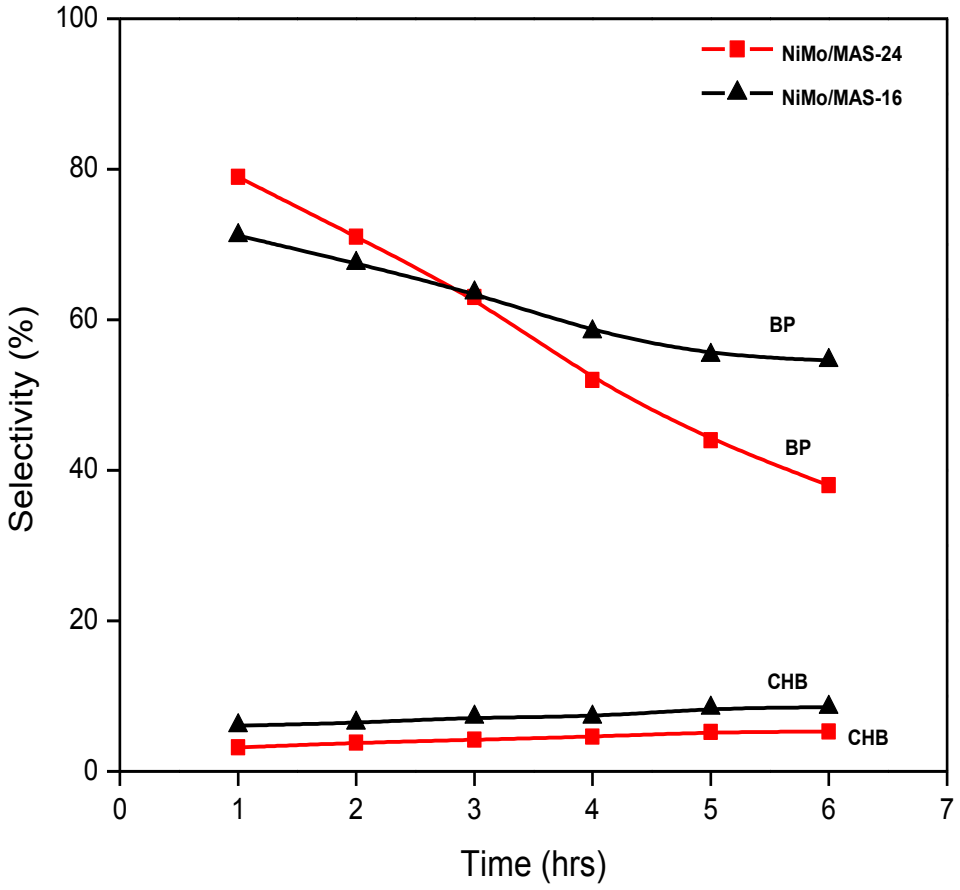

Figure 4.12 b): Product distribution of BP and CHB in the HDS of DBT over NiMo/MAS-24 and NiMo/MAS-16. Reactions conditions: Temperature – 325 ^{o}C, H_2 Pressure – 600 psi, Stirring speed – 1000 rpm

MAS materials with higher seeding times. CHB is formed by the hydrogenation of cyclohexen-1-yl- benzene (CHEB) which is a product of direct desulfurization of THDBT. The THDBT occurs as an intermediate when the HDS of DBT follows the hydrogenation route. The lower selectivity of CHB in NiMo/MAS-16 and NiMo/MAS-24 can be explained in two ways: 1) The hydrogenation pathway is less favored as compared to the DDS pathway, or 2) In presence of

strong acid sites and high reaction temperatures of 320 ^{o}C, CHEB may have undergone further hydrogenation to form Iso DM decalin and alkyl –CH (Zhang et al., 2010). The strong Bronsted acid sites in NiMo/MAS-16 and NiMo/MAS-24 appear to have promoted the further hydrogenation of CHEB at 320 ^{o}C. The former seems unlikely as the presence of acid sites is known to enhance hydrogenating properties as well which are ascribed to electronic effects of the acidity on metal sulfide phase (Welters et al., 1994). In either case the DDS pathway is accelerated more than the HYD pathway over catalysts supports with longer durations of hydrothermal treatment. The presence of acidic protons in MAS-16 and MAS-24 catalysts arising from the Bronsted acid sites help in the faster scission of the C-S bond.

4.4 Discussion: Effect of Hydrothermal Treatment on MAS

The catalytic performance tests combined with the physico-chemical characterization shows that the duration of hydrothermal treatment of the zeolite seed solution is a very important factor in deciding the nature of the final material. At low seeding times of t_{seed} = 4 hrs, the final material is essentially similar to mesoporous Al-SBA-15 with associated long range ordered structure exhibiting p6mm symmetry as observed from XRD at low angles. Further, no peaks associated with crystalline structure was observed for materials with t_{seed} = 16 hrs. In contrast MAS-24 exhibited sharp XRD peaks similar to ZSM-5. The absence of XRD peaks in MAS-16 may be attributed to the presence of very small particles which were not detected by XRD. Jacobs et al had previously reported a minimum particle size of 8 nm for it to be detected by X-ray diffraction techniques (Jacobs et al., 1981b). Zebib et al who have also shown that transition from a purely mesoporous material to a mixture of BEA zeolite and mesoporous material occurs abruptly between t_{seed} = 16 hrs and t_{seed} = 24 hrs (Zebib et al., 2005). The results confirm that in

addition to BEA zeolite the abrupt transition phase also occurs in materials assembled with ZSM-5 seeds. The induction period of the zeolite seeds into the mesoporous structure depends on the Si/Al ratio and the gel composition (Camblor et al., 1991). The transformation of the MAS material from amorphous to a zeolitic one is reflected on the physico-chemical properties of the final material. The contribution of mesopores to the total surface area of the material decreases with seeding time. This effect is particularly visible in the reduction of surface area of MAS-24 as compared to MAS-16. In MAS-16 mesopores constitute almost 70 % of the total surface area whereas the mesoporous area in MAS-24 is as low as 50 % of the total surface area. The decline in mesopores is accompanied with a rapid growth of micropores in the materials especially in MAS-24. The increase in microporosity in MAS-24 can be ascribed to the degree of connection of the alumino-silicate network of the hydrothermal gel. The alumino silicate framework after 24 hrs of hydrothermal treatment is nearly completely connected. The large connected alumino silicate network in MAS-24 is able to resist the capillary stress of evaporative drying and calcination. As a result the micropores are retained by the final material. In contrast, hydrothermal gel with low seeding durations (t_{seed} = 4 hrs.) possesses a very high content of silanols, which corresponds to interruption of the alumino-silicate framework. The presence of weaker silanol groups instead of a stronger alumino-silicate network allows the micropores to grow into mesopores (Morsli et al., 2007). The ^{27}Al NMR spectra of MAS-16 and MAS-24 provides evidence of the complete framework connectivity of the alumino-silicate network. Absence of octahedral extra framework aluminum and the relative shift of the tetrahedral Al peak to δ = 57 ppm suggests that Al is present mostly in a ZSM-5 like network. In contrast, Al-SBA-15 and MAS-4 exhibit the same peak at δ = 53 ppm. The occurrence of the tetrahedral peak for MAS-24 at higher chemical shifts is due to the difference in connectivity of Al in the silica

matrix. The near complete induction of ZSM-5 seeds in the framework gives the walls of MAS-24 a ZSM-5 like alumino silicate network.

The MoO_x phase supported only on MAS-16 was well dispersed on the surface of the material as revealed by the Raman spectra of the catalysts. The metal oxide phase supported on MAS-4 and MAS-24 exhibited Raman peaks at 820 cm^{-1} characteristic of bulk MoO_3. The presence of MoO_3 suggests agglomeration of MoO_x species on the support surface leading to the formation of bulk MoO_3. The poor dispersion in MAS-4 was probably due to the incomplete incorporation of Al into the silica framework of MAS-4. At 15 wt % Mo loadings, formation of bulk MoO_3 on silica based support has also been previously reported (Huang et al., 2008). Si-O-Mo bond strength in silica based support is known to be relatively weaker that Al-O-Mo resulting in low metal support interaction as compared to alumina supports. The tendency to form Mo-O-Mo bonds leading to formation of bulk MoO_3 is therefore more in pure silica supports or supports where the incorporation of the hetero atom into the silica framework is not proper. The formation of bulk MoO_3 in MAS-24 despite the complete incorporation of Al into tetrahedral framework could be attributed to the low surface and partial collapse of the mesoporous structure of MAS-24. Nevertheless MAS-16 has high surface area as well as extensive 4 coordinated Al in the framework. As a result the MoO_x exists as a very well dispersed phase on the surface of MAS-16.

Consistent with the characterization results, sulfided NiMo catalyst supported on MAS-16 was found to be most active in the hydrotreating of both model compound and real feed stock. The high activity of the NiMo/MAS-16 can be ascribed to the following reasons : 1)Excellent textural properties 2) Optimum concentration of strong Bronsted and Lewis acid sites 3) formation of a well dispersed active phase.

Large pores and a narrow pore size distribution can eliminate diffusion limitations and provides greater accessibility to the active sites for the reactant and product molecules. In this regard, the hydrodesulfurization activity of mesoporous material is well documented in literature for large molecules like DBT and 4,6 DMDBT (Turaga and Song, 2003). Previous works on HDS of bulky molecules with microporous zeolites have yielded low conversions (Solís et al., 2006). MAS-16 with an average pore size of 5.2 nm and a surface area of 650 m^2/g is 40 % more active than NiMo supported on MAS-24 in the HDS of DBT. In addition, the total surface area of MAS-24 is relatively low and predominantly microporous in nature. The low surface area causes agglomeration of the MoO_x particles leading to the formation of bulk MoO_3 which is known to be difficult to sulfide.

4.5 MAS-16 –γ Al_2O_3 as mixed support for hydrotreating Light Gas Oil

Considering the excellent properties of MAS-16, it was used as a component in the preparation of the catalysts support for hydrotreatment with real feed stock. Three different MAS-16-Al_2O_3 mixed supports were prepared such that the MAS-16 loading was 0 wt %, 5 wt % and 10 wt % respectively. The rest of the mixture was γ-Al_2O_3. NiMo loading was kept constant at 5 wt % and 15 wt % respectively. The hydrotreatment of the LGO was performed in the same 500 mL Parr reactor. After flushing out the air with nitrogen, the reactor was pressurized with H_2 to 1000 psi. The temperature of the system was maintained at 350 ^oC. The batch reactor was kept at a constant stirring speed of 1000 rpm to avoid mass transfer limitations. Products were collected after 6 hrs of reaction time.

The textural properties and the acidic sites evaluation is presented in Table 4.3. It is observed that the surface area of the catalysts increase gradually with increase in the weight of MAS-16 in the mixture. There is however, no appreciable change in the pore diameter. The pore diameter

was essentially found to be bimodal typical of alumina materials. One very interesting aspect is the change in the total acid sites of the catalyst. With the incorporation of MAS-16 to Al_2O_3, the Bronsted and Lewis acid sites increase.

Table 4.3: Textural and acidic properties of NiMo supported on MAS-16 and Al_2O_3 composite material

Support Composition				Amount of acid sites (μmol/gm)		
MAS-16 (wt%)	Al_2O_3 (wt%)	$S_{tot}(m^2/g)$	d_{BJH} (nm)	Lewis	Bronsted	Lewis + Bronsted
5	95	298	8.1	421	9	430
10	90	332	7.9	455	16	471
0	100	189	8.6	396	--	396

The HDS and HDN activities of MAS supported catalysts are presented relative to a commercial catalyst. The conversions for HDS and HDN of the commercial catalyst are standardized to 100 % due to low conversions in a batch type reactor. The HDS and HDN activity of NiMo/MAS-16 (5 wt %) is higher than the commercial catalyst. Further, the activity of this catalyst was also found to be higher that NiMo supported only on Al_2O_3. However, the NiMo/Al_2O_3 performed better than NiMo/MAS-16 (10 wt %). A boiling point distribution comparison of the three catalysts is given in Figure 4.14. The volume fraction of lighter naptha products (boiling point 90- 170 ^oC) in NiMo/MAS-16 (5 wt %) is more than NiMo/γ-Al_2O_3 .The Bronsted acid sites in MAS-16 may have promoted the cracking of large hydrocarbon molecules in LGO into lighter products. On the other hand γ Al_2O_3 is known to possess Lewis acid sites which do not favor cracking reactions.

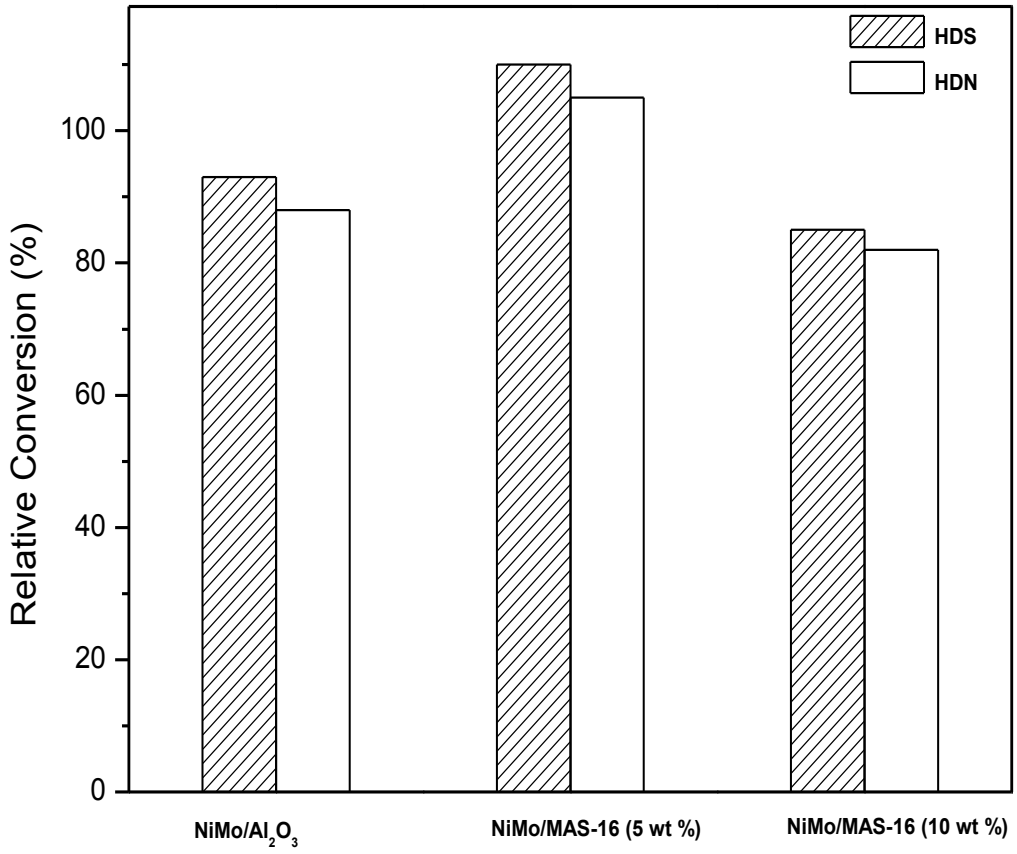

Figure 4.13: Hydrotreating activity of MAS supported NiMo catalysts relative to a commercial hydrotreating catalyst after 6 hrs of reaction time

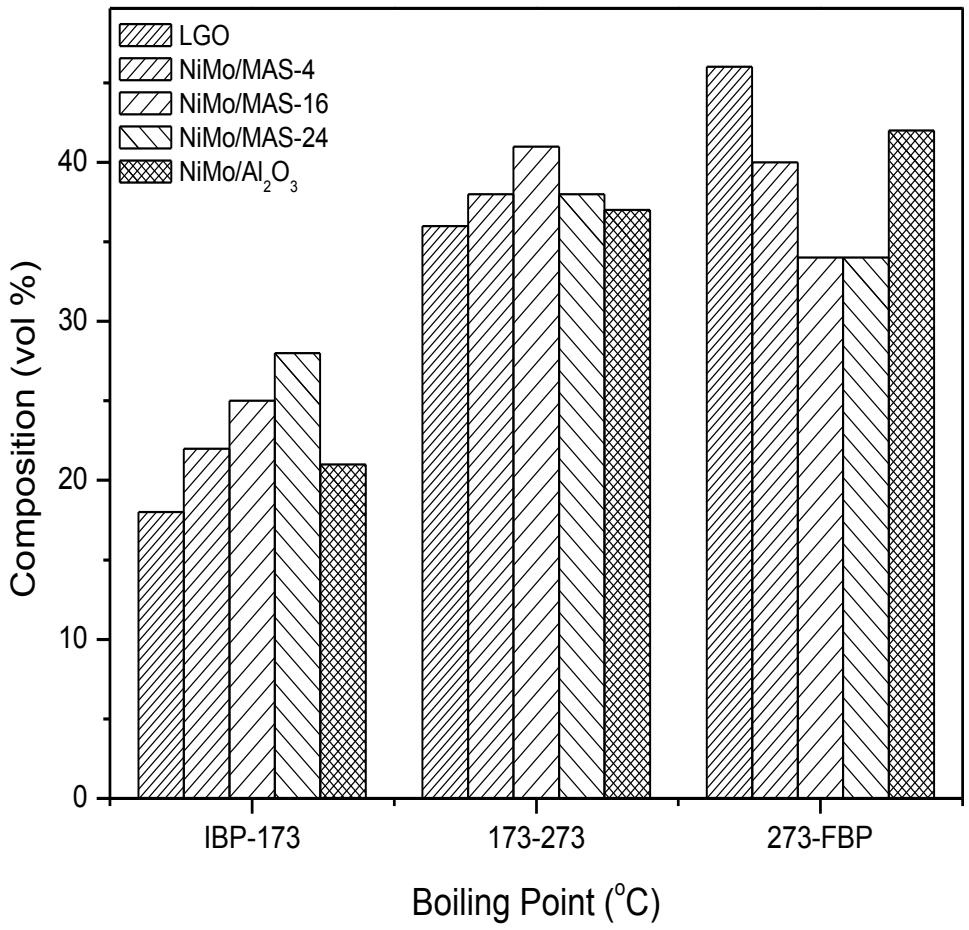

Figure 4.14: Boiling point distribution of the product of LGO hydrotreating after 6 hrs of reaction over different catalysts

4.6 Conclusions

Mesostructured alumino-silcate materials were synthesized from ZSM-5 nanoclusters and used as catalysts supports for the hydrotreatment of a model compound and real feed stock. The alumino-materials exhibited different acid strength and textural properties depending on the duration of hydrothermal treatment of the zeolite seeds. Three different MAS materials were synthesized using 4 hrs, 16 hrs and 24 hrs of hydrothermal treatment duration. Materials synthesized with low seeding time of 4 hrs showed properties similar to Al-SBA-15 prepared using the direct synthesis route, whereas material with high seeding time (t_{seed} = 24 hrs) resembled ZSM-5. The acidity of the MAS materials were found significantly higher than Al-SBA-15 and Al_2O_3 materials. The activity of NiMo catalysts supported on MAS materials were evaluated using the hydrodesulfurization of dibenzothiophene. The NiMo catalyst supported on mesoporous alumino silicate obtained after 16 hrs of hydrothermal treatment of the ZSM-5 precursors was found to be the most active in the HDS of DBT. Based on the preliminary catalytic tests, MAS-16 was selected as an additive to γ-Al_2O_3 to improve its acidic and textural properties. Three different MAS-16 –Al_2O_3 mixed supports were prepared using 0 wt%, 5 wt % and 10 wt % MAS-16. The hydrotreating activities of the NiMo catalyst supported on the prepared materials were evaluated in a batch reactor using light gas oil as the feedstock. From the hydrotreating tests, it was observed that the composition 5 wt % MAS-16 and 95 % Al_2O_3 has the highest promoting effect on the hydrotreating activity of the catalysts.

CHAPTER 5

EFFECT OF CITRIC ACID MODIFICATION

The effect of the addition of citric acid on the sulfidation properties and the hydrotreating activity of NiMo/MAS-16-Al_2O_3 have been described in this chapter. The synthesized catalysts were characterized extensively using different techniques like BET, FT-IR, Raman spectroscopy and X-Ray absorption spectroscopy. The chemical structure of the catalysts at various temperatures of sulfidation was probed using XANES and EXAFS. Finally, the hydrotreating activity of the catalysts was evaluated in a trickle bed reactor with heavy gas oil as the feedstock.

5.1 Synthesis and Characterization of catalysts

Three catalysts were synthesized by varying the citric acid (CA) to nickel (Ni) molar ratios. Three different ratios of CA/Ni = 0, 1 and 2 were used for preparing the catalysts. The catalysts were prepared using the pore volume impregnation procedure. Molybdenum was first loaded on the support followed by overnight drying and calcination at 550 ^{o}C. The molybdenum loading was followed by the impregnation of ctric acid and nickel in the desired molar ratio. Citric acid was first dissolved in a 20 % ammonium hydroxide solution followed by the addition of nickel nitrate hexa-hydrate. The catalysts in which citric acid was present were dried at 120 ^{o}C and not calcined. However the catalyst with CA/Ni = 0 was calcined after the impregnation of nickel nitrate solution at 550 ^{o}C.

The textural properties of the catalysts are listed in Table 5.1. It is observed that with increase in citric acid, the pore diameter and the surface area of the catalysts decreased. The relative deterioration of the textural properties can be attributed to the deposition of larger nickel citrate

and molybdenum-citrate complex on the face and the pores of the support. However, no major change in surface area and pore diameter were observed in the catalyst prepared without citric acid. The actual amount of metal present in the catalysts as determined through ICP-MS closely matched the targeted values, indicating that the loss of metals during the impregnation procedure was minimal.

Table 5.1: Textural properties of NiMo catalysts prepared with different CA/Ni ratios

Catalyst	Mo (wt%)	Ni (wt%)	CA/Ni (mol/mol)	BET Area (m^2/gm)	Pore Dia(nm)	Actual Loading Mo (%)	Ni (%)
Cat A	15	5	0	374	11.1	14.8	4.8
Cat B	15	5	1	324	10.9	14.9	4.7
Cat C	15	5	2	312	10.8	14.8	4.8

5.1.1 FT-IR Spectroscopy

FT-IR was carried out to investigate the formation of the nickel citrate complex on the catalysts. Figure 5.1 shows the FT-IR spectra of the 3 catalysts. The presence of a transmittance band at 1390 cm^{-1} in Cat B and Cat C, confirms the formation of Nickel-Citrate complex. The band at 1390 cm^{-1} is attributed to the symmetric stretching of the $RCOO^-$ group (Tsimbler et al., 1969). Cat A shows only one band at 1510 cm^{-1} which was assigned to the H-O-H bending mode of adsorbed water. No band at 1390 cm^{-1} is observed in Cat A. The FT-IR results confirm the presence of citric acid in Cat B and Cat C. Figure 5.2 shows the effect of calcination on the catalysts. This indicates that the nickel citrate complex decomposes on calcination at high

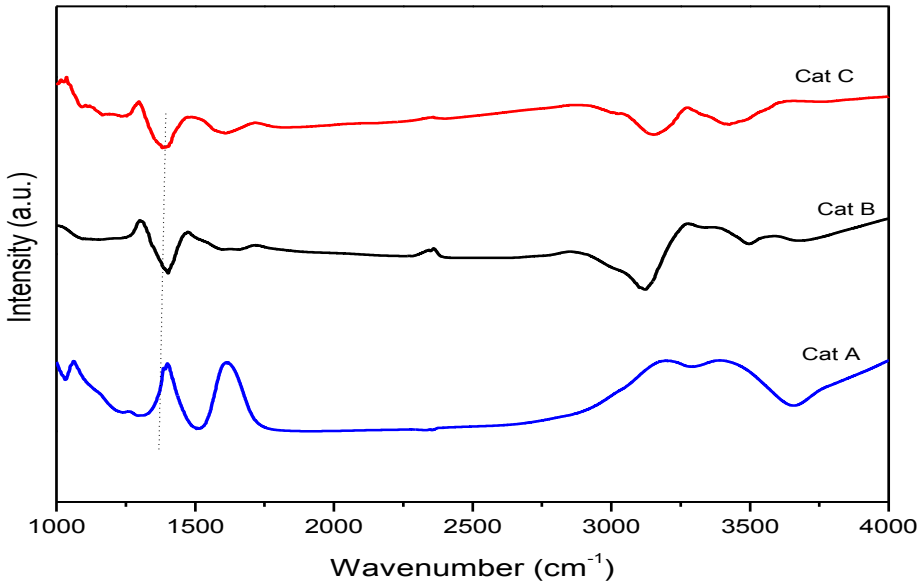

Figure 5.1: FT-IR spectra of the catalysts with different CA/Ni ratios

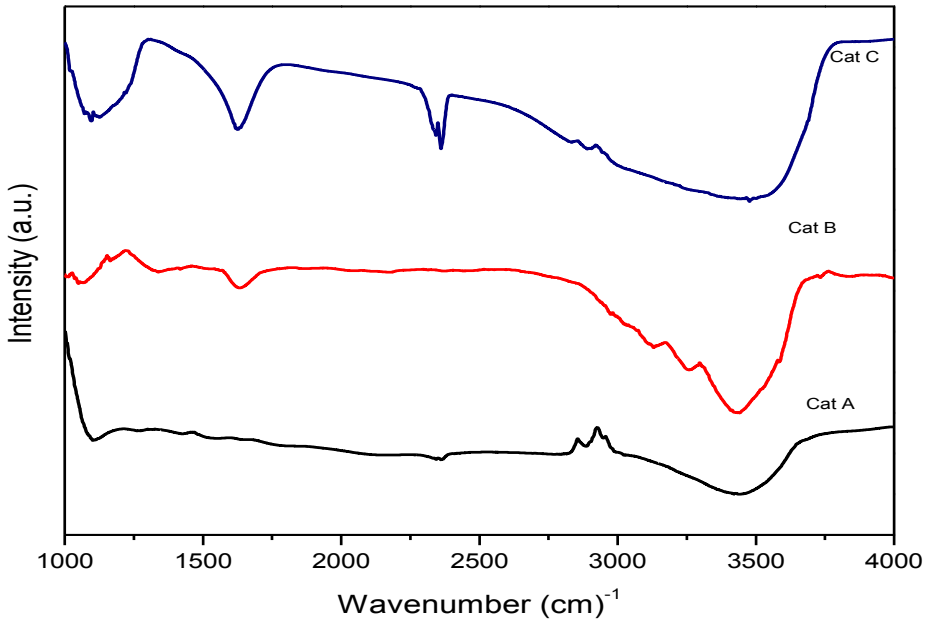

Figure 5.2: FT-IR spectra of the prepared catalysts after calcination

temperatures. Thus, it is important that the catalysts with citric acid be not calcined in order to preserve the metal citrate complex formed in the catalyst.

5.1.2 Raman Spectroscopy

Figure 5.3 shows the laser Raman spectra of the synthesized catalysts. The difference in the spectra of the catalyst is due to the nature of the Mo complex formed in the system. Cat C with the higest CA/Ni ratio of 2 shows gives peaks at 978 cm^{-1}, 950 cm^{-1} and 896 cm^{-1}. The peak at 978 cm^{-1} has been identified as the interaction species of MoO_x with the γ Al_2O_3 support (Wachs, 1996). An additional peak at 950 cm^{-1} can be identified as the Mo=O stretching band present in $Mo(H_xCitrate)O_3^{4-x}$ (Samotus et al., 1991) . Presence of this band indicates the formation of Mo-citrate complex in addition to the Ni-citrate complex already formed. Cat B with a CA/Ni of 1 gives a single peak at 977 cm^{-1} indicating the formation of a very well dispersed amorphous phase of MoO_x on the alumina support. Absence of peaks as those present in Cat C confirms that no Mo-Citrate complex formation has taken place and all the citrate ions are complexed with Ni only. In addition, no sharp peaks at 890 and 990 cm^{-1} show the absence of a crystalline MoO_3 phase in all three catalysts. Thus a 15 wt % Mo loading is sufficiently well dispersed on the support and no MoO_3 is observed from the Raman Spectroscopy results. As with the FT-IR spectroscopy, Raman spectra were recorded for the catalysts in order to observe the effects of calcination. Figure 5.4 shows the Raman spectra of the 3 catalysts after calcination. It is observed

that the peaks for molybdenum-citrate complex have completely vanished and there is hardly any

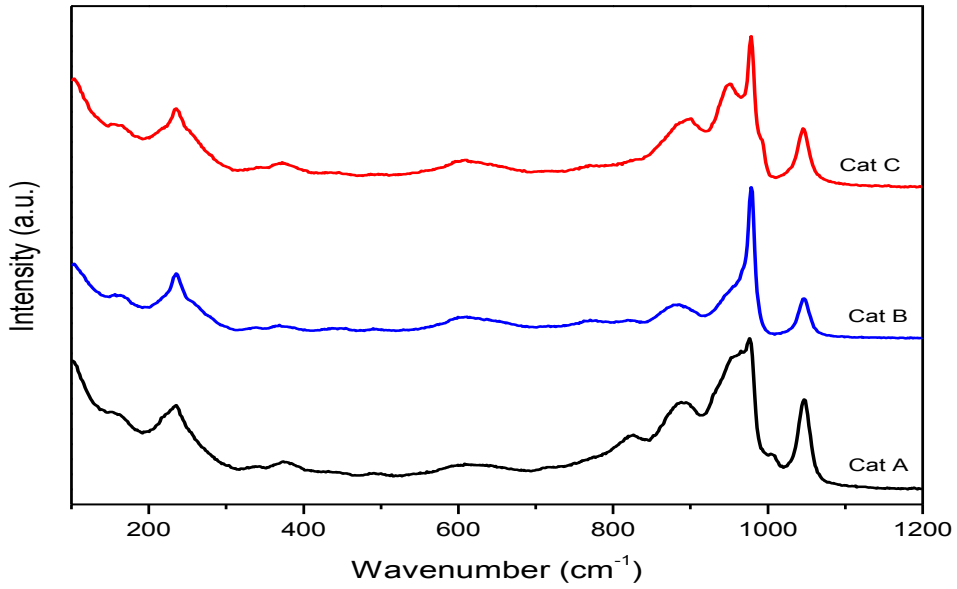

Figure 5.3: Raman spectra of the synthesized catalysts after drying

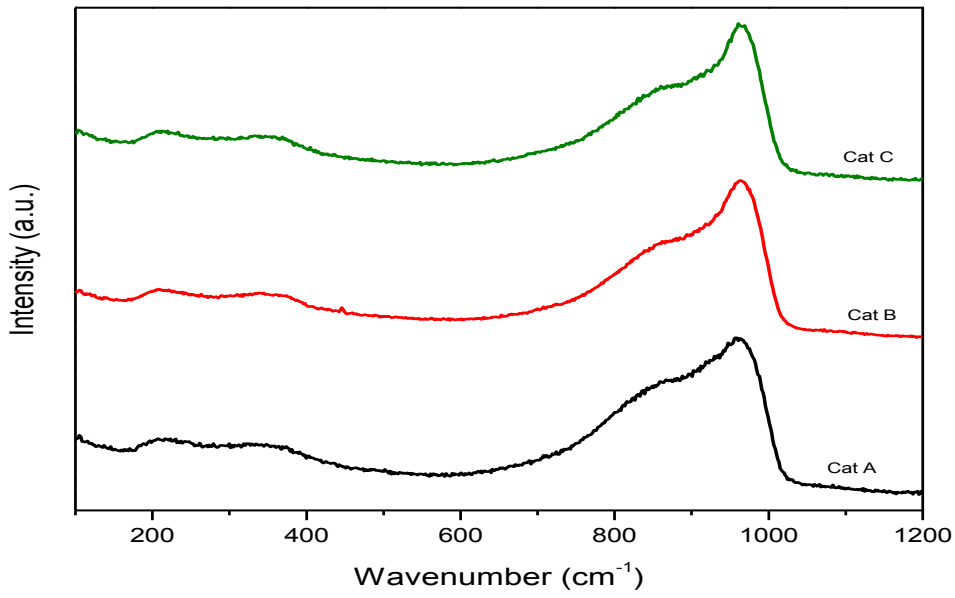

Figure 5.4: Raman spectra of the synthesized catalysts after calcination

difference between the three catalysts. Only one broad peak at 970 cm^{-1} is observed in all three catalysts which are typical of the well dispersed $MoO_x - Al_2O_3$ interacting species.

5.1.3 Mo K Edge EXAFS

The Mo K edge EXAFS spectra are shown in Figure 5.5 for the three catalysts. The near edge spectra of the three catalysts are shown in Figure 5.6. The pre-edge feature present in all the three catalysts can be attributed to the 1s – 4d bound state transition. The transition probability of this formally forbidden excitation is dependent on the local symmetry of the molybdenum atom.

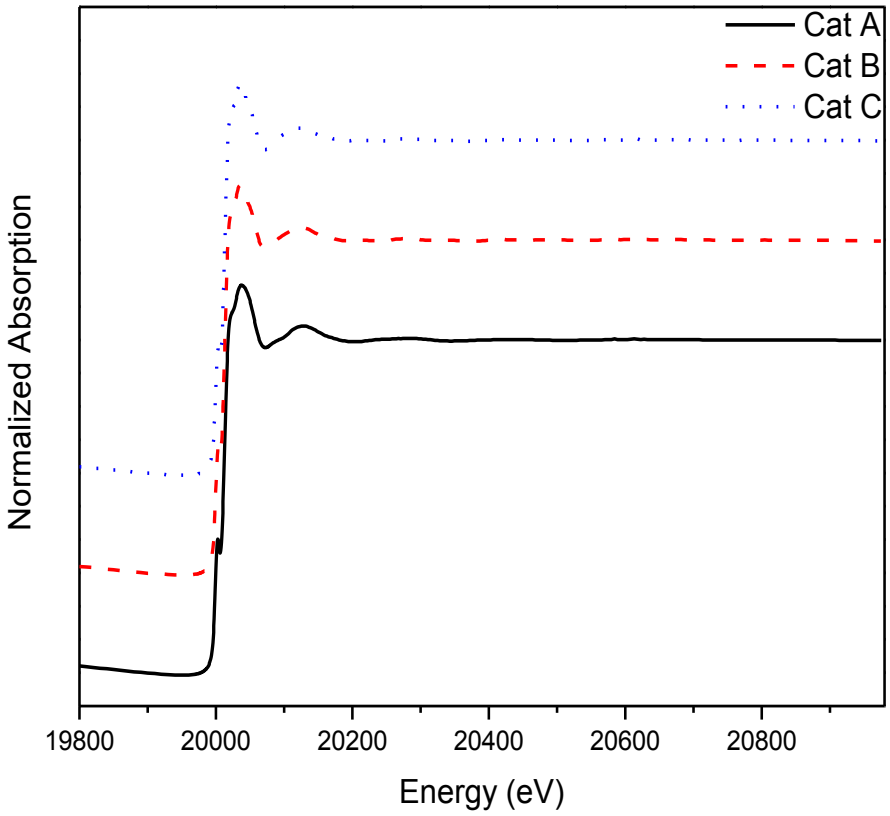

Figure 5.5: Mo K edge EXAFS spectra of the three catalysts

The effective mixing of metal d-states with ligand p-orbitals in case of tetrahedral symmetry gives rise to a more intense pre-edge feature. In case of a non perfect octahedral surrounding of the central atom the 1s-4d transition is only slightly allowed. The lower intensity of the pre-edge peaks in the spectra of the catalysts is thus an indicator of the distortion in the octahedral coordination around the molybdenum atom.

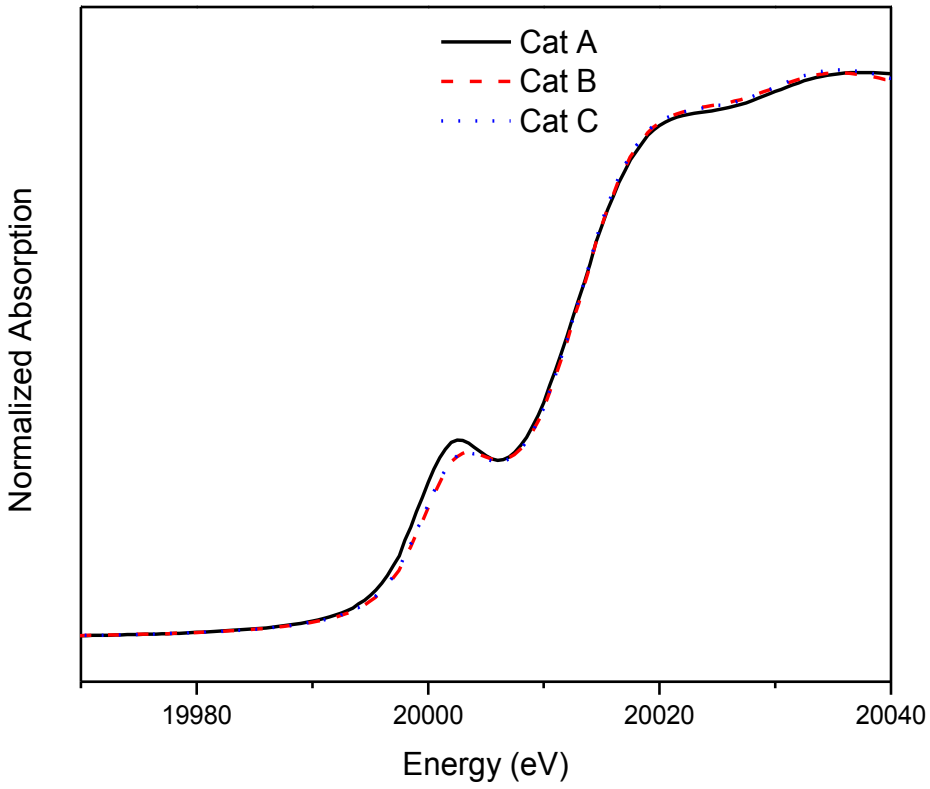

Figure 5.6: Mo K edge spectra of the three catalysts in the XANES region showing the pre-edge peak

As observed in Figure 5.6, Cat A has a relatively pronounced pre edge feature as compared to Cat B and Cat C. The distortion of the octahedral symmetry around the Mo atom is more in Cat A than Cat B and Cat C in which citric acid is present. Cat A has a very similar feature to MoO_3 which also exhibits a more distinct pre-edge peak. Or alternately, there is also a possibility of a higher percentage of tetrahedrally coordinated molybdenum oxide species when no citric acid is present. Further, it is also confirmed that at both the ratios of CA/Ni, some mount of citric acid always gets complexed with molybdenum.

Figure 5.7 shown below demonstrates the high signal to noise ratio of the collected data in k space even at higher k value of 12.

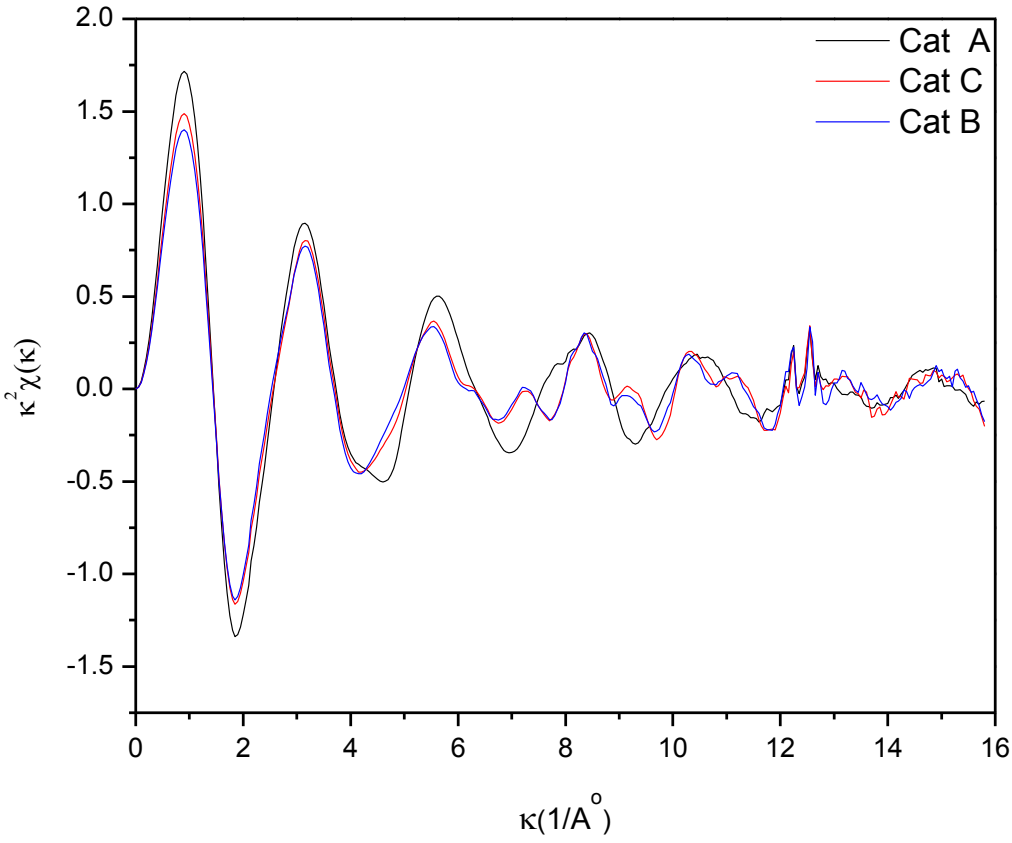

Figure 5.7: Mo K edge EXAFS spectra demonstrating the high signal to noise ratio of the collected data in k space even at higher k value of 12

The Fourier Transformation of the EXAFS spectra is shown in Fig.5.8. The k^3 weighted FT EXAFS function show that, in the presence of CA, both the first shell (0.5 - 1.5 A^o) and the second shell (2.5 – 4 A^o) are affected. Compared with Cat A, the FT of Cat B and Cat C show a strong decrease in intensity between 0.5 and 1.5 A^o. In contrast, the signal between 2.5 A^o and 4 A^o of Cat B and Cat C is much more intense and asymmetrical than that of Cat A. The results of the fit for Cat A, Cat B and Cat C is shown in Table 5.2.

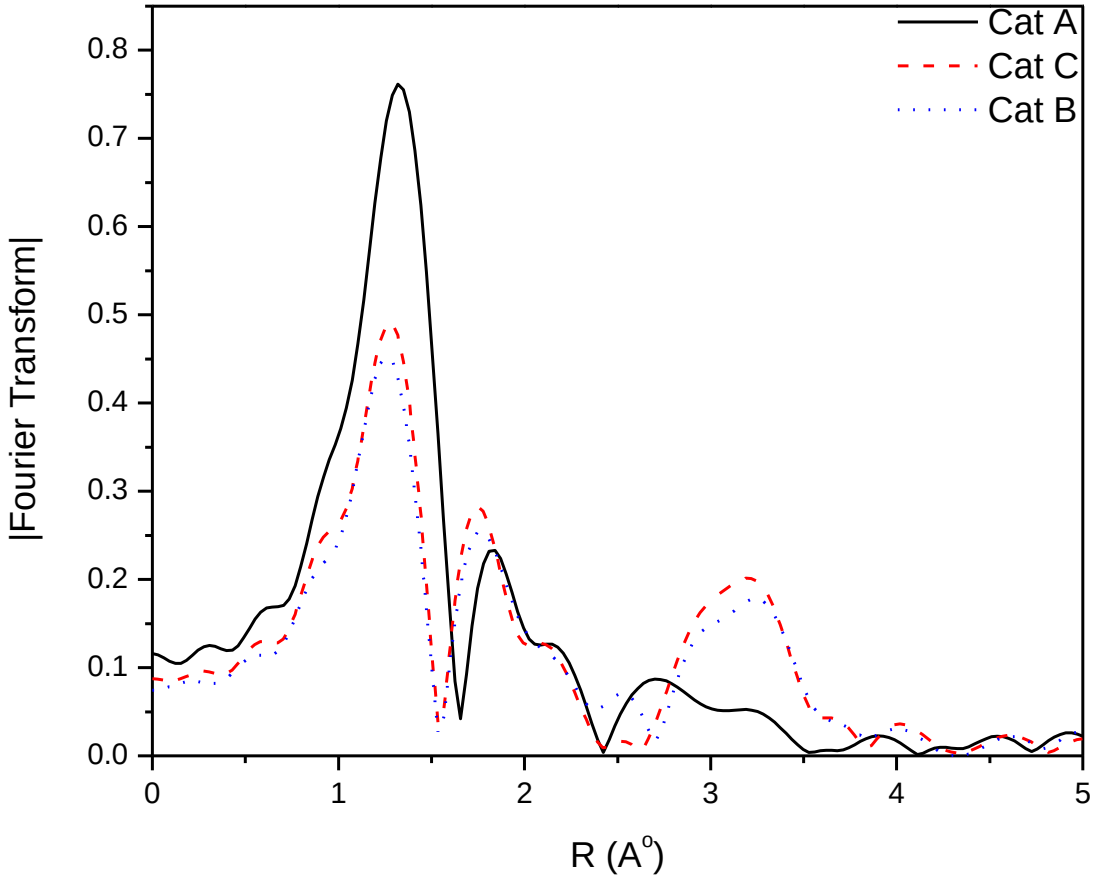

Figure 5.8: Radial Distribution Functions of the EXAFS spectra of the three catalysts in oxide state

The fitting results suggest that Mo in Cat A on an average is present in a distorted tetrahedral geometry. On the contrary, Cat B and Cat C have 3 O contributions at 1.71, 1.90 and 2.35 A^o indicating an octahedral geometry for Mo in Cat B and Cat C. Another interesting feature is the decrease in signal intensity from 2.5 - 4 A^o in Cat A.

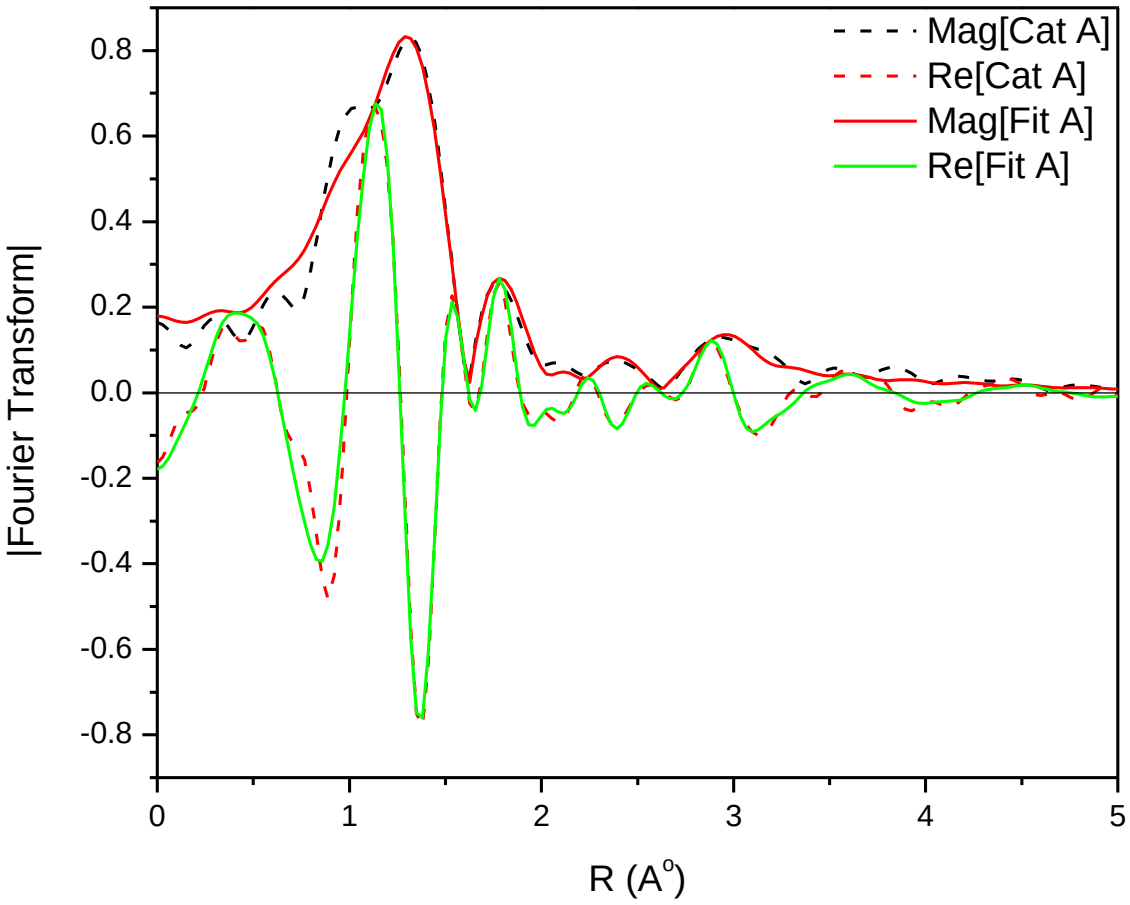

Figure 5.9: Magnitude and real part of the Fourier Transform of Mo K edge EXAFS spectra in Cat A. The solid line represents the fitted spectra

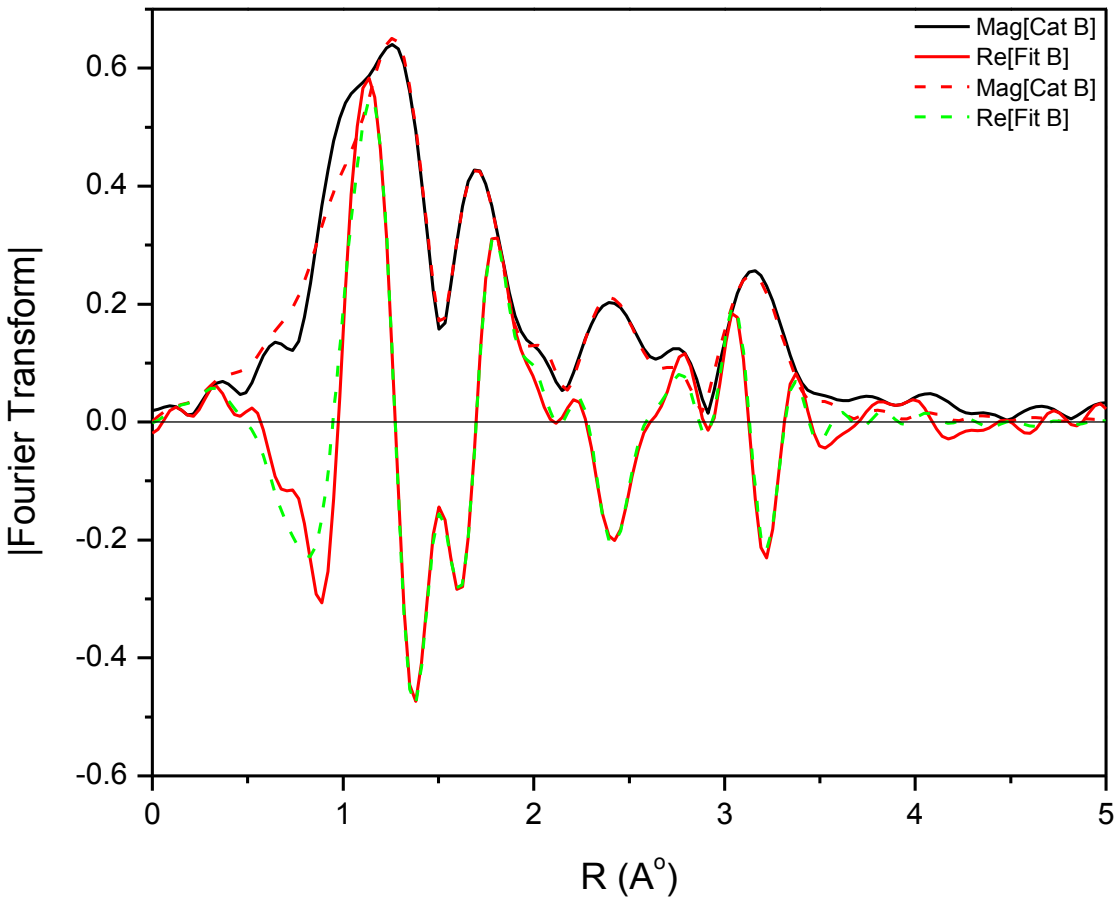

Figure 5.10: Magnitude and real part of the Fourier Transform of Mo K edge EXAFS spectra in Cat B. The solid line represents the fitted spectra

The contribution to this shell is primarily from Mo-Mo and Mo-Ni. The amplitude for this shell, which mainly consists of Mo-Mo contributions, is a measure of the size of the molybdenum oxide particles. The reduced intensity of this peak in Cat A indicates the MoO_x species in Cat A are smaller as compare to Cat B and Cat C. Indeed, calcination in Cat A leads to the formation of

isolated species of MoO_x which are primarily tetrahedral. However, in Cat B and Cat C a Mo-Citrate complex $[(MoO_2)_4O_3(C_6H_5O_7)_2 \cdot 6H_2O]^{4-}$ is formed with distorted octahedral geometry. This formation of this complex is more in Cat C than in Cat B. It is only obvious that at higher CA/Ni ratios, the tendency to form Mo-citrate complex will only be greater.

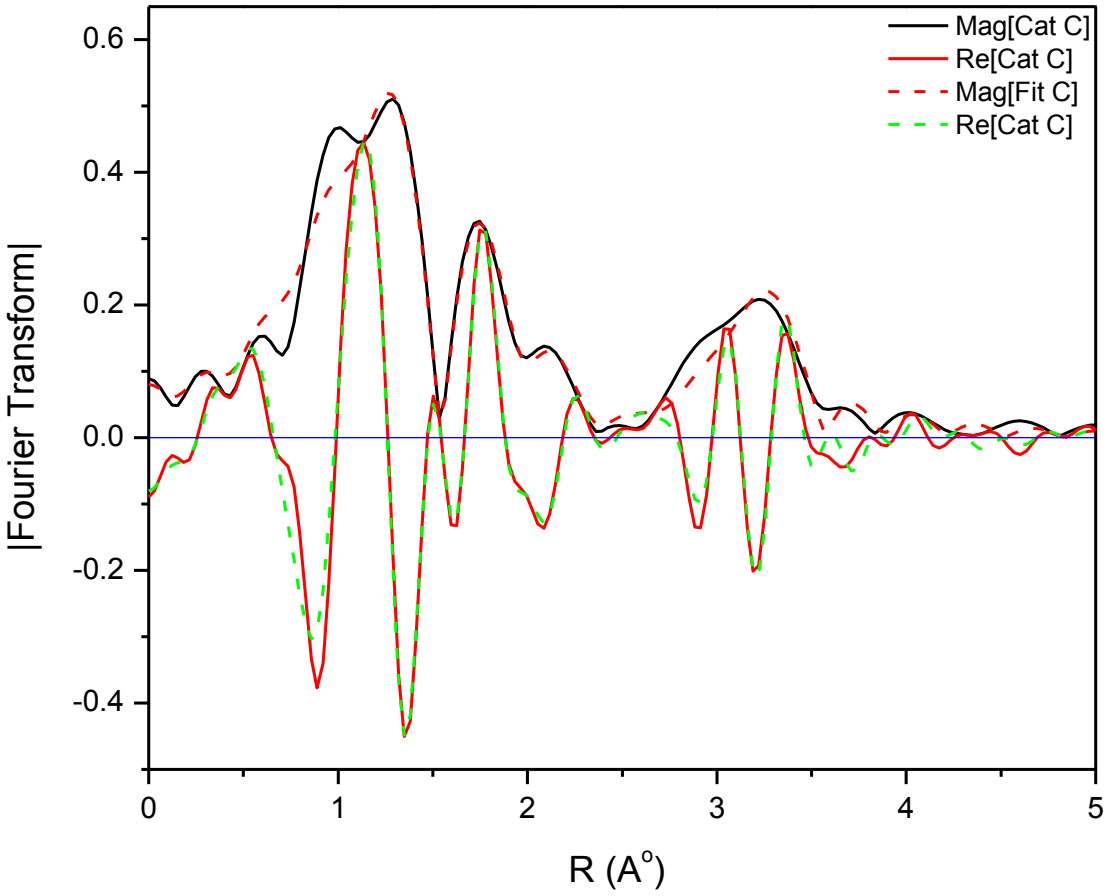

Figure 5.11: Magnitude and real part of the Fourier Transform of Mo K edge EXAFS spectra in Cat A. The solid line represents the fitted spectra

Table 5.2: Obtained fit parameters for bond distance (R), coordination number (N) and ΔE_o for the three catalysts

	Mo-O_1				Mo-O_2				Mo-O_3				Mo-Mo			
	R (A^o)	N	$\Delta\sigma^2$ (10^{-4} A^o)	ΔE_o(eV)	R	N	$\Delta\sigma^2$ (10^{-4} A^o)	ΔE_o (eV)	R	N	$\Delta\sigma^2$ (10^{-4} A^o)	ΔE_o(eV)	R	N	$\Delta\sigma^2$ (10^{-4} A^o)	ΔE_o(eV)
Cat A	1.75	2.3	36.7	-10.4	1.99	0.4	3.2	-11.2	2.37	1.5	42.1	3.5	-	-		
Cat B	1.71	1.9	40.3	-9.4	1.94	1.8	4.3	3.2	2.33	1.4	21.4	-2.4	3.3	1.7	82.3	-3.1
Cat C	1.73	2	28.9	2.3	1.94	1.9	16.6	2.1	2.31	1.5	94.7	-6	3.1	1.9	52.1	-4.6

5.1.4 Ni K Edge XANES

The Ni K-edge XANES spectra for the prepared catalysts along with the reference materials NiO and $NiMoO_4$ is presented in Fig. 5.12. The Ni K-edge mainly probes the electron transition from 1s orbital to the 4p orbital. The associated pre edge peak is assigned to the dipole forbidden Ni (1s) to Ni (3d) electronic transition. This feature is strictly forbidden in centro-symmetric octahedral configuration. However, such transitions are allowed in a tetrahedral field. The absence of any pre edge feature in the materials indicates that Ni is coordinated almost exclusively with oxygen atoms in an octahedral geometry. Another interesting feature is the reduction in the white line intensity of the 1s - 4p transition when citric acid is present. The formation of nickel-citrate complex may have attributed to this decrease in the white line intensity in Cat B and Cat C. In comparison, the peak position of the second reference NiO occurs at 8336.3 eV about 1.5 eV less than that of $NiMoO_4$ and the synthesized catalysts. Further, NiO exhibited additional broad features at 8356 eV and 8373 eV. It is interesting to note that these features are absent in the synthesized catalysts as well as pure $NiMoO_4$. On the basis of the above observations, it can be thus ascertained that the Ni present in Cat A is primarily as a $NiMoO_4$ phase after calcination, distinct from the pure NiO phase, whereas a nickel-citrate complex is formed in Cat B and Cat C confirming the FT-IR results.

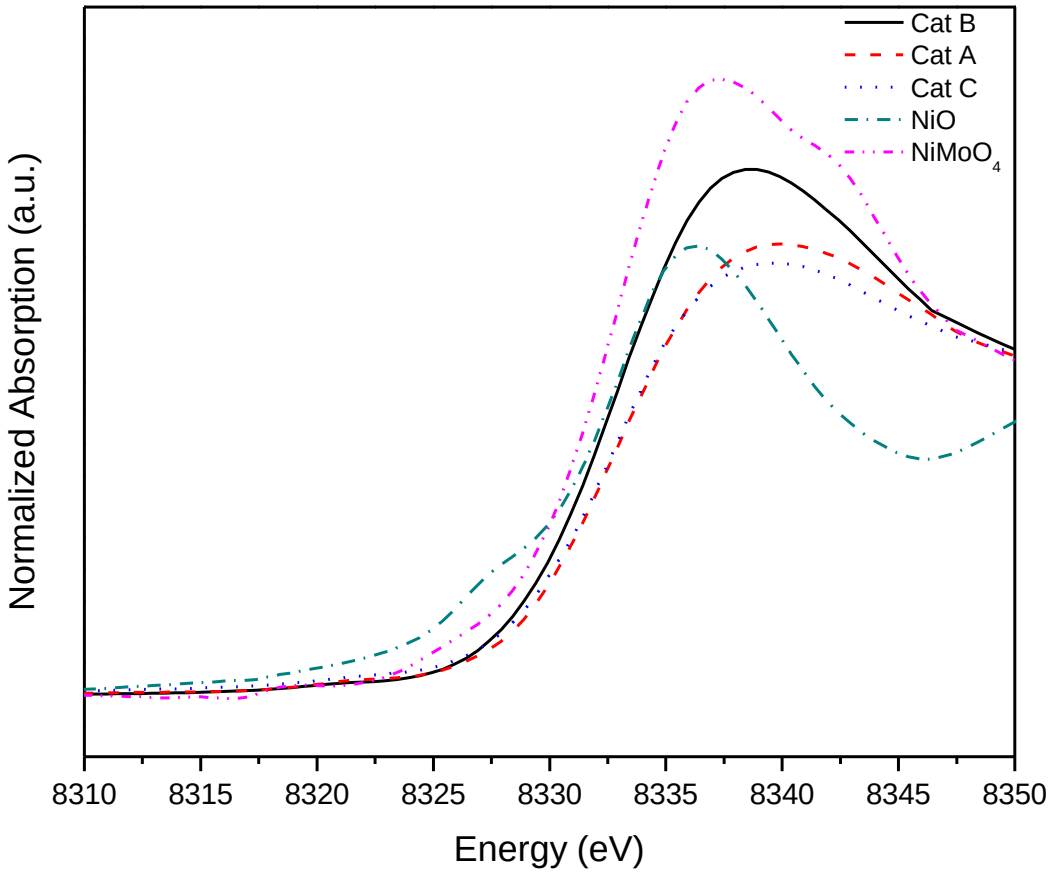

Figure 5.12: Ni K-edge XANES spectra in the pre-edge region for the prepared catalysts along with the reference materials NiO and $NiMoO_4$

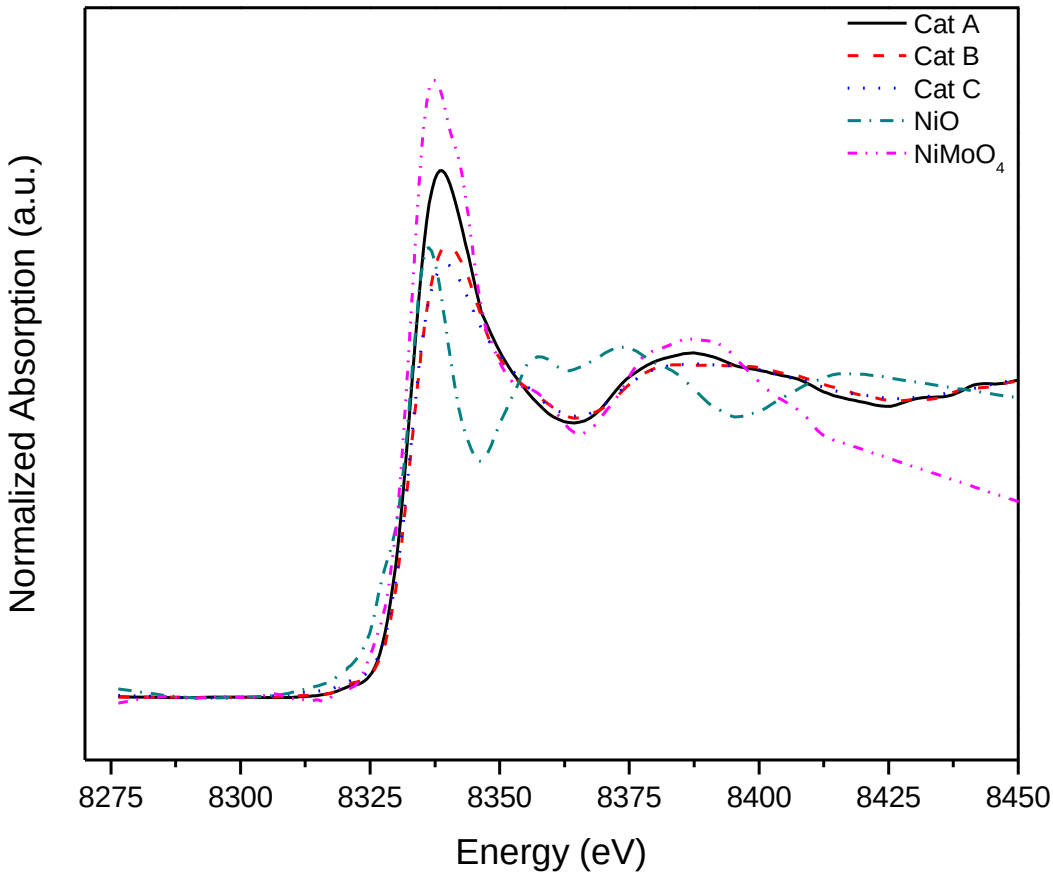

Figure 5.13: Ni K-edge XANES spectra for the prepared catalysts along with the reference materials NiO and $NiMoO_4$

5.2 Effect of Citric Acid on Sulfidation of Catalysts

The synthesized catalysts were sulfided at three different temperatures to trace the transition of the oxide catalysts into the sulfided state and the effect of citric acid on the sulfidation of the catalysts. The catalysts were sulfided at 150 ^{o}C, 250 ^{o}C and 350 ^{o}C and then the chemical state of the active metals were analyzed using X-ray absorption techniques.

5.2.1 Mo K Edge XAS

The Mo near edge spectra of three catalysts at different sulfiding temperatures is shown in Figure 5.14. With increase in temperature, the pre-edge peak attributed to the 1s – 4d bound state transition corresponding to a dissymmetric octahedral surrounding of the Mo atoms gradually vanishes. The disappearance of this peak is also marked by the shifting of the spectra to lower energies. In the presence of citric acid, this shift is less pronounced and the shape of the edge is closer to the oxidic sample indicating that the sulfidation is slowed down.

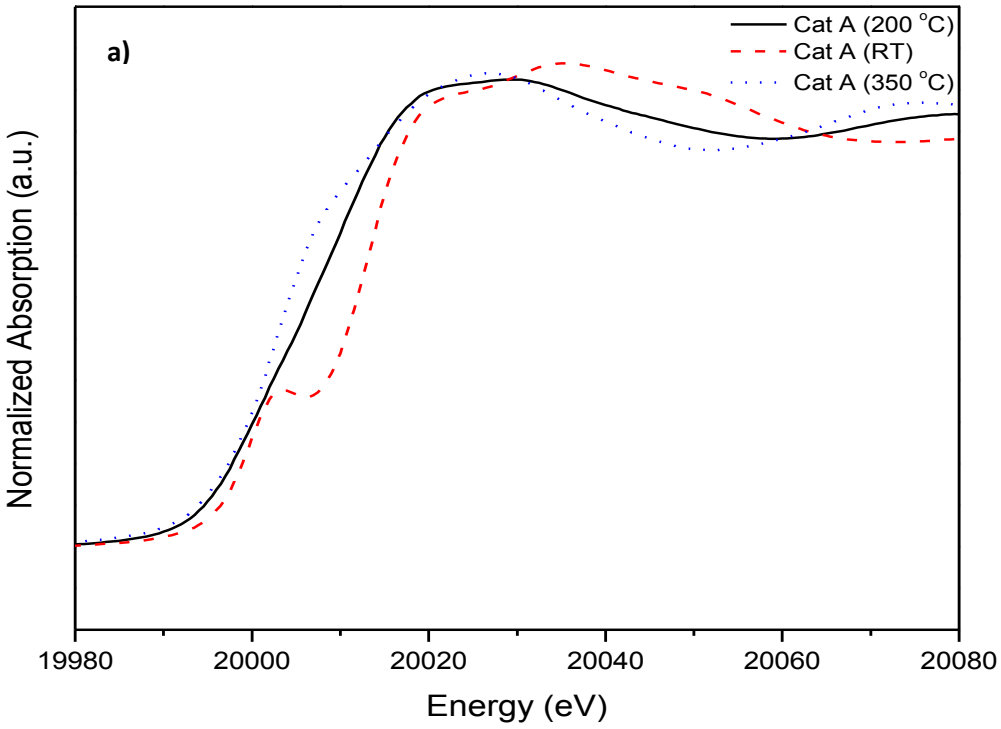

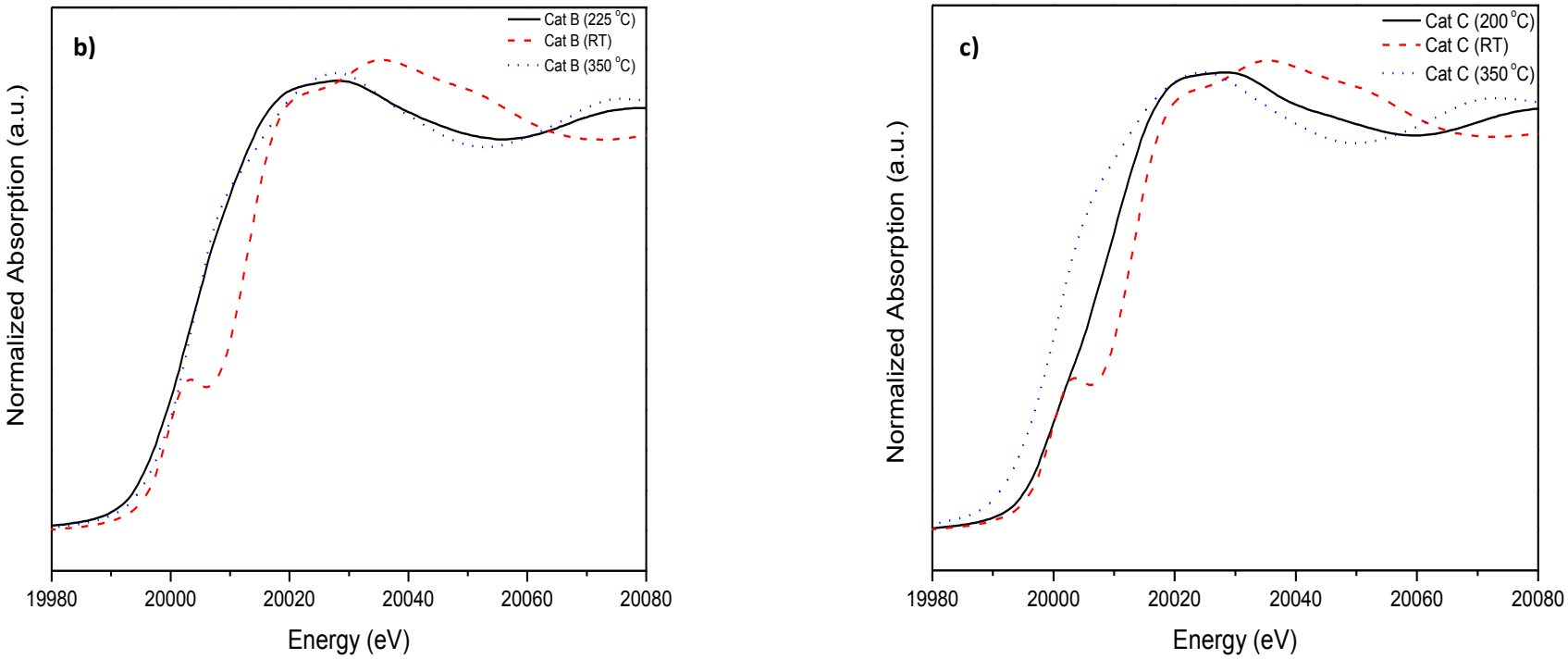

Figure 5.14: Mo near edge spectra of the catalysts at different sulfiding temperatures a) Cat A; b) Cat B; c) Cat C

Remarkable changes are observed in the Radial Distribution Function (RDF) curves for the catalysts sulfided at an intermediate temperature of 225 ^{o}C. The most distinct feature of the intermediate sulfided catalysts as compared to the oxide catalysts is the appearance of a new shell at 1.90 A^{o} (phase uncorrected) combined with the attenuation of the Mo-O signal at 1.72 A^{o}. Further, the Mo-O contributions at 1.93 A^{o} and 2.29 A^{o} have also vanished completely. Thus at 225 ^{o}C, the weaker Mo-O-Mo bridging bonds gets cleaved first to form the Mo-S bonds, similar to that in crystalline MoS_2. Indeed, the Mo-S bond distance calculated to be 2.42 A^{o} was very close to the reference MoS_2 (Dickinson and Pauling, 1923). Another interesting feature of the RDF curve, is the intensity of the Mo-S shell in Cat B as compared to Cat A and Cat C. The amplitude of the Fourier Transform of the EXAFS function is directly related to the coordination number of the scattering atom. It is clear that the extent of sulfidation in Cat A is much larger as compared to Cat B and Cat C at 225 ^{o}C. The results from the RDF curves are further confirmed by fitting the spectra with suitable standards. The results from the fits are listed in Table 5.3

Table 5.3: Fit parameters of the three catalysts after sulfidation at 225 ^{o}C

	Mo-O				Mo-S			
	R	N	$\Delta\sigma^2$ (10^{-4} A^{o})	ΔE_o(eV)	R	N	$\Delta\sigma^2$ (10^{-4} A^{o})	ΔE_o(eV)
Cat A	1.79	0.46	12.3	3.67	2.41	2.41	-53	1.32
Cat B	1.76	0.55	41	5.6	2.43	1.2	23	6.3
Cat C	1.78	0.6	65	-11	2.43	1.4	41	-4.1

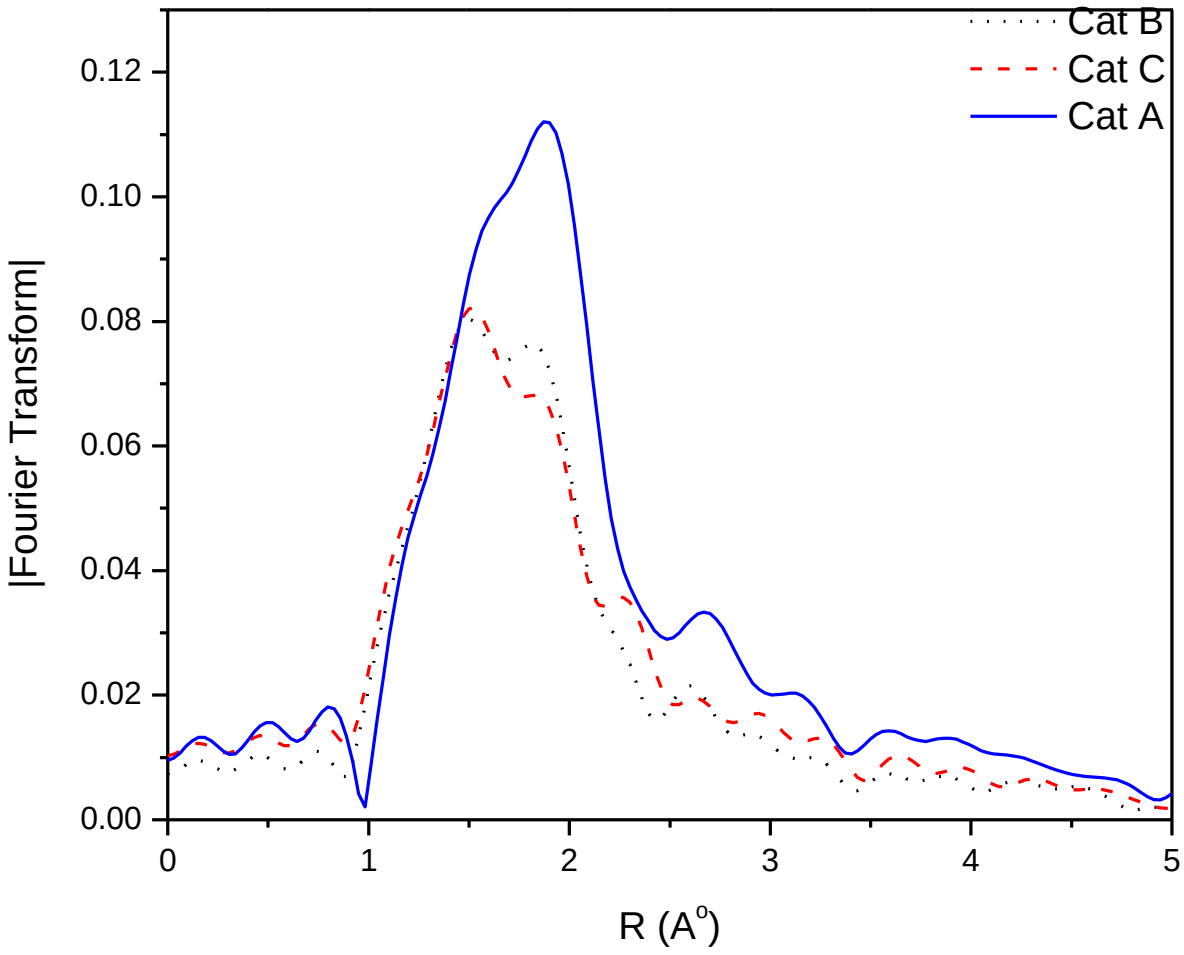

Figure 5.15: Radial Distribution Functions of the EXAFS spectra of the three catalysts after sulfidation at 225 ^{o}C

On increasing the sulfidation temperature further to 350 ^{o}C, it is observed that the strong bridging oxygen peaks are replaced by Mo-S peaks. There is also an appearance of Mo-Mo shell at 3.14 A^{o} (phase corrected). The Mo-S and Mo-Mo interatomic distances correspond to the structural parameters of bulk MoS_2, while the observed coordination Mo-Mo coordination number is lower than that of MoS_2 (N_{Mo-Mo}= 6). This indicates the formation of small crystallites of MoS_2 irrespective of the preparation method. The fit parameters of the Fourier Transformations of the

sulfided catalysts are given in Table 5.4. The higher coordination number for Mo-S and Mo-Mo shells in Cat B and Cat C indicates a better saturation of the MoS_2 edges as compared to Cat A. The smaller N_{Mo-S} and N_{Mo-Mo} coordinations in Cat A suggest a partial formation of Type II sites in Cat A. Further Cat A and Cat C also show Mo-O contributions at 1.72 and 1.98 A^o. These bonds can be attributed to the terminal and bridging oxygen atoms that remain unsulfided even at 350 ^oC. It is notable that these features are essentially absent in Cat B, possibly because of an optimal promotion of MoS_2 by Ni resulting in better sulfidation.

Table 5.4: Fit parameters of the three catalysts after sulfidation at 350 ^oC

	Mo-O				Mo-S				Mo-Mo			
	R	N	$\Delta\sigma^2$ (10^{-4} A^o)	ΔE_o (eV)	R	N	$\Delta\sigma^2$ (10^{-4} A^o)	ΔE_o (eV)	R	N	$\Delta\sigma^2$ (10^{-4} A^o)	ΔE_o (eV)
Cat A	1.79	0.6	34.2	2	2.41	5.5	28.3	3.1	3.14	3.1	38.2	2.7
Cat B	1.77	0.3	21.6	3.3	2.41	5.6	43.7	7.2	3.14	3.9	54.3	9.1
Cat C	1.79	0.5	43.8	6.3	2.41	5.3	72.4	2.9	3.14	3.7	56.2	3.8

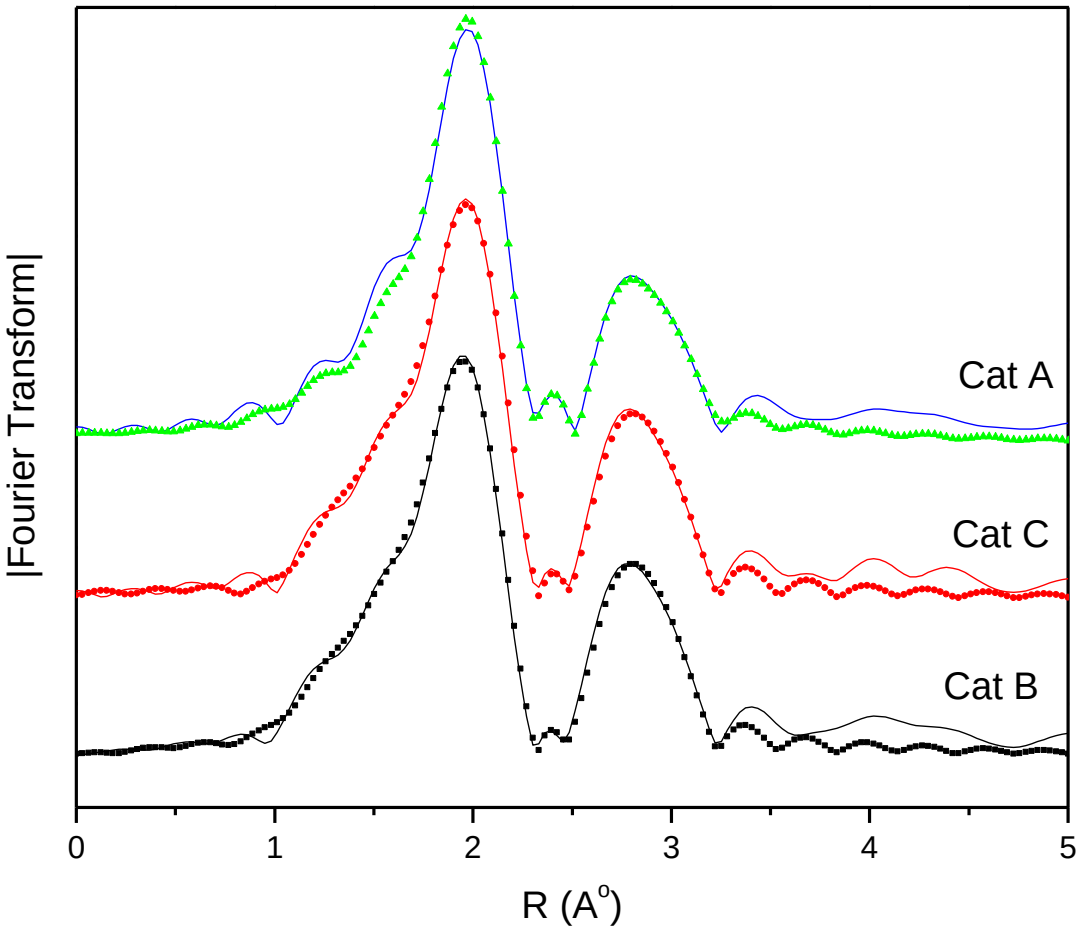

Figure 5.16: Magnitude of the Fourier Transform of Mo K edge EXAFS spectra in the three catalysts. The symbols represents the fitted spectra

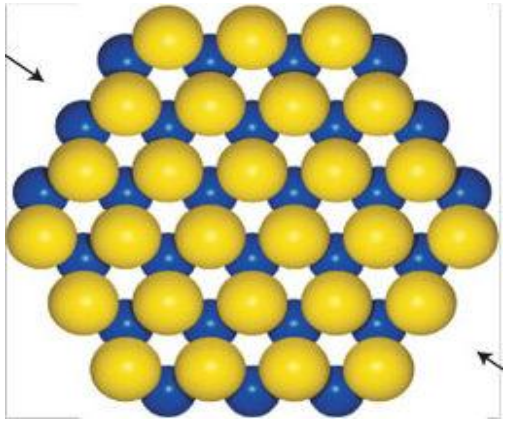

Figure 5.17a: Hexagonal MoS_2 stack formed after sulfidation

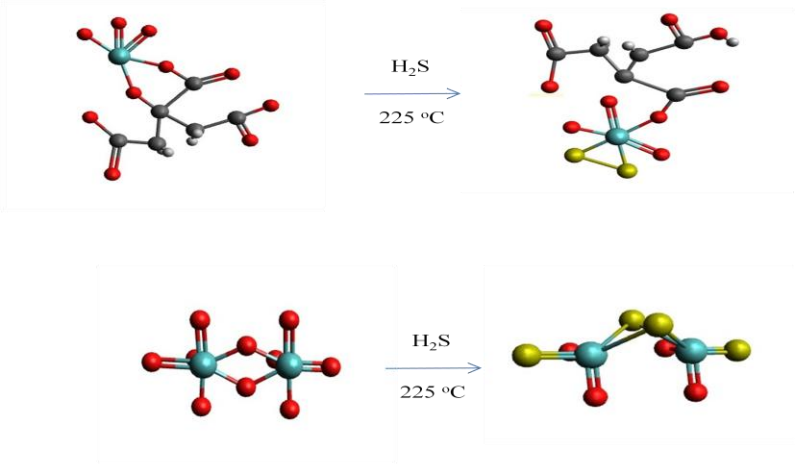

Figure 5.17b: Schematic showing sulfidation in Cat A and Cat B

Figure 5.17c: Picture depicting the interatcion of molybdenum with the support in Cat A (left) and complete sulfidation in Cat B (right)

5.1.1 Ni K Edge XANES and HRTEM

The effect of temperature on the sulfidation of Ni is studied using the near edge spectra of Ni K edge. Figure 5.18 shows a comparison of the Ni K edge spectra between Cat A and Cat B at sulfided at 150 ^{o}C, 250 ^{o}C and 350 ^{o}C. The sharp white line characteristic of the dipole allowed 1s-3p transition is observed for both the catalysts at room temperature whereas a slight pre edge feature around 8322 eV is observed only in Cat A. This feature is strictly forbidden in centro-symmetric octahedral configuration (Basu and Ghosh, 1973). However, such transitions are allowed in a tetrahedral field. The presence of this peak indicates that some Ni is also present in a tetrahedral coordination. This is in contrast with Cat B, where Ni is coordinated almost exclusively with oxygen atoms in an octahedral configuration. The formation of Ni-citrate complex wherein, Ni is coordinated with 6 oxygen atoms possibly results in this geometry. At 150 ^{o}C, no appreciable change in the Ni K edge spectra is observed in Cat B. However in Cat A, the white line characteristic of NiO is replaced by a broader curve similar to NiS_x. This suggests a possible delay in the sulfidation of Ni when citric acid is used. The formation of Ni-citrate complex in Cat B inhibits the sulfidation of Ni at lower temperatures. On increasing the temperature to 250 ^{o}C, Cat B and Cat A exhibit similar spectra. It is evident from the Ni and Mo K edge spectra that citric acid not only affects the Ni species but also the Mo species even at lower ratios of CA/Ni. The formation of Ni-citrate complex and Mo-citrate complex results in slower rate of sulfidation. However, larger CA/Ni (CA/Ni = 2) ratios results in an excessive formation of Mo-citrate complex which hinders the complete sulfidation of MoS_2. Nevertheless, use of citric acid as an additive promotes Type II Ni-Mo-S sites as compared to Cat A. This is further confirmed by the HRTEM images of the three catalysts (Fig 5.19). A statistical analysis of

the images reveals that the stacking of MoS_2 layers is larger in Cat B and Cat C. On the contrary Cat A mostly forms single layered MoS_2 slabs.

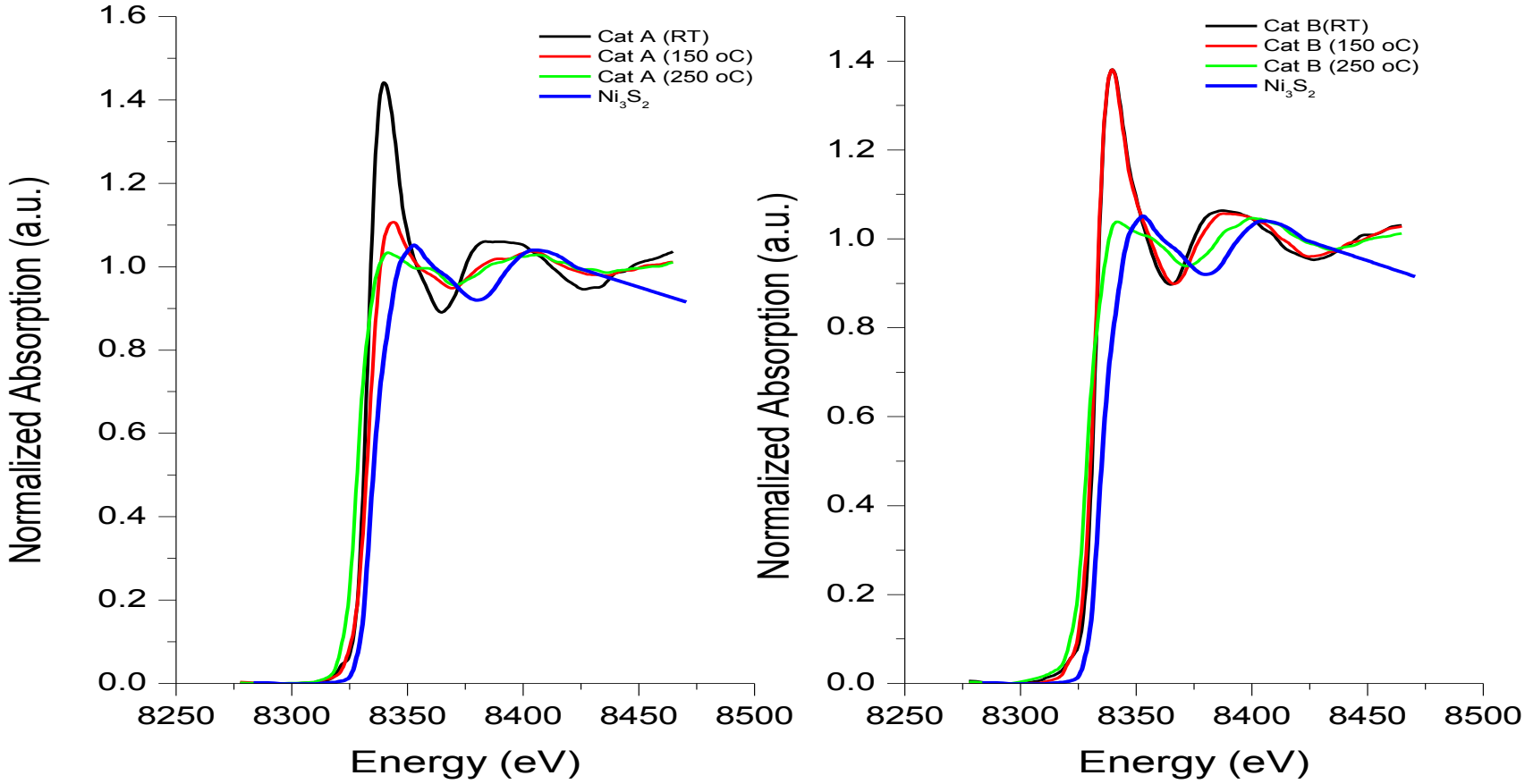

Figure 5.18 Comparison of the Ni K edge spectra between Cat A and Cat B at sulfided at 150 ^{o}C, 250 ^{o}C and 350 ^{o}C.

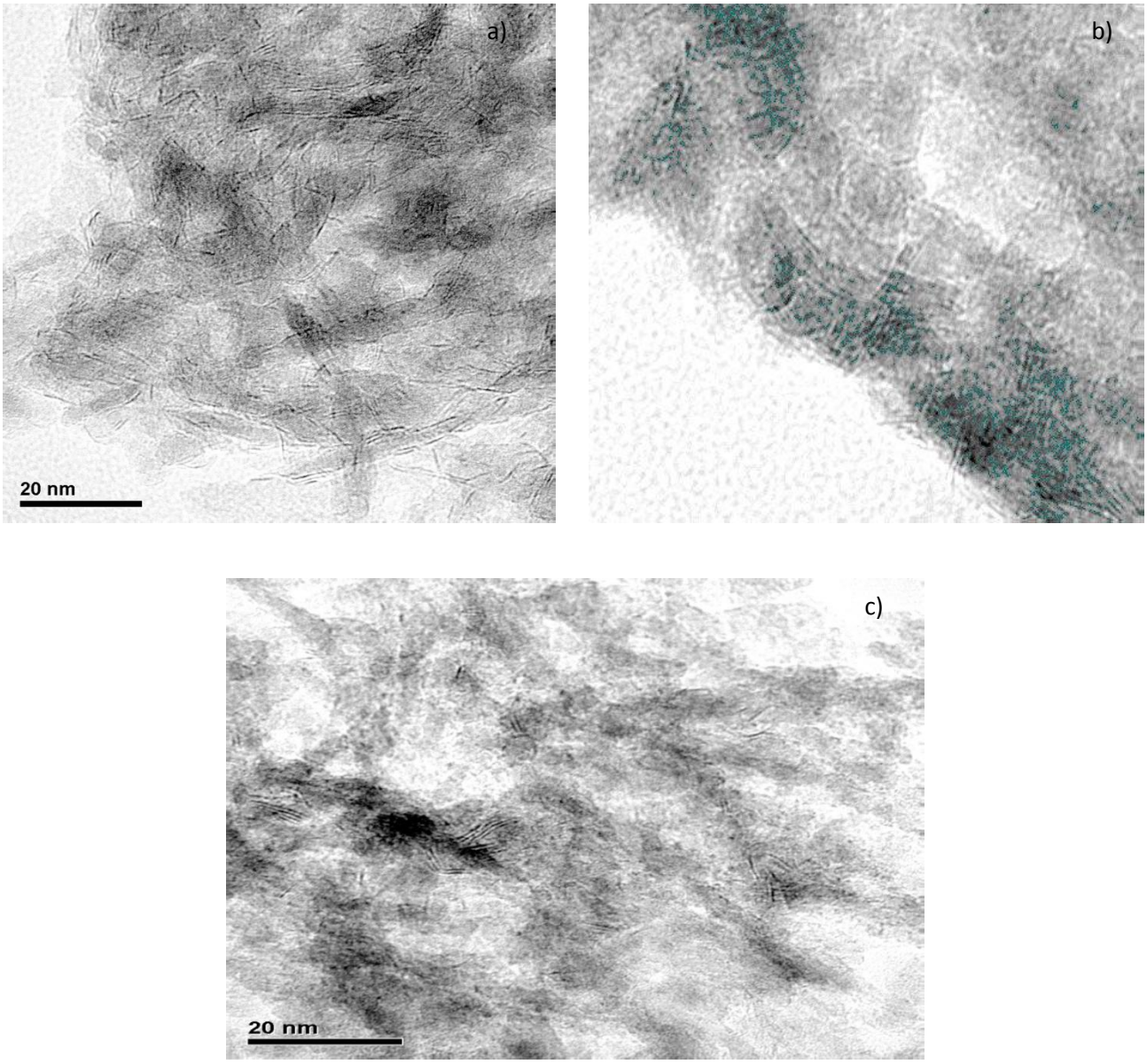

Figure 5.19: HRTEM images of catalysts with varying CA/Ni ratios sulfided at 350 ^{o}C a) Cat A; b) Cat B and c) Cat C

5.2 Hydrotreating Activity Evaluation

In the present study, the performance of all catalysts was evaluated based on hydrodesulfurization (HDS) and hydrodenitrogenation (HDN) activities exhibited during hydrotreatment of heavy gas oil (HGO) derived from Athabasca bitumen. In a typical run, 5 ml of catalyst was loaded in the reactor, and sulfidation of catalyst was carried out for 48 hrs. The sulfided catalyst was then precoked (stabilized) using HGO for 5 days (T = 370˚C, P = 8.9 MPa, LHSV = 1.0 h^{-1}, gas-to-oil ratio = 600 mL/mL). From the catalyst stabilization study (Figure 5.20) it was evident that the HDS and HDN activity decrease with time for an initial two days due to the coke deposition on catalyst surface and then level out.

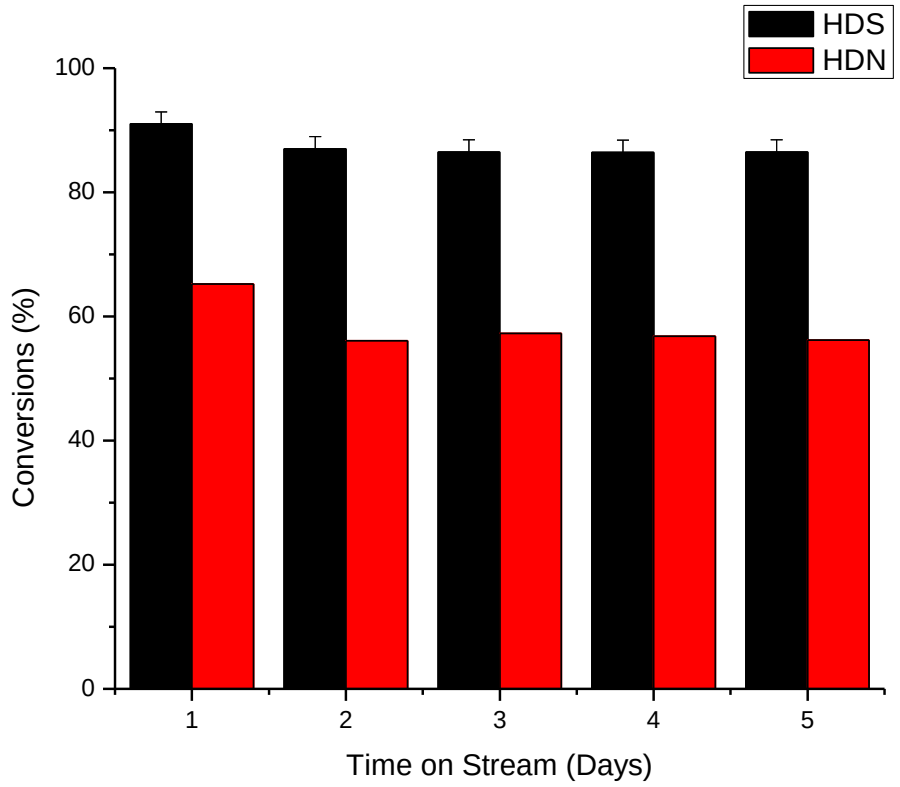

Figure 5.20: Activity study of Cat B during the stabilization and pre coking period

Figure 5.21 shows the HDS and HDN activity of the three catalysts in the hydrotreating of heavy gas oil. Cat B is found to be most active in both hydrodesulfurization and hydrodenitrogenation. The incorporation of citric acid seems to improve the HDN activity more than the HDS activity. Indeed, previous reports in literature have attributed this to the increase in the Type II Ni-Mo-S sites, which seem to favor the HDN activity by promoting the hydrogenation route.

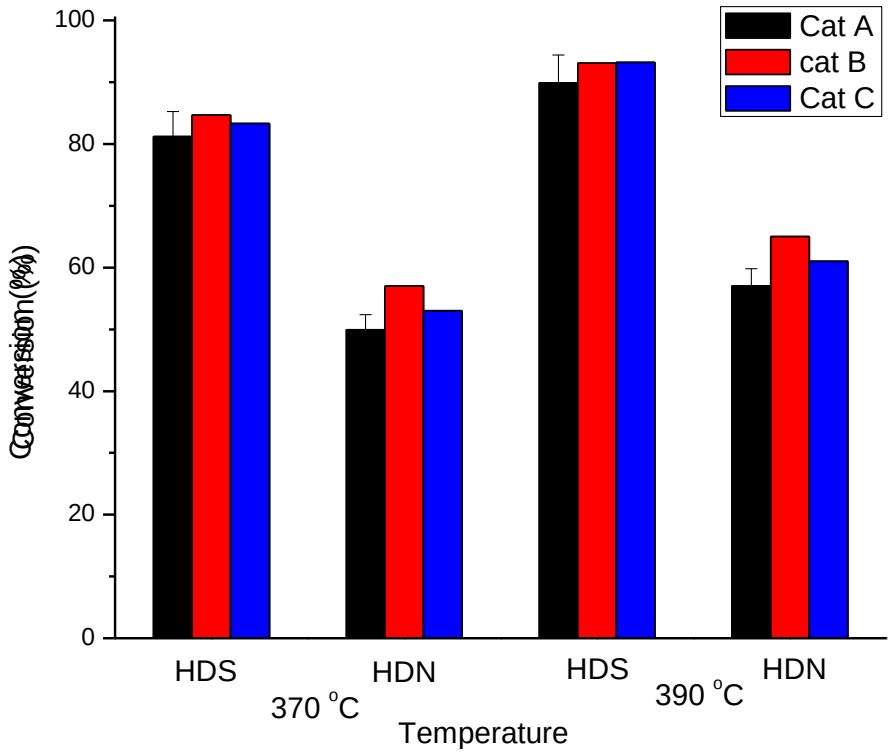

Figure 5.21: HDS and HDN activity of catalysts prepared with different CA/Ni ratios

Thus it is apparent that use of citric acid improves the intrinsic activity of the active sites. This promotion is possibly due to the formation of Ni-citrate complex which delays the sulfidation of Ni. A delayed sulfidation of Ni results in the better formation of the Type II Ni-Mo-S sites with multiple layers of MoS_2 slabs. In corroboration with the characterization results and hydrotreating activity tests, it is concluded that a CA/Ni molar ratio of 1 is optimal for further hydrotreating activity tests.

5.3 Conclusions

Three different catalysts were prepared by varying the citric acid to nickel molar ratios (CA/Ni = 0, 1 and 2) while keeping the Ni loading constant at 5 wt %, Mo loading at 15 wt %. All the catalysts were supported on the MAS-16 – Al_2O_3 mixed support. The detailed characterization of the catalyst revealed that both Ni and Mo form complex with citric acid. The formation of the metal-citrate complex was found to retard the sulfidation of both the metals. At CA/Ni = 1, the formation of nickel-citrate complex was favorable. The formation of the nickel-citrate complex was found to delay the sulfidation of Ni, such that nickel and molybdenum were observed to have near simultaneous sulfidation. However, at higher CA/Ni ratio of 2, some citric acid also formed complex with Mo. The formation of the molybdenum-citrate complex was found to be detrimental to the sulfidation of molybdenum. The hydrotreating activities of the catalyst using heavy gas oil as the feedstock also confirmed the results from the characterization studies. Cat B, with CA/Ni molar ratio of 1 was found to give the maximum sulfur and nitrogen conversions. The catalyst with CA/Ni ratio of 1 was selected for further metal optimization and hydrotreating tests.

CHAPTER 6

OPTIMIZATION OF METAL LOADING

This chapter deals with the synthesis, characterization and hydrotreating activity evaluation of the catalysts prepared by varying the active metal loading. In the first stage, four different catalysts were synthesized by varying the molybdenum loading (10 wt %, 13 wt %, 15 wt % and 17 wt %) keeping the nickel loading (5 wt %) and the citric acid to nickel molar ratio (CA/Ni = 1) constant. The hydrotreating activities of the catalysts were checked using the hydrodesulfurization and hydrodenitrogenation of heavy gas oil derived from Athabasca bitumen. Subsequently the catalysts with the optimal molybdenum loading were selected for varying the nickel content (3 wt %, 5 wt %, 7 wt % and 9 wt %) such that the citric acid to nickel molar ratio remained constant at 1. Finally the hydrotreating activities were evaluated using the above mentioned procedure.

6.1 Effect of Molybdenum Loading

From the previous chapter, it was concluded that a citric acid to nickel molar ratio of 1 was optimal for further studies. Four different catalysts with Mo loading of 10 wt %, 13 wt %, 15 wt % and 17 wt % were synthesized using the pore volume impregnation procedure described earlier. The nickel loading was kept constant at 5 wt %. The citric acid to nickel molar ratio was also maintained at 1 for all the four catalysts. The catalysts were supported on MAS-16 – γ Al_2O_3 mixture. The synthesis procedure for the catalysts has been described in the previous chapter. The catalysts were prepared using the successive pore volume impregnation method, with molybdenum being loaded first followed by calcination. Nickel was subsequently loaded with

citric acid in the desired ratio and finally dried overnight at 120 ^{o}C. The textural properties of the catalysts are listed in Table 6.1.

Table 6.1: Textural properties of the catalysts synthesized with different Mo loadings

Catalyst	Mo (wt%)	Ni (wt%)	CA/Ni (mol/mol)	BET Area (m^2/g)	Pore Dia (nm)	Actual Loading	
						Mo (wt %)	Ni (wt%)
Cat B1	10	5	1	367	11	9.4	4.7
Cat B2	13	5	1	349	10.6	12.8	4.8
Cat B3	15	5	1	324	10.9	14.8	4.8
Cat B4	17	5	1	278	10.8	16.7	4.9

It is observed that surface area of the catalysts calculated using the BET method, gradually decreases with increase in molybdenum loading. This may be ascribed to the formation of the more complex and bulky molybdenum citrate dimmers, trimers and tetramers. Upon drying there is a possibility that these complexes may be deposited on the pore mouths. This is also evident from the reduction in pore diameter of the supported catalysts. In order to probe the chemical state and nature of the molybdenum oxide species formed, the catalysts were analyzed using Raman spectroscopy. The Raman spectra of the four catalysts in oxide state is shown in Figure 6.1With increase in molybdenum loading it is obse

rved that the peak at 976 cm^{-1} for Cat B21 and Cat B22 shifts towards lower wave numbers. This Raman band at 976 cm^{-1} can be attributed to molybdenum citrate monomers and dimmers like $[MoO_4(cit)H_3]^{4-}$. In case of Cat B24 this peak is observed at 946 cm^{-1}. With increase in molybdenum loading, there may have been the formation of a molybdenum citrate tetramer complex like $[(MoO_2)_4)O_3(cit)_2]^{4-}$. Further,

the peak at 1046 cm^{-1} is generally ascribed to the aluminium molybdenum hydrate species formed when molybdenum reacts with the $-Al(OH)_6$ group of the support. The reaction can be represented as shown in equation 6.1:

$$6Mo_7O_{24}^{6-} + 7Al^{3+} + 24H_2O \rightarrow 7Al(OH)_6Mo_6O_{18}^{3-} + 6H^{+} \quad .....(6.1)$$

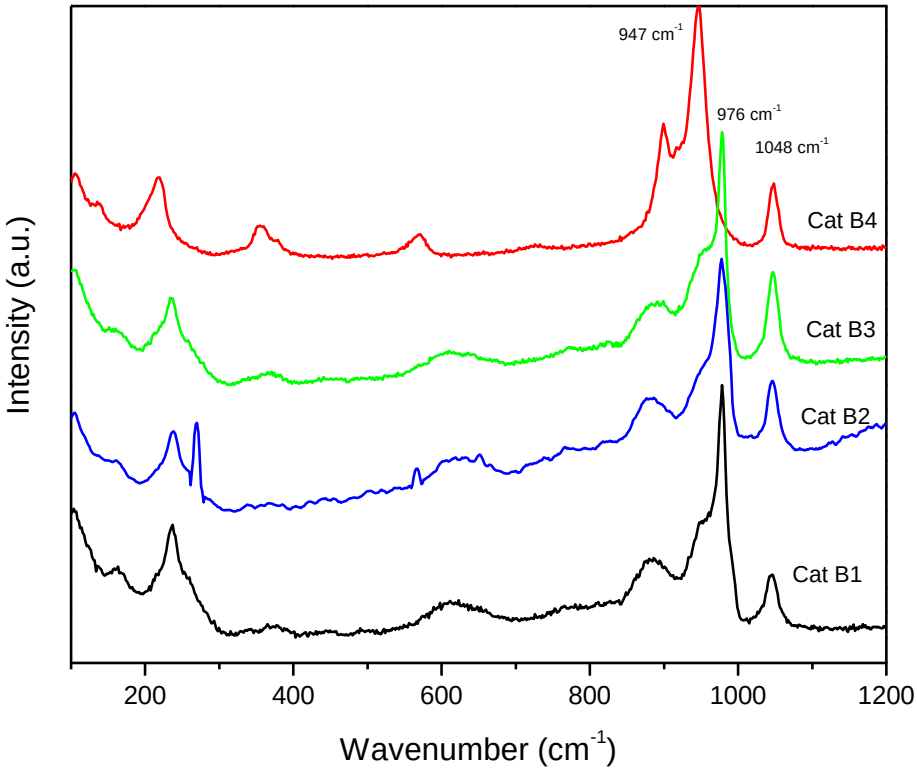

Figure 6.1: Raman spectra of the catalysts prepared with different molybdenum loadings

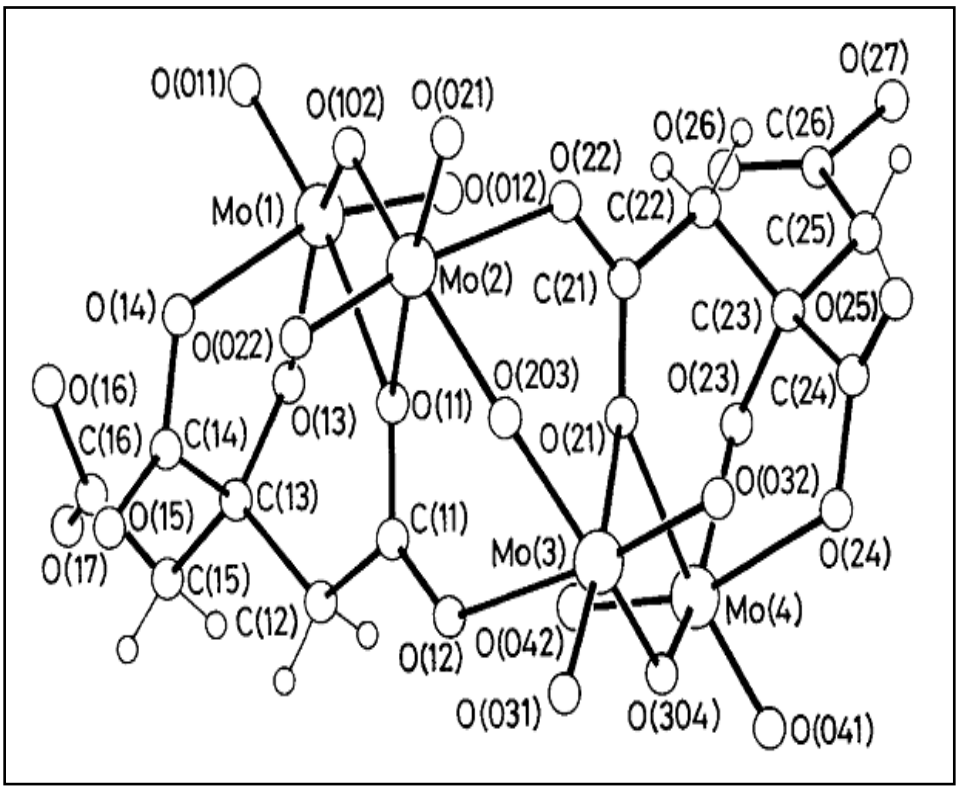

Figure 6.2: Structure of the molybdenum-citrate tetramer complex (Alcock et al., 1990)

XRD was used to study the crystallinity of the synthesized catalysts. Figure 6.3 shows the XRD pattern of the four catalysts. The catalysts were scanned in a region varying between 10^{o} and 40^{o}. Also shown are the diffraction pattern of the reference compounds MoO_3 and $NiMoO_4$. The broad and amorphous nature of the diffraction pattern observed for all the catalysts indicate the absence of crystalline MoO_3 in all the four catalysts. This indicates that, the Mo-citrate species are well dispersed over the support surface even at high molybdenum loadings. The results are in good agreement from the findings of Raman spectroscopy. However, it is difficult to determine the exact chemical nature of the Mo-citrate complex formed through XRD technique

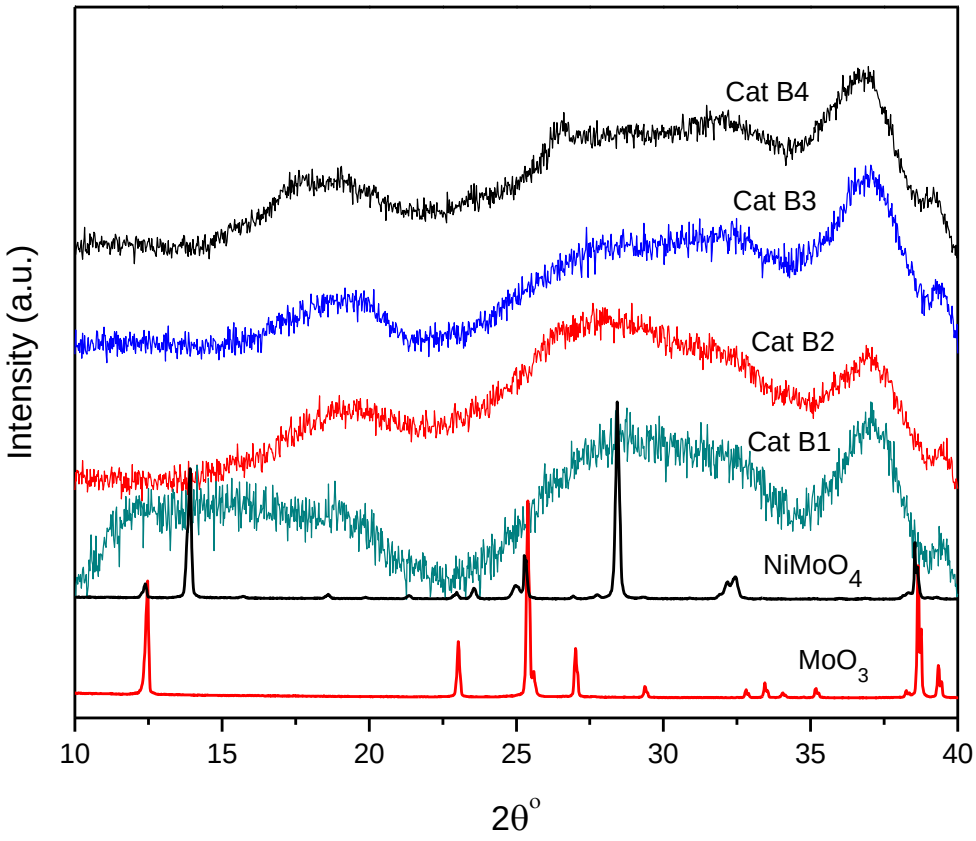

Figure 6.3: X-ray diffraction pattern of the catalysts with different Mo loadings. Also shown for reference are the XRD patterns of MoO_3 and $NiMoO_4$

The Mo K edge EXAFS spectra and fits from the sulfided catalysts are shown in Figure. 6.4. The Fourier transformed Mo spectra of the samples and the fits are presented in Figure 6.5. Also shown for consideration are the real part of the Fourier Transformed spectra and the corresponding fits in Fig.6.7. The EXAFS best fit values for all the catalysts are summarized in Table 6.2.

The low noise levels at high K values illustrate the high data quality of the spectral acquisitions. The Fourier Transformation of these samples revealed mainly 2 shells due to the Mo-S and Mo-Mo contributions. The corresponding peaks occur at 1.96 A^o and 2.79 A^o, both phase incorrected. Crystalline MoS_2 is well known to have a hexagonal strucuture with each Mo atom surrounded by 6 S atoms at 2.4 A^o and each S atom surrounded by 6 Mo atoms at 3.16 A^o (Dickinson and Pauling, 1923). From Table 6.2, it is evident that the S and Mo coordination in the sulfided samples is less than crystalline MoS_2. The reduction in the Mo-Mo coordination in the sulfided samples is due to the small particles size of the supported MoS_2 that are formed upon sulfidation. Further, a decrease in the Mo-S contribution in the catalysts with respect to MoS_2 is generally due to incomplete sulfidation or the presence of a Mo-O contribution in the EXAFS spectra. Indeed, the coordination parameters obtained from the fitting procedure revealed the presence of Mo-O shell at a distance of 1.96 A^o. Such a Mo-O contribution has also been previously observed by Leliveld et al, who reported the presence of O shell at 1.97 A^o for sulfided $NiMo/Al_2O_3$ catalysts (Leliveld et al., 1997). The occurrence of the Mo-O bond may be attributed to the presence of unsulfided Mo species possibly from MoO_3. The Mo-O coordination is highest for Mo loading of 17 wt % indicating low sulfidation caused due to the presence of molybdenum citrate tetramer which are difficult to sulfide. This is further corroborated by the low Mo-S coordination in Cat B4. Thus it is clear from the Mo K edge EXAFS best fit values that the sulfidation is highest in Cat B3 followed by Cat B2 and Cat B1. The results are in

agreement with the Raman results of the oxide phase. The presence of molybdenum-citrate tetramer, does indeed hampers the complete sulfidation of the catalysts.

Table 6.2: EXAFS best fit values for the catalysts with different Mo loadings

Scatterer	N	R (A^o)	$\Delta\sigma^2$ $(A^o)^2$	ΔE_o (eV)
Cat B1				
O	0.29	1.79	0.002136	-3.92
S	5.37	2.4	0.004238	4.32
Mo	3.67	3.16	0.004396	3.03
Cat B2				
O	0.26	1.77	0.007902	-8.99
S	5.63	2.4	0.004228	4.85
Mo	3.77	3.16	0.004565	3.63
Cat B3				
O	0.3	1.77	0.002162	3.35
S	5.6	2.41	0.004358	7.25
Mo	3.9	3.16	0.005432	9.08
Cat B4				
O	0.72	1.82	0.009163	-6.48
S	5.07	2.41	0.003724	3.43
Mo	3.79	3.16	0.004702	2.89

The HRTEM images of the sulfided catalysts are presented in Figure 6.7. The formation of MoS_2 stacks are clearly shown in the pictures with different stack heights and lengths. MoS_2 crystallites with lengths between 20 and 80 Å and stacking from two to six layers are formed on the supports.

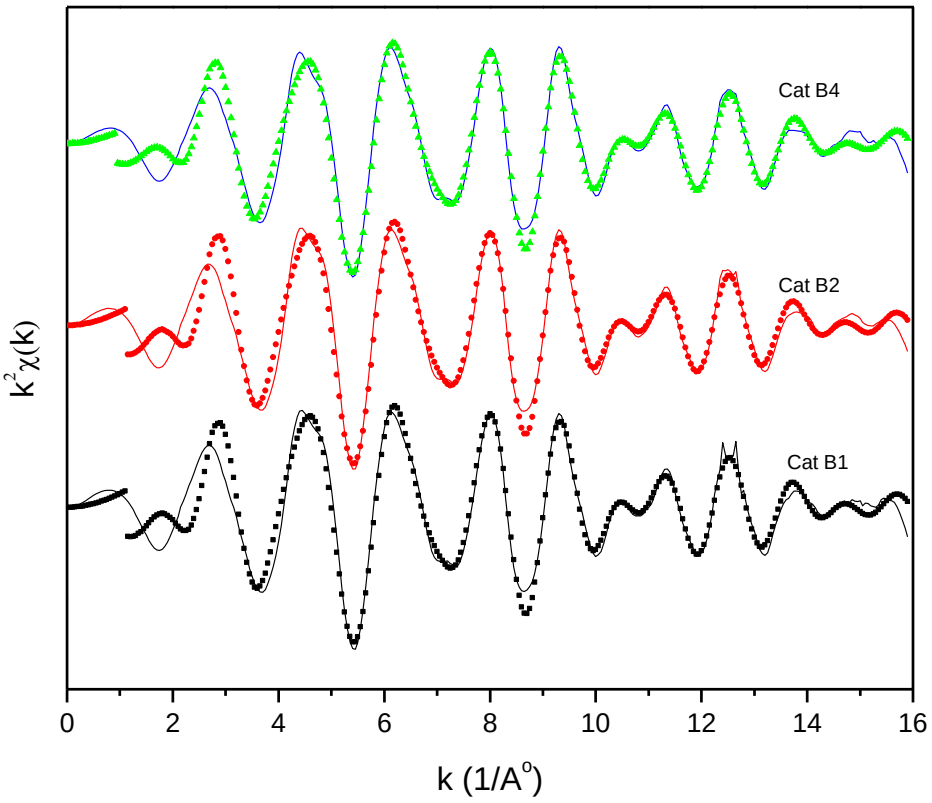

Figure 6.4: EXAFS spectra of sulfided catalysts (line) and corresponding fits (symbols)

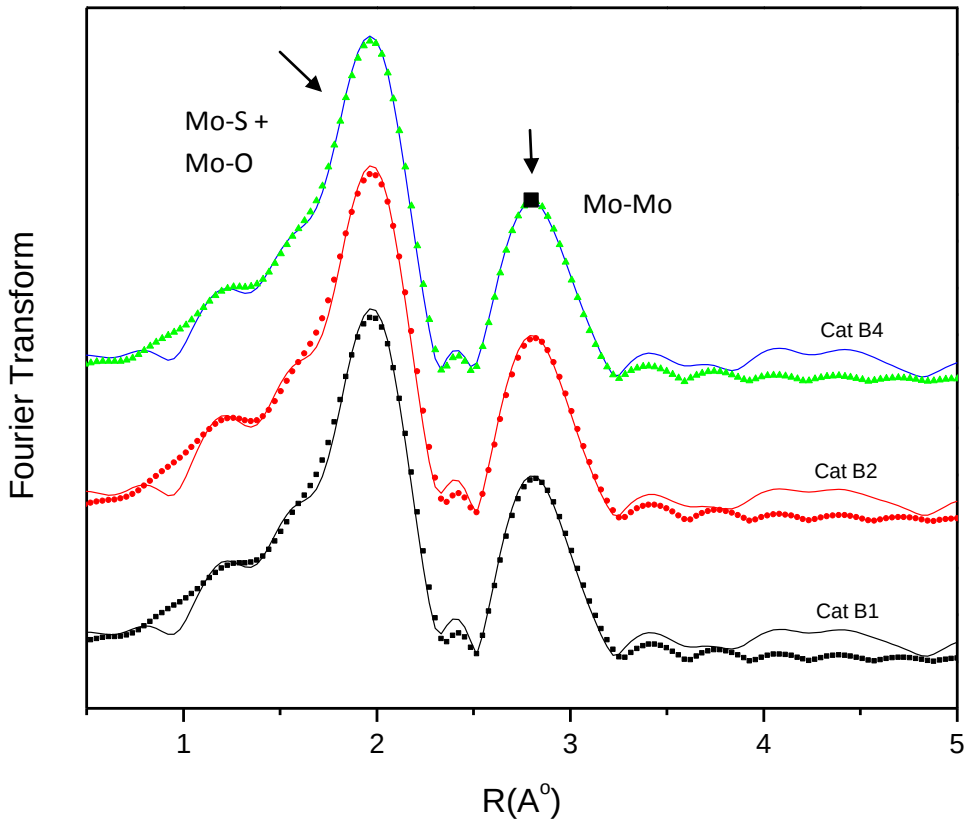

Figure 6.5: Magnitude of the Fourier transform of sulfided catalysts (line) and corresponding fits (symbols). The fit range for the spectra is 1- 4 A^o

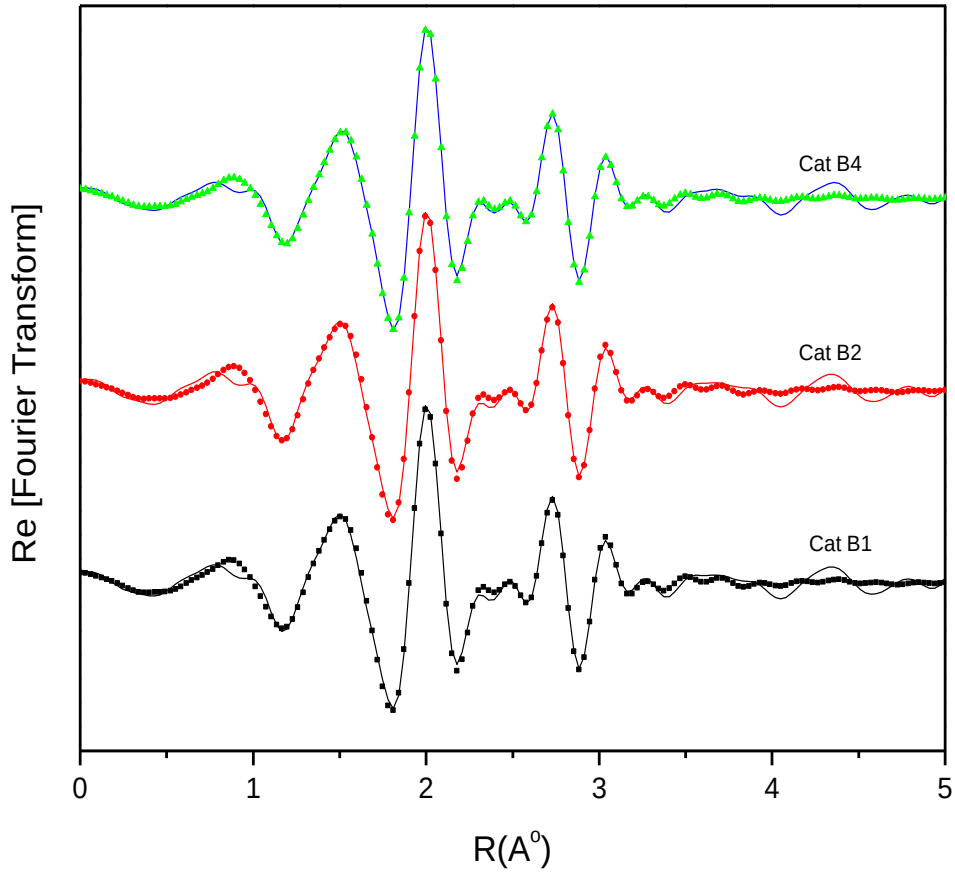

Figure 6.6: Real part of the Fourier transform of sulfided catalysts (line) and corresponding fits (symbols). The fit range for the spectra is 1- 4 A^o

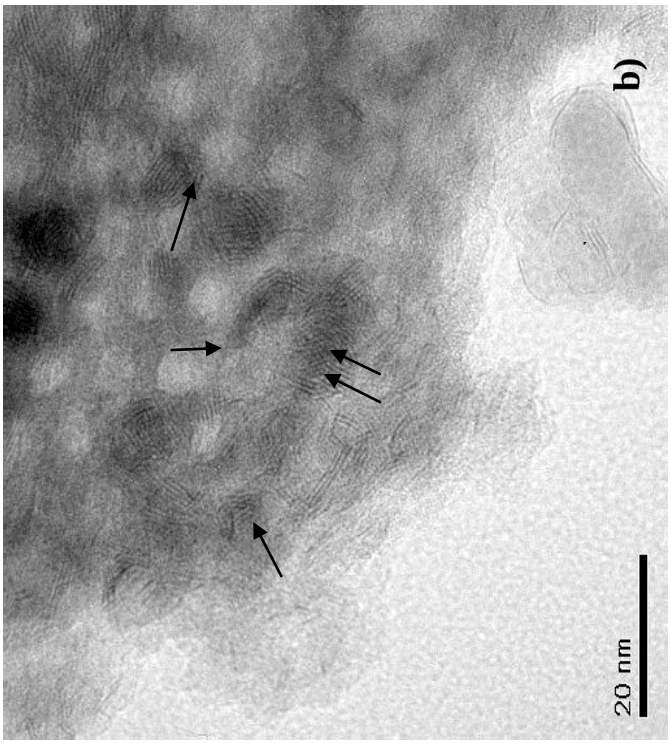
b)
20 nm

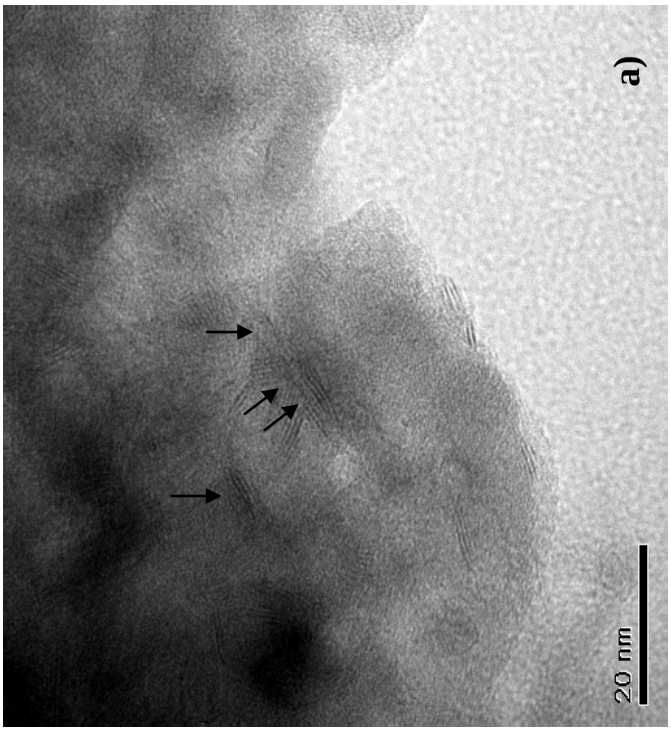
a)
20 nm

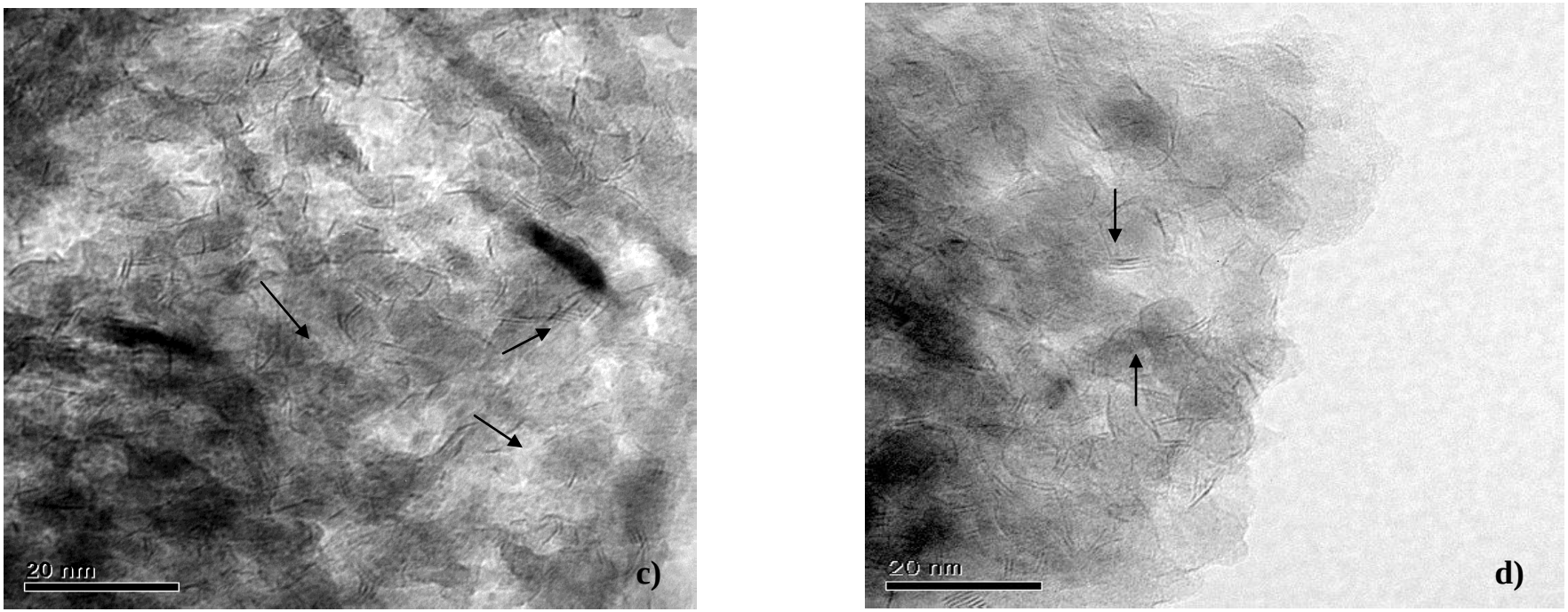

Figure 6.7: HRTEM images of sulfided a) Cat B1 b) Cat B2 c) Cat B3 and d) Cat B4. The arrows indicate the MoS_2 slabs

6.1.1 Hydrotreating Activity

The catalysts were evaluated for hydrodesulfurization and hydrodenitrogenation activities using heavy gas oil as the feedstock in a trickle bed reactor. The results of the catalytic activity tests are shown in Figure 6.8. It is observed that Cat B2 (Mo loading of 13 wt %) was the most active for HDS and HDN of heavy gas oil. The maximum sulfur and nitrogen conversion obtained were 94 % and 69 % respectively at 390 ^{o}C. In contrast, Cat B4 with 17 wt % Mo loading gave comparatively low S and N conversions.

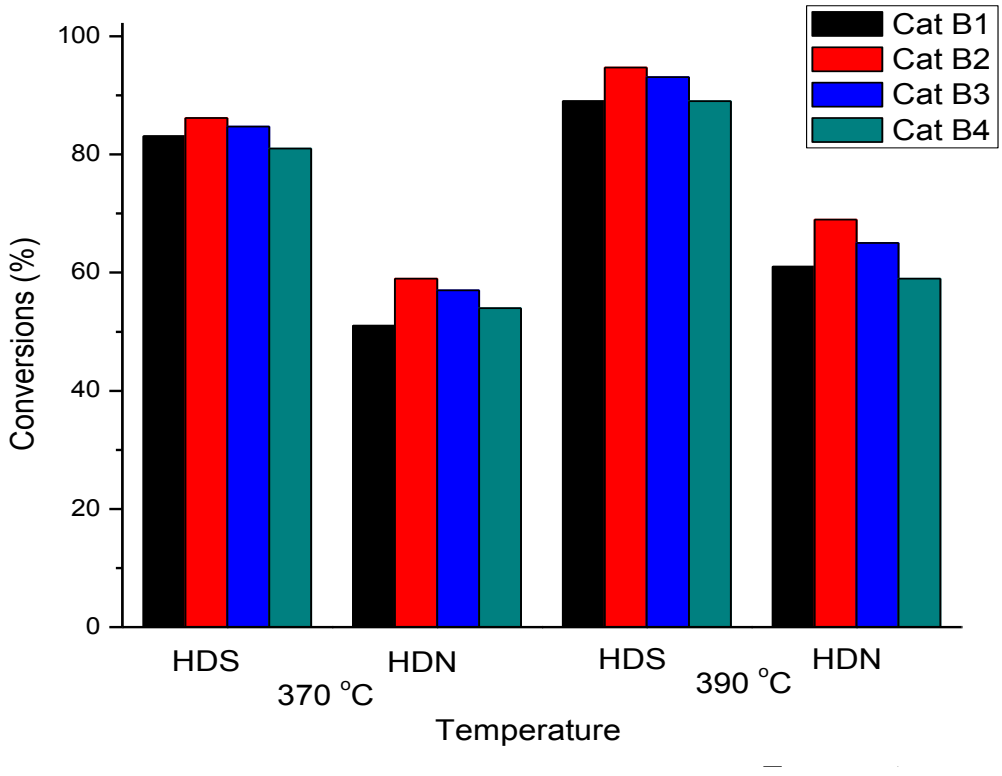

Figure 6.8 Hydrotreating activities of the catalysts synthesized with different Mo loadings at 370 ^{o}C and 390 ^{o}C

The formation of a molybdenum- citrate tetramer may have proved detrimental to the sulfidation of the molybdenum species. Due to the formation of the molybdenum citrate complex as against the nickel citrate complex, the sulfidation of molybdenum is retarded. As a result, nickel and molybdenum don not get sulfided at similar temperatures. The sulfidation of molybdenum occurs at higher temperature due to the complexation with citric acid. Cat B2 with Mo loading of 13 wt % was found to have the best molybdenum loading at the given conditions. Lower molybdenum loading was found to be generally favourable for higher hydrotreating activities. Molybdenum and nickel compete for the formation of complex with citric acid. There is an increased formation of nickel-citrate complex when the molybdenum loading is low. This may be the reason for higher hydrotreating activity observed in Cat B2.

6.2 Effect of Nickel Loading

After the determination of the optimal Mo loading, nickel loading on the catalysts were varied to synthesize four different catalysts such that the nickel content varied from 3 wt % to 9 wt % . Four catalysts were prepared with a constant Mo loading of 13 wt % and CA/Ni ratio of 1 while varying the Ni content. The catalysts were named as Cat B21, Cat B22, Cat B23 and Cat B24 with Ni loading of 3 wt %, 5 wt %, 7 wt % and 9 wt %. The textural properties of the synthesized catalysts are given in Table 6.3.

To study the effects of the different nickel loadings on the sulfidation of the catalysts, the Ni K edge XANES spectra of the catalysts sulfided at 150 ^{o}C is also shown in Fig 6.9. As can be observed, at low Ni loadings the intensity of the white line at 8339 eV is lower as compared to the catalysts with higher Ni loadings. Furthermore, no pre edge peak is observed for catalysts

with 3 and 5 wt % Ni loading. In contrast, this feature is prominent at 7 and 9 wt % Ni loadings. Additionally, the feature at 8389 eV is also stronger Cat B23 and Cat B24. The presence of the pre edge feature at 8321 eV and additional feature at 8389 eV in Cat B23 and Cat B24 and indicates that sulfidation of Ni is further retarded with increase in Ni concentration. This may be due to the increased formation of the nickel-citrate complex. The extensive formation of the nickel complex somewhat slows down the rate of sulfidation.

Table 6.3: Textural properties and metal loadings of catalysts prepared with different Ni loadings

Catalyst	Mo (wt%)	Ni (wt%)	CA/Ni (mol/mol)	BET Area (m^2/g)	Pore Dia (nm)
Cat B21	13	3	1	356	11.1
Cat B22	13	5	1	349	10.6
Cat B23	13	7	1	321	10.6
Cat B24	13	9	1	304	9.8

The results of the Ni K edge XANES are further corroborated by the S K edge XANES of the catalysts sulfided at 150 ^{o}C. The XANES spectrum of the S K edge is shown in Fig 6.10. Two prominent peaks are visible for the three catalysts at 2471 and 2481 eV. The peak occurring at 2471 eV is attributed to sulfur species in the reduced -2 oxidation state and the sulfur peak observed at higher energy is characteristic of sulfur in higher oxidation states mostly as sulphate (S^{+6}). .

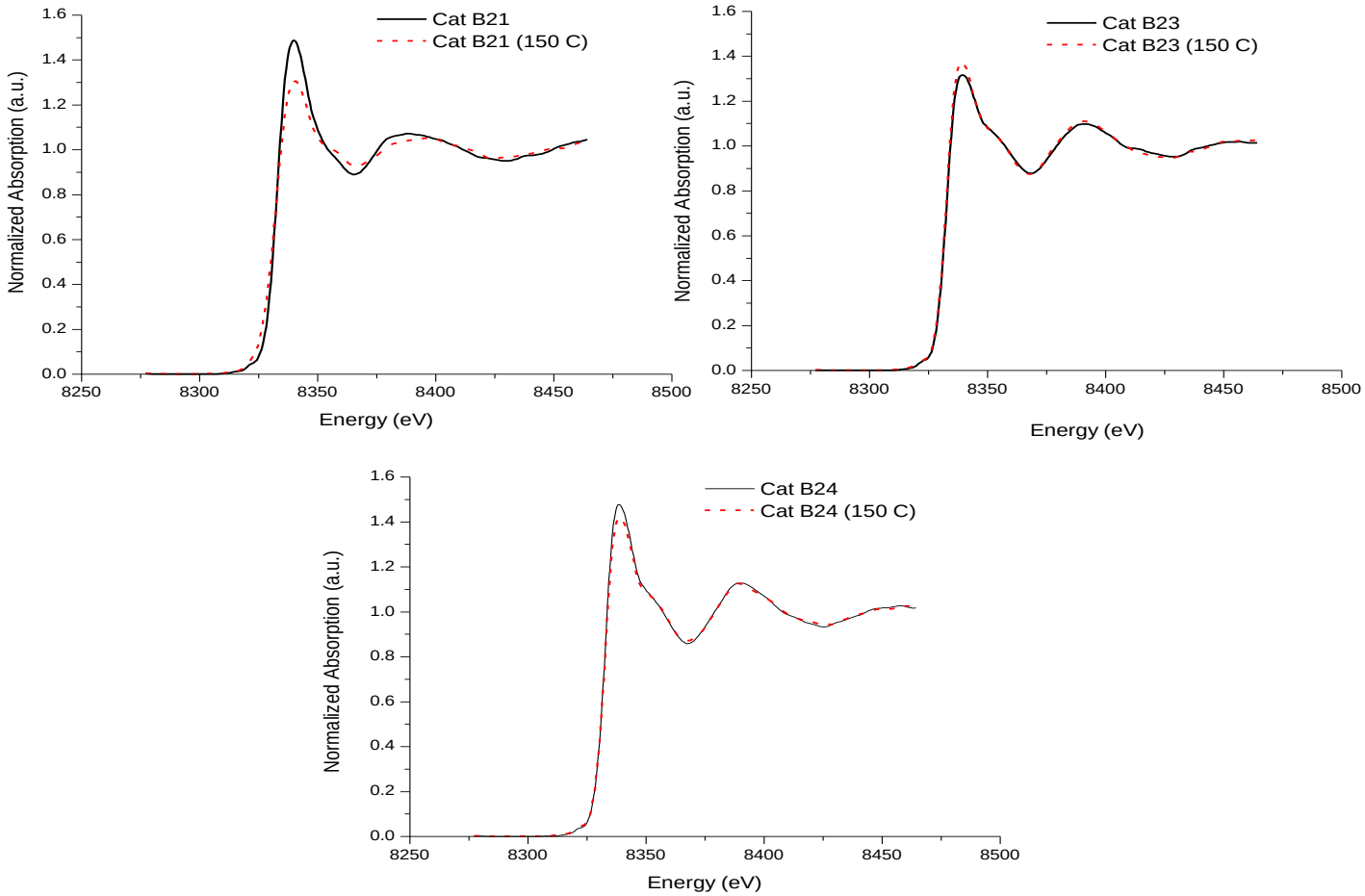

Figure 6.9: Ni K-edge XANES spectra of catalysts prepared with different Ni loadings, a) Cat B21 : Ni-3 wt% ; b) Cat B23 : Ni-7 wt% ; c) Cat B24 : Ni-9 wt%

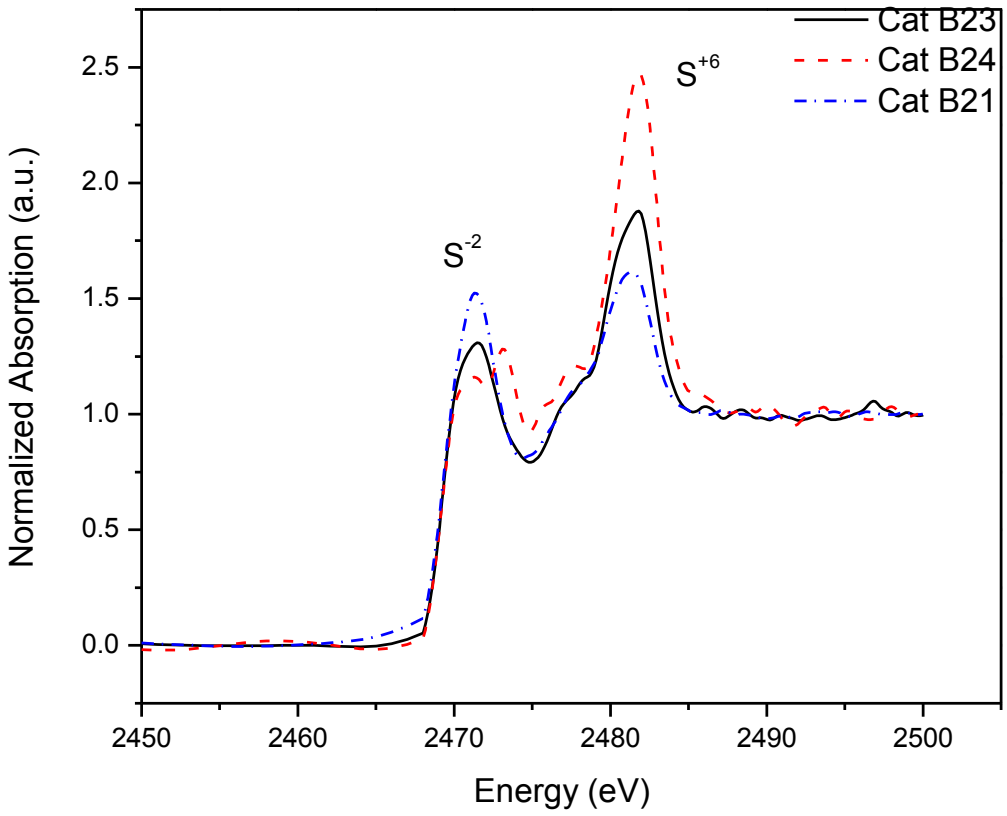

Figure 6.10: S K-edge XANES spectra of catalysts prepared with different Ni loadings. The peak at 2471 eV indicates S^{2-} and peak at 2481 eV indicates S in +6 state

The lower energy peak at 2471 eV progressively increases with decrease in nickel loading (Cat B21 > Cat B23 > Cat B24). Interestingly, the sulphate peak shows the opposite trend, with the S^{+6} peak intensity of Cat B24 being maximum while that of Cat B21 being the lowest. Presence of high oxidation states of S in Cat B24 and Cat B23 indicate that, reduction of S is relatively slower in these catalysts as compared to Cat B21. On the other hand Cat B21 with a lower loading of nickel, the reduction of sulfur into sulfide (S^{2-}) is rather accelerated. The increased formation of S^{2-} is due to the reduction of Ni into NiS or Ni_3S_2 even at low temperatures. On the

contrary, an increased Ni loading leading to the formation of the stable Ni(citrate) complex retards the reduction of Ni species. The results are in well agreement with the Ni K edge spectra which also confirm the same findings.

6.2.1 Hydrotreating Activity

The characterization results of the catalysts with varying Ni loadings are well reflected in the hydrotreating activity results (Figure 6.11). The catalytic activity in the HDS and HDN of heavy gas oil, increases monotonically with increase in Ni loadings till 7 wt % and then no appreciable change in observed in HDS and HDN conversions on further increase of Ni content.

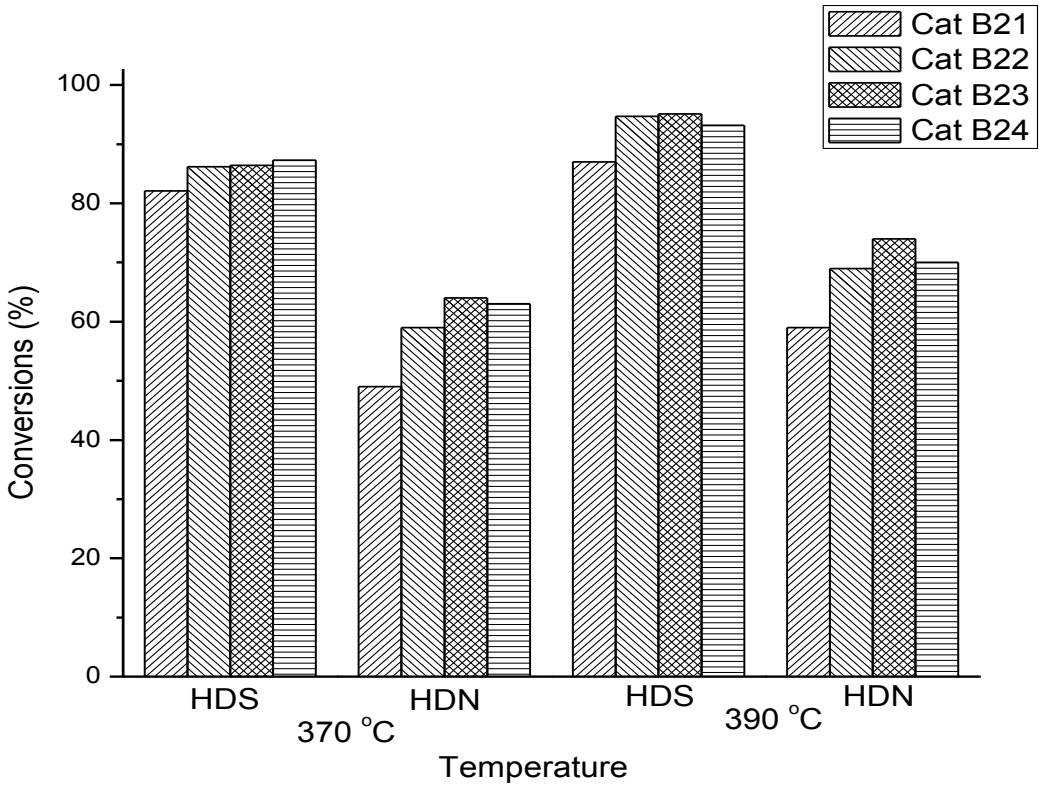

Figure 6.11: HDS and HDN activity of catalysts prepared with different Ni loadings

Despite of the formation of the nickel citrate complex, the stagnation in the catalytic activity of Cat B24 may be due to the excess Ni/Mo ratio. Previous works have shown that at very high nickel loadings, there may be agglomeration of Ni into bulk NiO. Further the possibility of some nickel getting into the alumina framework cannot also be ruled out. Nonetheless, maximum hydrodesulphurization conversion of 95 % was obtained with Cat B23 at reaction temperature of 390 ^{o}C. The corresponding HDN conversion was around 74 % at the same temperature. From the catalytic tests and characterization results, the metal content of the catalysts were optimized to a Mo loading of 13 wt %, Ni loading of 7 wt % and a CA/Ni molar ratio of 1. This catalyst (Cat B23) was found to be the most active for hydrotreating of heavy gas oil from Athabasca bitumen.

6.3 Conclusions

In the first stage, four different catalysts were synthesized by varying the molybdenum loading (10 wt %, 13 wt %, 15 wt % and 17 wt %) keeping the nickel loading (5 wt %) and the citric acid to nickel molar ratio (CA/Ni = 1) constant. It was observed that at higher Mo loadings, molybdenum formed trimers and tetramer complexes with citric acid. The formation of the molybdenum citrate tetramer severely retarded the sulfidation of molybdenum. Cat B2, with 13 wt % Mo loading was found to give the maximum sulfur and nitrogen conversions. In the second stage, the molybdenum loading was fixed at 13 wt % the CA/Ni molar ratio was maintained at 1, while the nickel loading was varied to prepare catalysts with 3 wt %, 5 wt %, 7 wt % and 9 wt % Ni loading. Ni and S K edge XANES revealed that with increase in Ni loading in Cat B23, the equilibrium reaction of nickel citrate was pushed in the forward direction resulting in an increased formation of nickel citrate. The hydrotreating of heavy gas oil showed that Cat B23 was the most active catalyst amongst all.

CHAPTER 7

LONG TERM ACTIVITY STUDY OF THE OPTIMIUM CATALYST

This chapter deals with the activity study of the optimized catalyst over an extended period of time. The catalyst was allowed to run for a period of 45 days at 390 ^{o}C and checked for stability and performance. Further, the effect of various reactions conditions and parameters on the hydrodesulfurization and hydrodenitrogenation activities is also studied in this chapter. Finally, the catalyst with optimum Mo loading of 13 wt %, Ni loading of 7 wt % and CA/Ni ratio of 1 supported on MAS-16 – γ Al_2O_3 is doped with 2.5 wt % phosphorus and the hydrotreating activity is compared with a commercial catalyst. Phosphoric acid (H_3PO_4) is used as the phosphorus precursor in the catalyst. The catalyst doped with phosphorus was prepared using the classical pore volume impregnation method. Required amount of ammonium heptamolybdate was dissolved in a mixture of water and H_3PO_4 and impregnated onto the support. The catalyst was then dried overnight and subsequently calcined at 550 ^{o}C for 4 hrs. Nickel and citric acid were loaded on the calcined catalyst using the procedure described in the earlier chapters.

7.1 Comparison with Commercial Catalyst

In order to compare the catalytic activity of Cat B23 with a commercial catalyst, Cat B23 was doped with 2.5 wt % phosphorus. The HDS and HDN conversions obtained after doping with phosphorus is shown in Fig 7.1. Further, the hydrotreating performance of this catalyst was found to be comparable to a commercial catalyst. An appreciable increase in the hydrodenitrogenation activity in particular was observed with the addition of phosphorus.

Maximum sulfur and nitrogen conversions of 95 % and 78 % respectively were recorded at 390 ^{o}C. Various authors have earlier attributed the improvements in hydrodenitrogenation activity to the increased formation of MoS_2 stacks. However, no significant improvement in the hydrodesulfurization activity was observed.

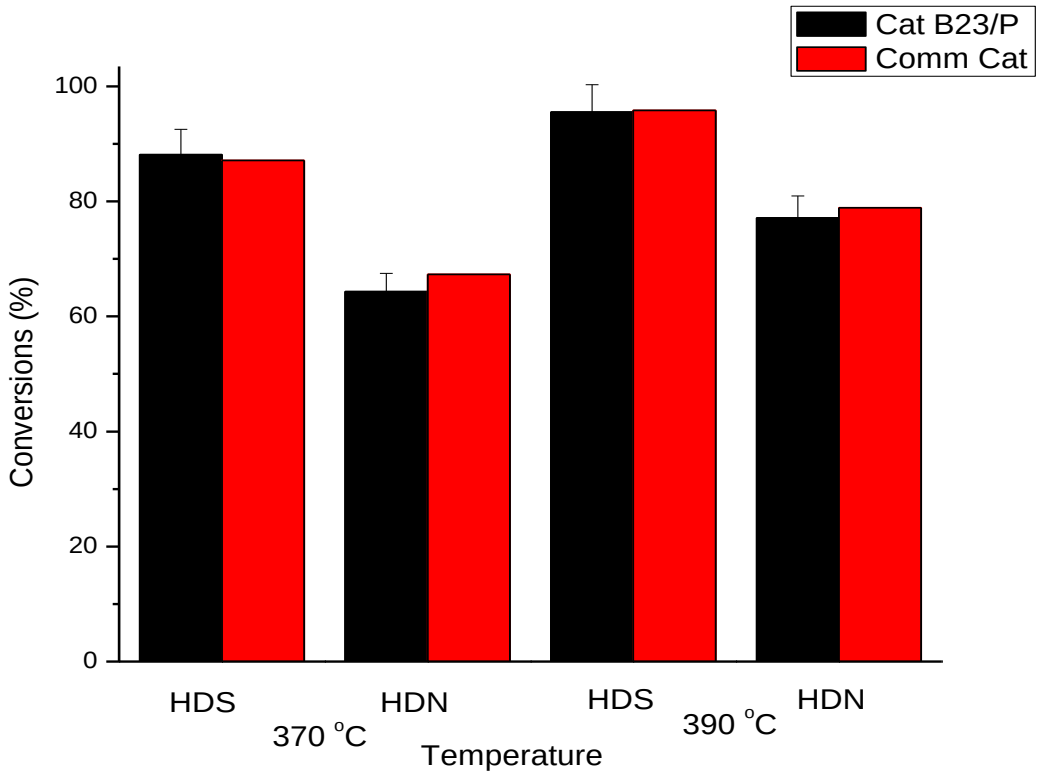

Figure 7.1: HDS and HDN activity comparison of commercial catalyst and Cat B23 doped with phosphorus. T = 370/390 °C, P=1300 psi, LHSV = 1 h^{-1}, H_2/oil ratio 600 Nm^3/m^3

7.2 Long Term Activity Study

In order to evaluate the stability and the performance of the phosphorus doped optimized catalyst (Cat B23/P), the hydrotreating run was allowed for an extended period of 45 days. The reaction conditions were kept constant at 390 ^{o}C, 1300 psi H_2 to oil ratio of 600 m^3/m^3 and LHSV of 1 hr^{-1}. Products were collected every 24 hrs and analyzed for sulfur and nitrogen contents. The long term activity study results are shown in Figure 7.2.

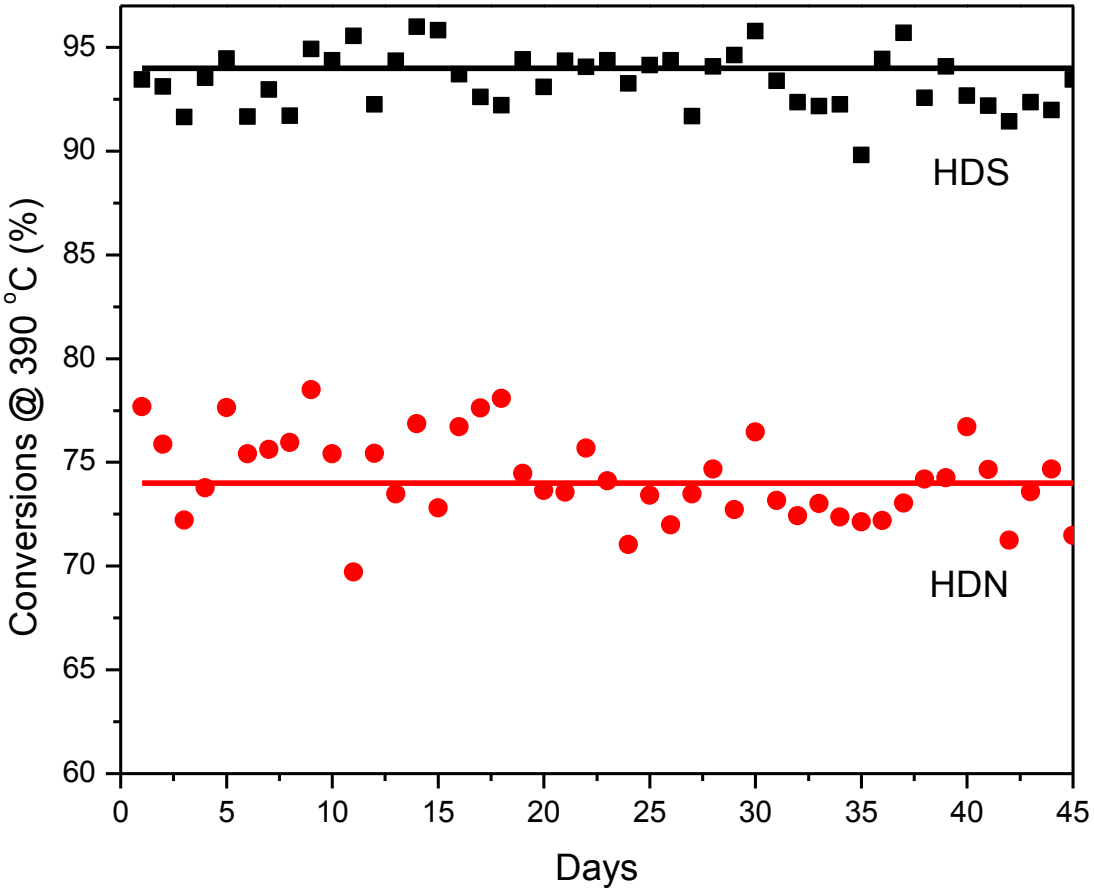

Figure 7.2: Long term HDS and HDN activation study of Cat B23/P over a period of 45 days.

T = 390 °C, P=1300 psi, LHSV = 1 h^{-1}, H_2/oil ratio 600 Nm^3/m^3

The hydrodesulfurization activity remained almost constant over the whole period with an average sulfur conversion of 94 %. The nitrogen conversion also exhibited similar behavior with average conversions of 75 %. The above results suggests that the catalyst was stable over a long period of time and that deactivation of the catalyst over a period of 45 days if any was negligible.

7.3 Effect of Reaction Conditions

7.3.1 Liquid Hourly Space Velocity

The liquid hourly space velocity is defined as the ratio of the hourly volume of feed processed to the volume of catalyst. In this study, the volume of the catalyst was kept constant at 5 ml. The feed flow rate of the heavy gas oil was varied in order to observe the effects of the change in LHSV on the HDS and HDN activity. Three different LHSV of 0.5 hr^{-1}, 1 hr^{-1} and 1.5 hr^{-1} were used for this study. The temperature, pressure and H_2 to oil ratio were kept constant at 390 ^oC, 1300 psi and 600 m^3/m^3 respectively. The effect of LHSV on the HDS and HDN is shown in Figure 7.3.

As the LHSV of heavy gas oil is decreased, the HDS conversion is increased due to increase in the contact time of the liquid with the catalyst. A maximum sulfur conversion of 97 % is achieved at LHSV of 0.5 hr^{-1}. Nitrogen conversion also shows a drop with increase in LHSV. However, the decrease in HDN activity is more significant as compared to the decrease in HDS activity. With increasing LHSV, the residence time decreases. As a result of the reduction in contact time, the hydrogenation activity seemed to get affected more as compared to the hydrogenolysis activity. The HDN reaction mainly proceeds through the hydrogenation pathway. This may be the reason for the steeper decline in the HDN activity as compared to HDS activity with increase in LHSV.

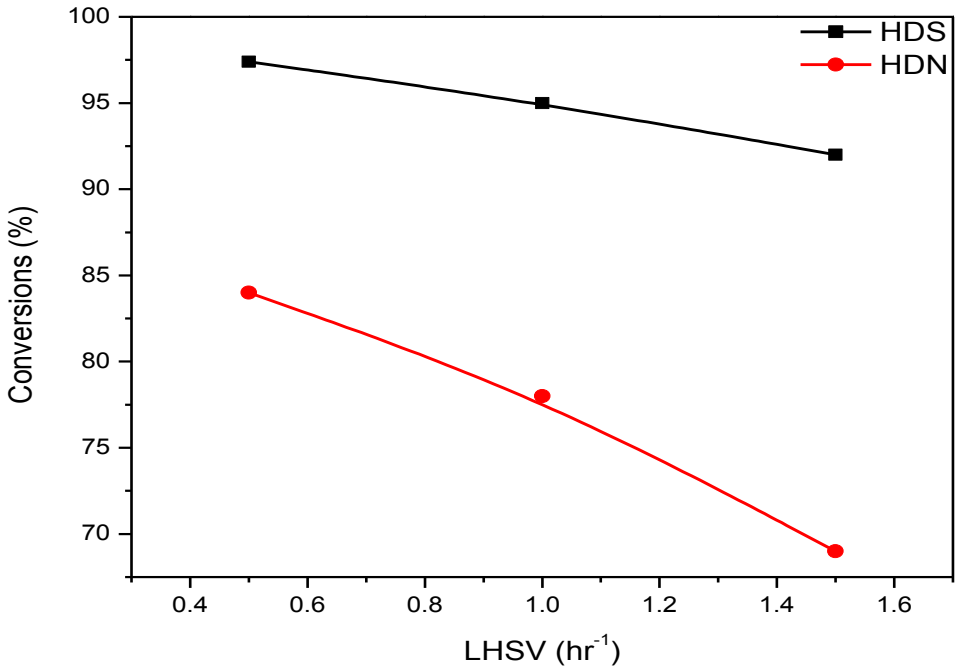

Figure 7.3: Effect of LHSV on the HDS and HDN activity of Cat B23/P. T = 390 °C, P=1300 psi, LHSV = 0.5/1/1.5 h^{-1}, H_2/oil ratio 600 Nm^3/m^3

7.3.2 Pressure

The effects of reaction pressure on the HDS and HDN activities of Cat B23/P were studied at three different pressure levels, 1100 psi, 1300 psi and 1500 psi, while keeping temperature, LHSV and gas/oil ratio at 385 °C, 1.0 h^{-1} and 600 m^3/m^3, respectively. The effects of pressure on HDS and HDN conversion are shown in Figure 6.3a. It can be observed that change in pressure on sulfur conversions in heavy gas oil was not very significant. Upon increase in pressure from 1100 psi to 1500 psi, sulfur conversion increases but only slightly. The maximum sulfur conversion of 97 % was obtained at 1500 psi. This increase in HDS activity may be

attributed to the desulfurization of some refractory molecules which proceeds only at very high pressures. The increase in sulfur conversion was relatively higher when the pressure was increase from 1300 psi to 1500 psi. The same trend was also observed in the hydrodenitrogenation of heavy gas oil. The increase in activity was more in the pressure range of 1300 psi -1500 psi as compared to 1100 psi – 1300 psi. The increase in hydrogenation activity may again be the reason for the improvement in HDN.

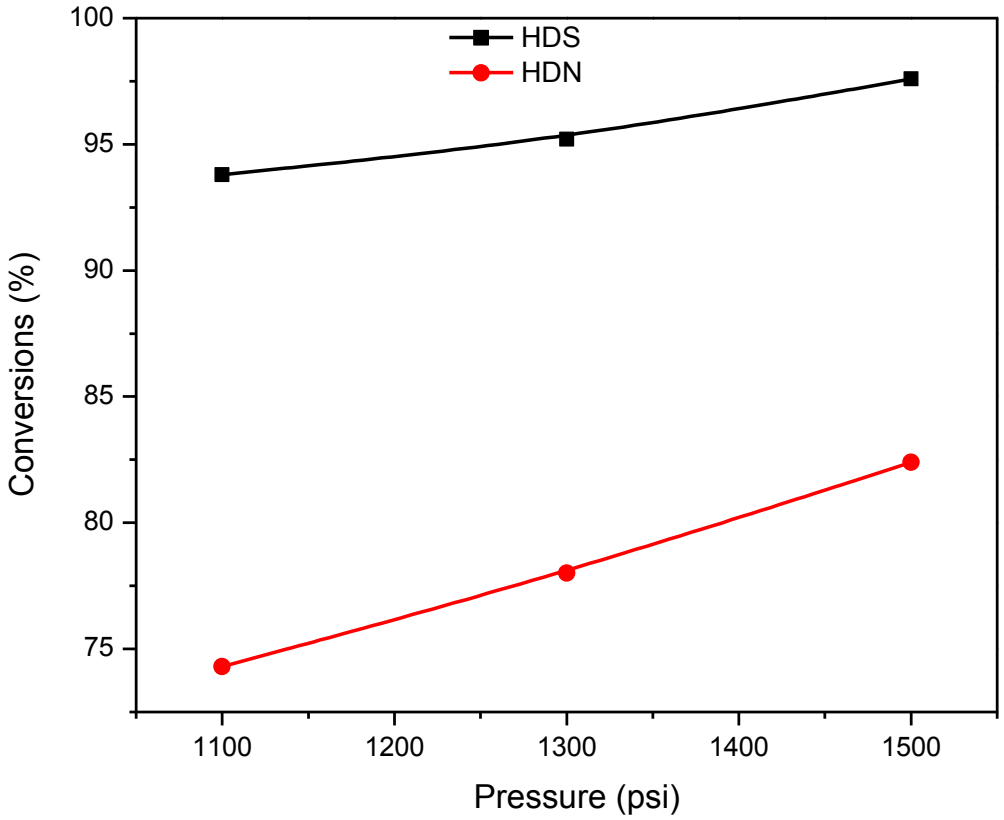

Figure 7.4: Effect of pressure on the HDS and HDN activity of Cat B23/P. T = 390 °C, P=1100/1300/1500 psi, LHSV = 1 h^{-1}, H_2/oil ratio 600 Nm^3/m^3

7.3.3 Sulfidation Temperature

The final sulfidation temperature was varied during the sulfidation of the catalysts in order to observe the effects of change in sulfidation conditions. Four different sulfidation temperatures namely, 320 ^{o}C, 340 ^{o}C, 350 ^{o}C and 370 ^{o}C were used in the study. All other reaction conditions were kept constant. Temperature, pressure, LHSV and H_2/oil were fixed at 390 ^{o}C, 1300 psi, 1 hr^{-1} and 600 m^3/m^3. The results are shown in Figure 7.5. As evident from the figure, change in sulfidation did not have a major effect in the hydrodesulfurization activity. Maximum HDS activity was observed close to 340 ^{o}C after which the sulfur conversions remained constant at 95 %. On the contrary the significant increase in the HDN activity was observed on increasing the sulfidation temperature from 320 ^{o}C to 370 ^{o}C.

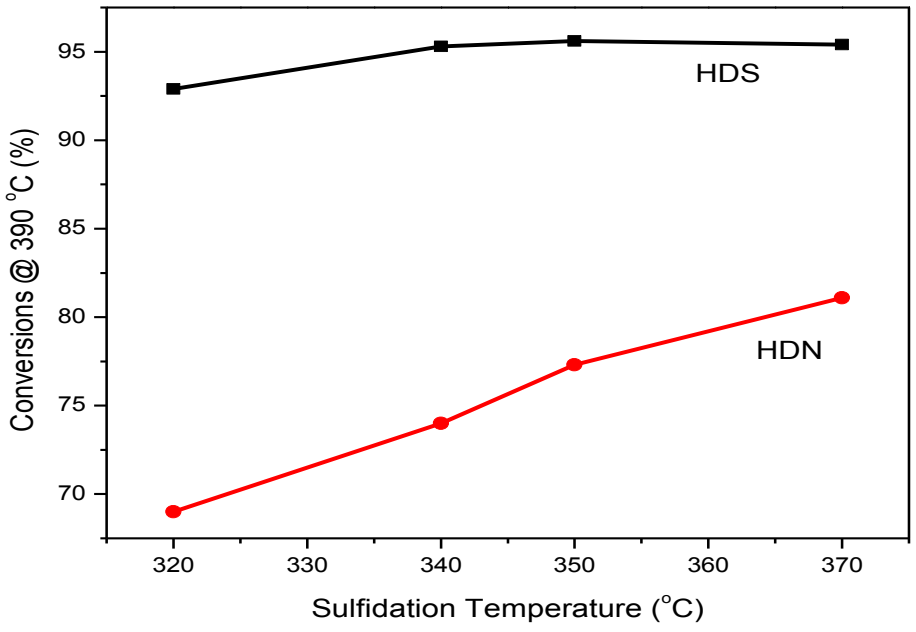

Figure 7.5: Effect of sulfidation temperature HDS and HDN activity of Cat B23/P at 390 ^{o}C. T = 390 °C, P=1300 psi, LHSV = 1 h^{-1}, H_2/oil ratio 600 Nm^3/m^3

On increasing the temperature of sulfidation, the Mo-O-Al bonds rapidly break resulting in the complete sulfidation of Mo. Further, various authors have also reported an increase in Type II NiMoS active sites on increasing the sulfiding temperature. This increase in Type II NiMoS sites may be the reason for the significant improvement in HDN activity.

7.3.4 H_2/Oil Ratio

The effect of the hydrogen/heavy gas oil volumetric ratio on the conversion HDS and HDN was studied by changing its value in the range from 450 to 1000 Nm^3/m^3while keeping temperature, pressure, and LHSV, at 390 °C, 1300 psi, and 1.0 h^{-1}, respectively. The effects of the gas/oil ratio on HDS and HDN are presented in Figure 7.6.

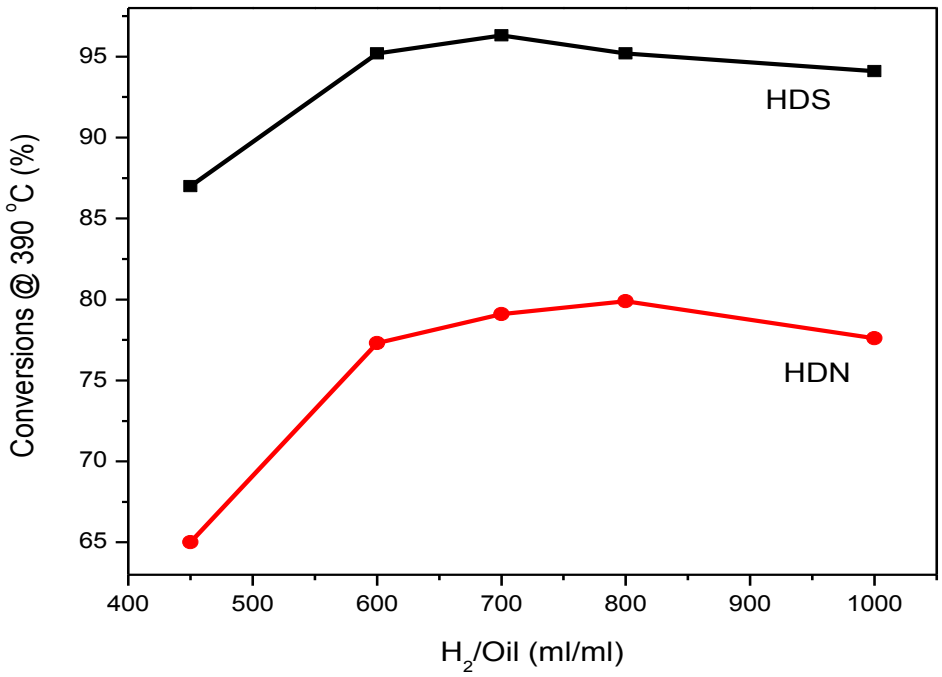

Figure 7.6: Effect of H_2 to oil ratio HDS and HDN activity of Cat B23/P at 390 °C. T = 390 °C, P=1300 psi, LHSV = 1 h^{-1}, H_2/oil ratio 450/600/700/800/1000 Nm^3/m^3

It is evident from the figure that there is increase of HDS and HDN activity due to increase in hydrogen/gas oil ratio. The sulfur conversion increases from 87 to 97 wt% as the hydrogen/heavy gas oil volumetric ratio is increased from 450 to 700 Nm^3/m^3. With further increase in the H_2/oil ratio, there is no significant change in the sulfur conversions. A similar pattern was also observed in the nitrogen conversions. The N conversion increased from 64.8 to 80 % on increasing the H_2/oil ratio from 450 to 700 Nm^3/m^3. Beyond this the nitrogen conversion plateaus and a slight decrease is observed at higher H_2/oil ratios.

7.4 Conclusions

The catalyst was allowed to run for a period of 45 days at 390 ^oC and checked for stability and performance. The optimum catalyst with Mo loading of 13 wt %, Ni loading of 7 wt % and CA/Ni ratio of 1 supported on MAS-16 - Al_2O_3 was doped with 2.5 wt % phosphorus and the hydrotreating activity is compared with a commercial catalyst. The HDS and HDN activities of the optimum catalyst (Cat B23) doped with phosphorus were found to be better than the hydrotreating activity of a commercial catalyst. Long term activity tests showed that there was no significant deactivation of the catalyst and the catalyst performance remained very much constant. The HDS and HDN activities were found to increase with decrease in the liquid hourly space velocity (LHSV). With increase in the pressure and the sulfidation temperature the catalyst activity was found to improve. Similarly, the catalyst activity increased with increase in the H_2 to oil ratio from 450 to 700 Nm^3/m^3, after which no significant change in catalyst activity was observed.

CHAPTER 8

SUMMARY & RECOMMENDATIONS

This chapter summarizes the most important findings and conclusions of the whole study. Further recommendations pertaining to development of highly active hydrotreating catalysts using citric acid as an chelating ligand are also suggested which could be interesting to explore for future studies and investigations. The most important results from all four phases of this work are summarized below.

8.1 Summary

- **Phase I - Synthesis and modification of γ-Al_2O_3 support with mesoporous alumino-silicates prepared from ZSM-5 nano-seeds**

Mesostructured alumino-silcate materials were synthesized from ZSM-5 nanoclusters and used as catalysts supports for the hydrotreatment of a model compound and real feed stock. The alumino-materials exhibited different acid strength and textural properties depending on the duration of hydrothermal treatment of the zeolite seeds. Three different MAS materials were synthesized using 4 hrs, 16 hrs and 24 hrs of hydrothermal treatment duration. Materials synthesized with low seeding time of 4 hrs showed properties similar to Al-SBA-15 prepared using the direct synthesis route, whereas material with high seeding time (t_{seed} = 24 hrs) resembled ZSM-5. The acidity of the MAS materials were found significantly higher than Al-SBA-15 and Al_2O_3 materials. The incorporation of Al in the silica matrix in a tetrahedral geometry resembling zeolites was found to increase the Bronsted acid sites. The activity of NiMo catalysts supported on MAS materials were evaluated using the hydrodesulfurization of

dibenzothiophene. The NiMo catalyst supported on mesoporous alumino silicate obtained after 16 hrs of hydrothermal treatment of the ZSM-5 precursors was found to be the most active in the HDS of DBT. The results of the catalytic tests were in corroboration with the characterization results. Optimum acidity, high dispersion of the active metals and excellent textural properties in MAS-16 were determined to be the reasons for the high activity in DBT hydrodesulfurization. Based on the preliminary catalytic tests, MAS-16 was selected as an additive to γ-Al_2O_3 to improve its acidic and textural properties. Three different MAS-16 –Al_2O_3 mixed supports were prepared using 0 wt%, 5 wt % and 10 wt % MAS-16. The hydrotreating activities of the NiMo catalyst supported on the prepared materials were evaluated in a trickle bed reactor using heavy gas oil as the feedstock. From the hydrotreating tests, it was observed that the composition 5 wt % MAS-16 and 95 % Al_2O_3 has the highest promoting effect on the hydrotreating activity of the catalysts. The high activity observed on this particular catalyst was attributed to an optimum combination of textural properties and acidic sites. Further, this particular composite (5 wt % MAS-16 + 95 wt % Al_2O_3) was selected as the support for all further hydrotreating reactions.

- **Phase II – Effect of citric acid modification**

The effect of the addition of citric acid on the sulfidation properties and the hydrotreating activity of NiMo/MAS-16-Al_2O_3 was described in this chapter. The synthesized catalysts were characterized extensively using different techniques like BET, FT-IR, Raman spectroscopy and X-Ray absorption spectroscopy. The chemical structure of the catalysts at various temperatures of sulfidation was probed using XANES and EXAFS. Finally, the hydrotreating activity of the catalysts was evaluated in a trickle bed reactor with heavy gas oil as the feedstock. Three different catalysts were prepared by varying the citric acid to nickel molar ratios (CA/Ni = 0, 1 and 2) while keeping the Ni loading constant at 5 wt %, Mo loading at 15 wt %. All the catalysts were supported on the MAS-16 – Al_2O_3 mixed support. The detailed characterization of the

catalyst revealed that both Ni and Mo form complex with citric acid, although Ni-citrate complex has a slightly higher stability than molybdenum-citrate complex. The formation of the metal-citrate complex was found to retard the sulfidation of both the metals. At CA/Ni = 1, an formation of nickel-citrate complex was favorable. The formation of the nickel-citrate complex was found to delay the sulfidation of Ni, such that nickel and molybdenum were observed to have near simultaneous sulfidation. However, at higher CA/Ni ratio of 2, some citric acid also formed complex with Mo. The formation of the molybdenum-citrate complex was found to be detrimental to the sulfidation of molybdenum. The results are also confirmed from the EXAFS spectra of the Mo K edge and XANES spectra of Ni K edge. The hydrotreating activities of the catalyst using heavy gas oil as the feedstock also confirmed the results from the characterization studies. Cat B, with CA/Ni molar ratio of 1 was found to give the maximum sulfur and nitrogen conversions. The catalyst with CA/Ni ratio of 1 was selected for further metal optimization and hydrotreating tests.

- **Phase III – Optimization of metal loading**

This chapter dealt with the synthesis, characterization and hydrotreating activity evaluation of the catalysts prepared by varying the active metal loading. In the first stage, four different catalysts were synthesized by varying the molybdenum loading (10 wt %, 13 wt %, 15 wt % and 17 wt %) keeping the nickel loading (5 wt %) and the citric acid to nickel molar ratio (CA/Ni = 1) constant. It was observed that at higher Mo loadings, molybdenum formed trimers nd tetramer complexes with citric acid. The formation of the molybdenum citrate tetramer severely retarded the sulfidation of molybdenum. The hydrotreating activities of the catalysts were checked using the hydrodesulfurization and hydrodenitrogenation of heavy gas oil derived from Athabasca bitumen. Cat B2, with 13 wt % Mo loading was found to give the maximum sulfur and nitrogen

conversions. In the second stage, the molybdenum loading was fixed at 13 wt % the CA/Ni molar ratio was maintained at 1, while the nickel loading was varied to prepare catalysts with 3 wt %, 5 wt %, 7 wt % and 9 wt % Ni loading. Ni and S K edge XANES revealed that with increase in Ni loading in Cat B23, the equilibrium reaction of nickel citrate was pushed in the forward direction resulting in an increased formation of nickel citrate. The increased formation of nickel citrate complex sufficiently delayed the sulfidation temperature of Ni. As a result of the near sulfidation of Ni and Mo, the formation of Type II NiMoS active sites was accentuated. The hydrotreating of heavy gas oil showed that Cat B23 was the most active catalyst amongst all. Near simultaneous sulfidation of Ni and Mo leading to the formation of highly active Type II NiMoS sites in Cat B23, was found to be the reason for its high HDS and HDN activity.

- **Phase IV – Long term activity study of the optimum catalyst**

This chapter dealt with the activity study of the optimized catalyst over an extended period of time. The catalyst was allowed to run for a period of 45 days at 390 ^{o}C and checked for stability and performance. Further, the effect of various reactions conditions and parameters on the hydrodesulfurization and hydrodenitrogenation activities was also studied in this chapter. Finally, the optimum catalyst with Mo loading of 13 wt %, Ni loading of 7 wt % and CA/Ni ratio of 1 supported on MAS-16 – γ Al_2O_3 was doped with 2.5 wt % phosphorus and the hydrotreating activity is compared with a commercial catalyst. The HDS and HDN activities of the optimum catalyst (Cat B23) doped with phosphorus were found to be better than the hydrotreating activity of a commercial catalyst. Long term activity tests showed that there was no significant deactivation of the catalyst and the catalyst performance remained very much constant. The HDS and HDN activities were found to increase with decrease in the liquid hourly space velocity (LHSV). With increase in the pressure and the sulfidation temperature the catalyst activity was

found to improve. Similarly, the catalyst activity increased with increase in the H_2 to oil ratio from 450 to 700 Nm^3/m^3, after which no significant change in catalyst activity was observed.

8.2 Recommendations

- Mesoporous alumino-silicate materials were prepared using ZSM-5 nano precursors in this work. Other zeolite precursors like those from Y-zeolite and β-zeolite can also be used as precursors for the synthesis of mesoporous alumino-silicate materials. Further, various other combination of mesoporous materials from zeolite precursors like, mesoporous titania-silicate, mesoporous zirconia-silicate materials can also be explored as support materials for hydrotreating reactions.
- Heavy gas oil was primarily used as the feedstock for the hydrotreating reactions. Heavy gas oil from Athabasca bitumen has high sulfur and nitrogen content making it difficult to hydrotreat. Other feedstocks like light gas oil, straight run gas oil, and middle distillate fraction can also be used to evaluate the performance of the catalysts.
- Only citric acid has been used as an additive in this work. Other chelating ligands like ethylene diammine tetraaceitic acid (EDTA) and nitrilo aceitic acid (NTA) can also be used to evaluate the catalytic performance in the hydrotreating of heavy gas oil.
- A detailed analysis of the feed and product needs to be done in order to understand fully the reactions that are taking place other than hydrodesulfurization and hydrodenitrogenation.
- A kinetic study of the catalysts also needs to be done to determine the rate constants and the inhibitory effects of nitrogen and some sulfur compounds.

REFERENCES

Absi-Halabi, M., A. Stanislaus and D.L. Trimm, "Coke formation on catalysts during the hydroprocessing of heavy oils," Applied Catalysis. **72**, 193-215 (1991a).

Aerts, A., L.R.A. Follens, M. Haouas, T.P. Caremans, M. Delsuc, B. Loppinet, J. Vermant, B. Goderis, F. Taulelle, J.A. Martens and C.E.A. Kirschhock, "Combined NMR, SAXS, and DLS Study of Concentrated Clear Solutions Used in Silicalite-1 Zeolite Synthesis," Chemistry of Materials. **19**, 3448-3454 (2007).

Alcock, N.W., M. Dudek, R. Grybos, E. Hodorowicz, A. Kanas and A. Samotus, "Complexation between molybdenum(VI) and citrate: structural characterisation of a tetrameric complex, $K_4[(MoO_2)_4O_3(cit)_2].6H_2O$," J. Chem. Soc. , Dalton Trans., 707-711 (1990).

Al-Dalama, K. and A. Stanislaus, "A comparative study of the influence of chelating agents on the hydrodesulfurization (HDS) activity of alumina and silica-alumina-supported CoMo catalysts," Energy and Fuels. **20**, 1777-1783 (2006).

Ancheyta, J., M.J. Angeles, M.J. Macias, G. Marroquin and R. Morales, "Changes in Apparent Reaction Order and Activation Energy in the Hydrodesulfurization of Real Feedstocks," Energy Fuels. **16**, 189-193 (2002).

Ancheyta, J., M.S. Rana and E. Furimsky, "Hydroprocessing of heavy petroleum feeds: Tutorial," Catalysis Today. **109**, 3-15 (2005).

Apecetche, M.A. and B. Delmon, "Experimental evidence for the existence of a Co-Mo bilayer on CoMo-Al_2O_3 hydrodesulfurization catalysts," Reaction Kinetics and Catalysis Letters. **12**, 385-392 (1979).

Arteaga, A., J.L.G. Fierro, P. Grange and B. Delmon, "Simulated regeneration of an industrial CoMo gamma -Al_2O_3 catalyst influence of steam," American Chemical Society, Division of Petroleum Chemistry, Preprints. **32**, 339-346 (1987).

Atwood, D.A. and M.J. Harvey, "Group 13 Compounds Incorporating Salen Ligands," Chem. Rev. **101**, 37-52 (2001).

Babich, I.V. and J.A. Moulijn, "Science and technology of novel processes for deep desulfurization of oil refinery streams: a review," Fuel. **82**, 607-631 (2003).

Ball, M. and M. Wietschel, "The Hydrogen Economy: Opportunities and Challenges," Cambridge University Press (2010).

Barrio, V.L., P.L. Arias, J.F. Cambra, M.B. Guemez, J. Campos-Martin, B. Pawelec and J.L.G. Fierro, "Evaluation of silica-alumina-supported nickel catalysts in dibenzothiophene hydrodesulphurisation," Applied Catalysis A: General. **248**, 211-225 (2003).

Barzetti, T., E. Selli, D. Moscotti and L. Forni, "Pyridine and ammonia as probes for FTIR analysis of solid acid catalysts," J. Chem. Soc. , Faraday Trans. **92**, 1401-1407 (1996).

Basu, C. and U.S. Ghosh, "Contribution of configuration interaction to the intensity of crystal field transitions in tetrahedral Fe2+ ion," Phys. Stat. Sol. (b). **60**, 97-106 (1973).

Bej, S.K., A.K. Dalai and J. Adjaye, "Kinetics of hydrodesulfurization of heavy gas oil derived from oil sands," Petrol Sci Technol. **20**, 867-877 (2002).

Bej, S.K., S.K. Maity and U.T. Turaga, "Search for an Efficient 4,6-DMDBT Hydrodesulfurization Catalyst: A Review of Recent Studies," Energy Fuels. **18**, 1227-1237 (2004).

Bej, S.K., A.K. Dalai and J. Adjaye, "Effect of Hydrotreating Conditions on the Conversion of Residual Fraction and Microcarbon Residue Present in Oil Sands Derived Heavy Gas Oil," Energy Fuels. **15**, 1103-1109 (2001).

Bentley, R.W., "Global oil & gas depletion: an overview," Energy Policy. **30**, 189-205 (2002).

Bergwerff, J.A., M. Jansen, B.R.G. Leliveld, T. Visser, K.P. de Jong and B.M. Weckhuysen, "Influence of the preparation method on the hydrotreating activity of MoS_2/Al_2O_3 extrudates: A Raman microspectroscopy study on the genesis of the active phase," Journal of Catalysis. **243**, 292-302 (2006).

Berkowitz, N. and J.G. Speight, "The oil sands of Alberta," Fuel. **54**, 138-149 (1975).

Botchwey, C., A.K. Dalai and J. Adjaye, "Product Selectivity during Hydrotreating and Mild Hydrocracking of Bitumen-Derived Gas Oil," Energy Fuels. **17**, 1372-1381 (2003).

Bouwens, S.M.A.M., D.C. Koningsberger, V.H.J. de Beer and R. Prins, "The structure of the cobalt sulfide phase in carbon-supported Co and Co-Mo sulfide catalysts as studied by exafs and xanes," Catalysis Letters. **1**, 55-59 (1988).

Bouwens, S.M.A.M., D.C. Koningsberger, V.H.J. De Beer, S.P.A. Louwers and R. Prins, "Exafs study of the local structure of Ni in Ni-MoS_2/C hydrodesulfurization catalysts," Catalysis Letters. **5**, 273-283 (1990).

Bouwens, S.M.A.M., F.B.M. Vanzon, M.P. Vandijk, A.M. Vanderkraan, V.H.J. Debeer, J.A.R. Vanveen and D.C. Koningsberger, "On the Structural Differences Between Alumina-Supported Comos Type I and Alumina-, Silica-, and Carbon-Supported Comos Type II Phases Studied by XAFS, MES, and XPS," Journal of Catalysis. **146**, 375-393 (1994).

Breysse, M., J.L. Portefaix and M. Vrinat, "Support effects on hydrotreating catalysts," Catalysis Today. **10**, 489-505 (1991).

Breysse, M., P. Afanasiev, C. Geantet and M. Vrinat, "Overview of support effects in hydrotreating catalysts," Catalysis Today. **86**, 5-16 (2003).

Breysse, M., C. Geantet, P. Afanasiev, J. Blanchard and M. Vrinat, "Recent studies on the preparation, activation and design of active phases and supports of hydrotreating catalysts," Catalysis Today. **130**, 3-13 (2008).

Camblor, M.A., A. Mifsud and J. Perez-Pariente, "Influence of the synthesis conditions on the crystallization of zeolite Beta," Zeolites. **11**, 792-797 (1991).

Carvill, B.T. and L.T. Thompson, "Hydrodesulfurization over model sulfide cluster-derived catalysts," Applied Catalysis. **75**, 249-265 (1991).

Cattaneo, R., T. Shido and R. Prins, "The Relationship between the Structure of $NiMo/SiO_2$ Catalyst Precursors Prepared in the Presence of Chelating Ligands and the Hydrodesulfurization Activity of the Final Sulfided Catalysts," Journal of Catalysis. **185**, 199-212 (1999).

Cheng, Y., L. Wang, J. Li, Y. Yang and X. Sun, "Preparation and characterization of nanosized ZSM-5 zeolites in the absence of organic template," Mater Lett. **59**, 3427-3430 (2005).

Chrones, J. and R.R. Germain, "Bitumen and heavy oil upgrading in Canada," Fuel Sci. Technol. Int. **7**, 783-821 (1989).

Chunshan, S., "An overview of new approaches to deep desulfurization for ultra-clean gasoline, diesel fuel and jet fuel," Catalysis Today. **86**, 211-263 (2003).

Clausen, B.S., H. Topsoe, R. Candia, J. Villadsen, B. Lengeler, J. Als-Nielsen and F. Christensen, "Extended X-ray absorption fine structure study of Co-Mo hydrodesulfurization catalysts," J. Phys. Chem. **85**, 3868-3872 (1981).

Cooper, B.H. and B.B.L. Donnis, "Aromatic saturation of distillates: an overview," Applied Catalysis A: General. **137**, 203-223 (1996).

Coulier, L., V.H.J. de Beer, J.A.R. van Veen and J.W. Niemantsverdriet, "On the formation of cobalt molybdenum sulfides in silica supported hydrotreating model catalysts," Topics in Catalysis. **13**, 99-108 (2000).

Craje, M.W.J., V.H.J. de Beer and d.K. van, "Some aspects of the stability of the So-called "Co-Mo-S" phase present in sulfided carbon-supported Co and CoMo catalysts. A Mossbauer emission spectroscopic study," Hyperfine Interactions. **69**, 799-802 (1991).

Craje, M.W.J., V.H.J. de Beer, J.A.R. van Veen and d.K. van, "On the identification of `Co-sulfide' species in sulfided supported Co and CoMo catalysts," American Chemical Society, Division of Petroleum Chemistry, Preprints. **39**, 538-547 (1994).

Daage, M. and R.R. Chianelli, "Structure-Function Relations in Molybdenum Sulfide Catalysts: The "Rim-Edge" Model," Journal of Catalysis. **149**, 414-427 (1994).

De Boer, M., A.J. Van Dillen, D.C. Koningsberger and J.W. Geus, "The structure of highly dispersed SiO2-supported molybdenum oxide catalysts during sulfidation," J. Phys. Chem. **98**, 7862-7870 (1994).

de Moor, Peter-Paul E. A., T.P.M. Beelen, B.U. Komanschek, L.W. Beck, P. Wagner, M.E. Davis and R.A. van Santen, "Imaging the Assembly Process of the Organic-Mediated Synthesis of a Zeolite," Chem. Eur. J. **5**, 2083-2088 (1999).

de Moor, Peter-Paul E. A., T.P.M. Beelen and R.A. van Santen, "In situ Observation of Nucleation and Crystal Growth in Zeolite Synthesis. A Small-Angle X-ray Scattering Investigation on Si-TPA-MFI," The Journal of Physical Chemistry B. **103**, 1639-1650 (1999).

de Moor, Peter-Paul E. A., T.P.M. Beelen, R.A. van Santen, L.W. Beck and M.E. Davis, "Si-MFI Crystallization using a dimer and trimer of TPA Studied with Small-Angle X-ray Scattering," The Journal of Physical Chemistry B. **104**, 7600-7611 (2000).

Delannay, F., "High resolution electron microscopy of hydrodesulfurization catalysts: A Review," Applied Catalysis. **16**, 135-152 (1985).

Delmon, B., "Mobility of atomic species on catalyst surfaces (spillover) : effects on creation of active sites and stability of catalysts," Applied Catalysis A: General. **113**, 121-124 (1994).

Delmon, B., "Dynamic processes in active phase-support interactions," Journal of Molecular Catalysis. **59**, 179-206 (1990).

Delmon, B., "Characterization of catalyst deactivation: Industrial and laboratory time scales," Applied Catalysis. **15**, 1-16 (1985).

Delmon, B., "A new hypothesis explaining synergy between two phases in heterogeneous catalysis the case of hydrodesulfurization catalysts," Bull. Soc. Chim. Belges. **88**, 979-987 (1979).

Delmon, B. and G.F. Froment, "Remote Control of Catalytic Sites by Spillover Species: A Chemical Reaction Engineering Approach," Catalysis Reviews. **38**, 69-100 (1996).

Dhar, G.M., B.N. Srinivas, M.S. Rana, M. Kumar and S.K. Maity, "Mixed oxide supported hydrodesulfurization catalystsâ€”a review," Catalysis Today. **86**, 45-60 (2003).

Dhar, G.M., G.M. Kumaran, M. Kumar, K.S. Rawat, L.D. Sharma, B.D. Raju and K.S.R. Rao, "Physico-chemical characterization and catalysis on SBA-15 supported molybdenum hydrotreating catalysts," Catalysis Today. **99**, 309-314 (2005).

Dickinson, R.G. and L. Pauling, " The crustal structure of molybdenite," J. Am. Chem. Soc. **45**, 1466-1471 (1923).

Eijsbouts, S., J.J.L. Heinerman and H.J.W. Elzerman, "MoS_2 structures in high activity hydrotreating catalysts. II. Evolution of the active phase during the catalyst life cycle. Deactivation model," Applied Catalysis A, General. **105**, 69-82 (1993a).

Eijsbouts, S., J.J.L. Heinerman and H.J.W. Elzerman, "MoS_2 structures in high-activity hydrotreating catalysts. I. Semi-quantitative method for evaluation of transmission electron microscopy results. Correlations between hydrodesulfurization and hydrodenitrogenation activities and MoS2 dispersion," Applied Catalysis A, General. **105**, 53-68 (1993b).

Emeis, C.A., "Determination of Integrated Molar Extinction Coefficients for Infrared Absorption Bands of Pyridine Adsorbed on Solid Acid Catalysts," Journal of Catalysis. **141**, 347-354 (1993).

Escobar, J., M.C. Barrera, l.R. de, J.A. Toledo, V. Santes and J.A. ColÃn, "Effect of chelating ligands on NiMo impregnation over wide-pore ZrO_2-TiO_2," Journal of Molecular Catalysis A: Chemical. **287**, 33-40 (2008).

Fantazzini, D., M. Hook and A. Angelantoni, "Global oil risks in the early 21st century," Energy Policy. **39**, 7865-7873 (2011).

Ferdous, D., A.K. Dalai and J. Adjaye, "Hydrodenitrogenation and Hydrodesulfurization of Heavy Gas Oil Using NiMo/Al_2O_3 Catalyst Containing Boron: Experimental and Kinetic Studies," Ind Eng Chem Res. **45**, 544-552 (2006).

Ferdous, D., A.K. Dalai and J. Adjaye, "A series of NiMo/Al_2O_3 catalysts containing boron and phosphorus: Part II. Hydrodenitrogenation and hydrodesulfurization using heavy gas oil derived from Athabasca bitumen," Applied Catalysis A: General. **260**, 153-162 (2004).

Follens, L.R.A., A. Aerts, M. Haouas, T.P. Caremans, B. Loppinet, B. Goderis, J. Vermant, F. Taulelle, J.A. Martens and C.E.A. Kirschhock, "Characterization of nanoparticles in diluted clear solutions for Silicalite-1 zeolite synthesis using liquid ^{29}Si NMR, SAXS and DLS," Phys. Chem. Chem. Phys. **10**, 5574-5583 (2008).

Frunz, L., R. Prins and G.D. Pirngruber, "ZSM-5 precursors assembled to a mesoporous structure and its subsequent transformation into a zeolitic phase--from low to high catalytic activity," Microporous and Mesoporous Materials. **88**, 152-162 (2006).

Fujikawa, T., "Highly active CoMo HDS catalyst for the production of clean diesel fuels," Catalysis Surveys from Asia. **10**, 89-97 (2006).

Fujikawa, T., M. Kato, H. Kimura, K. Kiriyama, M. Hashimoto and N. Nakajima, "Development of Highly Active Co-Mo Catalysts with Phosphorus and Citric Acid for Ultra-deep Desulfurization of Diesel Fractions (Part 1) Preparation and Performance of Catalysts," Journal of the Japan Petroleum Institute. **48**, 106-113 (2005a).

Fujikawa, T., M. Kato, T. Ebihara, K. Hagiwara, T. Kubota and Y. Okamoto, "Development of Highly Active Co-Mo Catalysts with Phosphorus and Citric Acid for Ultra-deep Desulfurization of Diesel Fractions (Part 2) Characterization of Active Sites," Journal of the Japan Petroleum Institute. **48**, 114-120 (2005b).

Furimsky, E. and F.E. Massoth, "Hydrodenitrogenation of Petroleum," Catalysis Reviews. **47**,

Furimsky, E. and F.E. Massoth, "Deactivation of hydroprocessing catalysts," Catalysis Today. **52**, 381-495 (1999).

Perot, G., "Hydrotreating catalysts containing zeolites and related materials - mechanistic aspects related to deep desulfurization," Catalysis Today. **86**, 111-128 (2003).

Garg, S., K. Soni, G.M. Kumaran, M. Kumar, J.K. Gupta, L.D. Sharma and G.M. Dhar, "Effect of Zr-SBA-15 support on catalytic functionalities of Mo, CoMo, NiMo hydrotreating catalysts," Catalysis Today. **130**, 302-308 (2008).

Gates, B.C. and H. Topsoe, "Reactivities in deep catalytic hydrodesulfurization: challenges, opportunities, and the importance of 4-methyldibenzothiophene and 4,6-dimethyldibenzothiophene," Polyhedron. **16**, 3213-3217 (1997).

Grajciar, L., C.O. Arean, A. Pulido and P. Nachtigall, "Periodic DFT investigation of the effect of aluminium content on the properties of the acid zeolite H-FER," Phys. Chem. Chem. Phys. **12**, 1497-1506 (2010).

Grange, P., "Catalytic hydrodesulfurization," Catalysis Reviews - Science and Engineering. **21**, 135-181 (1980).

Grange, P. and X. Vanhaeren, "Hydrotreating catalysts, an old story with new challenges," Catalysis Today. **36**, 375-391 (1997).

Gray, M.R., "Upgrading petroleum residues and heavy oils / Murray R. Gray," M. Dekker, New York : (1994).

Gruia, A., "Hydrotreating; Handbook of Petroleum Processing," in D. S. J. S. Jones and P. R. Pujado, Eds. Springer Netherlands (2006), pp. 321-354.

Grzechowiak, J.R., I. Wereszczako-Zielinska, J. Rynkowski and M. Ziolek, "Hydrodesulphurisation catalysts supported on alumina-titania," Applied Catalysis A: General. **250**, 95-103 (2003).

Gutierrez, O.Y., D. Valencia, G.A. Fuentes and T. Klimova, "Mo and NiMo catalysts supported on SBA-15 modified by grafted ZrO2 species: Synthesis, characterization and evaluation in 4,6-dimethyldibenzothiophene hydrodesulfurization," Journal of Catalysis. **249**, 140-153 (2007).

Gutierrez, O.Y., G.A. Fuentes, C. Salcedo and T. Klimova, "SBA-15 supports modified by Ti and Zr grafting for NiMo hydrodesulfurization catalysts," Catalysis Today. **116**, 485-497 (2006).

Gutierrez, O.Y., F. Perez, G.A. Fuentes, X. Bokhimi and T. Klimova, "Deep HDS over NiMo/Zr-SBA-15 catalysts with varying MoO_3 loading," Catalysis Today. **130**, 292-301 (2008).

Han, Y., S. Wu, Y. Sun, D. Li, F. Xiao, J. Liu and X. Zhang, "Hydrothermally Stable Ordered Hexagonal Mesoporous Aluminosilicates Assembled from a Triblock Copolymer and Preformed Aluminosilicate Precursors in Strongly Acidic Media," Chemistry of Materials. **14**, 1144-1148 (2002a).

Han, Y., F. Xiao, S. Wu, Y. Sun, X. Meng, D. Li, S. Lin, F. Deng and X. Ai, "A Novel Method for Incorporation of Heteroatoms into the Framework of Ordered Mesoporous Silica Materials Synthesized in Strong Acidic Media," J Phys Chem B. **105**, 7963-7966 (2001).

Harris, S. and R.R. Chianelli, "Catalysis by transition metal sulfides: A theoretical and experimental study of the relation between the synergic systems and the binary transition metal sulfides," Journal of Catalysis. **98**, 17-31 (1986).

Hauser, A., A. Marafi, A. Almutairi and A. Stanislaus, "Comparative Study of Hydrodemetallization (HDM) Catalyst Aging by Boscan Feed and Kuwait Atmospheric Residue," Energy Fuels. **22**, 2925-2932 (2008).

Hayden, T.F. and J.A. Dumesic, "Studies of the structure of molybdenum oxide and sulfide supported on thin films of alumina," Journal of Catalysis. **103**, 366-384 (1987).

Hayden, T.F., J.A. Dumesic, R.D. Sherwood and R.T.K. Baker, "Direct observation by controlled atmosphere electron microscopy of the changes in morphology of molybdenum oxide and sulfide supported on alumina and graphite," Journal of Catalysis. **105**, 299-318 (1987).

Hensen, E.J.M., P.J. Kooyman, d.M. Van, d.K. Van, V.H.J. De Beer, J.A.R. Van Veen and R.A. Van Santen, "The relation between morphology and hydrotreating activity for supported MoS_2 particles," Journal of Catalysis. **199**, 224-235 (2001).

Huang, L., J. Fu, Q. Guo and Y. Zhong, "Outlook on global refining and transportation fuel market in the future -A review of 2010 Hart Energy Conference," Petroleum Processing and Petrochemicals. **41**, 1-7 (2010).

Huang, L., W. Guo, P. Deng, Z. Xue and Q. Li, "Investigation of Synthesizing MCM-41/ZSM-5 Composites," The Journal of Physical Chemistry B. **104**, 2817-2823 (2000).

Huang, Z.-., W. Bensch, L. Kienle, S. Fuentes, G. Alonso and C. Ornelas, "SBA-15 as Support for MoS_2 and Co-MoS_2 Catalysts Derived from Thiomolybdate Complexes in the Reaction of HDS of DBT," Catalysis Letters. **122**, 57-67 (2008a).

Huang, Z., W. Bensch, W. Sigle, P. van Aken, L. Kienle, T. Vitoya, H. Modrow and T. Ressler, "The modification of MoO_3 nanoparticles supported on mesoporous SBA-15: characterization using X-ray scattering, N_2 physisorption, transmission electron microscopy, high-angle annular darkfield technique, Raman and XAFS spectroscopy," J. Mater. Sci. **43**, 244-253 (2008b).

Hughes, T.R. and H.M. White, "A study of the surface structure of decationized Y zeolite by quantitative infrared spectroscopy," J. Phys. Chem. **71**, 2192-2201 (1967).

Huo, Q., T. Dou, Z. Zhao and H. Pan, "Synthesis and application of a novel mesoporous zeolite L in the catalyst for the HDS of FCC gasoline," Applied Catalysis A: General. **381**, 101-108 (2010).

Isoda, T., S. Nagao, X. Ma, Y. Korai and I. Mochida, "Hydrodesulfurization Pathway of 4,6-Dimethyldibenzothiophene through Isomerization over Y-Zeolite Containing CoMo/Al2O3 Catalyst," Energy Fuels. **10**, 1078-1082 (1996).

Jacobs, P.A., E.G. Derouane and J. Weitkamp, "Evidence for X-ray-amorphous zeolites," J. Chem. Soc. , Chem. Commun., 591-593 (1981).

Jayne, D., Y. Zhang, S. Haji and C. Erkey, "Dynamics of removal of organosulfur compounds from diesel by adsorption on carbon aerogels for fuel cell applications," Int J Hydrogen Energy. **30**, 1287-1293 (2005).

John W., W., "Hydrocracking processes and catalysts," Fuel Process Technol. **35**, 55-85 (1993).

Kabe, T., A. Ishihara and H. Tajima, "Hydrodesulfurization of sulfur-containing polyaromatic compounds in light oil," Ind Eng Chem Res. **31**, 1577-1580 (1992).

Kabe, T., K. Akamatsu, A. Ishihara, S. Otsuki, M. Godo, Q. Zhang and W. Qian, "Deep Hydrodesulfurization of Light Gas Oil. 1. Kinetics and Mechanisms of Dibenzothiophene Hydrodesulfurization," Ind Eng Chem Res. **36**, 5146-5152 (1997).

Kameoka, T., H. Yanase, A. Nishijima, T. Sato, Y. Yoshimura, H. Shimada and N. Matsubayashi, "Catalytic performance tests and deactivation behavior of Ni-W/Al2O3 catalysts developed for upgrading coal-derived liquids," Applied Catalysis A, General. **123**, 217-228 (1995).

Kirschhock, C.E.A., R. Ravishankar, P.A. Jacobs and J.A. Martens, "Aggregation Mechanism of Nanoslabs with Zeolite MFI-Type Structure," The Journal of Physical Chemistry B. **103**, 11021-11027 (1999).

Kjarstad, J. and F. Johnsson, "Resources and future supply of oil," Energy Policy. **37**, 441-464 (2009).

Klimov, O., A. Pashigreva, D. Kochubei, G. Bukhtiyarova and A. Noskov, "The use of X-ray absorption spectroscopy for developing new-generation Co-Mo catalysts of hydrotreating of diesel fuel," Doklady Physical Chemistry. **424**, 35-39 (2009).

Klimov, O.V., A.V. Pashigreva, K.A. Leonova, G.A. Bukhtiyarova, S.V. Budukva and A.S. Noskov, "Bimetallic Co-Mo-complexes with optimal localization on the support surface: A way for highly active hydrodesulfurization catalysts preparation for different petroleum distillates," in "Studies in Surface Science and Catalysis; Scientific Bases for the Preparation of Heterogeneous Catalysts Proceedings of the 10th International Symposium, Louvain-la-Neuve, Belgium, July 11-15, 2010," E.M. Gaigneaux, M. Devillers, S. Hermans, P.A. Jacobs,J.A.Martens and P.Ruiz, Ed. Elsevier (2010a), pp. 509-512.

Klimov, O.V., A.V. Pashigreva, M.A. Fedotov, D.I. Kochubey, Y.A. Chesalov, G.A. Bukhtiyarova and A.S. Noskov, "CoMo catalysts for ultra-deep HDS of diesel fuels prepared via synthesis of bimetallic surface compounds," Journal of Molecular Catalysis A: Chemical. **322**, 80-89 (2010b).

Klimova, T., J. Ramirez, M. Calderon and J.M. Dominguez, "New Mo and NiMo catalysts supported on MCM-41/Alumina for thiophene hydrodesulfurization," Studies in Surface Science and Catalysis. **117**, 493-500 (1998).

Klimova, T., L. Pena, L. Lizama, C. Salcedo and O.Y. Gutierrez, "Modification of activity and selectivity of NiMo/SBA-15 HDS catalysts by grafting of different metal oxides on the support surface," Industrial and Engineering Chemistry Research. **48**, 1126-1133 (2009).

Klimova, T., J. Reyes, O. Gutiérrez and L. Lizama, "Novel bifunctional NiMo/Al-SBA-15 catalysts for deep hydrodesulfurization: Effect of support Si/Al ratio," Applied Catalysis A: General. **335**, 159-171 (2008).

Krishnan, J.M. and K.R. Rajagopal, "Review of the uses and modeling of bitumen from ancient to modern times," Appl. Mech. Rev. **56**, 149-214 (2003).

Kunisada, N., K. Choi, Y. Korai, I. Mochida and K. Nakano, "Optimum coating of USY as a support component of NiMoS on alumina for deep HDS of gas oil," Applied Catalysis A: General. **276**, 51-59 (2004).

Kwart, H., G.C.A. Schuit and B.C. Gates, "Hydrodesulfurization of thiophenic compounds: The reaction mechanism," Journal of Catalysis. **61**, 128-134 (1980).

Landau, M.V., D. Berger and M. Herskowitz, "Hydrodesulfurization of Methyl-Substituted Dibenzothiophenes:Fundamental Study of Routes to Deep Desulfurization," Journal of Catalysis. **159**, 236-245 (1996).

Larocca, M., S. Ng and H. De Lasa, "Fast catalytic cracking of heavy gas oils: modeling coke deactivation," Ind Eng Chem Res. **29**, 171-180 (1990).

Lecrenay, E., K. Sakanishi and I. Mochida, "Catalytic hydrodesulfurization of gas oil and model sulfur compounds over commercial and laboratory-made CoMo and NiMo catalysts: Activity and reaction scheme," Catalysis Today. **39**, 13-20 (1997).

Lecrenay, E., K. Sakanishi, I. Mochida and T. Suzuka, "Hydrodesulfurization activity of CoMo and NiMo catalysts supported on some acidic binary oxides," Applied Catalysis A: General. **175**, 237-243 (1998a).

Lecrenay, E., K. Sakanishi, T. Nagamatsu, I. Mochida and T. Suzuka, "Hydrodesulfurization activity of CoMo and NiMo supported on Al_2O_3-TiO_2 for some model compounds and gas oils," Applied Catalysis B: Environmental. **18**, 325-330 (1998b).

Leliveld, R.G., A.J. van Dillen, J.W. Geus and D.C. Koningsberger, "A Mo-K Edge XAFS Study of the Metal Sulfide-Support Interaction in (Co)Mo Supported Alumina and Titania Catalysts," Journal of Catalysis. **165**, 184-196 (1997).

Leyva, C., M.S. Rana, F. Trejo and J. Ancheyta, "On the Use of Acid-Base-Supported Catalysts for Hydroprocessing of Heavy Petroleum," Ind Eng Chem Res. **46**, 7448-7466 (2007a).

Linares, C. and M. Fernandez, "Study of the Individual Reactions of Hydrodesulphurization of Dibenzothiophene and Hydrogenation of 2-Methylnaphthalene on ZnNiMo/Î³-Alumina Catalysts," Catalysis Letters. **126**, 341-345 (2008).

Lipsch, J.M.J.G. and G.C.A. Schuit, "The $CoO¸MoO_3¸Al_2O_3$ catalyst: III. Catalytic properties," Journal of Catalysis. **15**, 179-189 (1969).

Liu, Y. and T.J. Pinnavaia, "Assembly of wormhole aluminosilicate mesostructures from zeolite seeds," J. Mater. Chem. **14**, 1099-1103 (2004).

Liu, Y. and T.J. Pinnavaia, "Aluminosilicate mesostructures with improved acidity and hydrothermal stability," J. Mater. Chem. **12**, 3179-3190 (2002).

Liu, Y., W. Zhang and T.J. Pinnavaia, "Steam-Stable MSU-S Aluminosilicate Mesostructures Assembled from Zeolite ZSM-5 and Zeolite Beta Seeds," Angew. Chem. Int. Ed. **40**, 1255-1258 (2001).

Liu, Y., W. Zhang and T.J. Pinnavaia, "Steam-Stable Aluminosilicate Mesostructures Assembled from Zeolite Type Y Seeds," J. Am. Chem. Soc. **122**, 8791-8792 (2000).

Louwers, S.P.A., M.W.J. Craje, A.M. Vanderkraan, C. Geantet and R. Prins, "The Effect of Passivation on the Activity and Structure of Sulfided Hydrotreating Catalysts," Journal of Catalysis. **144**, 579-596 (1993).

Lu, M., A. Wang, X. Li, X. Duan, Y. Teng, Y. Wang, C. Song and Y. Hu, "Hydrodenitrogenation of Quinoline Catalyzed by MCM-41-Supported Nickel Phosphides," Energy Fuels. **21**, 554-560 (2007).

Ma, X., K. Sakanishi and I. Mochida, "Hydrodesulfurization reactivities of various sulfur compounds in diesel fuel," Industrial and Engineering Chemistry Research. **33**, 218-222 (1994).

Ma, X., K. Sakanishi, T. Isoda and I. Mochida, "Hydrodesulfurization reactivities of narrow-cut fractions in a gas oil," Industrial and Engineering Chemistry Research. **34**, 748-754 (1995).

Madeley, R.A. and S. Wanke E., "Variation of the dispersion of active phases in commercial nickel-molybdenum-alumina hydrotreating catalysts during oxidative regeneration," Applied Catalysis. **39**, 295-314 (1988).

Maity, S.K., M.S. Rana, S.K. Bej, J. Ancheyta-Juarez, G. Murali Dhar and T.S.R. Prasada Rao, "Studies on physico-chemical characterization and catalysis on high surface area titania supported molybdenum hydrotreating catalysts," Applied Catalysis A: General. **205**, 215-225 (2001).

Mangnus, P.J., E.K. Poels and J.A. Moulijn, "Temperature programmed sulfiding of commercial CoO-MoO3/Al2O3 catalysts," Industrial and Engineering Chemistry Research. **32**, 1818-1821 (1993).

Mangnus, P.J., E.K. Poels, A.D. van Langeveld and J.A. Moulijn, "Comparison of the sulfiding rate and mechanism of supported NiO and Ni0 particles," Journal of Catalysis. **137**, 92-101 (1992).

Mann, R.S., I.S. Sambi and K.C. Khulbe, "Hydrofining of heavy gas oil on zeolite-alumina supported nickel-molybdenum catalyst," Ind Eng Chem Res. **27**, 1788-1792 (1988).

Massoth, F.E., G. Muralidhar and J. Shabtai, "Catalytic functionalities of supported sulfides. II. Effect of support on Mo dispersion," Journal of Catalysis. **85**, 53-62 (1984).

Massoth, F.E., "Characterization of Molybdena Catalysts," in "Advances in Catalysis," D.D. Eley,Herman Pines and Paul B.Weisz, Ed. Academic Press (1979), pp. 265-310.

Medici, L. and R. Prins, "Structure of Oxidic NiMo/SiO2Hydrotreating Catalyst Precursors," Journal of Catalysis. **163**, 28-37 (1996a).

Medici, L. and R. Prins, "The Influence of Chelating Ligands on the Sulfidation of Ni and Mo in NiMo/SiO2Hydrotreating Catalysts," Journal of Catalysis. **163**, 38-49 (1996b).

Mestl, G. and T.K.K. Srinivasan, "Raman Spectroscopy of Monolayer-Type Catalysts: Supported Molybdenum Oxides," Catalysis Reviews: Science and Engineering. **40**, 451-570 (1998).

Meyers, R.A., "Handbook of Petroleum Refining Processes (3rd Edition),".

Mignard, S., S. Kasztelan, M. Dorbon, A. Billon and P. Sarrazin, "Deep HDS of middle distillates using a high loading CoMo catalyst," in "Studies in Surface Science and Catalysis; catalysts in Petroleum Refining and Petrochemical Industries 1995 Proceedings of the 2nd International Conference on Catalysts in Petroleum refining and Petrochemical Industries," J. B. a. A. S. M. Absi-Halabi, Ed. Elsevier (1996), pp. 209-216.

Mochida, I. and K. Choi, "Current Progress in Catalysts and Catalysis for Hydrotreating; Practical Advances in Petroleum Processing," in C. Hsu and P. Robinson, Eds. Springer New York (2006), pp. 257-296.

Morsli, A., M.F. Driole, T. Cacciaguerra, R. Arletti, B. Chiche, F. Hamidi, A. Bengueddach, F. Quignard and F. Di Renzo, "Microporosity of the amorphous aluminosilicate precursors of zeolites: The case of the gels of synthesis of mordenite," Microporous and Mesoporous Materials. **104**, 209-216 (2007).

Nava, R., J. Morales, G. Alonso, C. Ornelas, B. Pawelec and J.L.G. Fierro, "Influence of the preparation method on the activity of phosphate-containing CoMo/HMS catalysts in deep hydrodesulphurization," Applied Catalysis A: General. **321**, 58-70 (2007).

Prabhu, A., L. Kumaresan, M. Palanichamy and V. Murugesan, "Synthesis and characterization of aluminium incorporated mesoporous KIT-6: Efficient catalyst for acylation of phenol," Applied Catalysis A: General. **360**, 59-65 (2009).

Prabhu, N., A.K. Dalai and J. Adjaye, "Hydrodesulphurization and hydrodenitrogenation of light gas oil using NiMo catalyst supported on functionalized mesoporous carbon," Applied Catalysis A: General. **401**, 1-11 (2011).

Pratt, K.C., J.V. Sanders and V. Christov, "Morphology and activity of MoS2 on various supports: Genesis of the active phase," Journal of Catalysis. **124**, 416-432 (1990).

Prins, R., De Beer, V. H. J. and G.A. Somorjai, "Structure and Function of the Catalyst and the Promoter in Coâ€"Mo Hydrodesulfurization Catalysts," Catalysis Reviews. **31**, 1-41 (1989).

Prins, R., M. Egorova, A. RÃ¶thlisberger, Y. Zhao, N. Sivasankar and P. Kukula, "Mechanisms of hydrodesulfurization and hydrodenitrogenation," Catalysis Today. **111**, 84-93 (2006).

Rajagopalan, K., A.W. Peters and G.C. Edwards, "Influence of zeolite particle size on selectivity during fluid catalytic cracking," Applied Catalysis. **23**, 69-80 (1986).

Ramirez, J. and F. Sanchez-Minero, "Support effects in the hydrotreatment of model molecules," Catalysis Today. **130**, 267-271 (2008).

Rana, M.S., B.N. Srinivas, S.K. Maity, G. Murali Dhar and T.S.R. Prasada Rao, "Catalytic functionalities of TiO2 based SiO2, Al2O3, ZrO2 mixed oxide hydroprocessing catalysts," in "Studies in Surface Science and Catalysis; Hydrotreatment and hydrocracking of oil fractions Proceedings ofthe 2nd International Symposium/7th European Workshop," G. F. F. a. P. G. B. Delmon, Ed. Elsevier (1999), pp. 397-400.

Rana, M.S., V. SÃ¡mano, J. Ancheyta and J.A.I. Diaz, "A review of recent advances on process technologies for upgrading of heavy oils and residua," Fuel. **86**, 1216-1231 (2007).

Ratnasamy, P. and S. Sivasanker, "Structural Chemistry of Co-Mo-Alumnina Catalysts," Catalysis Reviews. **22**, 401-429 (1980).

Ravel, B. and M. Newville, "ATHENA, ARTEMIS, HEPHAESTUS: data analysis for X-ray absorption spectroscopy using IFEFFIT," J. Synchrotron Rad. **12**, 537-541 (2005a).

Ravishankar, R., C. Kirschhock, B.J. Schoeman, P. Vanoppen, P.J. Grobet, S. Storck, W.F. Maier, J.A. Martens, F.C. De Schryver and P.A. Jacobs, "Physicochemical Characterization of Silicalite-1 Nanophase Material," The Journal of Physical Chemistry B. **102**, 2633-2639 (1998).

Rinaldi, N., T. Kubota and Y. Okamoto, "Effect of citric acid addition on the hydrodesulfurization activity of MoO_3/Al_2O_3 catalysts," Applied Catalysis A: General. **374**, 228-236 (2010).

Rinaldi, N., T. Kubota and Y. Okamoto, "Effect of citric acid addition on Co-Mo/B_2O_3/Al $_2O_3$ catalysts prepared by a post-treatment method," Industrial and Engineering Chemistry Research. **48**, 10414-10424 (2009).

Rinaldi, N., M. Yoshioka, T. Kubota and Y. Okamoto, "Hydrodesulfurization activity of Co-Mo/Al_2O_3 catalysts prepared with citric acid: Post-treatment of calcined catalysts with high Mo loading," Journal of the Japan Petroleum Institute. **53**, 292-302 (2010).

Rinaldi, N., Usman, K. Al-Dalama, T. Kubota and Y. Okamoto, "Preparation of Co-Mo/B2O3/Al2O3 catalysts for hydrodesulfurization: Effect of citric acid addition," Applied Catalysis A: General. **360**, 130-136 (2009).

Robinson, P. and G. Dolbear, "Hydrotreating and Hydrocracking: Fundamentals; Practical Advances in Petroleum Processing," in C. Hsu and P. Robinson, Eds. Springer New York (2006), pp. 177-218.

Robinson, W.R.A.M., J.A.R. van Veen, V.H.J. de Beer and R.A. van Santen, "Development of deep hydrodesulfurization catalysts: II. NiW, Pt and Pd catalysts tested with (substituted) dibenzothiophene," Fuel Process Technol. **61**, 103-116 (1999).

Soderbergh, B., F. Robelius and K. Aleklett, "A crash programme scenario for the Canadian oil sands industry," Energy Policy. **35**, 1931-1947 (2007).

Sambi, I.S. and R.S. Mann, "Rey-zeolite and silica-alumina mixed support for hydrotreating heavy gas oil," Can. J. Chem. Eng. **67**, 337-343 (1989).

Samotus, A., A. Kanas, M. Dudek, R. Grybos and E. Hodorowicz, "1:1 Molybdenum(VI) citric acid complexes," Transition Metal Chemistry. **16**, 495-499 (1991).

Scheffer, B., E.M. van Oers, P. Arnoldy, V.H.J. de Beer and J.A. Moulijn, "Sulfidability and HDS activity of Co-Mo/Al2O3 catalysts," Applied Catalysis. **25**, 303-311 (1986).

Schuit, G.C.A. and B.C. Gates, "Chemistry and engineering of catalytic hydrodesulfurization," AICHE J. **19**, 417-438 (1973).

Shabtai, J., G.J.C. Yeh, C. Russell and A.G. Oblad, "Fundamental hydrodenitrogenation studies of polycyclic nitrogen-containing compounds found in heavy oils. 1. 5,6-Benzoquinoline," Ind Eng Chem Res. **28**, 139-146 (1989).

Shabtai, J., Q. Guohe, K. Balusami, N.K. Nag and F.E. Massoth, "Catalytic functionalities of supported sulfides: V. Cî—¸N bond hydrogenolysis selectivity as a function of promoter type," Journal of Catalysis. **113**, 206-219 (1988).

Shimada, H., T. Sato, Y. Yoshimura, A. Hinata, S. Yoshitomi, A. Castillo Mares and A. Nishijima, "Application of zeolite-based catalyst to hydrocracking of coal-derived liquids," Fuel Process Technol. **25**, 153-165 (1990).

Smith, D.F., P. Rahimi, A. Teclemariam, R.P. Rodgers and A.G. Marshall, "Characterization of Athabasca Bitumen Heavy Vacuum Gas Oil Distillation Cuts by Negative/Positive Electrospray Ionization and Automated Liquid Injection Field Desorption Ionization Fourier Transform Ion Cyclotron Resonance Mass Spectrometry," Energy Fuels. **22**, 3118-3125 (2008).

Solís, D., A.L. Agudo, J. Ramírez and T. Klimova, "Hydrodesulfurization of hindered dibenzothiophenes on bifunctional NiMo catalysts supported on zeolite-alumina composites," Catalysis Today. **116**, 469-477 (2006).

Song, C., "New Approaches to Deep Desulfurization for Ultra-Clean Gasoline and Diesel Fuels: An Overview," ACS Division of Fuel Chemistry, Preprints. **47**, 438-444 (2002).

Soni, K., B.S. Rana, A.K. Sinha, A. Bhaumik, M. Nandi, M. Kumar and G.M. Dhar, "3-D ordered mesoporous KIT-6 support for effective hydrodesulfurization catalysts," Applied Catalysis B: Environmental. **90**, 55-63 (2009).

Soni, K., K. Mouli, A. Dalai and J. Adjaye, "Influence of Frame Connectivity of SBA-15 and KIT-6 Supported NiMo Catalysts for Hydrotreating of Gas Oil," Catalysis Letters. **136**, 116-125 (2010).

Sonja, E., "On the flexibility of the active phase in hydrotreating catalysts," Applied Catalysis A: General. **158**, 53-92 (1997).

Sonnemans, J. and P. Mars, "The mechanism of pyridine hydrogenolysis on molybdenum-containing catalysts. I. The monolayer MoO_3/Al_2O_3 catalyst: Preparation and catalytic properties," Journal of Catalysis. **31**, 209-219 (1973).

Speight, J.G., "Refining: Characterisation and analysis of resids," Petroleum Technology Quarterly. **8**, 103-104, 106 (2003).

Speight, J., "Liquid Fuels from Oil Sand," in "Handbook of Alternative Fuel Technologies," Anonymous CRC Press (2007), pp. 197-221.

Speight, J. and J. Ancheyta, "Hydroprocessing Chemistry," in "Hydroprocessing of Heavy Oils and Residua," Anonymous CRC Press (2007a), pp. 35-50.

Speight, J. and J. Ancheyta, "Hydroprocessing Chemistry," in "Hydroprocessing of Heavy Oils and Residua," Anonymous CRC Press (2007b), pp. 35-50.

Stanislaus, A. and B.H. Cooper, "Aromatic Hydrogenation Catalysis: A Review," Catalysis Reviews. **36**, 75-123 (1994).

Sun, M., D. Nicosia and R. Prins, "The effects of fluorine, phosphate and chelating agents on hydrotreating catalysts and catalysis," Catalysis Today. **86**, 173-189 (2003).

Sundaramurthy, V., A.K. Dalai and J. Adjaye, "Effect of EDTA on hydrotreating activity of $CoMo/Al_2O_3$ catalyst," Catalysis Letters. **102**, 299-306 (2005).

Sundaramurthy, V., I. Eswaramoorthi, A.K. Dalai and J. Adjaye, "Hydrotreating of gas oil on SBA-15 supported NiMo catalysts," Microporous and Mesoporous Materials. **111**, 560-568 (2008).

Swain, E.J., "U.S. crude slate gets heavier, higher in sulfur," Oil Gas J. **89**, 59-61 (1991).

Topsoe, H. and B.S. Clausen, "Active sites and support effects in hydrodesulfurization catalysts," Applied Catalysis. **25**, 273-293 (1986).

Topsoe, H., B.S. Clausen and F.E. Massoth, Catalysis Science and Technology, Vol.11., 1-231 (1996).

Topsoe, H., B.S. Clausen, N.-. Topsoe, E. Pedersen, W. Niemann, A. Muller, H. Bogge and B. Lengeler, "Inorganic cluster compounds as models for the structure of active sites in promoted hydrodesulphurization catalysts," Journal of the Chemical Society, Faraday Transactions 1: Physical Chemistry in Condensed Phases. **83**, 2157-2167 (1987).

Topsoe, H., B.S. Clausen, R. Candia, C. Wivel and S. Morup, "In situ Mossbauer emission spectroscopy studies of unsupported and supported sulfided CoMo hydrodesulfurization catalysts: Evidence for and nature of a CoMoS phase," Journal of Catalysis. **68**, 433-452 (1981).

Topsoe, N. and H. Topsoe, "Characterization of the structures and active sites in sulfided $CoMo/Al_2O_3$ and $NiMo/Al_2O_3$ catalysts by NO chemisorption," Journal of Catalysis. **84**, 386-401 (1983).

Topsoe, H. and B.S. Clausen, "Importance of Co-Mo-S type structures in hydrodesulfurization," Catalysis Reviews. **26**, 395-420 (1984).

Trong On, D., D. Lutic and S. Kaliaguine, "An example of mesostructured zeolitic material: UL-TS-1," Microporous and Mesoporous Materials. **44-45**, 435-444 (2001).

Tsimbler, S.M., L.L. Shevchenko and V.V. Grigor'eva, "The IR absorption spectra of the tartrate and citrate complexes of nickel, cobalt, and iron," Journal of Applied Spectroscopy. **11**, 1096-1101 (1969).

Turaga, U.T. and C. Song, "MCM-41-supported Co-Mo catalysts for deep hydrodesulfurization of light cycle oil," Catalysis Today. **86**, 129-140 (2003a).

Turaga, U.T., X. Ma and C. Song, "Influence of nitrogen compounds on deep hydrodesulfurization of 4,6-dimethyldibenzothiophene over Al2O3- and MCM-41-supported Co-Mo sulfide catalysts," Catalysis Today. **86**, 265-275 (2003b).

van Dillen, A.J., R.J.A.M. Terorde, D.J. Lensveld, J.W. Geus and K.P. deÂ Jong, "Synthesis of supported catalysts by impregnation and drying using aqueous chelated metal complexes," Journal of Catalysis. **216**, 257-264.

van Veen, J. A. Rob, E. Gerkema, d.K. van and A. Knoester, "A real support effect on the activity of fully sulphided CoMoS for the hydrodesulphurization of thiophene," J. Chem. Soc. , Chem. Commun., 1684-1686 (1987).

van Veen, J.A.R., H.A. Colijn, P.A.J.M. Hendriks and A.J. van Welsenes, "On the formation of type I and type II NiMoS phases in NiMo/Al2O3 hydrotreating catalysts and its catalytic implications," Fuel Process Technol. **35**, 137-157 (1993).

Van, D.K., M.W.J. Craje, E. Gerkema, W.L.T.M. Ramsela and V.H.J. De Beer, "So-called CoMoS" phase observed in carbon-supported cobalt sulfide catalyst by mossbauer emission spectroscopy," Applied Catalysis. **39**, L7-L10 (1988).

Voorhoeve, R.J.H., "Electron spin resonance study of active centers in nickel-tungsten sulfide hydrogenation catalysts," Journal of Catalysis. **23**, 236-242 (1971).

Voorhoeve, R.J.H. and J.C.M. Stuiver, "The mechanism of the hydrogenation of cyclohexene and benzene on nickel-tungsten sulfide catalysts," Journal of Catalysis. **23**, 243-252 (1971).

Wachs, I.E., "Raman and IR studies of surface metal oxide species on oxide supports: Supported metal oxide catalysts," Catalysis Today. **27**, 437-455 (1996).

Wang, A., Y. Wang, Y. Chen and P. Yao, "Hydrodesulfurization of dibenzothiophene over siliceous MCM-41-supported catalysts II. Sulfided Ni-Mo catalysts," Journal of Catalysis. **210**, 319-327 (2002).

Weber, T., J.C. Muijsers, van Wolput, J. H. M. C., C.P.J. Verhagen and J.W. Niemantsverdriet, "Basic Reaction Steps in the Sulfidation of Crystalline MoO3 to MoS2, As Studied by X-ray Photoelectron and Infrared Emission Spectroscopy," J. Phys. Chem. **100**, 14144-14150 (1996).

Welters, W.J.J., V.H.J. de Beer and R.A. van Santen, "Influence of zeolite acidity on thiophene hydrodesulfurization activity," Applied Catalysis A: General. **119**, 253-269 (1994).

Whitehurst, D.D., T. Isoda and I. Mochida, "Present State of the Art and Future Challenges in the Hydrodesulfurization of Polyaromatic Sulfur Compounds," in "Advances in Catalysis," D.D. Eley, Werner O. Haag,Bruce Gates and Helmut Knozinger, Ed. Academic Press (1998), pp. 345-471.

Wivel, C., R. Candia, B.S. Clausen, S. MÃ¸rup and H. Topsoe, "On the catalytic significance of a CoMoS phase in $CoMo/Al_2O_3$ hydrodesulfurization catalysts: Combined in situ Mossbauer emission spectroscopy and activity studies," Journal of Catalysis. **68**, 453-463 (1981).

Wiwel, P., B. Hinnemann, A. Hidalgo-Vivas, P. Zeuthen, B.O. Petersen and J.Ã. Duus, "Characterization and Identification of the most Refractory Nitrogen Compounds in Hydroprocessed Vacuum Gas Oil," Ind Eng Chem Res. **49**, 3184-3193 (2010).

Yoshimura, Y., "Temperature-programmed oxidation of sulfided cobalt-molybdate/alumina catalysts," Industrial and Engineering Chemistry Research. **30**, 1092-1099 (1991a).

Yoshimura, Y., H. Yokokawa, T. Sato, H. Shimada, N. Matsubayashi and A. Nishijima, "Temperature-programmed oxidation of sulfided nickel-molybdate/alumina catalysts Change of composition and structure of active metals," Applied Catalysis. **73**, 39-53 (1991b).

Yoshimura, Y., T. Sato, H. Shimada, N. Matsubayashi, M. Imamura, A. Nishijima, S. Yoshitomi, T. Kameoka and H. Yanase, "Oxidative regeneration of spent molybdate and tungstate hydrotreating catalysts," Energy and Fuels. **8**, 435-445 (1994).

Yue, Y., A. Gedeon, J. Bonardet, J. D'Espinose, J. Fraissard and N. Melosh, "Direct synthesis of AlSBA mesoporous molecular sieves: characterization and catalytic activities," Chem. Commun., 1967-1968 (1999).

Yui, S.M. and E.C. Sanford, "Mild hydrocracking of bitumen-derived coker and hydrocracker heavy gas oils: kinetics, product yields, and product properties," Ind Eng Chem Res. **28**, 1278-1284 (1989).

Yumoto, M., K. Usui, K. Watanabe, K. Idei and H. Yamazaki, "Development of a Cosmo deep HDS catalyst for diesel fuel," Catalysis Today. **35**, 45-50 (1997).

Zebib, B., S. Zeng, J.-. Krafft, J.-. Lambert, J. Blanchard, H. Nie, D. Li and M. Breysse, "High surface area supports with strong Brønsted acidity in an open porosity," in "Studies in Surface Science and Catalysis; Molecular Sieves: From Basic Research to Industrial Applications, Proceedings of the 3rd International Zeolite Symposium (3rd FEZA)," N. Z. a. P. N. J. Cejka, Ed. Elsevier (2005), pp. 517-524.

Zeng, S., J. Blanchard, M. Breysse, Y. Shi, X. Su, H. Nie and D. Li, "Mesoporous materials from zeolite seeds as supports for nickelâ€“tungsten sulfide active phases: Part 2. Catalytic properties for deep hydrodesulfurization reactions," Applied Catalysis A: General. **298**, 88-93 (2006).

Zeng, S., J. Blanchard, M. Breysse, Y. Shi, X. Su, H. Nie and D. Li, "Mesoporous materials from zeolite seeds as supports for nickel tungsten sulfide active phases: Part 1. Characterization and catalytic properties in hydrocracking reactions," Applied Catalysis A: General. **294**, 59-67 (2005).

Zhang, D., A. Duan, Z. Zhao and C. Xu, "Synthesis, characterization, and catalytic performance of NiMo catalysts supported on hierarchically porous Beta-KIT-6 material in the hydrodesulfurization of dibenzothiophene," Journal of Catalysis. **274**, 273-286 (2010).

Zhang, Z., Y. Han, L. Zhu, R. Wang, Y. Yu, S. Qiu, D. Zhao and F.-. Xiao, "Strongly Acidic and High-Temperature Hydrothermally Stable Mesoporous Aluminosilicates with Ordered Hexagonal Structure," Angewandte Chemie International Edition. **40**, 1258-1262 (2001).

Zhao, D., J. Feng, Q. Huo, N. Melosh, G.H. Fredrickson, B.F. Chmelka and G.D. Stucky, "Triblock Copolymer Syntheses of Mesoporous Silica with Periodic 50 to 300 Angstrom Pores," Science. **279**, 548-552 (1998).

APPENDIX A

Characteristics	Quantities
Sulfur (%)	4.21
Nitrogen (%)	0.38
Density (g/mL)	0.98
Simulated Distillation	Temperature (^{o}C)
Initial Boiling Point	211.2
Final Boiling Point	595.4
Boiling Point Distribution (^{o}C)	Fraction (%)
IBP-260	2
260-310	5
310-360	6
360-410	18
410-465	21
465-FBP	48

APPENDIX B1

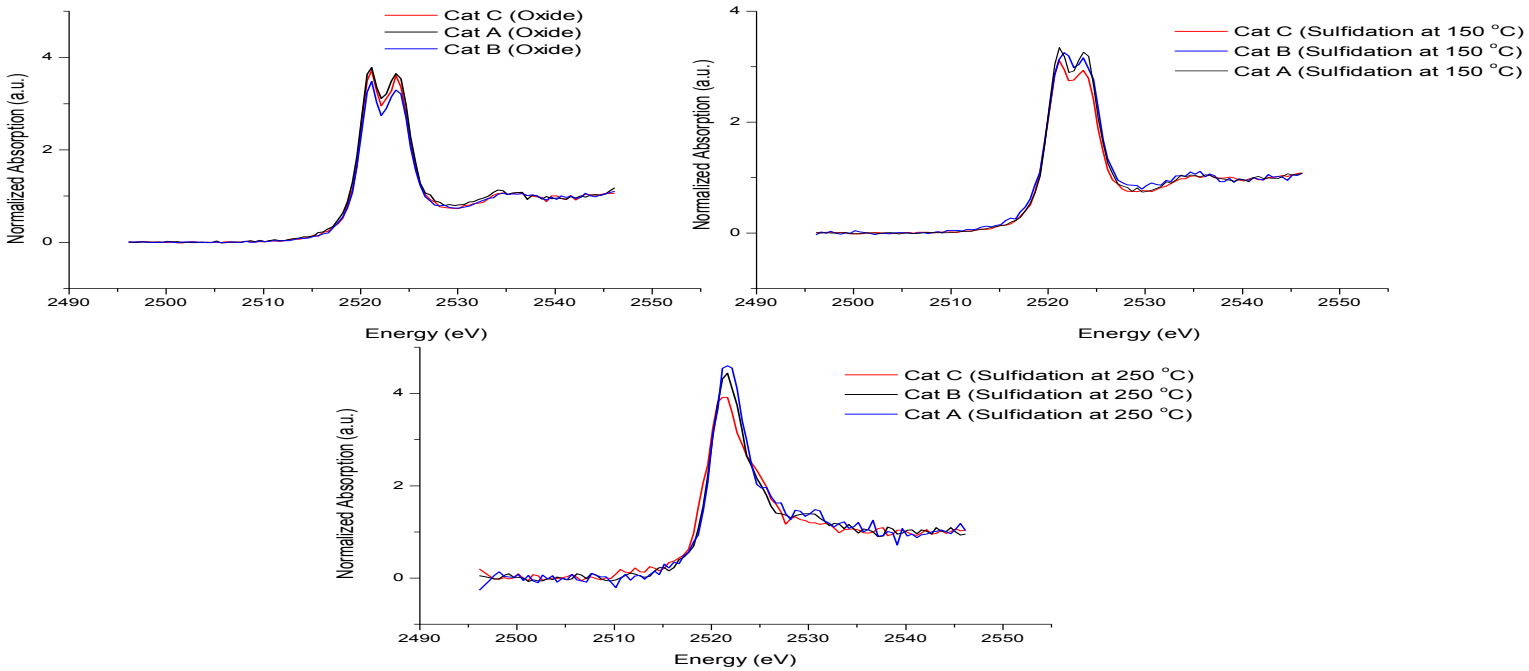

Mo L_3 Edge spectra of catalysts prepared with different CA/Ni (0, 1 and 2) molar ratios. Shown here is the effect of molybdenum-citrate complex on the sulfidation of the catalysts. The peak intensity for Cat A is highest and Cat C is lowest at 250 ^{o}C, indicating that sulfidation is rather retarded in Cat C

APPENDIX B2

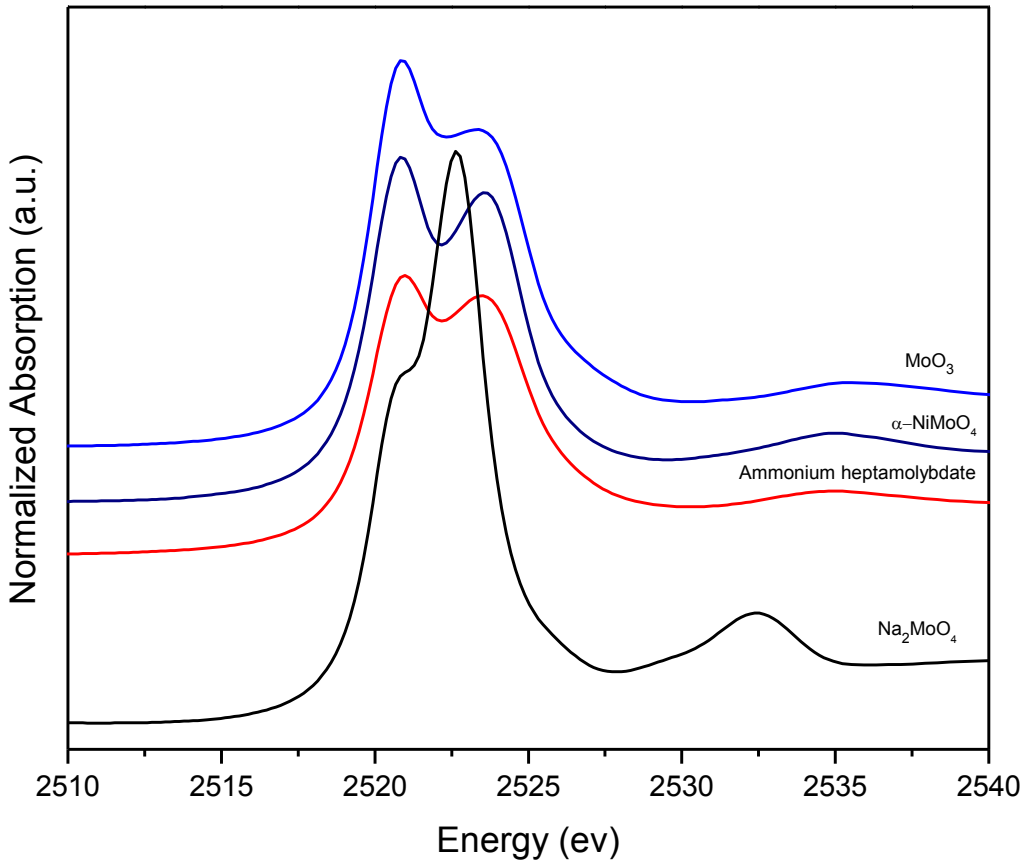

Mo L_3 Edge XANES spectra for some reference materials

APPENDIX C

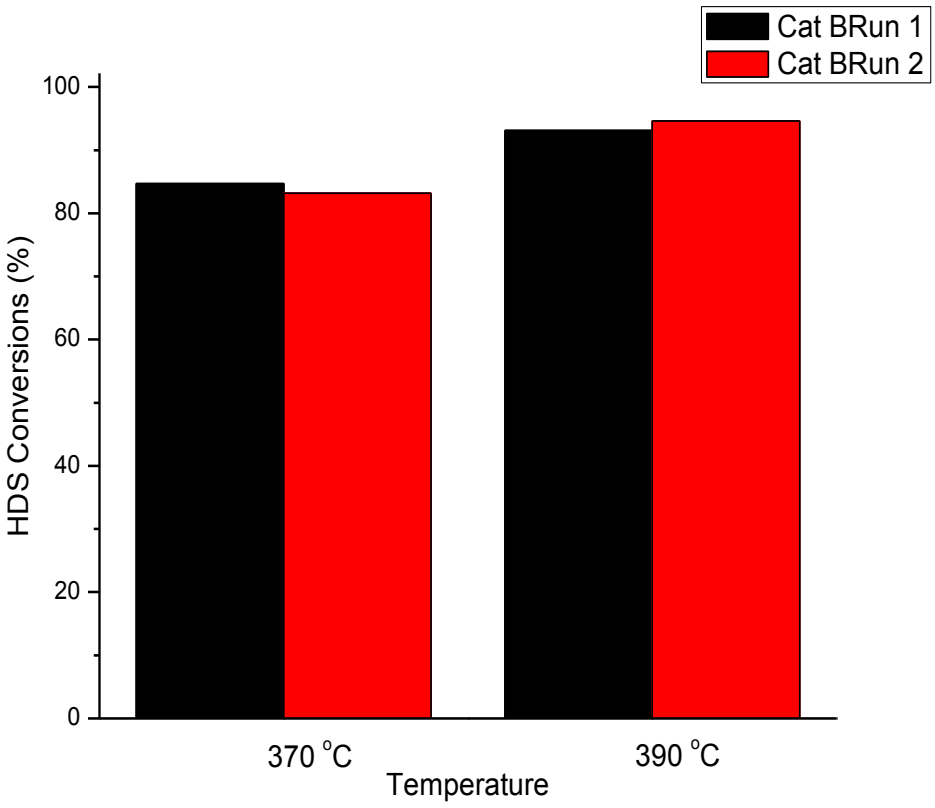

Hydrotreating activity test for Cat B to check for the reproducibility of the HDS results

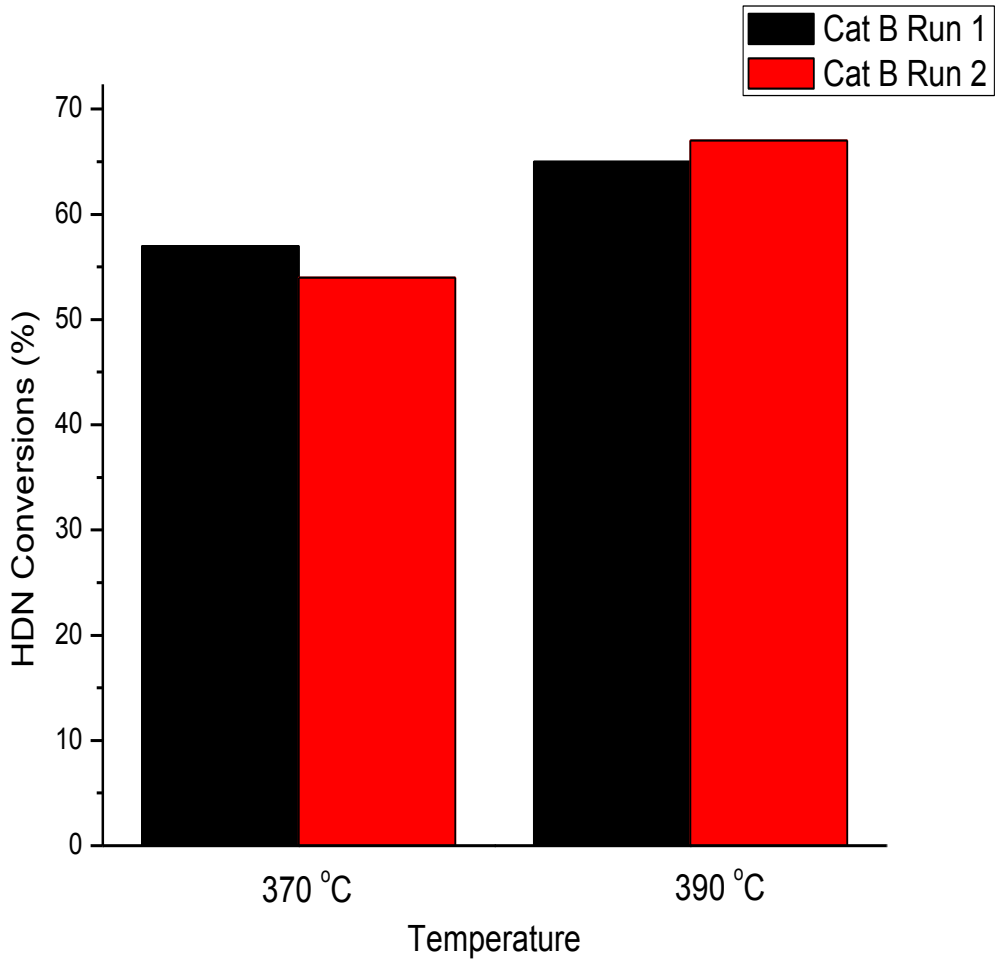

Hydrotreating activity test for Cat B to check for the reproducibility of the HDN results